Microplastic Mobility and Retention in Geosynthetic Clay Liners

By

Yifei Gao

A dissertation submitted to fulfilment requirements for the degree of

Doctor of Philosophy

(Civil Engineering)

at the

School of Civil Engineering

Faculty of Engineering

The UNIVERSITY OF SYDNEY

2026

Statement of Originality

This is to certify that the content of this thesis is my own work. This thesis has not been submitted for any other degree or purpose.

I certify that the intellectual content of this thesis is the product of my own work, and that all assistance received in preparing this thesis and all sources have been acknowledged.

Student Name: Yifei Gao

December 2025

Author Attribution Statement

This thesis contains materials that have been previously published or is currently in progress for which I am the first author. I am responsible for the design and execution of the experiments, data analysis, and drafting of the manuscripts. Permission to include the published data in this thesis has been granted by the corresponding author, Professor Abbas El-Zein.

Student Name: Yifei Gao

December 2025

As the primary supervisor for the PhD candidature of this thesis, I can confirm that the authorship attribution statement above is correct.

Supervisor Name: Abbas El-Zein

December 2025

Supervisor Declaration Statement

I have reviewed the content of this thesis and declare that it is free from plagiarism and of sufficient grammatical clarity to be examined. The research and writing are the candidate's own excepted as acknowledged in the Thesis Declaration. I confirm that the investigations were conducted in accordance with the ethics policies and integrity standards, and that the research data are presented honestly and without prejudice.

Supervisor Name: Abbas El-Zein

December 2025

AI Use Statement

During the preparation of the thesis, the author used ChatGPT (GPT-5 Thinking) for language polishing, wording suggestions and image reformatting. AI tools were not used for formulating research questions, conducting experiments or data collection, making statistical decisions, interpreting results, or drafting original scientific conclusions, nor were they used to generate raw data. All AI outputs were reviewed, verified, and, where necessary, rewritten by the author and checked by the supervisory team. The author accepts full responsibility for the thesis content and any errors.

Abstract

Microplastics (MPs) are plastic particles smaller than 5 mm which have recently emerged as environmental contaminants of concern. Landfills serve as major reservoirs of plastic, and potential sources of MP pollution, due to the accumulation and degradation of plastic waste. MPs have been detected in landfill leachate, with concentrations exceeding 30,000 pieces per litre, much higher than those typically observed in natural water bodies. Engineered barrier systems in landfills typically rely on geosynthetic clay liners (GCLs) and an underlying attenuation layer to restrict leachate migration. The swelling behaviour of bentonite in GCLs allows it to achieve low hydraulic conductivity and self-sealing capacity. While GCLs' ability to prevent the migration of dissolved organic and inorganic contaminants has been extensively investigated, their capacity to retain suspended particulate contaminants such as MPs remains poorly understood. This knowledge gap is especially concerning under field-representative conditions, where exposure to calcium-rich leachates and wet-dry cycles is known to reduce bentonite swelling and self-sealing behaviour, potentially compromising long-term barrier performance. An important methodological obstacle in addressing this gap is that conventional laboratory rigid soil columns, typically used to assess contaminant transport, are not suitable for low-permeability soils. Hence, the aims of this thesis are:

(1) To evaluate the influence of MPs on the swelling behaviour of bentonite in GCLs.

(2) To assess whether flexible wall permeameters (FWP) are suitable as soil columns for the study of MP transport through clay and sand-clay mixtures.

(3) To assess the ability of GCLs to prevent migration of small MPs under various GCL hydration conditions.

(4) To quantify MP transport through GCLs using advection-dispersion-reaction (ADR) models with first-order attachment/detachment kinetics and identify key processes at play.

Both non-fluorescent and fluorescently labelled polystyrene (PS) and polyethylene (PE) microspheres were used, with nominal sizes of 0.2, 0.5, 1, and 5 μm. The working

solutions were prepared from concentrated stock suspensions and quantified via ultraviolet-visible (UV-Vis) and fluorescence spectrophotometry. Two commercially available GCL products, including Bentomat® ST (granular sodium bentonite) and X-2000 (polymer-enhanced powder sodium bentonite), were tested. All transport experiments were conducted using an FWP, allowing controlled application of confining pressure and minimizing sidewall leakage. Prior to testing with soil specimens, baseline assessments were performed to evaluate instrument-induced artefacts and MP retention within the FWP system itself. GCL specimens were pre-hydrated in either deionized water or 10 mM, 100 mM and 300 mM $CaCl_2$ solutions, under continuously saturated or cyclic wet-dry conditions. The impact of hydration conditions on MP transport behaviour was critically assessed. MP breakthrough curves were generated by injecting MP-rich influent into near-saturated specimens, followed by deionized water flushing. Effluent was collected at fixed pore volumes, and MP concentrations were analysed to produce breakthrough profiles. The effects of GCL pre-hydration, bentonite type, and MP size and type on the extent and timing of breakthrough were quantified. Mercury Intrusion Porosimetry (MIP) and Scanning Electron Microscopy (SEM) of selected GCL and bentonite samples were used to help in interpreting soil column results. Derjaguin-Landau-Verwey-Overbeek (DLVO) interaction energy calculations were used to assess whether electrostatic interactions could explain the observed transport behaviour. Finally, eleven variants of the ADR model were compared to assess their ability to capture observed behaviour and hence identify relevant processes.

The main findings of this thesis can be summarised as follows. No significant change in swelling capacity was observed for GCLs containing polymer-enhanced powder bentonite when exposed to PS microspheres in either distilled water or 10 mM $CaCl_2$ solution. FWPs were evidenced to be suitable for MP transport studies in both coarse-grained and low-permeability soils. In all experiments with GCLs hydrated with deionized water, effluent MP concentration remained below the analytical detection limit, and no breakthrough was observed within the test durations, regardless of whether the bentonite was in powder or granulated forms. Similar outcomes were recorded in GCLs with powder bentonite that had undergone hydration under wet-dry cycles with solutions of up to 300 mM $CaCl_2$. By contrast, in GCLs containing granular bentonite that were exposed to 100 mM $CaCl_2$ and subjected to two wet-dry cycles, early breakthrough was observed of all studied MPs. MP retention in these GCLs was found to be dependent on particle size and polymer type. Larger particles (e.g., 1 μm PS) showed greater retention, likely due to

stronger attachment to the bentonite matrix and geotextile fibre. A ripening effect, characterized by a decline in effluent concentration following continuous MP injection, was observed for 1 μm PS particles but not for smaller sizes (0.2 and 0.5 μm), suggesting a particle size threshold for triggering clay surface modification. Additionally, PE particles exhibited higher retention than PS under comparable conditions, possibly due to differences in particle size distribution, hydrophobicity, or aggregation behaviour.

Numerical simulation showed that ADR formulations associated with time- and/or depth-dependent blocking terms reproduced the observed breakthrough behaviour more accurately than simpler models, highlighting the importance of progressive site blocking and depth-variable deposition in MP transport through GCLs.

This thesis is the first to provide a systematic experimental and numerical investigation of MP transport through GCLs. Future research can explore longer time experiments to assess whether breakthrough may occur in the longer term through powder bentonite as well as granular bentonite hydrated with deionised water. Laboratory experiments with permeants that are more representative of real leachates can provide better approximation of conditions in the field. On the other hand, field experiments would significantly enhance knowledge of the capacity of single- and double-lined barriers to prevent the migration of MPs. In addition, monitoring of aquifers underlying landfills can add valuable data on the extent of risk to aquifers and how to manage such risk.

Keywords: microplastics, GCL, landfill, swelling, transport and retention, hydration chemistry, wet-dry cycles, column experiments, numerical modelling

Acknowledgements

I would first like to express my sincere gratitude to my supervisor, Professor Abbas El-Zein, for his supervision, support and patience throughout my research. I feel fortunate and proud to have been one of his students. My heartfelt thanks go to my co-supervisor, Professor David Airey, for his invaluable guidance and insightful feedback throughout the course of my study. I would like to extend my appreciation to Professor R. Kerry Rowe, Professor Elizebeth A. Carter, Associate Professor Will Gates, and Professor Abdelmalek Bouazza for serving as co-investigators in this project. I am also grateful to Dr. Surya Sujathan for her continued attendance and constructive input during our weekly research meetings, and to Mr. Liam Duncan for his dedicated assistance with numerical modelling. This research was supported by the Commonwealth through an Australian Government Research Training Program (RTP) Scholarship DOI https://doi.org/10.82133/C42F-K220.

I wish to acknowledge the support of our laboratory technical officers, Ms. Caroline Tao, Ms. Ashalatha Indiradevi, Mr. Ross Barker, Mr. Garry Towell, and Mr. Paul Geddes, whose contributions to instrument training, equipment setup and sample preparation were essential to the research. My appreciations extend to all the researchers within Geoenvironmental Engineering Research Group, Dr. Steven Ding. Dr. Hamed Faizi, Dr. Joey Zhu, Linxue Zhao, and Christine Fink, for making my academic journey enriching and enjoyable.

Finally, I am deeply grateful to my parents, Jinhui Gao and Ping Xu, for their unconditional love, encouragement, and trust, which continually motivated me to pursue my passion. Special thanks go to Ms. Jiaqi Zhang for her understanding and support during our life together in Australia.

Publications and Awards

Journal papers

Gao, Y., Sujathan, S., Carter, E. A., Gates, W. P., Rowe, R. K., Bouazza, A., El-Zein, A. Performance of geosynthetic clay liners as hydraulic barriers against microplastic migration. (In progress).

Gao, Y., Sujathan, S., Carter, E. A., Airey, D., & El-Zein, A. (2025). Flexible wall permeameters for research on microplastic transport in soil: validity, advantages, and constraints. *Environmental Science & Technology, 59*(28), 14585-14596. https://doi.org/10.1021/acs.est.4c14274

Conference Papers

Gao, Y., Rowe, R. K., & El-Zein, A. (2024). Effect of microplastics on swelling behaviour of geosynthetic clay liners (GCLs). Proceedings of the XVIII European Conference on Soil Mechanics and Geotechnical Engineering (ECSMGE 24), 497-502. https://doi.org/ 10.1201/9781003431749

Gao, Y., Sujathan, S., & El-Zein, A. (2024). An insight into laboratory column experiments for microplastic transport in soil. Proceedings of GeoShanghai 2024, *6*(1), 012038. https://doi.org/10.1088/1755-1315/1335/1/012038

Awards

The paper “An insight into laboratory column experiments for microplastic transport in soil” was voted as “Best paper” candidate in GeoShanghai 2024.

Research Training Program Stipend (International) (SC3229).

Table of Contents

List of Figures

List of Tables

Notations

A_{123}	Hamaker constant for the two substances "1" and "3" in presence of solution "2", determined from the Hamaker constant of the three materials
C	Aqueous MP concentration
C_0	Initial concentration
C_{max}	Maximum effluent concentration
C_{max}/C_0	Maximum normalized concentration (plateau or peak)
d	Separation distance between particles or porous media
D	Particle diffusivity
k_a	First-order attachment coefficient
K	Boltzmann constant
kT	Thermal energy
$M_{MP\text{-}feed}$	Cumulative MP mass feed per unit area
$M_{MP\text{-}effluent}$	Cumulative transmitted MP mass per unit area
Pe	Peclet number
$PV_{initial\ breakthrough}$	Pore volumes at initial breakthrough when $C(t)/C_0$ exceeds 0.1
$PV_{0.5}$	Pore volumes at half-maximum
PV_s	Pore volumes to reach maximum (plateau)
r_p	Hydrodynamic radius of particulate particles
R^2	Coefficient of determination
S	Solid phase concentration of MPs
S_r	Degree of saturation
T	Absolute temperature
particles/L	Particles per liter
wt%	Mass percentage of a solute in solution or the mass percentage of specific material in bulk solid materials
v	Seepage velocity
λ	Cut-off wavelength
κ	Inverse of Debye length
k_{sat}	Saturated hydraulic conductivity

θ	Volumetric water content of porous media
ε_r	Relative dielectric constant
ε_0	Vacuum dielectric constant
η_p	Zeta potential of particle
η_c	Zeta potential of porous media
ρ	Soil bulk density
ψ	Dimensionless value to account for time- and depth-dependent blocking
ξ_{tot}	Total interaction energy
ξ_{vdw}	van der Waals attraction
ξ_{vdw}	Electrostatic double-layer interaction
γ	Overall transmission efficiency

Abbreviations

ADR	Advection-dispersion-reaction
AL	Attenuation layer
Bio-PMFs	Biodegradable polymer microfibers
BTCs	Breakthrough curves
CCL	Compacted clay liner
CFT	Colloidal filtration theory
DI	Deionised
DLVO	Derjaguin-Landau-Verwey-Overbeek
DW	Distilled
EC	Electrical conductivity
EDL	Electrostatic double-layer
ENPs	Engineered nanoparticles
FTIR	Fourier transform infrared
FWP	Flexible wall permeameter
GCL	Geosynthetic clay liner
GMB	Geomembrane
GSB	Granular sodium bentonite
HDPE	High-density polyethylene
IS	Ionic strength
LDPE	Low-density polyethylene
MIP	Mercury intrusion porosimetry
MPs	Microplastics
MSW	Municipal solid waste
PE	Polyethylene
PES	Polyester
PET	Polyethylene terephthalate
PP	Polypropylene
PPSB	Polymer-modified powdered sodium bentonite
PS	Polystyrene
PU	Polyurethane

PV	Pore volume
PVC	Polyvinyl chloride
RPs	Retention profiles
RWCs	Rigid wall columns
SB	Sand-bentonite
SEM	Scanning electron microscopy
SI	Swell index
SWRC	Soil-water retention curve
TIU	Toxic interface unit
UV-Vis	Ultraviolet-visible
WRC	Water retention capacity

Chapter 1 Introduction

1.1 Background

Plastics have become integral to modern society due to their versatility, durability and chemical resistance (Filiciotto and Rothenberg, 2021). Since the mid-20th century, global plastic production and consumption have increased exponentially, reaching approximately 380 million tons in 2015 (Geyer et al., 2017). A significant portion of plastic waste enters the environment through littering, mismanagement and improper disposal (Geyer et al., 2017), resulting in the accumulation of plastics in landfills, aquatic systems and coastal zones (Su et al., 2019; Mbedzi et al., 2020; Kushwaha et al., 2024).

Over time, plastic debris undergoes fragmentation, generating microplastics (MPs), commonly defined as plastic particles smaller than 5 mm (Thompson et al., 2004). The term *microplastic* was first introduced by Thompson et al. (2004), who used Fourier transform infrared (FTIR) spectroscopy to identify plastic debris of approximately 20 μm in marine beach samples. MPs are typically categorized as primary or secondary based on their origin (Ziani et al., 2023). Primary MPs are intentionally manufactured for specific applications, such as cosmetics and synthetic textiles, while secondary MPs are generated from the breakdown of larger plastic fragments (Ziani et al., 2023; Song et al., 2024). Secondary MPs account for most MPs encountered in the environment (Ziani et al., 2023).

MPs span a wide range of particle sizes, from millimetre-scale fragments to micrometre- and sub-micrometre-sized particles. In this thesis, the term *small microplastics* (small MPs) refers to particles between 0.2 and 5 μm, encompassing both sub-micron and few-micron fractions. These particles have increasingly been reported in landfill leachate and subsurface environments and may migrate more readily through soil pore networks and engineered barrier systems (Ma et al., 2025a). Their small size and environmental persistence may further complicate removal and containment. Consequently, the occurrence, transport and potential impacts of small MPs have attracted increasing research attention.

Soils are recognized as one of the largest environmental repositories of MPs, which can be introduced into the subsurface through urban runoff, industrial discharges, agricultural biosolids and plastic films (Deng et al., 2020; Huang et al., 2020; Horton et al., 2021; Wang et al., 2022a). The presence of MPs can alter soil properties and influence their migration from surface layers to deeper horizons through water flow (Bordoloi et al., 2022; Wang et al., 2022b). As a result, understanding MP behaviour and transport mechanisms in soils has become a critical research focus.

Municipal solid waste (MSW) management systems represent a major sink for plastic waste, with approximately 21-42% of managed plastics ultimately disposed of in landfills (Nizzetto et al., 2016; He et al., 2019; Kabir et al., 2023). Landfill leachate has been shown to contain significant quantities of MPs which originate from the physical, chemical and biological degradation of plastic waste, as well as from wastewater-treatment sludge disposed of in landfills (Xu et al., 2020; Kabir et al., 2023). In addition, MPs in leachate can act as vectors for organic and inorganic contaminants (He et al., 2019; Kabir et al., 2023). If MPs migrate through landfill barrier systems, they may pose a risk to underlying soils and groundwater. However, the extent to which landfill barrier systems can effectively limit the migration of MPs, particularly small MPs, remains uncertain and constitutes a key motivation for the research conducted in this thesis.

Sanitary landfills rely on engineered liner systems to prevent contaminant migration into the underlying subsoil and aquifer. A barrier system typically consists of three core components from bottom to top (Figure 1.1):

a) the underlying compacted soil attenuation layer (AL), constructed to achieve a hydraulic conductivity lower than 10^{-7} m/s and to separate the overlying liner from the aquifer (Rowe, 2012),

b) a low-permeability layer consisting of a geosynthetic clay liner (GCL) or compacted clay liner (CCL) (Rowe, 2011; Norris et al., 2023) and

c) a high-density polyethylene (HDPE) geomembrane (GMB) designed to provide chemical resistance against landfill leachate (Yu and El-Zein, 2019; Rowe et al., 2024).

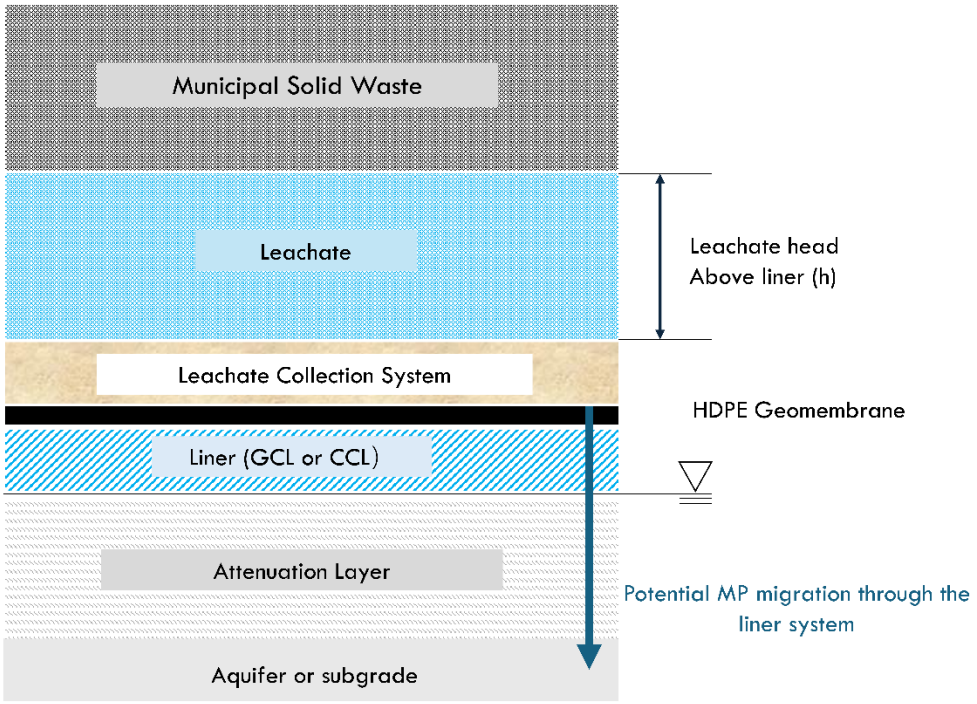

Figure 1.1. Conceptual diagram of microplastic (MP) migration pathways through a municipal solid waste (MSW) landfill liner system, including leachate, HDPE geomembrane, GCL/CCL liner, attenuation layer, and underlying aquifer, driven by leachate head.

Bentonite clay is a critical component of these barrier systems and can be present in several forms. First, GCLs consist of a thin layer of bentonite clay (typically less than 1 cm thick) sandwiched between woven or nonwoven geotextiles. When adequately hydrated, the bentonite forms a highly effective hydraulic barrier due to the swelling behaviour of montmorillonite, the principle swelling clay mineral in bentonite (Kaufhold et al., 2002). Compared with conventional CCLs, which require on-site compaction of natural clay soils, GCLs are prefabricated, lightweight, and easier to install (Rowe and Brachman, 2004; Bouazza and Gates, 2014; Rowe, 2014). Second, bentonite can be used to amend AL soils in order to reduce hydraulic conductivity and achieve regulatory or design targets (usually ~10^{-7} m/s). Bentonite-amended soils can provide a cost-effective solution when the desired hydraulic conductivity cannot be achieved through soil compaction alone (Fan et al., 2014; Proia et al., 2024). Third, bentonite powder is sometimes placed as a sealant in the gap between overlapping sides of two neighbouring GCLs to minimise leachate migration through panel interfaces and into the underlying soil (Brachman et al., 2010).

Landfill leachate can migrate through defects in the GMB and come into contact with the underlying GCL, where bentonite is relied on to prevent further contaminant

migration (Rowe and Hamdan, 2023). However, very little is known about the capacity of bentonite to prevent MP migration and, more generally, the interaction between bentonite and MPs. For example, when a GCL is installed, it is allowed to hydrate from the underlying subsoil so that the bentonite can swell and achieve the desired low hydraulic conductivity (usually $<10^{-9}$ m/s). In some cases, however, the GCL may be exposed to MP-rich leachate before adequate swelling has occurred. Hence, the potential effect of MPs on bentonite swelling remains an important but poorly understood issue.

The movement of MPs in soils, including landfill liner components, is influenced by several factors, including (i) MP particle type, size, shape and surface functional groups, aging and surface charge, (ii) soil hydro-mechanical and chemo-physical properties and (iii) environmental conditions (Ren et al., 2021; Yu et al., 2022; Li et al., 2024b). While extensive research has been conducted on MP mobility in coarse-grained soils (Ren et al., 2021; Fei et al., 2022; Yu et al., 2022), the interactions between MPs and clay-rich materials remain poorly understood (Yang et al., 2022). This knowledge gap constitutes a significant obstacle to any attempt at understanding the capacity of landfill liner systems to prevent MP migration into the surrounding environment.

One of the major impediments to research on MP transport in clay soils is the limitation of one of the most commonly used laboratory apparatus for contaminant transport studies, namely rigid-wall columns (RWCs). Soil column experiments using RWCs have been widely employed to investigate the transport and retention of contaminants, including MPs, in porous media. In these tests, soil is packed into a cylindrical column and saturated with water or other background solution (e.g., NaCl) before an MP suspension is introduced under controlled hydraulic conditions. Effluent samples collected during testing are used to generate breakthrough curves (BTCs), while post-test analysis of retained particles along the soil column can provide retention profiles (RPs). BTCs and RPs provide insight into transport and retention behaviour under different experimental conditions.

The use of RWCs in column tests offers fixed boundary conditions, a relatively simple setup, and is particularly suitable for cohesionless soils. However, several limitations reduce their suitability for fine-grained and cohesive soils. These include the absence of confinement, limit control of effective stress conditions, and extremely low flow rates under low hydraulic conductivity conditions. Although higher pressure gradients can be applied to increase flow rates, the lack of confinement may raise the risk of shrinkage, cracking and

sidewall leakage. Hence, alternative methodologies are required for investigating MP transport in clay-rich soils.

In summary, given the widespread presence of plastic waste in MSW, there is a need to assess the ability of landfill lining systems to prevent the migration of MPs from landfill leachate into underlying aquifers. However, based on the above discussion, such an assessment cannot be achieved without addressing the following knowledge and methodological gaps:

1. The effects of MPs on the swelling capacity of bentonite and its capacity to develop low hydraulic conductivity remain poorly understood.
2. RWCs, which are widely used in contaminant transport studies, are not well suited for clay-rich soils, including GCLs and bentonite-amended soils; alternative experimental methodologies are therefore needed.
3. No investigation has been reported on MP transport through GCLs and hence little knowledge of their capacity to prevent MP migration is currently available.
4. No attempts have been made to numerically simulate MP transport in GCLs, leaving the governing processes and their relative importance insufficiently understood.

1.2 Research Aims and Questions

By addressing the research gaps identified above, this thesis aims to contribute to the knowledge required to assess the ability of landfill lining systems to prevent MP migration into underlying aquifers. The thesis focusses on near sub-micron particle sizes (0.2, 0.5, 1 and 5 μm) because large MPs are less likely to migrate through the porous microstructure of a hydrated bentonite and smaller ones more likely to cross biological membranes and hence cause harm to plants and animals including humans (Lalrinfela et al., 2024). The following research questions and associated tasks guide the investigation:

1. How does MP exposure affect the swelling capacity of the bentonite in GCLs? This question is addressed through laboratory experiments to evaluate the swelling index and vertical deformation of GCL bentonite exposed to $CaCl_2$ and MP suspensions.
2. What are the key methodological considerations when using a flexible wall permeameter (FWP) to investigate MP transport, and what are its advantages and limitations? To address this question, a series of mass-balance tests are conducted to establish the

suitability of FWPs for MP transport experiments. Specifically, these tests assess the extent to which the FWP may act as a source or sink of MPs and hence influence transport measurements. The effects of porous stone type, filter paper type, pressure differential, MP size, concentration and ionic strength (IS) are investigated.

3. How effective are GCLs in preventing MP transport, and how do MPs interact with GCL components, including bentonite and geotextiles? A series of column transport experiments using FWPs are conducted to investigate MP transport through GCLs. Following the experiments, geotextiles and bentonite are analysed using scanning electron microscopy (SEM) to identify retained MPs. Mercury intrusion porosimetry (MIP) is further used to investigate changes in bentonite microstructure following exposure to different chemical conditions (i.e., deionised water versus $CaCl_2$). In addition, Derjaguin-Landau-Verwey-Overbeek (DLVO) interaction energies are calculated to estimate colloidal interactions between MPs and bentonite and to help interpret the observed transport and retention behaviour.

4. How effectively can advection-dispersion-reaction (ADR) models with first-order attachment/detachment kinetics describe MP transport through GCLs, and what transport and retention mechanisms do the modelling results imply?

The relationships between these four research components are shown in Figure 1.2.

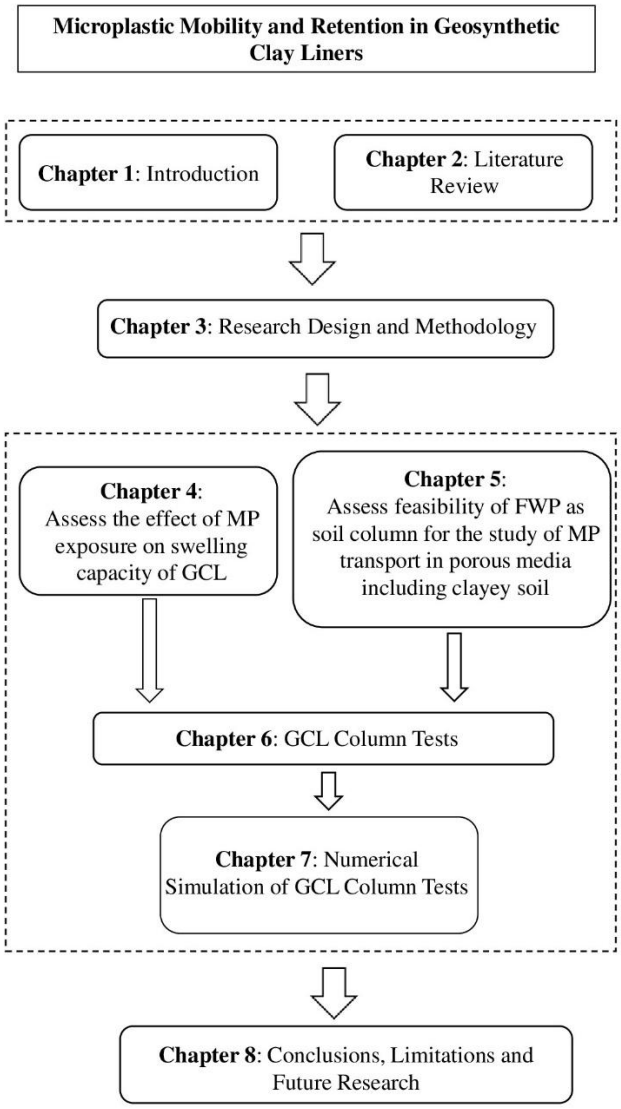

Figure 1.2 Summary of the main components of the study.

1.3 Novel Contributions

The thesis makes the following novel contributions:

1. Assessment of how exposure to small MPs affects the swelling of bentonite in GCLs.

2. Quantification of MP mass loss in a FWP, with analysis of influencing factors including MP particle size, filter paper and porous stone type, pressure differential and solution ionic strength.

3. Validation of a FWP as a soil column for MP transport, demonstrating near 100% recovery when no filter paper is used.

4. Assessment of MP transport through GCLs under different experimental variables.

5. Modelling of MP transport experiments through GCLs with one- and two-site ADR equations.

1.4 Outline of the Dissertation

The thesis is organized into eight chapters.

Chapter 2 presents an extensive literature review, with a focus on experimental and theoretical approaches to MP contamination in soil, presence of MP in landfill leachates and the performance of landfill barrier systems especially those with Na-bentonite GCLs. The aim of the chapter is to build a rationale, grounded in existing knowledge, for the research objectives and methodological choices pursued in this thesis.

Chapter 3 presents a summary of the overall research design of the project, as well as details of material choice and test conditions.

Chapters 4 to 7 address the four research questions outlined earlier, in the order presented above. Each one of these chapters first presents the methodology pursued followed by a discussion of the results and their implications. Chapter 4 examines the swelling behaviour of GCLs exposed to MPs, including an analysis of the swelling index and vertical swell deformation. Chapter 5 details the mass-balance experiments on FWP to assess its suitability for use as a soil column for the study of MP transport in soil. Chapter 6

investigates the barrier performance of GCLs against MP contamination and discusses results from FWP column studies as well as SEM and MIP analysis of GCL specimens. The DLVO interaction energy is used to help interpret experimental results. Chapter 7 explores the ability of eleven ADR model variants, with single or double attachment/detachment sites, to reproduce the GCL breakthrough curves. The variants are compared to identify the key processes controlling transport behaviour.

Finally, chapter 8 summarizes the key findings of this project, discusses their practical implications, and outlines limitations and potential avenues for future research.

Chapter 2 Literature Review

2.1 Introduction

Microplastics (MPs) are increasingly detected across terrestrial environments, yet their transport and fate within engineered containment systems remain insufficiently understood. This chapter critically reviews the current state of knowledge on MPs in soils, particularly in landfill environments. Section 2.2 summarizes evidence of MP contamination in soils, including their effects on physical and hydraulic properties, and evaluates column studies used to investigate transport behaviour. Section 2.3 describes the theoretical basis for MP mobility in porous media, focusing on retention mechanisms within an advection-dispersion-reaction (ADR) framework, colloidal filtration theory and DLVO interaction theory. Section 2.4 reviews detections of MPs in landfill environments and assesses the performance of landfill liner systems under field-realistic chemical and hydro-mechanical conditions. Finally, section 2.5 identifies the key research gaps that motivate this thesis and summarizes the research questions addressed in subsequent chapters.

2.2 Microplastic Contamination in Soils

2.2.1 Effects of MP Exposure on Soil Physical and Hydraulic Properties

MPs can influence key soil properties including soil structure, bulk density, porosity, hydraulic conductivity and water retention (Zhang et al., 2019). These effects arise from interactions between MP particles and soil grains that modify aggregate stability, packing behaviour and pore network geometry (Wang et al., 2023). MPs may disrupt interparticle bonding, act as rigid inclusions that alter packing arrangements, or accumulate within pore spaces, thereby affecting both soil structure and hydraulic behaviour (Lehmann et al., 2019; Solly et al., 2020; Li et al., 2025b). As a result, MPs can influence water flow, pore connectivity and physical retention processes in porous media.

Experimental studies have reported a wide range of outcomes depending on MP characteristics (e.g., polymer type, particle size, morphology and concentration), soil texture, and chemical conditions (Lehmann et al., 2019; Solly et al., 2020; Wang et al., 2022b; Yu et al., 2022; Li et al., 2025b). For example, reductions in hydraulic conductivity have been attributed to pore blocking and particle accumulation (Guo et al., 2022), whereas other studies report negligible changes or increases associated with macropore formation and structural disruption (Herath et al., 2013). Similarly, MPs may either decrease or increase soil water retention depending on particle shape and soil texture (Qi et al., 2020). These contrasting findings suggest that the effects of MPs on soil behaviour are highly dependent on particle characteristics, soil properties and chemical conditions.

However, most existing studies investigated homogenised MP-soil mixtures under controlled laboratory conditions, often at relatively high MP concentrations. Such experimental configurations differ from environmental scenarios, where MPs are transported with flowing water through intact soil structures or engineered barrier materials. Consequently, although previous work provides insight into MP-soil interactions, its implications to advective transport and retention processes remains limited. A detailed review of studies on individual soil properties is provided in Appendix X1, while the following sections focus on transport processes relevant to this thesis.

2.2.2 Column Studies of MP Transport in Soils

Understanding MP mobility and retention in porous media requires laboratory apparatus that can reproduce relevant hydro-chemo-mechanical boundary conditions. Apparatus selection is critical because it affects (i) control of saturation state, (ii) application of effective stresses representative of field conditions, and (iii) minimisation of experimental artefacts such as sidewall leakage, particle loss, and pump-induced pulsation. For low-permeability soils and engineered barrier systems, even minor artefacts, such as preferential flow along column walls or incomplete saturation, may significantly distort breakthrough behaviour and lead to erroneous interpretation of MP transport. Reliable measurement of breakthrough curves (BTCs) and mass balance therefore depends strongly on the suitability of the experimental equipment.

Several experimental approaches have been used to investigate contaminant transport, including rigid-wall columns (RWCs), geotechnical centrifuges, and flexible-wall

permeameters (FWPs). Their key characteristics, advantages, and limitations are summarised in Table 2.1.

Table 2.1. Comparison of experimental approaches for MP transport studies.

Apparatus	Key features	Advantages	Disadvantages
Rigid-wall column	Fixed-wall columns; constant head; peristaltic pump	Simple; low cost; widely used in literature; easy replication	No stress control; potential sidewall leakage and preferential flow; limited suitability for low-permeability soils
Geotechnical centrifuge	Elevated gravitational field; large specimen size	Accelerates transport processes; improved boundary realism	Complex operation; difficult flow control; particle-scaling forces do not scale with g-level
Flexible wall permeameter	Membrane confinement; controlled confining stress and back pressure; automated flow/pressure control	Minimises sidewall leakage; allows full saturation; replicates field stress conditions; suitable for low-permeability soils	More complex setup; potential particle retention in system components; requires a careful mass balance validation

Column experiments are widely employed to simulate contaminant transport by passing an MP suspension through a packed column of porous medium (Chu et al., 2019; Dong et al., 2021). RWCs are the most commonly used apparatus for MP transport studies, in which suspensions are passed through packed soils under controlled water head or flow conditions (Figure 2.1). Although RWCs are relatively simple to construct and operate, their inability to apply confining stress and the potential for sidewall leakage limit their suitability for fine-grained and low-permeability soils, where preferential flow paths may dominate transport behaviour (Guo and Fei, 2023).

Geotechnical centrifuges provide an alternative by accelerating advective transport through increased gravitational acceleration, enabling long-term transport behaviour to be simulated within shorter laboratory timescales (Huang et al., 2025). They also allow testing of larger specimens, improving boundary realism (Huang et al., 2025). However, interpretation of MP transport in centrifuge tests is complicated by the fact that particle-scale physicochemical interactions do not scale with gravitational acceleration, and flow

control in the rotating frame remains challenging. A more detailed discussion of RWCs and geotechnical centrifuges is provided in Appendix X2.

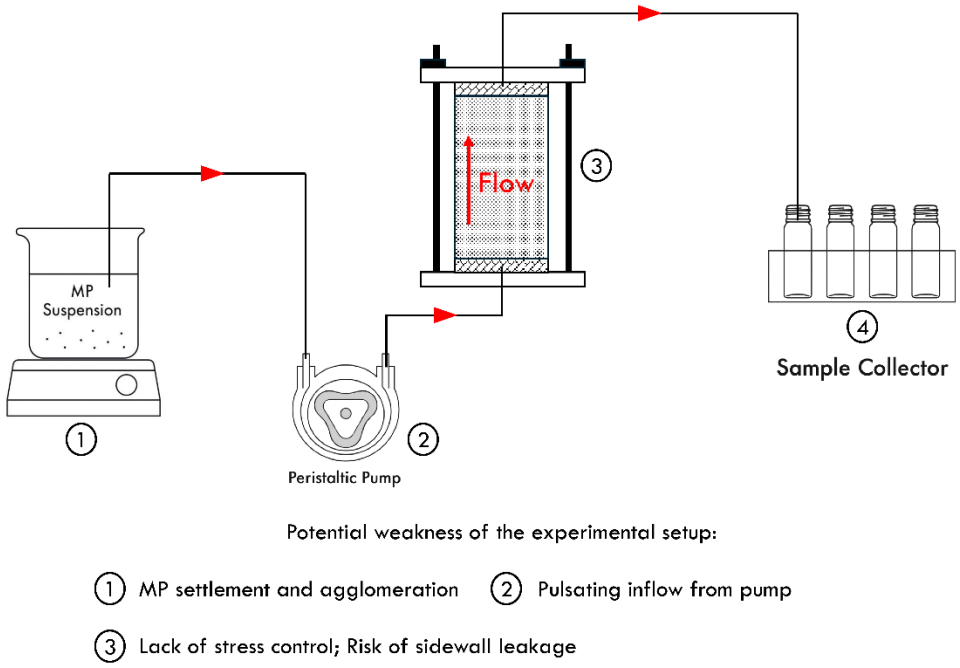

Figure 2.1. A typical rigid wall column set up for MP transport study with showing limitations for each instrument component (figure generated with AI assistance).

FWPs, originally developed for measuring hydraulic conductivity of fine-grained soils, overcome many of these limitations (Sterpi, 2015; Benson and Yesiller, 2016). The specimen is enclosed within a flexible rubber membrane and subjected to confining pressure, ensuring intimate radial contact and effectively minimising sidewall leakage. The application of back pressure enables full saturation, which is essential for reproducible transport measurements in low-permeability soils. In addition, automated pressure and volume control systems allow precise regulation of hydraulic gradients and monitoring of flow behaviour (Rowe and Li, 2020; Yu et al., 2020). These features make FWPs particularly suitable for simulating field-relevant hydraulic and mechanical conditions for low permeability soils with k <10^{-7} m/s (Kamon et al., 2002; Liu et al., 2019c). A further practical benefit is the ability to accommodate undisturbed cores without precise trimming of irregular surfaces (Daniel et al., 1985; Petrov et al., 1997; Jørgensen et al., 2004).

FWPs have been successfully adapted for solute transport studies in low-permeability media, demonstrating their capability to capture coupled advective–diffusive processes (Jørgensen et al., 2004; Zhou et al., 2013; Shackelford and Hong, 2019; Shackelford, 2021; Chaudhary et al., 2024). For example, Chaudhary et al. (2024) designed an FWP apparatus with contaminant reservoir to introduce and flush fluoride through soil-bentonite mixtures (30-70% bentonite by mass) relevant to landfill liners. Flow was monitored in real time using a volume fraction collector, and effluent samples were filtered and analysed after ~1-1.5 pore volumes (PV) were applied. Under the 30% bentonite scenario, flushed silt produced the highest normalised peak concentration (C_{max}/C_0 =0.90), whereas river sand yielded a much lower peak (C_{max}/C_0 <0.02), demonstrating how matrix texture and bentonite content influence contaminant breakthrough in low-permeability systems. The contrast was attributed to differences in diffusive mass transfer within immobile regions (Chaudhary et al., 2024). These results highlight the capability of FWPs for investigating solute transport in porous media with very low hydraulic conductivity.

However, their application to MP transport remains limited. Unlike dissolved solutes, MPs may undergo unintended retention within system components such as porous stones, membranes and tubing, introducing potential artefacts (Jørgensen et al., 2004; Zhou et al., 2013). Accordingly, rigorous baseline testing and mass balance assessment are required to ensure reliable interpretation of results. To the best of the author's knowledge, only one published study has applied FWPs to MP transport experiments but did not report any baseline mass recovery assessment (Chen et al., 2023), representing an important methodological gap in the literature. If addressed, it can lead to significant advances in the study of MP transport in low permeability soils, given the widespread availability of FWPs and the extensive practical experience associated with their use worldwide.

Given these considerations, FWPs were selected as the primary experimental platform in this study. Their ability to control confining stress, achieve full saturation, and minimise sidewall leakage makes them suitable for investigating MP transport in low-permeability soils and engineered barrier systems such as GCLs. By addressing methodological challenges associated with particle retention and mass balance, this study aims to extend the application of FWPs to MP transport and provide more reliable insights into MP mobility under field-relevant conditions.

2.2.3 Experimental Evidence of MP Transport in Soils

Laboratory studies show that MPs rarely behave as conservative tracers, exhibiting significant retention compared to inert solutes (Yu et al., 2022). The obtained BTCs commonly display three features: (i) early breakthrough, expressed as the time or the number of PV at which C/C_0=0.1, (ii) the peak normalised concentration $C_{max}/C_{0,}$ and (iii) tailing, a gradual decline in C/C_0 after the peak that reflects detachment or mass transfer into immobile domains (Thilagan et al., 2015; Pedretti and Bianchi, 2018). Complementary retention profiles (RPs), obtained by axial sectioning after the test, reveal how MPs are distributed within the column (Li et al., 2024d). Interpreted together under a verified mass balance, BTCs and RPs provide insights into MP mobility and the underlying deposition mechanisms across various porous media.

The literature on MP transport in porous media has expanded rapidly since 2016 (Miao et al., 2023; Li et al., 2024b). Most studies employ RWCs with varying dimensions and hydraulic controls (e.g., constant head or constant flow). Guo and Fei (2023) synthesised this body of work and grouped the governing variables into four categories: (i) experimental apparatus and boundary conditions; (ii) MP particle properties; (iii) porous media properties; and (iv) solution properties. This framework provides a basis for experimental design across scenarios and for interpreting observed transport and retention behaviours.

2.2.3.1 Effects of Experimental Apparatus and Boundary Conditions

Direct comparison of MP breakthrough across studies requires caution because laboratories use different devices and analytical workflows. Device geometry (e.g., column length and inner diameter), device materials (e.g., glass, acrylic), and hydraulic control (e.g., hydraulic head, flow rate) all influence transport outcomes (Pak et al., 2023). Analytical methods also vary in terms of filter pore size, staining protocols, and the spectral resolution/thresholds of FTIR or Raman, which affect detection limits and polymer identification accuracy (Dey et al., 2025). In addition, experimental boundary conditions differ across studies, including soil stress state (e.g., effective confining pressure), hydraulic gradient and water flux, and temperature (Haque and Fan, 2023; Guo et al., 2025b; Maqbool et al., 2025). Together, these factors influence attachment-detachment, straining, and mass transfer, thereby determining the form of both BTCs and RPs.

2.2.3.2 Effects of MP Particle Properties

Across column studies, MP mobility is influenced by polymer type, particle size and shape, surface chemistry (e.g., aging/weathering), and influent concentration. Particle size controls the geometric likelihood of straining and bridging. Larger particles are more readily intercepted at pore constrictions, whereas smaller ones are more likely to travel through pore networks even under saline conditions (Pradel et al., 2020; Yu et al., 2022). Composition and shape of MP particles are also important. Differences in density and hydrophobicity help explain trends such as PP<PET<PE in mobility for equal sizes (O'Connor et al., 2019; Gao et al., 2021). Waldschläger and Schüttrumpf (2020) reported greater deposition for fibres and irregular fragments than for spheres because the former shapes span pore throats and reorient or deform in flow, enhancing interception and straining. They also noted that fibre diameter is more influential than length in controlling transport behaviour. Surface properties exert a significant influence on breakthrough behaviour: negatively charged or hydrophilic particles (e.g., carboxylate/sulphonated MPs) exhibit greater breakthrough, whereas positively charged, amine-modified particles show enhanced deposition (Dong et al., 2019; Rong et al., 2021). Ageing (e.g., ultraviolet exposure) tends to increase oxygenated functional groups on MP surfaces, leading to more negative zeta potentials, reduced hydrodynamic size, and thereby enhanced mobility, while simultaneously increasing co-contaminant sorption capacity (Liu et al., 2019b; Xi et al., 2022). Finally, higher influent concentrations promote particle-particle and particle-collector collisions, aggregation, site blocking, and pore occlusion, generally lowering effluent recovery (Yu et al., 2022). At sufficiently high flow velocities, a critical concentration may be reached beyond which additional increases have little further effects (Hou et al., 2020).

2.2.3.3 Effects of Porous Media Properties

Properties of the porous medium significantly influence MP transport and retention (Li et al., 2024b). Collector type is particularly important. Smooth, chemically inert glass beads typically yield higher effluent recoveries than quartz sand, whereas natural soils with diverse mineralogy and organic matter retain substantially more MPs (Wang et al., 2016). For example, adding a loam fraction to sand increased deposition by roughly an order of magnitude, highlighting the role of clays in promoting retention (Quevedo and Tufenkji, 2012). Grain size also determines MP mobility, with larger grains reducing specific surface

area and the number of available attachment sites, while finer textures create smaller pore throats and more tortuous pathways that enhance straining and reduce transport (Dong et al., 2022).

Surface chemistry and surface roughness also exert important effects. Metal-oxide coatings, including Mn-, Fe-, and Al-oxides, enhance electrostatic attraction and contribute to particle deposition (Tan et al., 2021; Zhang et al., 2023a), while the development of biofilms increases retention by roughening collector surfaces and forming hydrogen bonds with MPs, leading to greater particle capture in biofilm-coated media compared with uncoated collectors (Mitzel et al., 2016; Ventura et al., 2024). Mineralogical composition contributes in a comparable effect, as higher Fe/Al-oxide contents and increased clay fractions reduce MP mobility through stronger adsorption, increased surface heterogeneity, and lower effective porosity (Wu et al., 2020; Ye et al., 2022b). In contrast, the specific roles of swelling clays, particularly smectites such as montmorillonite, remain less well understood and warrant targeted investigation.

Taken together, these findings suggest that mechanistic insights derived from simplified collectors, such as glass beads or clean quartz sands, may overestimate MP mobility under environmental conditions, highlighting the need for greater soil realism in both experiments and models.

2.2.3.4 Effect of Solution Properties

The hydro-chemical properties of the pore fluid exert a significant influence on MP transport behaviour (Dong et al., 2021; Ren et al., 2021; Li et al., 2024b). Solution pH can enhance MP mobility by driving more negative zeta potentials, and for some polymers such as PET, reducing aggregation, thereby increasing effluent recovery (Dong et al., 2021). In contrast, increasing ionic strength (IS) compresses the electrical double layer surrounding both collectors and MPs, weakens electrostatic repulsion, promotes aggregation, and consequently reduces transport (Lu et al., 2021a; Ye et al., 2022a). Salinity effects are often more pronounced for smaller particles, which are more sensitive to changes in electrostatic interactions (Dong et al., 2018).

Cation valence and identity further influence MP mobility (Lu et al., 2021a; Ma et al., 2025b). Multivalent ions, such as Ca^{2+}, Mg^{2+}, and Al^{3+}, enhance retention through cation bridging and charge neutralisation mechanisms (Quevedo and Tufenkji, 2012; Zhang et al.,

2023a). For ions with the same valence, smaller hydrated radii yield more effective charging screening and are therefore typically associated with reduced MP transport (Dong et al., 2021).

Hydrodynamic effects interact with influent concentration to influence MP transport behaviour (Zheng et al., 2014; Hou et al., 2020; Qi et al., 2022). Increasing flow velocity enhances hydrodynamic shear, which promotes particle detachment and reduces residence time, leading to higher effluent recovery at low and moderate concentrations (Hou et al., 2020; Qi et al., 2022). At high concentrations, however, greater velocities also increase the frequency of particle-collector and particle-particle collisions, thereby enhancing aggregation and accelerating the occupation of available attachment sites. As a result, MP transport may exhibit a non-monotonic response to increasing velocity, with mobility initially increasing due to shear-induced release before declining once collision-induced capture and pore-scale interception dominate beyond a critical influent concentration (Hou et al., 2020).

Co-contaminants can further modify MP surface chemistry and, in turn, influence mobility. Nanometre-scale PS particles have been shown to facilitate the transport of non-polar and weakly polar organic compounds (e.g., pyrene), while exerting negligible effects on more polar phenolic species (Liu et al., 2018). Different organic co-contaminants may have opposite effects. For example, naphthalene can reduce MP mobility through charge shielding, whereas nonylphenol may enhance transport by increasing electrostatic repulsion from quartz surfaces (Hu et al., 2020; Xu et al., 2022). Among inorganic species, fertiliser-released ammonium (NH_4^+) has been reported to increase MP retention by decreasing energy barrier (Rong et al., 2022), while divalent metal cations such as Cd^{2+} and Ba^{2+} promote deposition through charge screening and cation bridging with oxygenated functional groups on MP surfaces (Lu et al., 2021b; Tan et al., 2021).

Collectively, solution chemistry, flow regime, and co-contaminant presence act jointly to determine MP transport and retention. Rigorous reporting and control of these parameters are essential for meaningful comparison across studies and for robust interpretation of breakthrough and retention behaviour.

2.3 Theory of Microplastic Transport in Soils

2.3.1 Key Transport Processes

Understanding MP migration through soils is essential for predicting contaminant transport and assessing the performance of engineered barrier systems. Although extensive literature exists on the transport of colloids and engineered nanoparticles (ENPs), MPs differ in particle size, morphology, hydrophobicity and degree of surface aging, all of which can modify their transport and retention behaviour (Zhang et al., 2024). Nevertheless, classical colloid transport theory provides a useful conceptual framework for interpreting MP behaviour in porous media.

The key transport processes considered in this study include advection, hydrodynamic dispersion (mechanical dispersion and Brownian diffusion), physical interception and straining, and site-evolution processes such as blocking and ripening.

2.3.1.1 Advection, Dispersion and Diffusion

Particle transport by advection occurs through the bulk movement of pore water at the seepage velocity, while hydrodynamic dispersion causes spreading of particle distributions within porous media. Hydrodynamic dispersion arises from two main mechanisms: (i) mechanical dispersion, which results from pore-scale velocity variations and tortuous flow pathways, and (ii) molecular diffusion driven by Brownian motion, which causes particle motion down concentration gradients (Zhong et al., 2017; Mao et al., 2023). Mechanical dispersion depends on flow velocity and results from pore-scale variations in flow paths, whereas diffusion is independent of advective velocity and is governed by temperature, fluid viscosity and particle size.

The relative importance of advection versus diffusion and dispersion is commonly characterised by the Peclet number:

$$Pe = vL/D$$

where v is seepage velocity, L is the characteristic length, and D is particle diffusivity. Values of $Pe \gg 1$ indicate advection-dominated transport, whereas $Pe \ll 1$ indicates diffusion-dominated behaviour (Huysmans and Dassargues, 2005). At low flow velocities, diffusion can contribute appreciably to particle spreading, while under typical groundwater

flow conditions, mechanical dispersion generally dominates (Keller et al., 2004; Molz, 2015).

Particle size strongly influences diffusive transport. Brownian motion decreases rapidly with increasing particle diameter. Diffusion is often negligible for particles larger than approximately 1 μm but becomes increasingly important for sub-micron particles (Wang and Sedighi, 2023). Diffusion may also become significant in fine-grained porous media, where pore-scale velocities are low and pore lengths are short (Chowdhury et al., 2012). Quantitatively, particle diffusivities are typically three or more orders of magnitude lower than those of dissolved solutes (Batchelor, 1976). Nevertheless, for ENPs, diffusion can still exert a measurable influence on transport and retention processes (He et al., 2009). These transport processes provide the theoretical basis for interpreting MP breakthrough curves observed in the column experiments presented in this thesis. In Chapter 7, the relative importance of advection and dispersion is further evaluated during analysis of particle migration through low-permeability barrier materials.

2.3.1.2 Straining and Bridging

Straining refers to the geometric interception of particles at pore throats that are too small to permit passage (Figure 2.2a). It is controlled primarily by the relationship between particle size and shape and the pore throat size distribution within the porous medium (Njie et al., 2023). Retention by straining can occur at different locations and through several distinct modes. Surface straining occurs when multiple particles arrive simultaneously at a pore entrance and jam by arching (a process favoured at higher influent concentrations and, in some cases, mitigated by increased flow velocities that disrupt particle arches) (Bi et al., 2025). Wedging describes the capture of a single particle between adjacent collector surfaces, while bridging occurs when clusters of particles accumulate at a pore throat and form an interlocking blockage (Lin et al., 2021). In addition, particles may become trapped within sheltered pore regions formed by irregular packing, where stabilising interfacial forces inhibit remobilisation.

Classical filtration theory suggests that straining becomes significant when the particle-to-collector diameter ratio exceeds approximately 0.008 (Xu et al., 2006). However, many experimental studies have reported appreciable straining at smaller ratios, down to ~0.002-0.003, due to surface roughness, irregular particle geometries, and access to intra-

aggregate micro-pores that effectively narrow local throats (Bradford et al., 2007). When straining dominates, BTCs typically exhibit delayed breakthrough and reduced plateau concentrations, yielding low overall MP recovery in the effluent. In this study (Chapter 6), straining and bridging are used to interpret particle-size-dependent retention, reductions in effluent concentrations, and the retention of MPs within soil and GCL matrices.

2.3.1.3 Reversible and Irreversible Electro-Chemical Attachment

In addition to geometric interception, particles may be retained through interfacial interactions that promote attachment to collector surfaces (Figure 2.2b). These interactions occur over two characteristic distance ranges. At very short separation distances, typically on the order of a few nanometres, hydration forces, hydrogen bonding, and dipole-dipole interactions can dominate once particles approach collector surfaces at very small separation distances (Hedley et al., 2023). At longer ranges, particle behaviour is governed by the balance between electrostatic double-layer (EDL) interactions and van der Waals attraction, which together determine whether the net interaction energy is attractive or repulsive (Hedley et al., 2023).

Classical Derjaguin-Landau-Verwey-Overbeek (DLVO) theory describes these long-range interactions and predicts two principal attachment states. Particles may be captured within a primary energy minimum, leading to effectively irreversible deposition under steady hydraulic conditions, or they may reside transiently within a secondary energy minimum when a repulsive energy barrier persists, resulting in weak and reversible attachment (Ohshima, 2012). Solution chemistry strongly influences the height of this energy barrier. Increasing ionic strength compresses the EDL and reduces electrostatic repulsion, increasing the likelihood of primary minimum deposition (Chowdhury et al., 2014). Surface heterogeneity and roughness can reduce energy barriers and create contact points that render attachment quasi-irreversible over experimental timescales. In contrast, particles retained within a secondary minimum are readily detached by hydraulic shear or modest changes in solution chemistry that increase repulsive interactions (Ting, 2023).

For MPs in particular, polymer hydrophobicity and surface ageing processes, including oxidation and biofilm conditioning, can modulate attachment-detachment behaviour (Liu et al., 2019a). Oxidation or adsorption of natural organic matter generally increases surface electronegativity, which may weaken attachment and promote

remobilisation. Conversely, cation bridging involving multivalent ions such as Ca^{2+} and Al^{3+}, as well as hydrophobic interactions, tend to strengthen adsorption. These mechanisms provide a practical framework for interpreting BTC plateaus and hysteresis observed during MP transport experiments. In this thesis, DLVO-based interaction energy calculations are used in Chapter 6 to interpret MP-bentonite interactions under different chemical conditions. Theoretical predictions are compared with experimental transport results to evaluate the role of electrochemical interactions in MP retention.

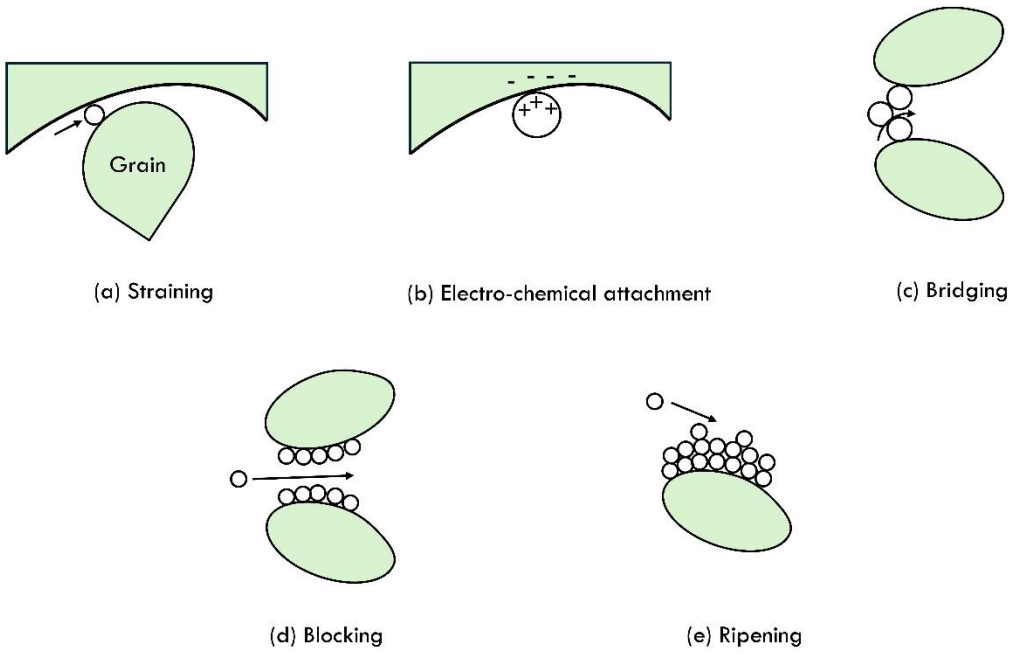

Figure 2.2. Classical particle transport mechanisms in porous media (a) straining; (b) electro-chemical attachment; (c) bridging; (d) blocking; and (e) ripening.

2.3.1.4 Blocking and Ripening

Collector surfaces have a finite capacity for particle attachment, which evolves as deposition progresses (Liu et al., 2020). Blocking occurs when favourable attachment sites become progressively occupied and particle-particle repulsion inhibits further deposition (Figure 2.2d). As a result, the effective attachment coefficient decreases over time, typically producing BTCs with rising plateau concentrations and reduced retention along the column (Kasel et al., 2013). Blocking is most commonly observed under relatively smooth collector

conditions, at low to moderate influent concentrations, and under solution chemistries that yield weak particle-collector attraction (Liu et al., 2020).

In contrast, ripening occurs when interactions between deposited particles promote continued deposition and multilayer accumulation (Figure 2.2e) (Bradford and Torkzaban, 2008). Previously deposited particles act as secondary collectors, enhancing further attachment and increasing the effective attachment rate over time (Katzourakis and Chrysikopoulos, 2024). Ripening is typically observed at higher MP loadings and/or solution chemistries that enhance interparticle attraction, and it often manifests as BTCs with declining plateau concentrations. In this thesis, blocking and ripening processes are used in Chapter 6 to interpret the evolution of breakthrough curve plateaus and time-dependent changes in MP deposition behaviour.

2.3.2 Continuum and Pore Scale Theories of Colloid Transport

BTCs from soil column studies of MP transport are commonly interpreted by fitting transport models to infer physically meaningful parameters (Lee et al., 2021; Cao et al., 2023). Two modelling scales are typically used (Lim et al., 2023). At the pore scale, fluid flow and particle motion are resolved within individual pore geometries, and interfacial interactions are often quantified using DLVO theory (Liu et al., 2023). While pore-scale approaches provide mechanistic insight, they are difficult to integrate with centimetre-scale column experiments because resolving the pore structure of an entire specimen is computationally prohibitive, and individual realisations may not adequately represent column-scale heterogeneity.

For this reason, many studies adopt continuum scale formulations that upscale pore-scale processes into an advection-dispersion-reaction (ADR) framework, commonly coupled with colloid filtration theory (Xiao et al., 2024; Yang and Tang, 2025). Within ADR models, one-site formulations treat all collector surfaces as a single kinetic domain with irreversible attachment (detachment set to zero), whereas two-site models partition retention into concurrent reversible and irreversible processes. No single formulation has yet emerged as a standard for MP transport, and model selection and parameter identifiability remain case-specific. These modelling approaches provide the basis for quantitative interpretation of MP breakthrough curves in this study, linking pore-scale processes with continuum-scale transport behaviour.

2.3.2.1 One-Site and Two-Site Advection-Dispersion-Reaction (ADR) Equations

Soil column tests of MP transport is most commonly interpreted with one-dimensional ADR models enriched with first-order attachment-detachment kinetics (Li et al., 2024e). Simple equilibrium formulations rarely reproduce both BTCs and RPs, so recent studies favour non-equilibrium kinetics that allow distinct attachment and detachment rates and accommodate heterogenous retention (Schijven and Šimůnek, 2002; Guo and Fei, 2023).

Two modelling families are commonly used (Guo and Fei, 2023). First, one-site models treat all collector surfaces as a single kinetic domain, and the coupled balance is:

$$\frac{\partial C}{\partial t} + \frac{\rho}{\theta}\frac{\partial S_1}{\partial t} = D\frac{\partial^2 C}{\partial x^2} - v_x\frac{\partial C}{\partial x} \tag{2.1}$$

where C [$M.L^{-1}$] is the aqueous MP concentration, θ [-] is the volumetric water content of porous media, ρ [$M.L^{-3}$] is soil bulk density, t [T] is time, v_x [$L.T^{-1}$] is pore-water velocity, x [L] is the spatial coordinate along flow direction, D [$L^2.T^{-1}$] is the dispersion coefficient, S_1 [$M.M^{-1}$] is the solid phase concentration of MPs. The second term on the left-hand side of equation 2.1 can be written as:

$$\frac{\rho}{\theta}\frac{\partial S_1}{\partial t} = k_{a1}\psi_1 C \tag{2.2}$$

where k_{a1} [T^{-1}] is the first-order (irreversible) attachment coefficient, and ψ_1 [-] is a dimensionless value to account for time- and depth-dependent blocking.

Second, two-site models simultaneously capture reversible attachment-detachment and irreversible attachment. The general form of two-site model is:

$$\frac{\partial C}{\partial t} + \frac{\rho}{\theta}\frac{\partial S_1}{\partial t} + \frac{\rho}{\theta}\frac{\partial S_2}{\partial t} = D\frac{\partial^2 C}{\partial x^2} - v_x\frac{\partial C}{\partial x} \tag{2.3}$$

where S_1 [$M.M^{-1}$] and S_2 [$M.M^{-1}$] are the retained MP mass per mass of porous media at the two sites 1 and 2, which correspond to irreversible and reversible attachment, respectively. The second and third term on the left-hand side of equation 2.3 can be written as:

$$\frac{\rho}{\theta}\frac{\partial S_1}{\partial t} = k_{a1}\psi_1 C \tag{2.4}$$

$$\frac{\rho}{\theta}\frac{\partial S_2}{\partial t} = k_{a2}\psi_2 C - \frac{k_{d2}\rho S_2}{\theta} \tag{2.5}$$

where k_{a1}, k_{a2} [T^{-1}] are the attachment coefficients for site 1 and 2, respectively, to capture irreversible and reversible attachment, k_{d2} [T^{-1}] is the detachment coefficient for site 2, and ψ_1 and ψ_2 are the blocking functions for sites 1 and 2, respectively.

To reproduce BTC plateaus and hyper-exponential RPs, time- and depth-dependent modifiers to the blocking function ψ are introduced. In practice, the time modifier modulates site evolution (e.g., blocking, ripening) by adjusting the effective deposition rate as sites fill, while the depth modifier scales attachment with distance from the inlet to represent near-inlet filtration (frequently using an empirical decay tied to grain size and a maximum solid loading). In this thesis, one-site and two-site ADR models are applied to fit experimental breakthrough curves and quantify attachment-detachment processes, with model selection and parameter interpretation discussed in Chapter 7.

2.3.2.2 Colloidal Filtration Theory

Colloidal filtration theory (CFT) provides a classical framework for describing the transport and removal of suspended particles as they migrate through porous media (Liang et al., 2024a). In CFT, the porous medium is idealised as an array of collector grains (e.g. sand particles), with colloids transported by advection and dispersion while undergoing collisions with collector surfaces that may result in attachment (Tufenkji and Elimelech, 2005). Particle deposition is commonly expressed as a first-order process with respect to aqueous concentration, yielding an exponential decline in concentration with travel distance. At the continuum scale, this behaviour is incorporated within ADR formulations using attachment and detachment rate coefficients that describe mass transfer between the mobile aqueous phase and one or more solid-phase retention domains. These effective coefficients combine hydrodynamic collection mechanisms (interception, sedimentation, Brownian diffusion) and physicochemical interactions at the particle-collector interface.

CFT was developed primarily for coarse granular media with well-connected pore spaces, where particle retention is often dominated by surface attachment (Kamai et al., 2015). Its application to clay-rich soils and engineered clay barriers requires additional consideration. In compacted clays and bentonite-based materials, pore structures span nano- to micro-scales, and the solid phase forms aggregates and tactoids rather than discrete spherical grains. As a result, collector surfaces are highly heterogeneous, and the boundary between surface attachment and mechanical straining is less distinct. Nonetheless, several CFT concepts remain relevant. Clay fabrics provide extensive internal surface area and charged mineral surfaces that can enhance electrostatic interaction and promote attachment (Fu et al., 2025b). Changes in pore-water chemistry (ionic strength, ion valence, and pH)

alter double-layer thickness and interaction energies, thereby influencing the likelihood of particle deposition (Chen et al., 2018a). In addition, first-order attachment-detachment formulations can still be applied at the continuum scale to represent net retention within complex pore networks.

In terms of bentonite and GCLs, CFT therefore offers a useful conceptual and mathematical basis for interpreting MP and colloid transport, provided that its clean-bed assumptions and simplified collector geometries are recognised as approximations of the microstructure and retention processes in clay barriers.

2.3.2.3 DLVO Interaction Energy Theory

DLVO theory provides a classical framework for describing the interaction energy between a suspended particle and a collector surface, or between two particles, as they approach one another in an aqueous medium (Shen et al., 2010). In its simplest formulation, the total interaction energy (ξ_{tot}) is expressed as the sum of two dominant contributions: a short range van der Waals attraction (ξ_{vdw}) and a longer range electrostatic double-layer interaction (ξ_{edl}) (Cao et al., 2023). The balance between these terms as a function of separation distance yields an interaction energy profile that typically features an energy barrier (the primary maximum) and one or more local minima (Bhattacharjee et al., 2000).

At very small separation distances, a deep primary minimum may develop, corresponding to strong attraction and effectively irreversible attachment. At larger separations, a shallower secondary minimum may exist, corresponding to weak and reversible attachment, from which particles may detach under modest hydrodynamic shear or Brownian forces (Hahn et al., 2004). Whether particles ultimately reach the primary minimum depends on their ability to overcome the primary energy barrier. When the barrier height greatly exceeds thermal energy (kT), primary-minimum attachment is unlikely, and deposition occurs predominantly within the secondary minimum. Conversely, when the barrier is small or negligible, particles readily access the primary minimum and attachment becomes effectively irreversible (Shen et al., 2012).

DLVO interaction energy profiles are highly sensitive to solution chemistry and surface properties (Abdelfatah et al., 2017; Liang et al., 2020). Increasing ionic strength or cation valence compresses the electrostatic double layer and reduces the height of the

primary maximum, increasing the likelihood of primary-minimum attachment. In contrast, low ionic strength and high surface charge magnitude enhance electrostatic repulsion, raising the energy barrier and favouring particle mobility or, at most, weak secondary-minimum attachment. Changes in pH and surface functional groups modify surface potentials and thus influence both the depth of energy minima and the height of the barrier (Nagar and Sharma, 2025). Particle size and collector curvature also affect interaction energies, as van der Waals forces scale with particle radius (Walz, 1998). For MP transport in clay-rich media, these factors may determine whether MPs remain largely mobile, undergo frequent attachment-detachment within a secondary minimum, or become strongly retained in a primary minimum.

The DLVO interaction energies applied in this study are calculated as follows (Ye et al., 2022b):

$$\xi_{vdw}(I_S, d) = \frac{-A_{123} r_p}{6d\left[1+\left(\frac{14d}{\lambda}\right)\right]} \tag{2.6}$$

$$\xi_{edl}(I_S, d) = \pi \varepsilon_r \varepsilon_0 r_p \{2\eta_p \eta_c \ln\left[\frac{1+e^{-\kappa d}}{1-e^{-\kappa d}}\right] + \left(\eta_p^2 + \eta_c^2\right)\ln\left[1 - exp(-2\kappa d)\right]\} \tag{2.7}$$

$$\xi_{tot}(I_S, d) = \xi_{vdw}(I_S, d) + \xi_{edl}(I_S, d) \tag{2.8}$$

where A_{123} is the Hamaker constant for the two substances "1" and "3" in presence of solution "2", determined from the Hamaker constant of the three materials, r_p is the hydrodynamic radius of particulate particles, λ is the cut-off wavelength, d is the separation distance between particles or porous media, ε_r is the relative dielectric constant, ε_0 is the vacuum dielectric constant, η_p, η_c are the zeta potential of particle and porous media, respectively, κ is the inverse of Debye length, K is the Boltzmann constant, and T is the absolute temperature.

In this thesis, column-scale MP transport is described using the ADR framework, which provides continuum-scale mass balances for the aqueous and solid phases, while DLVO theory supplies the mechanistic interpretation of the reaction terms representing attachment and detachment. Within CFT, particle removal is described using a single-collector removal efficiency and an attachment efficiency, which determine the first-order deposition rate. DLVO interaction energy profiles underpin these efficiencies. Hence, a high energy barrier combined with a shallow secondary minimum corresponds to low attachment efficiency and predominantly reversible attachment, whereas negligible barriers and a deep

primary minimum are associated with high attachment efficiency and largely irreversible deposition. In two-site ADR models, these two regimes are commonly represented by a reversible retention domain associated with secondary-minimum attachment and an irreversible domain associated with primary-minimum attachment. Interaction energy calculations based on DLVO theory are applied in Chapter 6 to evaluate MP-bentonite interactions under different solution chemistries and to support interpretation of reversible and irreversible retention processes observed in transport experiments.

2.4 Microplastic Contamination in Landfills

Terrestrial environments are increasingly recognised as major sources of MPs to aquatic systems (He et al., 2019; Wang et al., 2022c), with land-based waste management systems warranting particular attention. Landfills serve as the final repository for most managed plastic waste and represent a major long-term reservoir of plastic materials with the potential to generate and release MPs over time. Despite their importance, landfills remain under-studied with respect to MP occurrence, transport pathways, and controls on mobility. This section reviews current knowledge on MPs in landfills and is organised into the following components: (i) MP occurrence and abundance in landfill leachate, (ii) composite liner systems in landfills and the effects of chemical exposure on their barrier performance, and (iii) current knowledge on MP presence in lining systems.

2.4.1 Distribution and Abundance of MPs in Landfills

Landfills receive a wide range of wastes, including municipal solid waste (MSW), industrial residues, and hazardous materials (Szulc et al., 2022; Kabir et al., 2023; Lodh et al., 2025). In many developing countries, limited recycling and inadequate waste segregation have resulted in the direct disposal of large volumes of plastic materials (Browning et al., 2021). By 2015, approximately 79% of the 6,300 million tonnes of global plastic waste had accumulated in MSW landfills, where plastics accounted for an estimated 21-42% of total waste mass (Nizzetto et al., 2016; Geyer et al., 2017). Plastics can persist for decades to centuries due to their resistance to biodegradation, fragmenting into smaller particles while releasing chemical additives (Verma et al., 2016; Huang et al., 2022).

MPs in landfills originate from primary sources (e.g., cosmetic microbeads, industrial abrasives, synthetic microfibres) and secondary sources generated in situ by fragmentation of larger plastic debris, including macroplastics (>25 mm) and mesoplastics (5-25 mm) (Dehal et al., 2024). Fragmentation is driven by abiotic and biotic factors, including variable pH (4.5-9), elevated temperatures (60-90 °C), microbial activity, and mechanical abrasion during compaction and settlement (Zhu et al., 2018; Andrady et al., 2022; Born and Brüll, 2022).

Landfill leachate, generated during MSW decomposition, serves as both a reservoir and a transport medium for MPs (Dagwar and Dutta, 2024). MPs can migrate vertically through waste layers and concentrate in leachate that eventually interacts with liner systems. Given their small size and durability, MPs may challenge engineered barriers, with migration potential governed by particle size, surface chemistry and liner design.

A Web of Science search conducted in February 2025 (keywords: microplastic AND landfill leachate AND concentration OR distribution OR occurrence) identified 70 publications, of which 26 peer-reviewed studies reported MP concentrations in landfill leachate (Table 2.2). He et al. (2019) were among the first to identify landfill leachate as a potential MP source, reporting concentrations of 0.96-1.38 particles/L in closed sites and 0.42-24.58 particles/L in active sites across six landfills in southern China. However, their analysis was constrained by a detection limit of 100 μm, excluding finer MPs. Subsequent investigations in China, Lithuania and Indonesia generally observed lower leachate MP concentrations in older landfills compared with younger facilities, consistent with historical trends in plastic production, consumption, and waste management practices (Su et al., 2019; Sholokhova et al., 2023; Sembiring and Ramadan, 2024). PE and PP were the most frequently reported polymers in leachate, consistent with observations in landfill-adjacent soils (Kim et al., 2023; Mahesh et al., 2023; Saengchut et al., 2024; Ma et al., 2025a).

Ma et al. (2025a) reported size-dependent distributions in which larger MPs tended to remain near source zones, whereas smaller MPs penetrated deeper into surrounding soils (Figure 2.3). Reported MP concentrations in leachate range from below detection to ~200 particles/L at detection limits near ~50 μm (Sun et al., 2021; Kara et al., 2023). Substantially higher concentrations are reported when finer particles are quantified. Verma et al. (2024) and Ma et al. (2025a) measured 1,473-2,067 particles/L in India and 4,010-33,213 particles/L in China using analytical techniques with 20-30 μm detection limits. Apparent discrepancies reflect not only site differences but also methodological variability (e.g., filter

pore size, imaging/spectral resolution, and chemical pre-treatment). For example, fine-pored filtration and advanced spectroscopy improve recovery of small MPs, whereas aggressive digestion procedures can degrade certain polymers (Hu et al., 2021; Savino et al., 2022). Likewise, density-based separation approaches may underrepresent high-density polymers such as PVC and PET, introducing bias (Nandikes et al., 2024).

In summary, MPs are prevalent in landfill leachate, although reported concentrations vary widely across studies due to environmental variability and analytical limitations. A key limitation evident from Table 2.2 is the lack of consistent size-resolved data, particularly for small MPs. Most studies employed detection limits greater than 10-20 µm, with only one study reporting MPs down to ~450 nm and another down to ~1 µm. As a result, the abundance and distribution of small MPs in landfill leachate remain poorly constrained, despite their potentially greater mobility in subsurface environments.

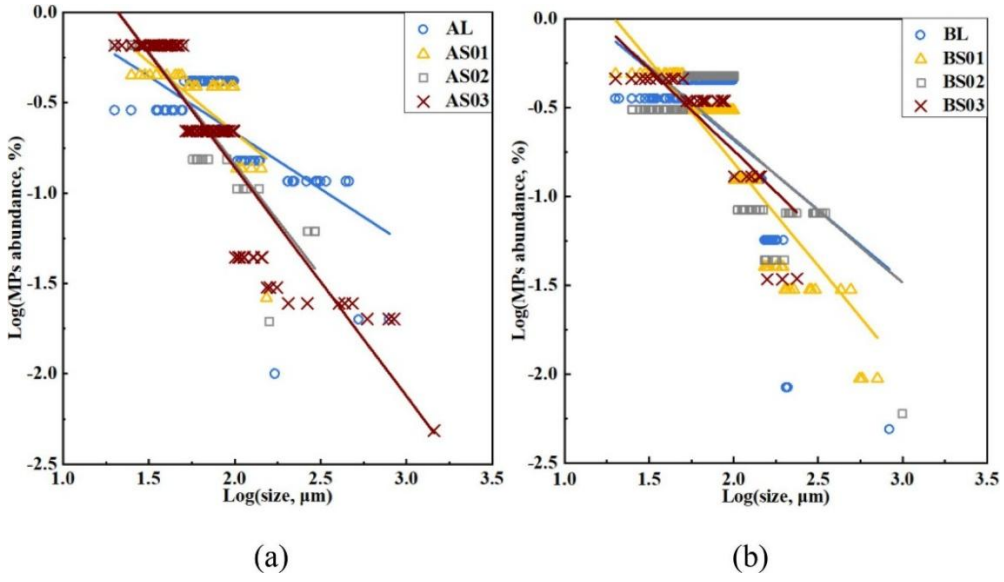

Figure 2.3. Size-dependent pattern of MP abundance in soil layers and leachate samples from two landfills: (a) Landfill A (closed for over 20 years); and (b) Landfill B (closed for 6 years). Sample codes use the site prefix (A or B) followed by L for leachate or S01-S03 for soils collected at depths of 0-1 m, 1-2 m, and 2-3 m. MPs abundance % in y-axis indicated the proportion of MP abundance in specific size ranges of the total abundance. Horizontal axis represents $\log_{10}$ of MP size. The slope of fitting line represents the degree of MP fragmentation. Adopted from Ma et al. (2025a).

Table 2.2. Summary of reported MP distribution and characteristics in landfill leachate, adjacent soils and refuse. Studies are listed in chronological order by publication year and, within each year, alphabetically by first author. Data were accessed from the Web of Science (search completed February 2025).

	References	Location	Landfill Type	MP Mass/Number Concentration			Detected Size Range	Predominant MP Type
				Leachate	Soil	Refuse		
1	Kilponen (2016)	Finland	Old-closed (closed for over 30 years)	0.080-0.261 fibres/L, 0.002-0.017 particles/L	Not specified	Not specified	>1 mm	Not specified
2	van Praagh et al. (2018)	Iceland, Norway and Finland	Hazardous and non-hazardous	0-2.36 µg/L	Not specified	Not specified	50-5000 µm	PE, PP & PS
3	He et al. (2019)	China	Active (10~20 years) and closed (closed for 10 years)	0.42-24.58 particles/L	Not specified	Not specified	100-1000 µm	PE & PP
4	Puthcharoen and Leungprasert (2019)	Thailand	ND	20.90 (±4.96) particles/kg	1457.99 (±489.71) particles/kg	Not specified	Not specified	PE, PP & PET
5	Su et al. (2019)	China	Young (<3 years), medium-aged (~10 years) and old (>20 years)	8 (±3) particles/L	Not specified	62 (±23) pieces/g	70-3670 µm	Cellophane in leachate PE in refuse
6	Xu et al. (2020)	China	MSW	291 (±91) particles/L	Not specified	Not specified	20-100 µm	PP, PA & rayon
7	Cordova and Riani (2021)	Indonesia	Informal (open dumping)	15.56 (±3.33) particles/L	Not specified	Not specified	80-5000 µm	PE, PP & PS
8	Narevski et al. (2021)	Southeast Europe	Sanitary and non-sanitary	0.64-2.16 mg/L	Not specified	Not specified	>23 µm	Not specified
9	Sun et al. (2021)	China	MSW	235.4 (±17.1) particles/L and 11.4 (±0.8) µg/L	Not specified	Not specified	10-150 µm	PE & PP
10	Mohammadi et al. (2022)	Iran	MSW	63-92 particles/L	Not specified	Not specified	0.45-5000 µm	Nylon, PP & PS
11	Nayahi et al. (2022)	Thailand	Formal (controlled) and informal (open dumping)	8.8 particles/L in formal landfill 9.93 particles/L in informal landfill	Not specified	Not specified	20-5000 µm	PP, PE & PS
12	Wan et al. (2022)	China	Informal	3-25 particles/L	570-14,200 particles/kg	590-103,080 particles/kg	>20 µm	PE, PP & PET
13	Kara et al. (2023)	Turkey	Sanitary	147-196 particles/L	Not specified	Not specified	100-2000 µm	Not specified
14	Ledieu et al. (2023)	France	Old-closed (closed for ~40 years)	0.71-106.7 particles/L	Not specified	Not specified	>25 µm	PE & PP

15	Salikova et al. (2023)	Kazakhstan	MSW	Not specified	0.81 particles/g	Not specified	5000-20,000 µm	Not specified
16	Sekar and Sundaram (2023)	India	MSW	9-21 particles/L	Not specified	Not specified	Not specified	PE, PP, PET, CA & nitrile
17	Sholokhova et al. (2023)	Lithuania	Old-closed (closed for over 20 years), medium-aged-closed (closed for over 10 years) and young (open)	Not specified	Not specified	9.1-48.9 g/kg	50-5000 µm	PE, PP & PS
18	Trihadiningrum et al. (2023)	Indonesia	MSW	9.00 (±0.85) particles/L	Not specified	Not specified	1-5000 µm	PE & PS
19	Chamanee et al. (2024)	Sri Lanka	MSW	2.06 (±0.62) mg/L	363 (±111) mg/kg	Not specified	1000-5000 µm	PE, PP & PS
20	Nakayama et al. (2024)	Japan	MSW	3 particles/L	47-120 particles/kg	Not specified	>100 µm	Not specified
21	Saengchut et al. (2024)	Thailand	MSW	13.75-38.33 particles/L	122.67-2453 particles/kg	Not specified	Not specified	PE & PP
22	Sembiring and Ramadan (2024)	Indonesia	Active (20 years) and closed (closed for 20 years)	12.00-56.33 particles/L	Not specified	Not specified	100-5000 µm	PP, PE & PVC
23	Verma et al. (2024)	India	Old (30-100 years)	1473-2067 particles/L	Not specified	Not specified	30-5000 µm	PE, PP, cellulose acetate & PVC
24	Hartini and Warsito (2025)	Indonesia	Active and closed	Not specified	Not specified	920-2,340 pieces/kg	Not specified	PP, PE & PS
25	Lodh et al. (2025)	India	Formal and informal	53.4 (±6.69) particles/L in informal landfill 34.7 (±4.73) particles/L in formal landfill	Not specified	Not specified	25-5000 µm	PE, PP, PET & PS
26	Ma et al. (2025a)	China	Informal-closed (closed for 6 and over 20 years)	4,010–33,213 particles/L	870–47,819 particles/kg	Not specified	20-1500 µm	PET, PU & PS

Note: PE = polyethylene; PP = polypropylene; PET = polyethylene terephthalate; PS = polystyrene; PA = polyamide; CA = cellulose acetate; PU = polyurethane.

2.4.2 Composite Liner Systems in Landfills

Composite liner systems are widely used in landfills, tailings storage facilities, lagoons and wastewater impoundments to restrict leachate and contaminant transport (Rowe, 2014; Rowe and Hosney, 2015). Modern waste containment facilities commonly employ multi-layer composite liners to provide chemical resistance and protect subsoils and groundwater from surface-derived contaminants (Rowe and Brachman, 2004). A typical system consists of a chemically resistant geomembrane (GMB) underlain by either a geosynthetic clay liner (GCL) or a compacted clay liner (CCL), and overlain by a granular drainage layer for leachate collection (Rowe and Brachman, 2004). A prepared subgrade serves as an attenuation layer (AL), reducing water flux and partially retarding the migration of dissolved contaminants (Rowe and Brachman, 2004; Peng et al., 2021).

High-density polyethylene (HDPE) GMBs (typically 0.5-3.0 mm thick) provide an effective hydraulic barrier but are susceptible to installation- and service-related defects, including punctures, wrinkles, stress cracking (Rowe and Brachman, 2004; Chappel et al., 2012). Contaminants may migrate through localised defects, and volatile organic compounds (VOCs) can diffuse through intact GMBs (Rowe and Brachman, 2004; Eun et al., 2017). To mitigate these pathways, a GCL or CCL is placed beneath the GMB to form a composite liner. The clay layer provides very low hydraulic conductivity and additional filtration and sorption capacity, while close GMB-clay contact minimises interface transmissivity and leakage.

GCLs and CCLs are the principal clay-based components employed in MSW landfills, mine tailings, and surface impoundments (Hosney and Rowe, 2014; Rowe, 2014; AbdelRazek and Rowe, 2019b). Both rely on the low hydraulic conductivity k_{sat} and swelling capacity of clay minerals, particularly bentonite, but they differ substantially in configuration, construction, and field performance.

CCLs are constructed in situ by placing and compacting natural or amended clayey soils at specified water contents and densities, typically to a thickness of ~0.75-1.0 m (Aldaeef and Rayhani, 2014). Performance is governed by clay mineralogy, degree of compaction and post-construction moisture conditions (Kasanin-Grubin, 2013; Aldaeef and Rayhani, 2014; Wan et al., 2014). CCLs can be cost-effective and provide high attenuation capacity when suitable clays are locally available. They can achieve k_{sat} below 1×10^{-9} m/s, but the large volumes of material required and the need for consistent quality control over

extensive areas are challenging (Zhai and Benson, 2006; Aldaeef and Rayhani, 2014). Inadequate compaction can increase macroporosity and thus k_{sat}, while uneven surfaces may impair contact with overlying GMB, increasing interface transmissivity and leakage (Ebina et al., 2004; Li et al., 2023). CCLs are also prone to desiccation cracking and root penetration, both of which can compromise long-term containment performance (Ghazizade and Safari, 2017; Bi et al., 2022).

GCLs have increasingly replaced CCLs in many engineering applications because they are quick to install, provide a thin and uniform barrier, and can self-seal when properly hydrated (Rowe, 2014; Rowe and Li, 2020). They are factory-manufactured composites consisting of a thin (~5-10 mm) layer of bentonite encapsulated between geotextiles (often needle-punched) or bonded to a geomembrane (AbdelRazek and Rowe, 2019a; Rowe et al., 2023). Product variants, including granular, powdered, and polymer-enhanced bentonites, affect swelling, chemical compatibility, and durability (Yu et al., 2020; Liang et al., 2024b). Supplied in rolls, GCLs enable rapid installation and more uniform properties than field-compacted clays. When adequately hydrated and confined, GCLs typically achieve hydraulic conductivities on the order of 10^{-10} to 10^{-11} m/s and exhibit beneficial self-sealing around small defects (Rowe and Li, 2020). Bentonite swelling also promotes intimate GCL-GMB contact, further reducing interface transmission and leakage (Rowe and Jabin, 2021).

2.4.3 Hydration and Swelling of Bentonite

Bentonite is widely employed as a clay amendment in CCLs or Als, and it is the key sealing component in GCLs (Rowe, 2014; Nath et al., 2023). When adequately hydrated, its high swelling capacity and correspondingly low hydraulic conductivity provide effective barrier performance (Ören and Akar, 2017). Mineralogically, bentonite typically contains ~70-90 wt% smectite, with the remainder comprising quartz, feldspar and minor carbonates and/or sulphates (Gómez-Espina and Villar, 2010; Grim and Guven, 2011). Montmorillonite (MMT), the principal smectite mineral in bentonite, is a dioctahedral 2:1 phyllosilicate that can be represented by the idealised composition (Yaghmaeiyan et al., 2022):

$$(Na, Ca)_{0.3}(Al, Mg)_2[Si_4O_{10}](OH)_2 \cdot n(H_2O)$$

MMT consists of tetrahedral-octahedral-tetrahedral (T-O-T) stacks, in which two silica tetrahedral sheets sandwich an octahedral sheet containing Al-, Mg- and Fe-hydroxyl units (Figure 2.4). Individual T-O-T layers are ~0.96-1.0 nm thick and stack quasi-parallel,

with interlayers hosting exchangeable cations and water molecules. Isomorphic substitution (e.g., Mg^{2+} for Al^{3+} in the octahedral sheet, or Al^{3+} for Si^{4+} in the tetrahedral sheet) generates a net negative layer charge, which is balanced by interlayer cations and their hydration shells (García-Romero et al., 2021; Prasad et al., 2023). The negatively charged basal surfaces electrostatically attract surrounding water molecules and cations, forming an electrical double layer (EDL), in which the outer Boltzmann-distributed region constitutes the diffuse double layer (DDL) (Sposito and Prost, 1982).

Hydration and swelling unfold in two coupled stages (Malusis and Shackelford, 2002; Shackelford et al., 2010). First, crystalline (interlayer) swelling occurs when water penetrates the interlayer space and hydrates exchangeable cations, overcoming the relatively weak van der Waals attractions between adjacent T-O-T layers (Rao et al., 2013). This process increases basal spacing from ~9.6-10 Å in nearly dry states to ~20 Å as hydrated cations expand the interlayer galleries (Li et al., 2024a). Second, osmotic swelling arises when a concentration difference develops between the interlayer solution and the external pore water. Under these conditions, clay surfaces act as a semi-permeable, ion-selective medium, and water flows into the interlayers to reduce the chemical potential gradient (Rao et al., 2013). As the adjacent DDLs separate to tens of Å, repulsive forces increase and swelling can exceed that associated with crystalline expansion (Gilbert et al., 2015). Osmotic swelling is highly sensitive to solution chemistry, particularly ionic strength and cation valence (Hotton et al., 2025). Monovalent cations (notably Na^{+}) favour greater swelling, whereas divalent and trivalent cations and high salinity suppress swelling and tend to increase hydraulic conductivity (Hotton et al., 2025).

The characteristic interaction range of electrostatic repulsion is described by the Debye length, κ^{-1} (AL-Bazali, 2022). For monovalent electrolytes in water at 25 °C (Liu, 2021),

$$\kappa^{-1}\,(\text{nm}) \approx \frac{0.304}{\sqrt{IS}}$$

where IS is ionic strength in mol/L. Thus, low ionic strength yields a larger κ^{-1}, allowing electrostatic repulsion to dominate, forcing layers apart and promoting osmotic swelling. In contrast, high ionic strength or the presence of multivalent cations reduces κ^{-1}, compresses the DDL, and supresses swelling. Because $I = \frac{1}{2}\sum z_i^2 c_i$ (where c_i is molar concentration and z_i is ionic charge), di- and trivalent electrolytes produce higher ionic

strength than monovalent electrolytes at the same molarity, leading to shorter κ^{-1}, reduced swelling, and typically higher hydraulic conductivity k (Alziyadi and Denton, 2021).

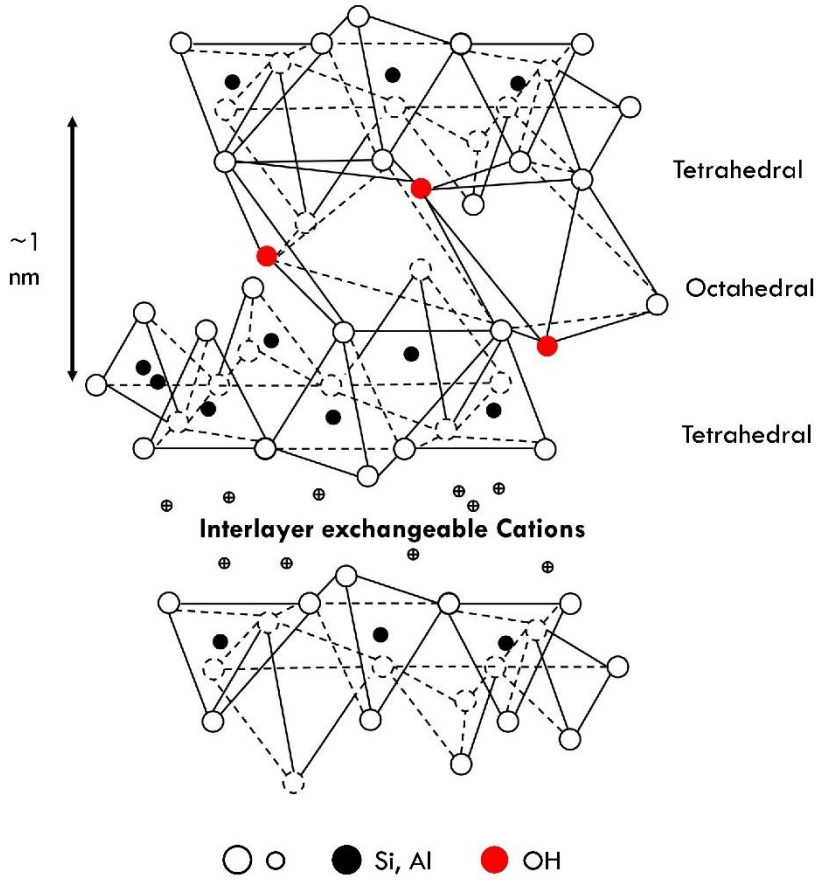

Figure 2.4. Crystal structure of montmorillonite clay, showing aluminum-centered octahedra sandwiched between tetrahedra (normally silicon-centered).

2.4.4 Impacts of Chemical Aggression and Wet-Dry Cycles on Barrier Performance

Barrier systems in landfills are routinely exposed to chemically aggressive solutions, either through localised defects in the GMB or through hydration by saline porewaters within the subgrade and backfill (Rowe and Li, 2021; Cen et al., 2025). The long-term performance of bentonite-based barriers therefore depends strongly on the chemical compatibility between bentonite and the permeating liquid (Shackelford et al., 2000; Rowe, 2012; Rowe and Li, 2021). Chemical compatibility refers to the ability of a clay liner to maintain sufficient swelling and low hydraulic conductivity when exposed to a given leachate or pore fluid (Bohnhoff and Shackelford, 2014; Xu et al., 2019).

The hydraulic behaviour of GCLs is determined primarily by the chemo-physical behaviour of bentonite during hydration (Alzamel et al., 2022). In sodium bentonite systems, expansion of the DDL promotes swelling and reduces effective pore space, resulting in low hydraulic conductivity. Exposure to electrolyte solutions alters this behaviour through cation exchange and DDL compression, particularly in the presence of multivalent cations such as Ca^{2+}. These interactions reduce swelling capacity, modify bentonite microstructure, and increase hydraulic conductivity.

Numerous studies since the 1990s have shown that hydraulic conductivity increases with ionic strength and cation valence because compression of the diffuse double layer (DDL) reduces bentonite swelling capacity (Lee and Shackelford, 2005). Shackelford et al. (2000) evaluated the hydraulic behaviour of GCLs permeated with non-standard liquids and identified the effects of permeant chemistry, bentonite quality and pre-hydration conditions as key factors governing hydraulic performance. Calcium-rich solutions are particularly detrimental because Ca^{2+} replaces exchangeable Na^{+} ions within sodium bentonite, thereby reducing swelling and increasing conductive pore space (Shackelford et al., 2000). For example, Vasko et al. (2001) reported a three order-of-magnitude increase in k_{sat} when the molarity of the hydrating solution increased from 5 to 100 mM $CaCl_2$. Comparative testing on Na-bentonite GCLs showed k_{sat} rising from ~10^{-9}-10^{-8} cm/s in water to ~10^{-8}-10^{-5} cm/s as $CaCl_2$ concentration increased from 50 to 200 mM (Xue et al., 2012). Long-term permeation studies further demonstrated that chemically induced increases in hydraulic conductivity may continue over extended periods and large cumulative pore volumes. Jo et al. (2005), for example, permeated GCLs with NaCl, KCl and $CaCl_2$ solutions for more than 2.5 years and observed hydraulic conductivity increasing with electrolyte concentration and cation valence, highlighting the potential for short-term tests to underestimate long-term chemical degradation. Lee and Shackelford (2005) further showed that the magnitude of hydraulic conductivity increase depends strongly on bentonite quality, with lower-quality sodium bentonite exhibiting increases of approximately two orders of magnitude when permeated with 100 mM $CaCl_2$.

In parallel with hydraulic conductivity studies, considerable research has examined the semipermeable membrane behaviour of bentonite barriers (Malusis and Shackelford, 2002). Semipermeable membrane behaviour refers to the partial restriction of solute migration caused by electrostatic interactions between dissolved ions and negatively charged clay surfaces (Malusis and Shackelford, 2002). The degree of membrane behaviour

is commonly quantified using the membrane efficiency coefficient ω, where ω=0 corresponds to no solute restriction and ω=1 corresponds to ideal semipermeable behaviour.

Malusis and Shackelford (2002) demonstrated that sodium bentonite GCLs can exhibit measurable membrane efficiency during exposure to electrolyte solutions, with membrane efficiency decreasing as electrolyte concentration increased. Subsequent studies showed that membrane behaviour is highly sensitive to boundary conditions, stress state and chemical environment. Kang and Shackelford (2009) developed flexible-wall testing procedures under closed-system conditions to minimise artefacts associated with solute leakage and chemical disequilibrium, while Kang and Shackelford (2011) showed that consolidation can enhance membrane behaviour.

The coupled relationship between membrane behaviour and solute diffusion has also been examined extensively. Shackelford and Lee (2003) showed that diffusion progressively weakens membrane behaviour because solute transport reduces the concentration gradient responsible for chemico-osmotic flow. This interaction highlights the transient nature of membrane behaviour in bentonite barriers subjected to long-term chemical exposure. Malusis et al. (2015) subsequently demonstrated restricted salt diffusion in GCLs, while Malusis and Daniyarov (2016) quantified the relationship between membrane efficiency and diffusive tortuosity in dense pre-hydrated GCLs. More recently, Shackelford et al. (2016) evaluated the limiting membrane and diffusion behaviour of GCLs and showed that membrane efficiency approaches a limiting value under highly compacted and chemically favourable conditions.

Several studies have also investigated approaches to improving membrane performance under chemically aggressive conditions. Bohnhoff and Shackelford (2013) reported that polymer amendment of bentonite can substantially improve membrane efficiency and reduce the detrimental effects of electrolyte exposure. Bohnhoff et al. (2014) further demonstrated calcium-resistant membrane behaviour in a polymer-amended bentonite, indicating that polymer modification may partially mitigate the effects of Ca^{2+} on bentonite structure and solute restriction. More recently, Fu et al. (2025a) showed that composite polymer amendment enhanced the containment performance of GCLs exposed to bauxite liquor, further supporting the potential of polymer modification to improve chemical resistance in bentonite barriers.

The relevance of membrane behaviour to MP transport requires careful interpretation because MPs are particulate colloids rather than dissolved solutes. MP migration through porous media is additionally influenced by processes such as straining, wedging, attachment, aggregation and pore-scale flow heterogeneity. Nevertheless, the same bentonite structure governing solute restriction also controls the effective pore network available for colloidal transport. Under chemically compatible conditions, extensive bentonite swelling produces small pore throats, low hydraulic conductivity and tortuous flow pathways that favour retention of suspended particles. Conversely, exposure to concentrated $CaCl_2$ solutions reduces swelling and increases conductive pore space within the bentonite, thereby increasing the potential for MP migration.

Composite barrier systems are also subjected to wet-dry cycles driven by seasonal temperature and moisture fluctuations. These cycles can induce desiccation cracking, panel shrinkage, and increases in hydraulic conductivity (Rowe and Hamdan, 2021). Bentonite undergoes substantial swelling and shrinkage during wetting and drying cycles, respectively, and repeated shrink-swell cycling may initiate and propagate cracks, creating preferential flow paths and increasing permeability.

Rowe and Hamdan (2021) examined these effects through a series of hydraulic conductivity tests (Figure 2.5). GCL specimens were conditioned under repeated wetting (8 hours) and drying (ranging from 16 hours to 14 days, depending on the test case) prior to permeation with tap water under confinement. For specimens dried for 16 hours per cycle, k_{sat} increased from 3×10^{-11} m/s (no wet-dry cycling) to 3×10^{-9}-3×10^{-8} m/s following cycling.

Differences in hydraulic conductivity associated with drying duration were linked to changes in the geometry of needle-punched fibre bundles (Figure 2.6). The average bundle diameter increased from 1.5-1.8 mm before testing to 2.0-2.3 mm after testing, indicating reduced swelling pressure acting on the bundles and localised bentonite washout (Figure 2.6, a_2-d_2). Rowe and Hamdan (2021) emphasised that the effects of wet-dry cycle number and drying duration depended on GCL structure and bentonite type and therefore cannot be predicted a priori.

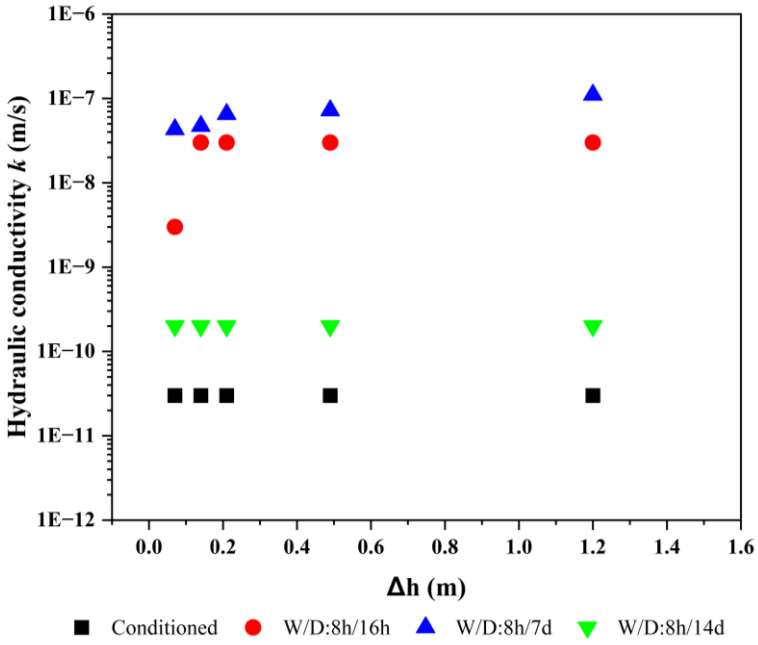

Figure 2.5. Hydraulic conductivity *k* of GCL specimens subjected to wet-dry (W/D) cycles with DI water under different drying durations and water heads (Δh). The conditioned case corresponds to hydration without W/D cycles. Based on data from Rowe and Hamdan (2021).

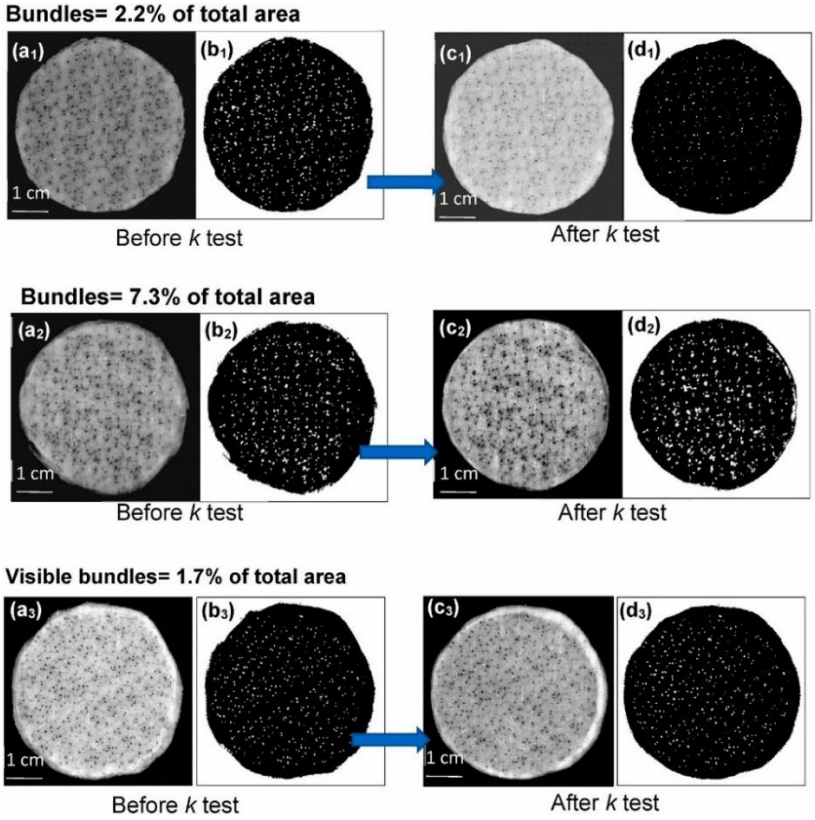

Figure 2.6. X-ray images for GCL specimens subjected to wet-dry cycles before and after hydraulic conductivity tests. (b) and (d) are the binary images of (a) and (c) to show punch bundles. The subscript 1, 2 and 3 represent drying durations of 16-hour, 7-day, and 14-day, respectively. Adopted from Rowe and Hamdan (2021).

2.4.5 MPs Mobility in GCLs

A substantial body of work has established the ability of GCLs to attenuate dissolved inorganic and organic contaminants through a combination of low hydraulic conductivity, diffusion restriction, sorption, and membrane behaviour (Lange et al., 2010; Scalia IV et al., 2018). In comparison, far less is known about the movement of suspended particulates, particularly small MPs. Studies examining MP mobility in GCLs are currently very limited, and the mechanisms controlling particulate migration through bentonite-based barriers have not yet been systematically established.

Some insight can be obtained from previous studies on colloid transport through compacted clays and bentonite-rich porous media. Research on bacteria, viruses, and engineered nanoparticles (ENPs) has shown that particulate mobility in low-permeability materials is governed by physicochemical interactions and pore-scale processes, including attachment-detachment, aggregation, diffusion limitation, and physical straining (McCarthy et al., 2002; Liu et al., 2020). These findings suggest that hydrated bentonite barriers may similarly restrict MP mobility.

Studies examining the transport of viruses and bacteria through clay-rich soils have shown that retention is strongly influenced by ionic strength, clay mineralogy, and electrostatic interactions between particles and mineral surfaces (McCarthy et al., 2002; Syngouna and Chrysikopoulos, 2015).

Das and Bharat (2022) reported that montmorillonite exhibits strong sorption behaviour towards poliovirus due to physicochemical interactions between exchangeable cations and negatively charged spike protein and montmorillonite clay surfaces. Similar mechanisms have also been proposed for coronavirus adsorption onto clay minerals, where electrostatic and hydrophobic interactions may contribute to viral retention (Yadav et al., 2023). Yadav et al. (2023) further investigated coronavirus transport through bentonite barriers and reported that high-quality bentonite with a specific surface area of approximately 635 m^2/g achieved near-complete virus removal. This study also reported low diffusion coefficients (around 1.67×10^{-9} m^2/s) and high retardation factors in compacted bentonite layers, suggesting that compacted bentonite can effectively restrict viral migration. These findings further highlight the important role of bentonite quality and surface interactions in restricting particulate transport through clay-based barrier systems.

Several studies have investigated the behaviour of ENPs in GCLs and bentonite barriers (Yang et al., 2018a; Yang et al., 2018b; Yang et al., 2020; Liu and Jiang, 2024). For example, using an osmotic control set-up, zinc oxide nanoparticles (~2-40 nm) became increasingly retarded with increasing osmotic pressure, and the breakthrough behaviour could be reproduced using a two-site kinetic framework that captured concurrent reversible and irreversible attachment within bentonite pore networks (Yang et al., 2018a). In GCL column tests with graphene oxide, hydrostatic pressure and influent concentration influenced particle mobility, while bentonite modification (i.e., thermal or sodium treatment) altered deposition and retention (Yang et al., 2020). A geomembrane-over-CCL configuration also exhibited strong retention of silver nanoparticles (<100 nm) at compliance-grade hydraulic conductivities ($<10^{-7}$ cm/s), highlighting the combined roles of sorption and physical straining in bentonite matrices (Lee et al., 2021).

Despite providing useful mechanistic insight, studies on viruses, bacteria, and ENPs cannot be directly extrapolated to MPs, which differ in composition, morphology and surface ageing processes (Hüffer et al., 2017; Gigault et al., 2021). As a result, transport behaviour observed for these colloidal particles may not be fully representative of MPs in bentonite-based barriers. Nevertheless, these studies remain relevant because small MPs overlap in size with many colloids and microorganisms previously investigated, and the bentonite microstructure controlling colloid and microbial retention is also likely to influence MP transport.

The mechanisms controlling colloid transport and retention in GCLs remain insufficiently understood. In particular, pre-hydration chemistry (e.g., DI water versus $CaCl_2$) and wet-dry cycling can alter interlayer spacing and gel development in bentonite, thereby changing effective pore-throat sizes and interfacial interaction energies. An important unresolved question is whether increases in hydraulic conductivity caused by divalent cations and/or desiccation-induced structural changes reduce straining and increase MP breakthrough. GCL product formulation is also likely to influence transport behaviour. Differences between granular and powdered bentonite, as well as polymer-enhanced variants, may affect swelling behaviour and chemical resilience, potentially leading to different capacities for MP retention under field-relevant conditions.

Bordoloi et al. (2022) proposed a conceptual model for MP retention in bentonite (Figure 2.7), suggesting that small MPs are preferentially entrapped within intra-aggregate pore spaces, whereas nanoscale and weathered particles with modified surface chemistry

may attach to mineral surfaces. To date, however, this conceptual framework has not been validated by laboratory transport studies, and, to the best of our knowledge, MP transport through GCLs has not yet been systematically investigated in the peer-reviewed literature.

In addition to acting as contaminant barriers, composite landfill liner systems may themselves represent an emerging secondary source of MPs. This concern arises because liners are constructed largely from polymer-based geosynthetics, including HDPE GMBs and PP/PES geotextiles and geonets. Accelerated ageing tests on HDPE GMBs immersed in synthetic landfill leachate at field-relevant temperatures (23-50 °C) showed that the liners can shed 475-1689 particles/m^2 within four months, with emissions dominated by <20 μm fragments, providing direct evidence that GMBs can contribute MPs to leachate (Krishnendu and Varghese, 2025). Field and laboratory studies on PET and PP geotextiles, which are widely used as protection and drainage/filter layers in landfill liners, showed that ultraviolet exposure can generate large numbers of microfibres and fragments (Bai et al., 2022). For coastal reclamation applications, global emissions from geotextiles have been estimated at 0.24-0.79 million tonnes of fibres per year (Bai et al., 2022). A national assessment in Sweden similarly identified geotextiles as potential MP sources and projected geotextile-derived emissions of 2-32 tonnes per year because of abrasion and water movement (Gustavsson et al., 2022). Studies on geosynthetics used in hydraulic engineering also show that ageing can generate MP releases in aquatic systems, reinforcing concerns that polymeric components of landfill liners, although designed as barriers, may become long-term sources of secondary MPs to leachate, subsoils and groundwater (Scholz et al., 2021).

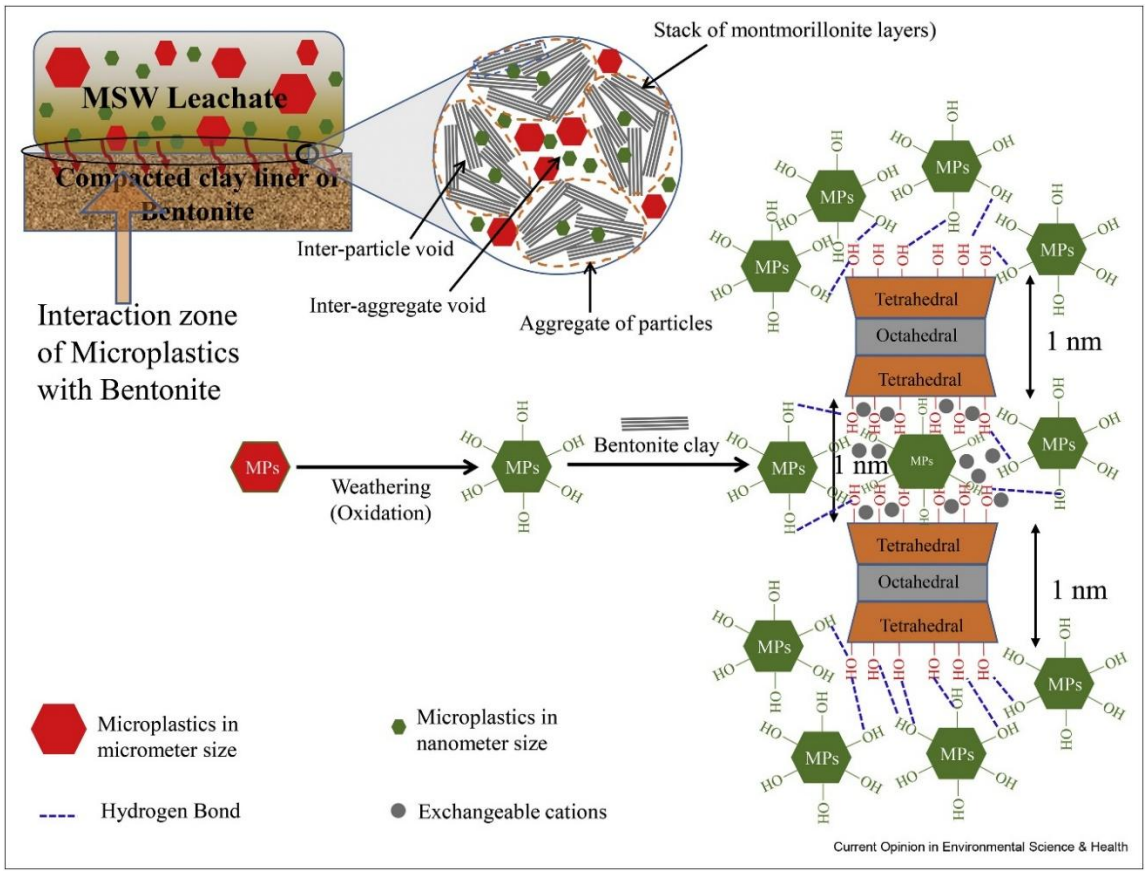

Figure 2.7. Schematic diagram of MP retention in bentonite. Adopted from Bordoloi et al. (2022).

2.5 Summary and Research Gaps

2.5.1 Summary of Current Knowledge

The literature demonstrates that MPs are widely distributed in soils and landfill systems and can be transported through porous media under favourable conditions. Key findings from the literature can be summarised as follows:

1. MPs can alter soil physical and hydraulic properties, including structure, porosity, hydraulic conductivity, and water retention, although reported effects vary widely depending on particle characteristics, soil properties, and experimental conditions.
2. MP transport behaviour is governed by a combination of processes, including advection, dispersion, straining, and physicochemical attachment, which can be interpreted using established colloid transport frameworks.

3. Laboratory column studies provide important insights into MP mobility and retention, but results are strongly influenced by experimental configuration and potential artefacts such as sidewall leakage and incomplete saturation.
4. Landfill leachate is recognised as a significant source and transport pathway for MPs, with reported concentrations spanning several orders of magnitude depending on site conditions and analytical methods.

2.5.2 Critical Knowledge Gaps

Despite the advances summarised above, several important knowledge gaps remain in understanding MP transport in soils and engineered barrier systems:

1. Lack of size-resolved field data for small MPs

Most field studies of landfill leachate are limited by analytical detection thresholds (>10-20 μm), resulting in a scarcity of reliable data for sub-micrometre MPs. Only a few studies have extended measurements to ~1 μm or below. Consequently, the abundance and distribution of small MPs, which are expected to exhibit greater mobility in porous media, remain poorly constrained. This limitation restricts the ability to define environmentally representative conditions for laboratory transport studies.

2. Methodological limitations in experimental apparatus

Commonly used experimental platforms (e.g., rigid-wall columns) subjected to artefacts such as sidewall leakage, lack of stress control, and pump pulsation, which may bias transport observations. The suitability of alternative systems for MP transport, particularly in low-permeability materials, remains insufficiently evaluated.

3. Limited understanding of MP transport in low-permeability barrier materials

Most experimental studies focus on coarse-grained soils or homogenised mixtures, whereas relatively few investigate MP transport in low-permeability systems such as compacted clays or geosynthetic clay liners (GCLs), where transport mechanisms may differ significantly.

4. Uncertainty in transport mechanisms under chemically hydrated conditions

While individual processes such as straining and electrochemical attachment are well described, their relative importance following chemical pre-hydration of soils and barrier

materials remains unclear. In particular, exposure to different pore water chemistries and wet-dry cycles can significantly alter soil structure, pore network geometry, and surface properties prior to transport. However, most studies do not systematically isolate the effect of such conditioning history on subsequent MP transport behaviour under controlled hydraulic conditions. This is especially relevant for small MPs, where changes in pore structure and surface interactions may strongly influence mobility.

2.5.3 Scope and Contribution of This Thesis

This thesis addresses the above knowledge gaps through a systematic experimental and modelling investigation of MP transport in soils and engineered barrier materials.

First, to address the lack of size-resolved field data, this study focuses on small MPs in the 0.2-1 μm size range, which are expected to represent a critical yet poorly characterised fraction of environmental MPs. Given the absence of reliable field concentration data for this size range, experimental concentrations are selected based on a combination of reported leachate concentrations and methodological considerations, as discussed in Chapter 3.

Second, to address methodological limitations, FWPs are employed as the primary experimental platform, enabling control of confining stress, saturation, and hydraulic gradients while minimising artefacts such as sidewall leakage. Additional validation is conducted to assess system-specific particle losses and ensure reliable mass balance.

Third, to improve understanding of transport in low-permeability systems, this research investigates MP migration through GCLs under controlled hydraulic conditions.

Finally, to better resolve transport mechanisms, the study integrates experimental observations with theoretical frameworks, including ADR modelling and DLVO interaction energy analysis, to interpret attachment, detachment, and retention processes.

Chapter 3 Overall Research Design and Methodology

3.1 Overall Research Design

This thesis is structured around the four research questions (RQs) discussed in section 1.2 and summarised here for convenience: (i) how does exposure to MPs affect the swelling behaviour of bentonite; (ii) are FWPs suitable as soil columns for investigating MP transport in low-permeability soils; (iii) how effective are GCLs at preventing MP transport; and (iv) can an ADR model of MP transport through GCLs reproduce observed behaviour in column studies, and what does it reveal about the dominant retention processes? These questions are addressed through a staged research program that progresses from material characterisation and swelling testing to permeation experiments and, finally, modelling-aided interpretation using ADR equations with both reversible and irreversible attachment. Figure 3.1 shows the overall research design.

First, the effects of MP exposure on bentonite swelling and pore structure are investigated in distilled water and $CaCl_2$ solutions (Task 1; Chapter 4). Second, a stress-controlled and leakage-resistant experimental platform for particulate transport testing is established using FWPs, including a baseline mass-balance assessment to quantify potential sources and sinks of MPs within the apparatus (Task 2; Chapter 5). Third, MP breakthrough and retention are evaluated for two commercial GCLs with powdered and granular bentonite. Specimens are pre-hydrated using either deionised (DI) water or $CaCl_2$ solutions, with the latter cases subjected to wet-dry cycling, and transport experiments are conducted using sub-micron and micron-scale PS and PE MPs. The effects of different hydration conditions on microstructure and hydraulic conductivity are assessed, BTCs are determined from FWP effluent, and post-test SEM is conducted on recovered GCL components to characterise MP retention locations (Task 3; Chapter 6). Fourth, ADR models with first-order attachment-

detachment kinetics are fitted to the GCL transport datasets to interpret the observed BTCs (Task 4; Chapter 7).

The rationales for key methodological and material choices are presented in the remainder of this chapter. On the other hand, details of methodologies adopted for each task are not discussed here but described instead in subsequent chapters. This formal structure was adopted for the thesis (rather than presenting all methodological details in a single chapter) because the methodologies followed in Tasks 1-4 are very different to each other. Hence, it is believed that, for a given task, presenting methodologies and results consecutively in the same chapter makes for a better reading experience.

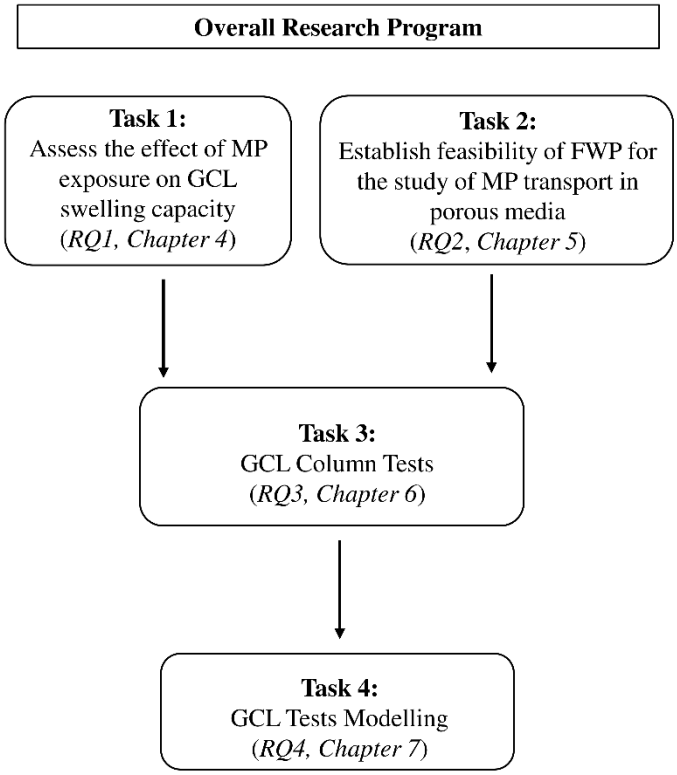

Figure 3.1. Overall research design (RQ1 to RQ4: Research questions listed in section 1.2)**.**

3.2 Materials Choice

3.2.1 Distilled versus Deionized Water

In this thesis, deionised (DI) water refers to high-purity laboratory water produced by a Millipore purification system (Millipore, Bedford, MA), whereas distilled water was supplied by the purification unit in the soil mechanics laboratory. Both water types exhibited very low electrical conductivity (as specified by the suppliers), indicating negligible ionic strength compared with the electrolyte solutions investigated in this study. Their effects on bentonite swelling and MP transport are therefore expected to be indistinguishable.

For practical reasons, distilled water was used in procedures where MP concentrations in effluents were not measured (e.g. swelling tests in Chapter 4), while DI water was used where accurate MP quantification was required (e.g. specimen preparation and permeant solutions in Chapter 5-6). Because the distilled water system does not include a final filtration stage, residual contaminants may be present that could interfere with MP measurements. This consideration motivates the use of DI water in all experiments involving MP analysis. Within each task, the same water type was used consistently to allow comparison among tests.

3.2.2 Geosynthetic Clay Liners (GCLs)

Two commercial GCLs were used in this research: Bentomat® ST (Minerals Technologies Inc., Australia; hereafter GCL-1), and Elcoseal X-2000 (Geofabrics Australia Pty. Ltd, Australia; hereafter GCL-2), as shown in Figure 3.2. GCL-1 consists of granular sodium bentonite (GSB) sandwiched between a nonwoven cover geotextile and a woven slit-film carrier geotextile. The layers are needle-punched through the thickness without thermal reinforcement (Makusa et al., 2014). GCL-2 is a thermally treated, needle-punched product in which a nonwoven cover is mechanically anchored through a layer of powdered polymer-amended sodium bentonite (PPSB) into a scrim reinforced composite carrier (nonwoven + woven). The polymer is an anionic additive, with proprietary formulation and dosage not disclosed (Gates et al., 2018). This configuration provides enhanced internal reinforcement and shear strength (Gates et al., 2018).

As-received rolls were sectioned into ~1 m sub-rolls or 0.5 m × 1.0 m sheets and stored in sealed plastic bags (or film-wrapped) to minimize moisture loss or uptake prior to

testing. Circular specimens were punched from sheet stock using a 50 mm diameter stainless-steel cutter under press load. To limit bentonite loss at cut edges, a small amount of DI water was applied around the cutter perimeter immediately prior to punching (Beck et al., 2008). Mass per unit area was determined gravimetrically from 50 mm discs and normalised by disc area. The mean value for GCL-1 was 5.0 kg/m^2, slightly lower than the 5.5 kg/m^2 reported by Makusa et al. (2014). The difference is plausibly attributable to bentonite loss during specimen cutting and subsequent handling and transport. Key properties of the two GCLs are summarized in Table 3.1.

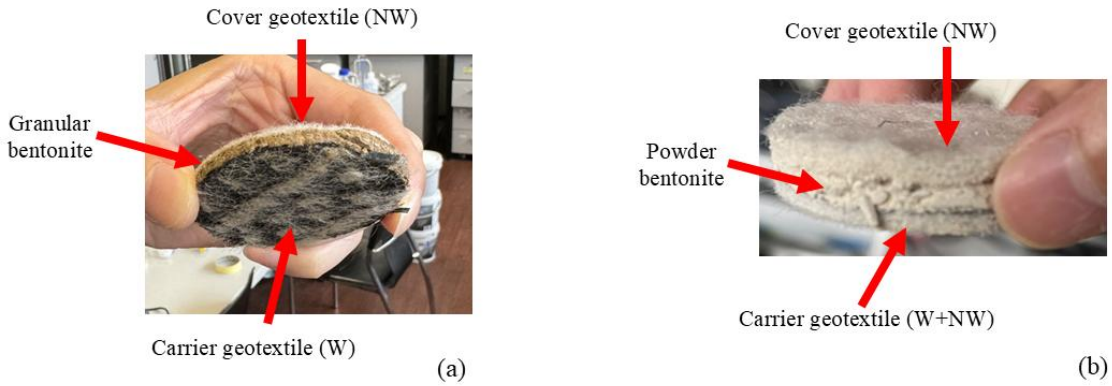

Figure 3.2. Photos of (a) GCL-1 and (b) GCL-2 samples with 50 mm diameter prior to testing.

Table 3.1. Key properties of GCLs used in this study.

	Values or Descriptions	
	GCL-1	GCL-2
Thickness (mm)	6.78	11.32
Gravimetric water content (%)	16.2	9.6
Cover geotextile	Nonwoven	Nonwoven
Carrier geotextile	Woven (slit-film)	Scrim reinforced (woven +nonwoven)
Dry mass of bentonite per unit area (kg/m^2) [1]	3.6 (Supplier)	3.7 (Supplier)
Dry mass of geotextiles per unit area (g/m^2) [1]	340 (Supplier)	550 (Supplier)
Mass per unit area (kg/m^2)	5.0 (Test)	5.9 (Test)
Bentonite type	Granular Na-bentonite	Powder anionic polymer modified Na-bentonite

Swelling index (mL/2g) [1]	24 (Supplier) 24 (Test)	24 (Supplier) 18 (Test)
Hydraulic conductivity permeated with deionised water (m/s) [1]	5×10^{-11} (Supplier) 4.1×10^{-11} (Test)	3×10^{-11} (Supplier) 3.7×10^{-11} (Test)
Mineralogy	84% montmorillonite 9% quartz [2]	74% montmorillonite 14% quartz [3]
Cation exchange capacity ($cmol^{+}/kg$)	83 [2]	-

[1] Supplier values are minimum average roll values (MARV), indicating at least 97.5% of the results are expected to exceed this value. "Test" values are mean values determined in the laboratory.

[2] Data from Makusa et al. (2014).

[3] Data from Qin et al. (2025).

3.2.3 Sand, Feldspar and Clay Minerals

Two natural Australian sands were used in Task 2 (Chapter 5) to evaluate the suitability of the FWP as a soil column for MP transport testing. The particle size distributions (PSD) of both sands are presented in Figure 3.3. Sand-1 exhibited a relatively narrow particle-size distribution with characteristic particle sizes of D_{10} =0.15 mm, D_{30} =0.26 mm, and D_{60} =0.36 mm, corresponding to C_u =2.4 and C_c =1.3. In contrast, Sand-2 showed a broader particle-size distribution with D_{10} =0.16 mm, D_{30} =0.42 mm, and D_{60} =0.85 mm, giving C_u =2.4 and C_c =1.3. Characteristic particle sizes D_{10}, D_{30}, and D_{60} represent the particle diameters corresponding to 10%, 30%, and 60% finer passing on the PSD curve, respectively. The coefficients of uniformity C_u and curvature C_c were calculated using:

$$C_u = \frac{D_{60}}{D_{10}} \text{ and } C_c = \frac{D_{30}^2}{D_{10} \times D_{60}}$$

Sand-1 is classified as poorly graded sand (SP) under the Unified Soil Classification System (USCS) according to ASTM D6913-04 (2009), whereas Sand-2 is a well-graded sand with little fines (SW).

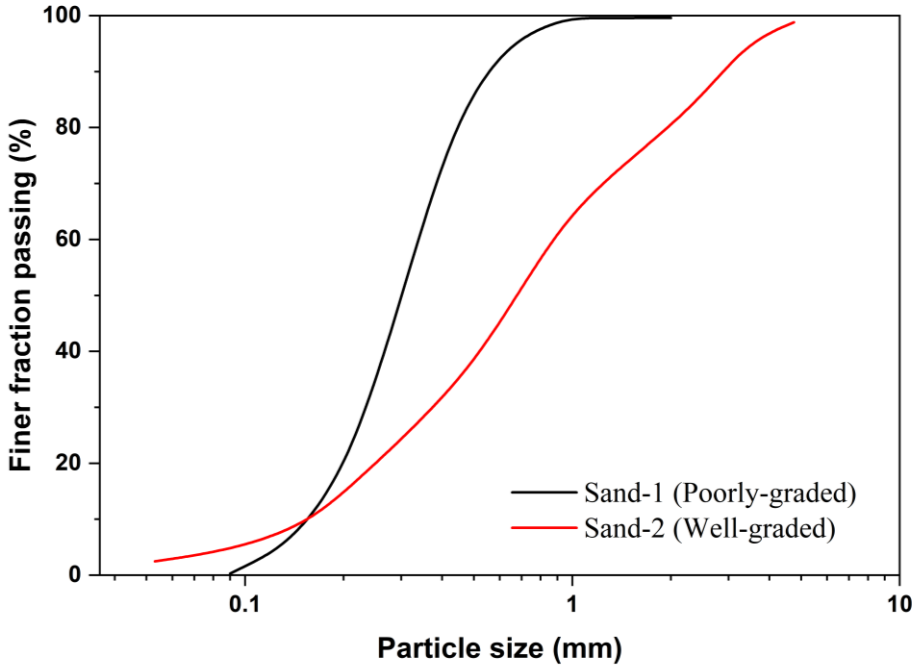

Figure 3.3. Particle size distributions of the two sands in this study.

Feldspar and bentonite (BT) powders were used as fine amendments to Sand-2. The feldspar was sourced from IMDEX Ltd. (Australia) and the bentonite from Global Synthetics Pty. Ltd. (Australia). The sodium bentonite corresponds to the grade used in Bentofix NSP 4900 GCLs and has a maximum particle size of ~67 μm, with ~90% of particles finer than 5 μm (Taheri and El-Zein, 2023). Because the finest fraction in Sand-2 is ~53 μm, direct mixing of Sand-2 with very fine bentonite would create a significant coarse-fine gap in the PSD. Such gap-graded mixtures are susceptible to internal instability under seepage, including erosion and leaching of fines (Li and Fannin, 2008, 2022). The instability can degrade soil structure and interfere with effluent MP quantification (Sujathan and El-Zein, 2025). To bridge this gradation gap, a feldspar powder with intermediate particle sizes (Figure 3.4) was selected as a non-plastic, filler, improving continuity of the PSD and reducing the risk of fines loss.

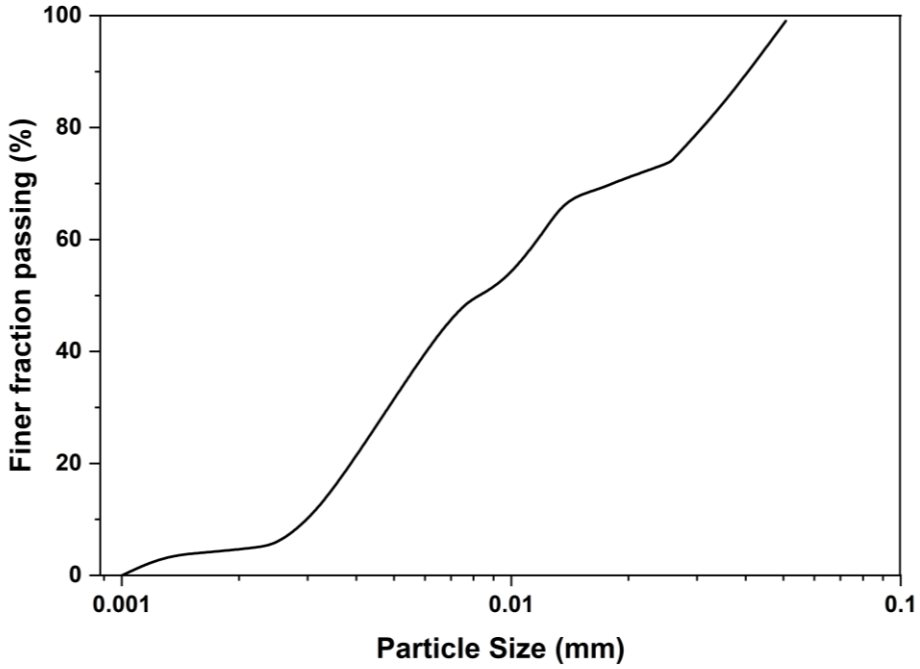

Figure 3.4. Particle size distribution of feldspar.

3.2.4 Microplastic Selection and Characterisation

PS and PE were selected as representative MP polymers due to their frequent detection in landfill leachate and adjacent soils (Kabir et al., 2023; Zaman et al., 2024). Nominal particle diameters of 0.2-5 μm were chosen for two primary reasons. First, smaller particles are generally more mobile in porous media and therefore more likely to migrate through soils and reach groundwater. Second, sub-micrometre MPs are more capable of crossing biological membranes, increasing their potential risks to cause harm to flora and fauna including humans (Anik et al., 2025).

Reported MP concentrations in landfill leachate vary widely among studies and are often reported without consistent information on particle size distributions or polymer composition. As shown in Table 2.2, many field investigations report particle counts per unit volume but do not provide size-resolved concentration data, making direct comparison with laboratory mass-based concentrations difficult. The experimental concentrations adopted in this study were therefore selected to represent realistic but measurable conditions for transport experiments, while acknowledging the uncertainty associated with currently available field data.

Two categories of MPs were used: non-fluorescent and fluorescently labelled particles. Non-fluorescent PS microspheres were employed in Tasks 1 and 2 (Chapters 4 and 5), where either MP concentrations did not need to be measured, or the matrices were clay-free, minimising interference in effluent measurements. When clay minerals were introduced (Tasks 3), fluorescent PS and PE particles were adopted because clay minerals can bias quantification of non-fluorescent MPs through light scattering and adsorption, whereas fluorescence-based detection provides more reliable and matrix-tolerant results (Sujathan and El-Zein, 2025). Fluorescent PS was also used in Task 2 for sand-felspar and sand-feldspar-bentonite mixtures to maintain analytical consistency.

3.2.4.1 Non-fluorescent Microplastics

Non-fluorescent PS microspheres with nominal diameters of 0.5, 1, and 5 μm were used for Tasks 1 and 2 (swelling tests and FWP assessment in Chapters 4 and 5), and are hereafter noted as PS0.5, PS1 and PS5, respectively. Aqueous stock suspensions (particle density 1.05 g/cm^3) were purchased from Sigma-Aldrich (PS0.5 and PS5) and Bioscientific Pty. Ltd., Australia (PS1). PSDs and surface morphology were examined using laser instrument (Mastersizer 3000, Malvern, UK) and scanning electron microscopy (Sigma HD, Zeiss). Detailed methods are given in Appendix X1 and X2. All PS particles were spherical and monodispersed in their supplied dispersant (Figure 3.5 and Figure 3.6).

Working suspensions were prepared immediately prior to experiments by ultrasonicating the stock solution, followed by pipetting off specific volumes and diluting them with background solutions (i.e., distilled water, Milli-Q DI water with resistivity of 18.2 MΩ·cm at 25 ℃, or $CaCl_2$ solutions) to achieve target concentrations. Freshly prepared suspensions were ultrasonicated for 5 minutes and gently agitated before use to minimise aggregation and settling. No chemical modification or additional surface treatment was applied. Stock suspensions were stored at 2-5 °C between preparations. In addition, PS1 dry powder (Bioscientific Pty Ltd, Australia) was used in Chapter 4 and stored at 20-25 ℃ prior to use.

Ultraviolet-visible (UV-Vis) spectrophotometer (Cary 60, Agilent Technologies, CA, USA), whose valid photometric range (absorbance) is up to 4, was used to quantify non-fluorescent MP concentrations in suspensions. A 3.5 mL aliquot of suspension was pipetted into a quartz cuvette, and the UV-Vis spectrum was collected in dual-beam mode

at wavelengths between 200-800 nm with an interval of 0.5 nm. The reference (blank) cuvette was filled with background solution (DI water or $CaCl_2$). MP concentrations were determined by plotting calibration curves based on respective peak absorbance values for PS0.5, PS1 and PS5 at wavelengths of 279, 438 and 246 nm, respectively (Figure 3.7). In some cases, alternative wavelengths were found to provide more reliable quantification, and were hence used, as will be detailed in the results section of Chapter 5.

3.2.4.2 Fluorescent Microplastics

Fluorescent MPs with nominal diameters ≤1 μm were used in Tasks 2 and 3 (FWP assessment and GCL transport tests). Monodisperse fluorescent PS microspheres with 0.2, 0.5 and 1 μm nominal diameters (f-PS0.2, f-PS0.5, and f-PS1) were obtained from Bioscientific Pty Ltd, Australia (catalogue numbers 24050, 24054, and 24062) as 2.6% (w/v) aqueous stock suspensions (particle density 1.05 g/cm^3). Based on the nominal diameters and assuming spherical geometry, the surface areas were approximately 3.14, 0.786, and 0.126 μm^2/particle for f-PS1, f-PS0.5, and f-PS0.2, respectively. Each size class carried three fluorescent labels with excitation wavelengths at 377, 517, and 588 nm. Supplier-reported coefficients of variation were 5% for f-PS0.2 and 3% for both f-PS0.5 and f-PS1, indicating high monodispersity.

Fluorescent PE microspheres with a mean diameter of 572 nm (f-PE0.5) were sourced from Lab 261, USA (catalogue number 951302) as a 1% (w/v) aqueous suspension (particle density <1.00 g/cm^3). Although the particle density was slightly lower than that of water, the very small particle size resulted in a negligible buoyant rise velocity (~0.24 mm/day based on Stokes' law), and the suspension reservoir was continuously agitated during testing to maintain particle dispersion. The particles exhibited a fluorescence excitation peak at 460 nm and a reported polydispersity index of 0.241. Compared with f-PS particles, f-PE0.5 displayed a dominant size peak at ~460 nm with two minor secondary peaks near 106 nm and 5 μm (Figure 3.8d and 3.8e). For f-PE0.5, the estimated surface area was approximately 0.786 μm^2/particle based on the mean particle diameter, noting that the polydisperse size distribution introduces additional uncertainty. Preparation of working suspensions followed the same procedures described in section 3.2.4.1.

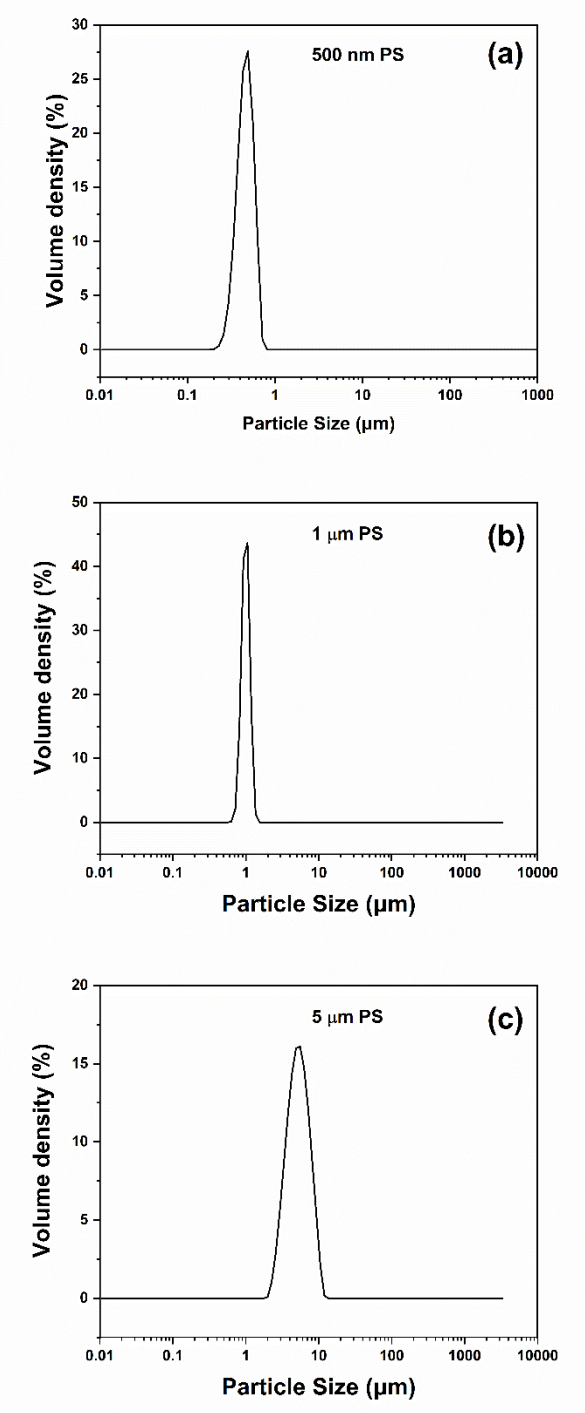

Figure 3.5. Particle size distributions (volume density plots) of the three-sized non-fluorescent MPs in stock suspensions.

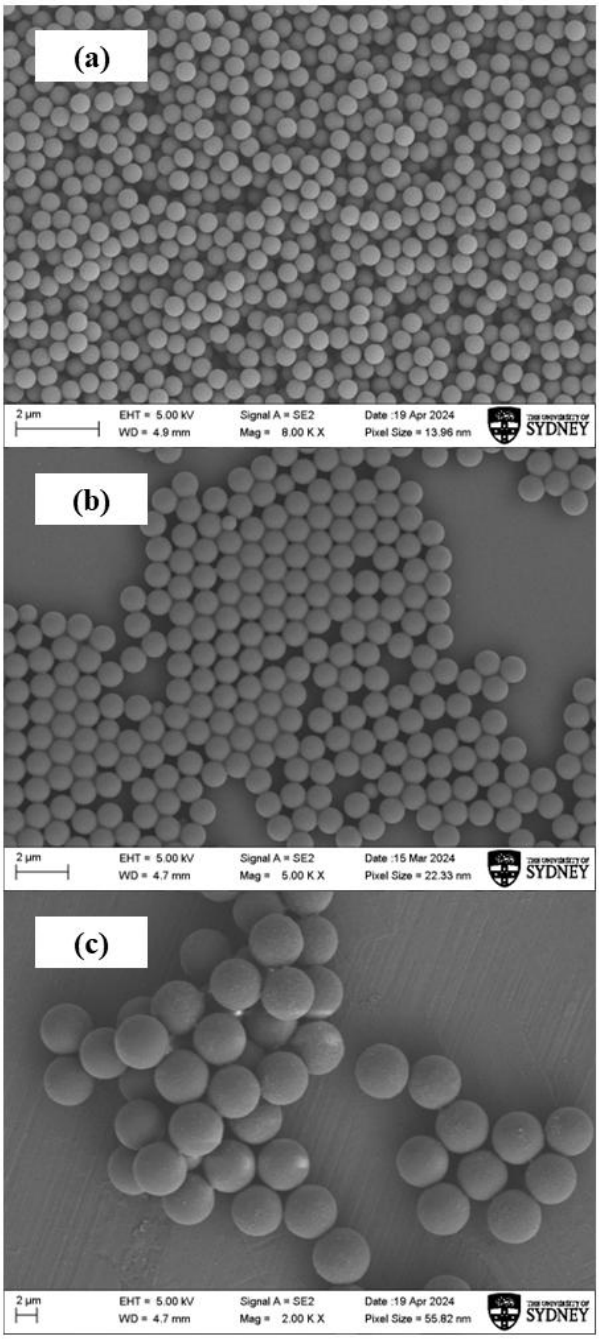

Figure 3.6. Surface morphology of non-fluorescent MPs in stock suspensions (images taken by scanning electron microscopy).

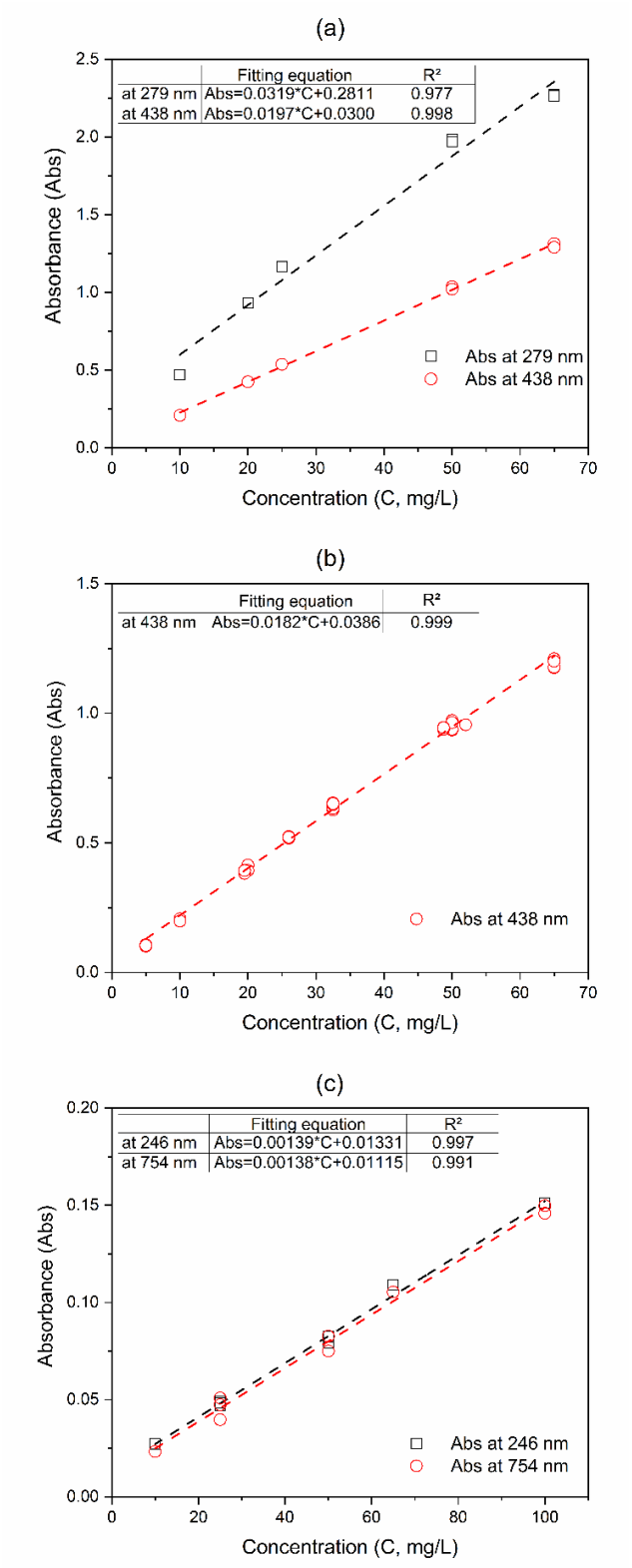

Figure 3.7. Calibration curves of MP concentration and UV-Vis absorbance (a) PS0.5, (b) PS1, and (c) PS5 (DI water was used as background solution).

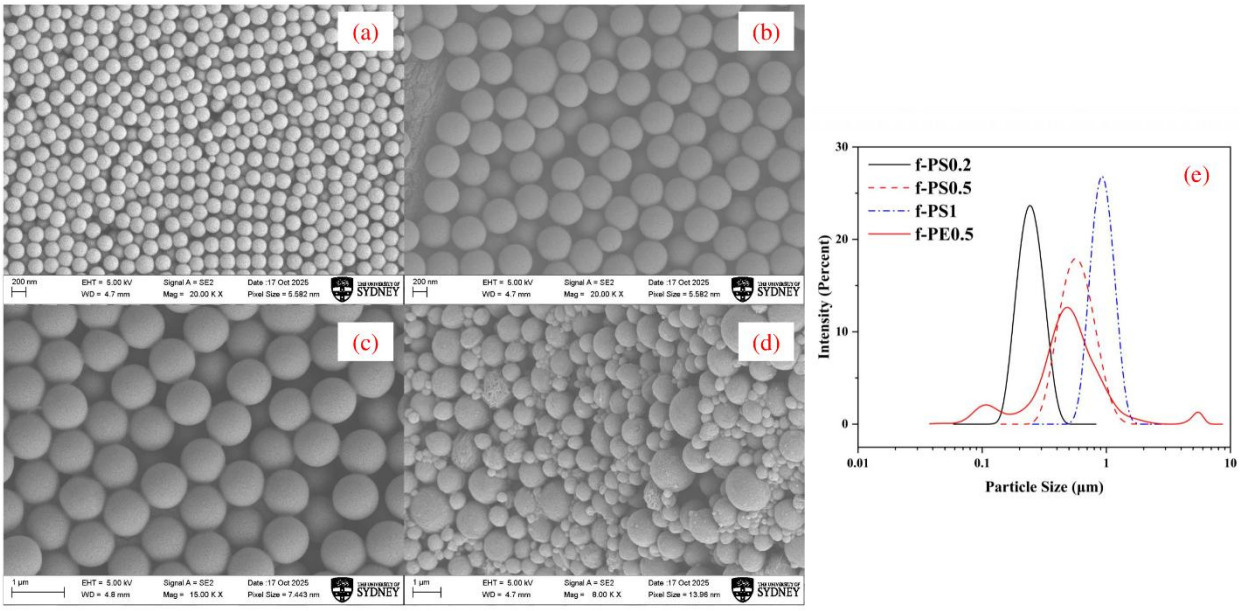

Figure 3.8. Scanning electron microscopy images of (a) f-PS0.2, (b) f-PS0.5, (c) f-PS1, (d) f-PE0.5 and (e) particle size distributions of these particles.

Effluent MP concentrations were quantified at room temperature using a Fluoromax-4 spectrofluorometer (Horiba Jobin-Yvon, USA). Prior to measurement, the instrument was warmed up, baseline-corrected using DI water, and operated with spectral correction enabled for sample (S1) and reference (R1) detectors, yielding corrected signals S1c and R1c. The ratio S1c/R1c was used to compensate for lamp fluctuations and detector response. Measurements were conducted in 1 cm path-length quartz cuvettes using emission-scan mode at fixed excitation wavelengths matching dye maxima. For PS and PE, the 517 (606) and 460 (503) nm excitation (emission) wavelengths were used, respectively.

Concentration calibration indicated that concentrations down to approximately 1 mg/L produced stable and repeatable fluorescence responses, whereas lower concentrations were associated with substantial signal noise and reduced measurement reliability. Given the influent concentration of 50 mg/L used in Task 3, this corresponds to a practical quantification threshold of approximately $C/C_0 \approx 0.02$. Consequently, “no breakthrough” should be interpreted as no detectable breakthrough above this practical measurement threshold rather than complete absence of MP transport. Very low-level breakthrough below the reliable measurement range of the method therefore cannot be ruled out.

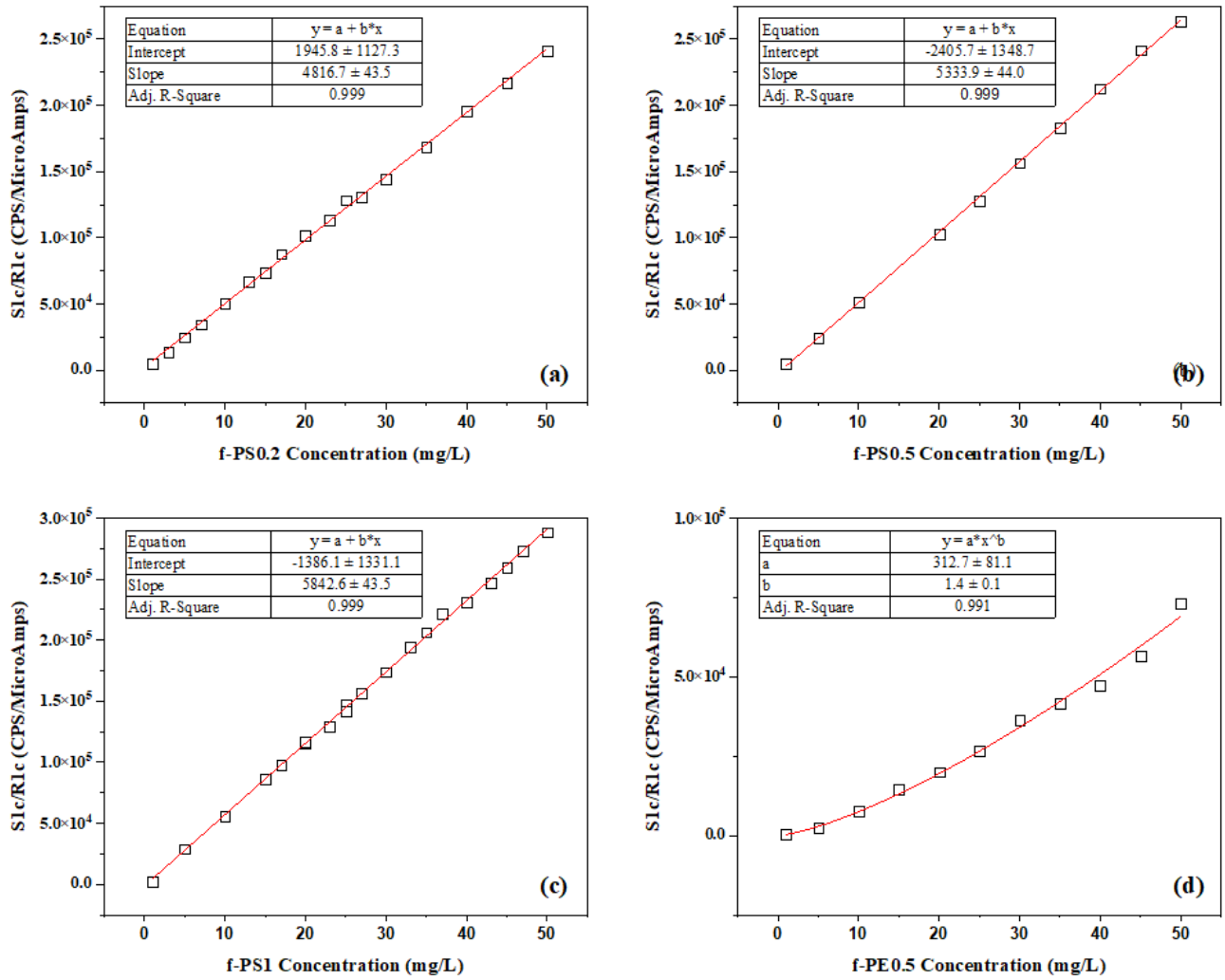

Figure 3.9. Calibration curves for fluorescent MPs in this study (a) f-PS0.2, (b) f-PS0.5, (c) f-PS1, and (d) f-PE0.5 (DI water was used as background solution).

During method development, saturation of the S1 detector occurred at concentrations around 50 mg/L when slit widths of 3-5 nm were used (S1 capacity ≈2×10^6 counts/second). Therefore, excitation and emission slit widths were set to 2 nm for PS and 3 nm for PE to avoid saturation while maintaining adequate spectral resolution. Calibration curves of S1c/R1c versus MP concentration were developed for each polymer and size class and used to determine MP concentrations in effluents (Figure 3.9).

3.3 Rationale for Testing Conditions

3.3.1 Task 1: Effect of MP Exposure on Bentonite Swelling

Most prior swelling studies have examined soil-MP composites prepared by premixing MPs into soils prior to hydration in clean water or chemical solutions. In landfill practice, however, barrier materials and subgrade soils are exposed to leachate containing suspended MPs, not to soil-MP composites prepared *ex ante*. Accordingly, this thesis adopts an exposure-to-suspension scenario in which bentonite specimens are hydrated with MP-rich solutions. This approach captures more realistic interactions and avoids artefacts from pre-mixed composites.

Swelling capacity is quantified under controlled chemistries (distilled water and $CaCl_2$ solutions) using swell index and odometer swell strain tests. Swell index is also quantified during GCL pre-hydration in Task 3. These measurements establish the baseline sensitivity of bentonite swelling to pore water chemistry and MP exposure, with the aim of assessing likely changes in hydraulic conductivity that may influence transport behaviour. In task 1, the effects of several variables on swelling are assessed including solution chemistry (distilled water and 10 mM $CaCl_2$), MP presence and concentration (0, 50, and 100 mg/L), and particle attributes, primarily under suspended particle exposure, with a powder-mixed variant used for comparison.

3.3.2 Task 2: Suitability of FWPs as Soil Columns for MP Transport

As reviewed in Chapter 2, FWPs are standard instruments for measuring hydraulic conductivity of low-permeability soils and have been used as soil columns for the study of dissolved contaminant transport. Extending this practice to MP transport is not straightforward because particles can be strained, filtered, or adsorbed by apparatus components (e.g., porous stones, pedestals, and filter papers), leading to artificial retention and biased transport estimates. Only one study has reported using FWPs to study MP transport and did not provide a mass-balance assessment (Chen et al., 2023). Task 2 therefore establishes such a baseline as a prerequisite for reliable use of FWPs in particulate-contaminant research and assesses their suitability for MP transport testing.

The Task 2 testing program was designed to identify potential sources of particles or interfering substances (e.g., release from tubing, filter papers, porous stones, and pedestals) and potential sinks (e.g., straining and/or adsorption at porous stones, pedestals, filter papers, and fittings) by varying the components most likely to interact with MPs. Alternative end-constraints and filtering elements (e.g., filter paper and porous stones) were compared to determine whether these components induce MP loss. Performance was also evaluated across MP sizes within sub-micron to micron scales to capture size-dependent sensitivity to straining and attachment. In parallel, the FWP was assessed under hydraulic conditions representative of low-permeability clayey media and higher-permeability granular or sand-clay mixtures**,** to determine whether the FWP can reproducibly generate interpretable BTCs under both slow- and fast-flow conditions. Finally, a full mass balance framework was embedded to distinguish porous-media retention from apparatus-induced losses, thereby establishing boundary conditions under which the FWP can be used with confidence for MP transport experiments.

3.3.3 Task 3: MP Transport in GCL

Task 3 evaluates GCL barrier performance against MP transport under controlled stress and hydration conditions. GCL specimens are pre-hydrated using either a) DI water or b) $CaCl_2$ with wet-dry cycling to represent chemical aging sometimes encountered under field conditions. The selected hydration solutions were intended to represent progressively aggressive chemical conditions relevant to landfill barrier systems rather than exact replication of a single field leachate composition. DI water was used as a low-ionic-strength condition representing ideal hydration, whereas 10 mM $CaCl_2$ represents moderate divalent-cation exposure that may occur in saline subsoils, construction water, or dilute leachate environments. The 100 and 300 mM $CaCl_2$ conditions were adopted as chemically aggressive scenarios intended to accelerate cation exchange and swelling suppression in bentonite. These concentrations are more representative of severe localised calcium-rich exposure conditions or long-term chemical degradation scenarios than of typical well-managed landfill operating conditions. Wet-dry cycling was applied as an accelerated degradation approach to induce structural and hydraulic changes in bentonite, including reduced swelling capacity, increased pore connectivity, and elevated hydraulic conductivity. The selected two-cycle regime is not intended to reproduce a specific landfill chronology,

but rather to produce representative degraded conditions within a practical laboratory timeframe. This approach enables comparison between intact and chemically conditioned GCLs.

All tests are conducted in FWPs with effective stress control, and each experiment follows a documented mass-balance protocol (system blanks and recovery checks) to quantify MP transmission and retention.

The testing program consisted of several sequential stages. Firstly, hydraulic conductivity and indicative swelling response are characterized under the selected hydration chemistries. Secondly, BTCs and effluent recoveries are quantified for defined MP attributes (polymer type and size class), with retained mass assessed using post-test analyses. Flow rate and pressure head are continuously recorded via the volume/pressure controllers to define hydraulic gradients and calculate seepage velocities. Effluent is collected at fixed intervals of number of pore volume (No. of PV), defined as $\text{No. of PV} = \frac{V_{effluent}}{V_{pore}}$. After test completion, the geotextiles and bentonite are recovered, gently cleaned to remove loosely adhering particles, dried, and prepared for SEM to visualise retained MPs and pore-scale features. Selected specimens are also analysed using mercury intrusion porosimetry (MIP) to assess the effect of pre-hydration chemistry on bentonite microstructure and to identify possible effects on MP transport behaviour.

Effluent concentrations are normalized as C/C_0 and plotted against PV to obtain BTCs, which are initially interpreted qualitatively. Quantitative metrics (defined in Chapter 6) are subsequently extracted to characterise breakthrough timing, recovery, and overall filtering capacity.

All transport experiments in this study are conducted under near fully saturated conditions. In practice, GCLs are commonly installed in an initially unsaturated state and may require extended periods to reach full saturation depending on subgrade conditions, hydration source and overburden stress. Saturated testing was adopted intentionally in this study because it represents conditions most favourable for advective transport by maximising hydraulic conductivity within the bentonite layer. The experiments therefore represent a conservative assessment of potential MP migration through GCLs under fully hydrated conditions.

Under unsaturated conditions, lower hydraulic conductivity and discontinuous flow pathways would likely further restrict MP movement. These effects were not examined

explicitly in the present study. Accordingly, the reported breakthrough behaviour should be interpreted as representative of saturated transport conditions rather than field performance under partially saturated conditions.

3.3.4 Task 4: Numerical Modelling of MP Breakthrough in GCLs

Task 4 uses one-site and two-site ADR models with first-order attachment-detachment kinetics to interpret BTCs generated in Task 3 and to infer plausible MP retention mechanisms in GCLs. First, candidate one- and two-site model formulations, including alternative blocking functions, are fitted to the measured BTCs and evaluated to identify best-performing models. Second, fitted transport and retention parameters (e.g., dispersivity, attachment and detachment coefficients, and maximum solid-phase capacities) are compared across test conditions, including hydraulic conductivity, MP size and polymer type, to assess how these factors influence MP mobility and retention behaviour.

3.3.5 Statistical Considerations

The number of replications adopted in this study reflected a balance between experimental repeatability and the practical constraints associated with long-duration permeameter testing. Replication was prioritised for baseline conditions to assess the consistency of the experimental procedures, whereas fewer replicates were conducted for exploratory conditions involving different particle sizes and polymer types in order to investigate a broader range of variables within the available experimental timeframe.

For the base-case condition, multiple replicates were conducted to quantify variability in measured outputs, including BTCs, peak normalised concentration (C_{max}/C_0), and cumulative mass recovery. Variability between tests is expected to arise mainly from heterogeneity in bentonite-based specimens, differences in hydraulic conductivity and pore structure. These repeated tests provided an indication of the variability associated with specimen preparation, hydraulic control, and effluent sampling. For the remaining test conditions, fewer replicates were performed to identify general trends in transport behaviour.

Formal statistical hypothesis testing was not undertaken because replication was limited for several conditions and because prior information on variability in MP transport through low-permeability materials was not available. In addition, individual permeameter

tests commonly required several months to complete, which constrained the number of replicates that could be performed within the scope of the study. Accordingly, the results are interpreted primarily in terms of consistent experimental trends and relative differences between conditions.

Chapter 4 Effects of Microplastics on Swelling Behaviour of Geosynthetic Clay Liners

4.1 Introduction

MPs have been reported to modify the bio-chemo-physical properties of soils (Mondol et al., 2025). The physical effects most relevant to barrier performance are summarised in Chapter 2. Most existing studies have investigated MP effects by premixing MPs with soils in the dry state before hydration. In landfills, by contrast, barrier materials and subgrade soils encounter leachate carrying suspended MPs rather than pre-blended MP-soil composites. This distinction matters for GCLs, whose bentonite ideally hydrates first under low-salinity conditions to develop swelling and achieve low hydraulic conductivity. Early exposure to chemically aggressive leachate can suppress swelling through cation exchange and electrical double layer compression (Tian et al., 2016).

To the best of the author's knowledge, the effects of MP exposure during hydration on the swelling capacity of GCLs have not been systematically evaluated. This chapter (Task 1 as described in Chapter 3) addresses this gap by (i) conducting swell index (SI) tests on sodium bentonite extracted from commercial GCLs following exposure to MP suspensions under controlled chemistries, (ii) performing oedometer swell strain tests on intact GCL specimens hydrated using the same MP-rich solutions, and (iii) applying SEM to post-test bentonite to visualize retained MPs and any associated microstructure changes. These experiments establish whether suspended MPs measurably influence bentonite swelling under landfill-relevant hydration conditions, thereby framing expectations for MP transport behaviour examined in subsequent chapters.

4.2 Materials and Methods

4.2.1 Materials

Materials used in this chapter are described in Section 3.2. Briefly, a commercially available GCL-2 and non-fluorescent 1 μm PS microspheres (PS1) were used in this chapter. Circular specimens (50 mm diameter) were punched from sheet stock using a stainless-steel cutter under press load. The PS1 particles were selected to represent small MPs relative to hydrated bentonite pore throats, thereby increasing the likelihood of detecting any influence of suspended MPs on swelling behaviour. Stock suspensions were ultrasonicated immediately before use and diluted to prepare working suspensions of 50 and 100 mg/L in the specified test solutions.

Although reported MP concentrations in landfill leachate are often lower, many surveys are constrained by detection limits that under-represent particles smaller than 10 μm (as summarized in section 2.4.1). Accordingly, elevated yet practically achievable concentrations were adopted to increase experimental sensitivity.

4.2.2 Swell Index Test

Swell index (SI) tests were conducted to assess bentonite swelling following ASTM D5890 (2019), with modification to accommodate MP exposure (Wireko et al., 2020). Four exposure scenarios were evaluated (Table 4.1). Given the lower density of PS (~1.05 g/cm^3) relative to bentonite (~2.6-2.7 g/cm^3), a specimen-first approach was adopted to minimise phase separation during wetting (Wireko et al., 2020).

For each test, 2 g of bentonite powder extracted from the GCL (with or without co-dosed PS1 powder, as specified) was placed at the bottom of an empty 100 mL graduated cylinder. The working solution (distilled water or PS1 suspension) was then added slowly along the sidewall in ~10 mL aliquots at 10-minute intervals until the 100 mL mark was reached, avoiding agitation and visible air entrapment. The specimen was left undisturbed at room temperature until no further swelling was observed. The gel volume was read to the nearest millilitre. Given the unevenness of the swelling surface of the sample, both the lowest and highest levels were recorded. Scenarios 1.1 and 1.2 were repeated to confirm the reproducibility.

Table 4.1. Test plan for SI tests.

Test No.	Sample	Working Solution	PS/Bentonite Mass Ratio
1.1	2 g of bentonite	Distilled water	/
1.2	2 g of bentonite + 10 mg PS1 powder	Distilled water	1:200
1.3	2 g of bentonite	Distilled water with 100 mg/L PS1	1:200
1.4	2 g of bentonite	Distilled water with 50 mg/L PS1	1:400

4.2.3 Oedometer Swell Strain Test

GCL panels were trimmed to 50 mm diameter using a circular punch under hydraulic load, and the initial specimen thickness H_0 was measured with a vernier calliper. The vertical swell deformation ΔH was measured at different points in time in a rigid oedometer (Figure 4.1) comprising a stainless-steel cell (50 mm inner diameter, 53 mm height), a stainless-steel reservoir, and a dial gauge (25.4 mm travel and 0.0254 mm resolution). The specimen was placed in the cell with a top quartz porous stone and a top cap. No bottom porous stone or filter paper was used to avoid trapping MPs in ancillary media during hydration. A seating pressure of 2 kPa was applied via the top cap to maintain contact while approximating near-free-swell conditions. Extra care was taken during installation to minimise bentonite loss from specimen edges.

Four permeating solutions were chosen to represent onsite hydration conditions: (i) distilled water (baseline), (ii) PS suspension in distilled water, (iii) $CaCl_2$ solution, and (iv) PS suspension in $CaCl_2$ solution (Table 4.2). After applying the seating pressure and allowing the dial gauge reading to stabilise, permeant was introduced into the reservoir until the specimen was fully submerged. Testing followed ASTM D4546 (2021). Dial gauge readings were taken at 15 s, 30 s, 1, 2, 4, 8, 15, 30 min, 1, 2 and 3 h on the first day, and then daily (i.e., 24 h, 48 h, etc) until the swelling rate decreased below 0.01 mm/hour. The swell strain was calculated as:

$$\varepsilon_s(t) = \frac{\Delta H(t)}{H_0} \times 100\%.$$

Duplicate tests were conducted to assess reproducibility. The test scenarios are shown in Table 4.2.

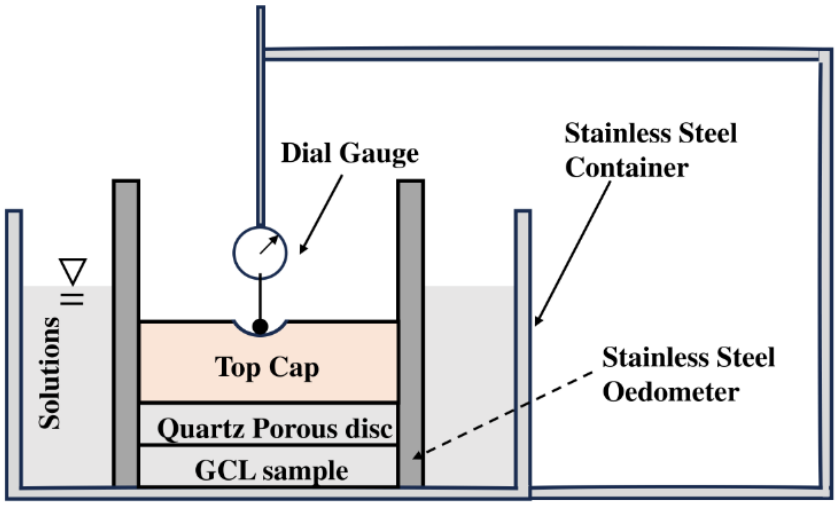

Figure 4.1. Oedometer test apparatus (not in scale).

Table 4.2. Test plan for oedometer swell strain tests.

Test No.	Specimen information		Permeating solution
	Initial thickness (mm)	Initial GCL mass (g)	
2.1	10.7	12.2 g	Distilled water
2.2	10.6	12.5 g	Distilled water
2.3	10.8	11.0 g	Distilled water with 100 mg/ L PS1
2.4	10.5	10.3 g	Distilled water with 100 mg/L PS1
2.5	10.7	11.3 g	10 mM $CaCl_2$
2.6	10.4	11.5 g	10 mM $CaCl_2$
2.7	10.1	11.5 g	10 mM $CaCl_2$ with 100 mg/L PS1
2.8	10.2	10.6 g	10 mM $CaCl_2$ with 100 mg/L PS1

4.2.4 Scanning Electron Microscopy

SEM was used to visualise possible bentonite-PS interactions and microfabric changes after the oedometer swell strain tests. A field-mission SEM (Sigma VP HD, Zeiss) was employed. Immediately after testing, GCL specimens were freeze-dried at -50 °C under vacuum to preserve pore structure. Small quantities of bentonite were then extracted from both the specimen edge and centre, and a fragment of the carrier geotextile was also collected. Samples were mounted on aluminium stubs using conductive carbon tape and sputter-coated with 10 nm gold to reduce charging. Imaging was conducted at an accelerating voltage of

5kV with a 30 μm aperture. These conditions provided high-contrast surface morphology while limiting beam damage. Images were acquired from both edge and centre locations, as well as from geotextile fibres to assess spatial variability in MP retention.

4.3 Results and Discussion

4.3.1 Swell Index Test

Swell index results are shown in Figure 4.2 as mean values with standard deviation. Replication was limited to duplicate tests for the MP-exposure conditions (n=2) and triplicate tests for the DI water control (n=3). Given the limited replication, formal statistical hypothesis testing was not performed, and comparisons between conditions are based primarily on the magnitude of observed differences relative to experimental variability.

Although ASTM D5890 (2019) specifies swell index measurement after 16-24 hours, swelling in the experiments continued beyond 24 hours and approached a quasi-steady value after approximately 10 days. A quasi-steady condition was defined as an increment of less than 1 mL per 2 g over a 16-hour period. Continuous swell index-time measurements were not recorded during hydration, and the experiments were not designed to determine swelling kinetics or equilibrium times. Accordingly, swell volumes were monitored over a ten-day period before final readings were recorded, and the results are shown in Figure 4.2.

Figure 4.2 indicates reasonable repeatability between replicate tests. The mean swell index for bentonite hydrated with distilled water was 29 mL/2 g. Addition of 1 μm PS particles at concentrations of 50 mg/L and 100 mg/L produced mean swell indices of 29 mL/2 g and 27 mL/2 g, respectively. These differences were small relative to the experimental variability represented by the standard deviation error bars.

No discernible difference was observed between pure bentonite and bentonite-PS mixture hydrating with distilled water. The average values were both 29 mL/2 g (Test 1.1 and Test 1.2). At a PS-to-bentonite mass ratio of up to 0.5% (10 mg PS1 mixed with 2.00 g bentonite and suspension exposure of 50-100 mg/L PS1 in distilled water), PS1 did not measurably alter the SI of the powdered sodium bentonite.

Tests 1.2 and 1.3 compared dry co-dosing (premixing PS1 powder with bentonite) with suspension exposure (PS1 in distilled water). Swell indices were indistinguishable within measurement uncertainty, indicating that the exposure mode did not measurably

affect free swelling under the conditions tested. Although the 100 mg/L PS1 condition yielded a slightly lower average SI than the 50 mg/L condition, additional testing would be required to determine whether this difference represents a reproducible trend or normal experimental variability.

At these low MP loadings and under low ionic strength conditions, 1 µm PS particles are unlikely to perturb double-layer interlayer swelling of Na-bentonite or change porewater chemistry. Overall, the results indicate that exposure to 1 µm PS particles at the concentrations examined did not produce a substantial reduction in swell index under low ionic strength conditions.

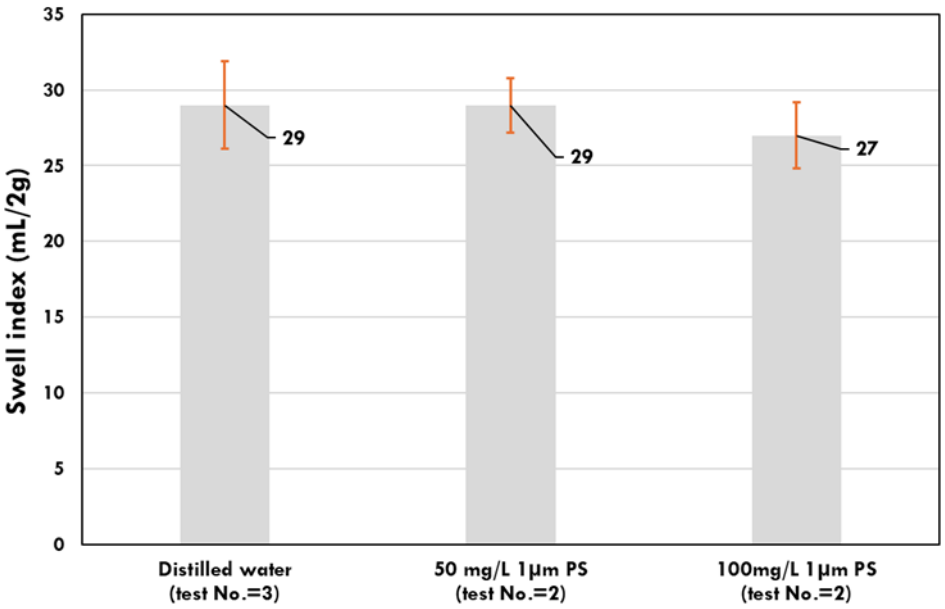

Figure 4.2. Swell index (SI) results of bentonite in distilled water (Test 1.1), bentonite in 100 mg/L (Test 1.3), and 50 mg/L (Test 1.4) PS1 solutions.

4.3.2 Oedometer Swell Strain Test

Figure 4.3 presents vertical swell strain as a function of time for all test scenarios. The instantaneous swelling rate initially increased to 0.9 mm/hour, and then slowly declined after 4 minutes. The swell strains reported below correspond to the time t_{limit}, defined as the point at which the swelling rate first decreased to 0.01 mm/hour. Values of t_{limit} were obtained by interpolation of the rate-time curves.

Table 4.3 and Figure 4.3 show generally good repeatability, with two notable exceptions. First, Tests 2.7-2.8 (10 mM $CaCl_2$ with 100 mg/L PS1) differed more than other replicate pairs, with terminal swell strains of 34.8% and 39.7%. Second, Test 2.3-2.4 (distilled water with 100 mg/L PS1) reached t_{limit} at 65 h and 35 h, respectively, despite converging to similar terminal swell strains. These discrepancies likely reflect specimen-scale heterogeneity, such as variation in bentonite distribution or needle-punch bundle density, as well as small differences in initial moisture content or seating/contact conditions.

As expected, exposure to $CaCl_2$ reduced swelling. Swell strains in 10 mM $CaCl_2$ were 38.3% and 38.9% (Tests 2.5-2.6), compared with 43.0% and 43.1% for distilled water controls (Tests 2.1-2.2). The resulting reduction of ~4-5 percentage points (~10% relative) is consistent with suppression of osmotic swelling by cation exchange and electrical double-layer compression in Na-bentonite.

Table 4.3. Elapsed time and swell strain at 0.01 mm/hour swell rate of oedometer swell strain tests.

Test No.	Hydration solution	t_{limit} (hour)	Swell strain (%)
2.1	Distilled water (DW)	83	43.0
2.2	DW (repeat)	95	43.1
2.3	PS1 100 mg/L in DW	65	42.4
2.4	PS1 100 mg/L in DW (repeat)	35	38.7
2.5	10 mM $CaCl_2$	51	38.3
2.6	10 mM $CaCl_2$ (repeat)	61	38.9
2.7	PS1 100 mg/L in 10 mM $CaCl_2$	45	34.8
2.8	PS1 100 mg/L in 10 mM $CaCl_2$ (repeat)	59	39.7

* DW is distilled water; t_{limit} is the time it takes to reach 0.01 mm/hour swell rate

Adding 100 mg/L PS1 to distilled water yielded swell strains of 42.4% and 38.7% (Tests 2.3-2.4). The small reduction relative to distilled water controls falls within experimental scatter and replicate variability in t_{limit} cautions against over-interpretation. Under distilled water conditions, effect of PS1 exposure appears negligible to modest and is not statistically resolved by the present dataset.

For combined exposure to 10 mM $CaCl_2$ and 100 mg/L PS1, one replicate (34.8%, Test 2.7) was lower than the $CaCl_2$-only range, while the second (39.7%, Test 2.8) was comparable to $CaCl_2$ controls. Given this mixed response and the magnitude of replicate variability, a consistent co-effect of PS with $CaCl_2$ on swell strain was not demonstrated by

these tests. Additional replication would be required to establish whether the observed differences are significant.

4.3.3 SEM of MPs and Clay Microstructure

As shown previously in Figure 3.6, the PS1 particles appear smooth and near spherical as described by the supplier (additional images are provided in section 3.2.3). Their regular geometry and high roundness make them easy to distinguish from platy bentonite tactoids and fibrous geotextile structures in SEM images. Polymer identity was inferred from morphology, and no spectroscopic confirmation was performed.

In Test 2.3, discrete PS particles were observed on bentonite sampled from the specimen edge (Figure 4.4a). Particles occurred as individual spheres or small clusters and appeared to rest on, or weakly adhere to, clay surfaces. Micrometre-scale voids (around 1 μm in size) were also present within the clay fabric; however, these features could result from freeze-drying or handling artefacts (e.g., sublimation pits or particle pull-out during sampling). Accordingly, a causal link between these voids and PS exposure cannot be established from SEM imaging alone.

On the carrier geotextile (Figure 4.4b), many PS1 particles were observed where bentonite residuals coated the fibres, whereas few particles were found directly on clean fibre surfaces. This spatial distribution suggests preferential association with bentonite rather than the geotextile itself. However, it is not possible to determine from these tests whether this is accidental or indicative of selective attachment to the bentonite.

No PS1 particles were identified in bentonite extracted from the specimen centre (Figure 4.4c). Within the limits imposed by SEM field of view and sampling volume, this indicates negligible penetration of 1 μm PS into the interior of the hydrated GCL under the tested conditions. At the same time, sparse particles below the detection density of the surveyed areas cannot be ruled out.

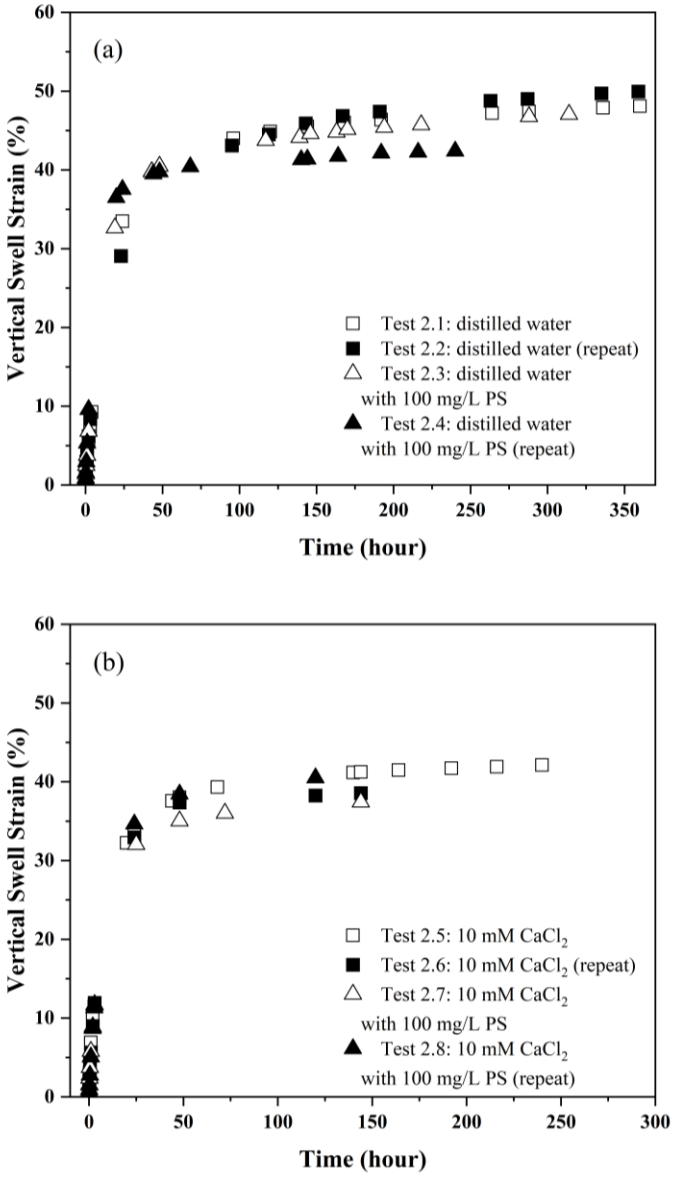

Figure 4.3. Oedometer swell strain test results (a) Tests 1-4 in distilled water with/without PS1; (b) Tests 5-8 in 10 mM $CaCl_2$ with/without PS1.

4.4 Conclusion

This chapter investigated whether exposure to suspended 1 μm PS microspheres influences the swelling behaviour of GCLs. Swelling behaviour was evaluated using swell index tests on extracted sodium bentonite and oedometer swell-strain tests on intact GCL specimens. Under the conditions examined, exposure to PS particles produced only minor changes in swelling behaviour relative to the control specimens. Slightly lower swell indices were observed in some tests involving 100 mg/L PS suspensions. However, additional testing is

required to determine whether these differences represent reproducible trends or fall within the range of experimental variability.

Post-test SEM observation showed that retained PS particles were located primarily on bentonite attached to the carrier geotextile during hydration. No clear evidence was obtained to suggest that suspended MPs significantly disrupted bentonite swelling or hydration behaviour at the MP concentrations examined. However, SEM analysis sampled only a limited specimen area, and sparse or spatially heterogeneous particle distributions within the bentonite cannot be excluded. More imaging approaches, including fluorescence-based sectioning or micro-CT analysis, would be required to better resolve MP distributions within hydrated bentonite.

The findings from this task should also be interpreted within the limitations of the experimental programme. First, the number of experiments was insufficient to support robust statistical analysis of the effects of MPs on bentonite swelling. Second, investigation of a broader range of variables (e.g., ion concentration and cation type) and additional MP sizes and polymer types would provide a more comprehensive assessment. Third, the experiments employed simplified aqueous chemistries and pristine commercially produced MPs, which do not fully represent the complexity of landfill leachate and environmentally aged particles. Future work should therefore include swelling tests using real landfill leachate, and where feasible, compare hydration using leachate before and after MP removal (e.g., filtration) to more directly isolate MP-specific effects.

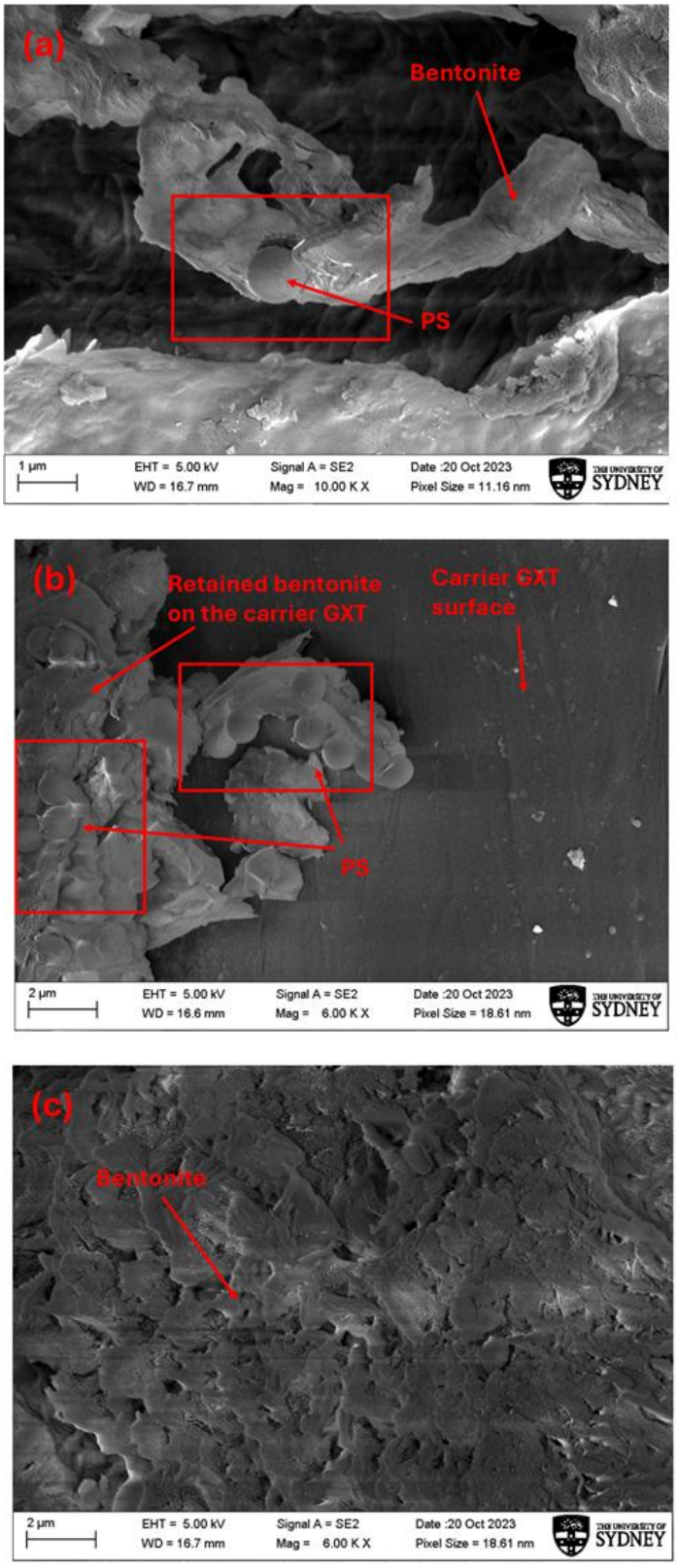

Figure 4.4. SEM images of the GCL specimen in test 2.3 (a) bentonite taken from the edge of GCL; (b) carrier geotextile (GXT) specimen with bentonite attached; (c) bentonite taken from the centre of GCL.

Chapter 5 Flexible-Wall Permeameters for Research on Microplastic Transport in Soil: Validity, Advantages and Constraints

5.1 Introduction

Assessing how MPs migrate through soils and are retained within porous media is essential for understanding long-term environmental risks. As reviewed in Chapter 2, most laboratory studies of MP transport have used RWCs. While RWCs perform adequately for coarse and relatively permeable matrices, they are less than ideal for fine-grained or low-permeability soils. Sidewall leakage, limited control of effective stress, and difficulty in maintaining saturation can introduce artefacts that bias breakthrough behaviour and mass recovery. These limitations motivate the use of alternative experimental devices that (i) minimise boundary artifacts, (ii) allow independent control of stress and hydraulic conditions, and (iii) remain applicable across a wide range of soil types, including expansive and very low-permeability materials.

Flexible wall permeameters (FWPs) meet these requirements and are well established in geotechnical engineering for measuring hydraulic conductivity of fine-grained soils (typically $k_{sat}<10^{-7}$ m/s) and for investigating the transport of dissolved contaminants.

Despite their widespread use for solute transport, FWPs have rarely been applied to particulate contaminants, and a systematic assessment of mass recovery and mass balance for MPs in FWPs remains a notable gap. In particular, MPs may be retained by permeameter components such as porous stones, filter papers, tubing, and fittings, potentially leading to biased transport estimates if such artefacts are not quantified.

The goal of this chapter (Task 2 in Chapter 3) is to establish a mass-balance baseline for MP transport experiments conducted in FWPs. Controlled experiments are performed to

evaluate whether FWPs, when paired with ultraviolet-visible (UV-Vis) and fluorescent spectroscopy for MP quantification, introduce measurable sources or sinks of MPs. The effects of key experimental variables, including MP size and concentration, permeant ionic strength, porous stone type, filter paper type, and hydraulic gradient, are assessed. In addition, based on findings from this investigation, the advantages and constraints of FWPs are discussed in comparison with RWCs. The results reported in this chapter provide the experimental foundation for subsequent chapters, in which FWPs are used to study MP transport and retention in GCLs.

5.2 Materials and Methods

5.2.1 Materials

This chapter used the GCLs, sands and MP suspensions described in Section 3.2. Non-fluorescent PS microspheres with nominal diameters of 0.5, 1 and 5 μm (PS0.5, PS1 and PS5), together with fluorescent PS microspheres of nominal diameter 0.5 μm (f-PS0.5), were used as representative MPs. Working influent suspensions (20-75 mg/L) were prepared by diluting stock suspensions in the specified background solutions and were ultrasonicated immediately before use.

Two sands were used in the validation experiments. Sand-1 (SP) was sieved to achieve a size range between 300 μm and 600 μm and then washed with DI water until the supernatant was clear to minimise residual fines. The washed sand was oven-dried at 105 ℃ overnight and stored in a dry environment until use. Sand-2 (SW) was sieved to retain the 53 μm-1.18 mm fraction. The retained fraction was oven-dried at 105 ℃ overnight and stored in sealed containers at room temperature. Pre-washing Sand-2 was avoided to prevent preferential removal of the finest particles and distortion of the particle size distribution. Feldspar and bentonite (BT) powders were stored in sealed bags to minimise moisture uptake prior to use.

Clay-based transport tests were conducted using GCL-1, a granular sodium bentonite GCL described in Section 3.2. The GCL roll was sealed in plastic film and stored in a dry, light-shielded environment prior to specimen preparation. Swell index tests on extracted bentonite (ASTM D5890, 2019) yielded 23 mL/2 g when hydrated in DI water, decreasing to 9 mL/2 g after hydration in 100 mM $CaCl_2$ with two wet-dry cycles. The latter

condition was selected to represent a chemically aggressive and cyclic moisture conditions relevant to potential field exposure conditions.

5.2.2 Flexible Wall Permeameter Setup

Figure 5.1 shows a conceptual diagram of the FWP device (GDS Instrument, UK) used in this study. All tests were conducted following ASTM D5084 (2016). Porous stones were placed on the bottom stainless-steel pedestal either with or without filter paper, and covered with an acrylic top cap. This assembly was wrapped by a flexible latex membrane and placed inside an acrylic cell chamber filled with tap water.

During the experiment, cell pressure was applied using pressure/volume controllers (GDS Instrument, UK) to maintain an average effective confining pressure of 35 kPa. Additional pressure controllers were used to regulate permeant pressures and flow rates in order to maintain a specified pressure gradient through the specimen. Toxic interface units (TIUs, GDS Instrument, UK) were used between the controllers and the permeant solutions to isolate the controllers from chemical exposure and avoid damage. A Bellofram diaphragm within each TIU ensures pressure transmission from the controller to the permeant solution. All fittings were made of stainless steel, and 1/8-inch diameter Teflon tubing was employed throughout the system.

The experiments were conducted in two operating modes. In the first mode, corresponding to conventional permeability testing, two pressure controllers and two TIUs were connected to the inlet and outlet of the FWP cell. This configuration was used for all source and sink experiments (Test Sets 1 and 2; Table 5.1). Hydraulic gradients were established by independently controlling pressures at the inlet and outlet. The influent suspension was introduced via the inlet TIU, while the outlet TIU was pre-injected with the same solution to facilitate concentration tracking. This pre-injected solution allowed for easier measurement of concentration changes after testing using UV-Vis spectroscopy, leveraging the method's higher sensitivity at high concentrations. Effluent concentrations were back calculated from the changes in MP concentration in the outlet TIU (details in 'Test Set 2: "Sink Experiments": FWP as sink of particles').

Given the reported concerns about this testing method's inadequacy for flow-through transport experiments, particularly its tendency to retain residual particles in the TIU and bias transport parameters (Mazzieri et al., 2015), an alternative modus operandi

was considered for column tests with porous media (Test Set 3). In this alternative method, the influent solution was introduced via an inlet TIU, and effluent was directly collected in a 12 mL glass vial at atmospheric pressure. This approach enabled time-series effluent sampling, reduced the number of experimental components, and allowed effluent MP concentrations to be measured directly rather than inferred from the MP concentration in the outlet TIU. Although this method reduces the precision with which hydraulic gradients and hydraulic conductivity can be quantified, this drawback was acceptable since the primary aim of these experiments was MP transport assessment rather than accurate permeability measurement.

Volume changes in the pressure controllers were recorded by GDSLAB v2.8.4 software (GDS Instrument, UK). For Test Sets 1 and 2, steady-state hydraulic conditions were considered reached when the absolute ratio of inflow to outflow rates remained below 1.25 (ASTM D5084, 2016). The FWP cell, TIUs and tubing were carefully cleaned after each test to avoid cross-contamination.

Preliminary tests were conducted to assess the stability of MP suspension within the inlet TIU. As the sink experiments (Test Set 2) did not exceed 40 minutes, rotational shaking using an orbital shaker was found to be sufficient to minimize settlement of particles (Figure 5.2) and was hence used in all tests. For MP transport experiments through GCL-1 hydrated with DI water, hydraulic conductivity was less than 5×10^{-9} cm/s, resulting in very slow flow rates and extended test durations. In this case, the MP suspension in the inlet TIU was replaced with fresh solutions every three days to maintain a consistent influent concentration. In addition, MP concentrations in the inlet TIU were measured before and after each test to identify any loss of MPs attributed to particle settling.

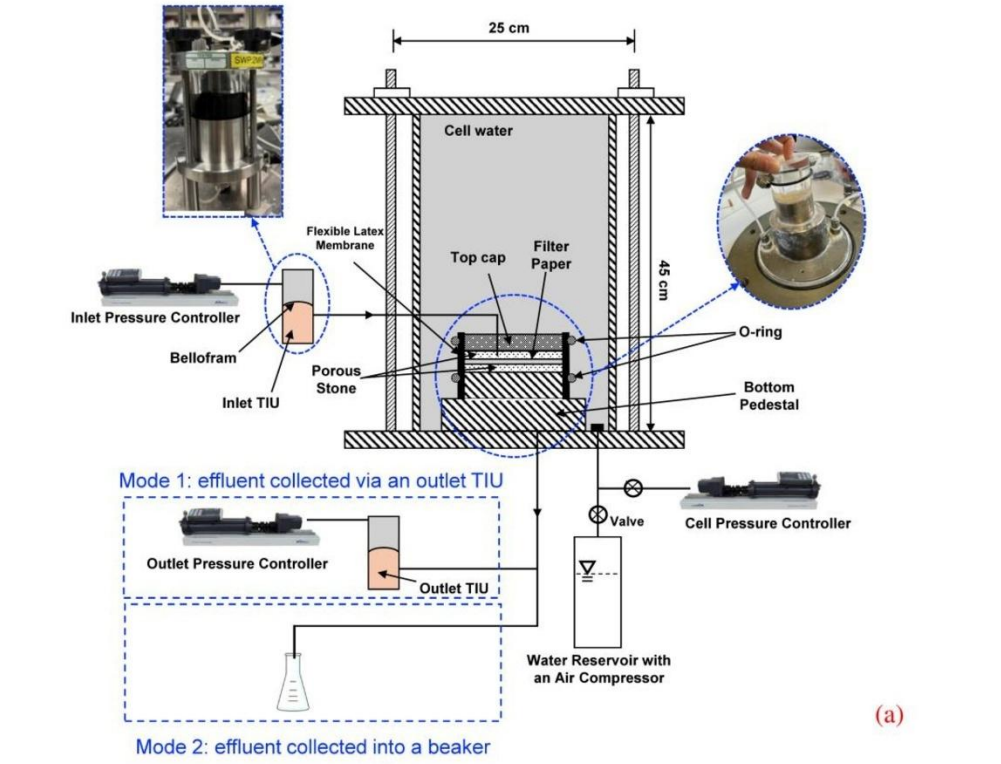

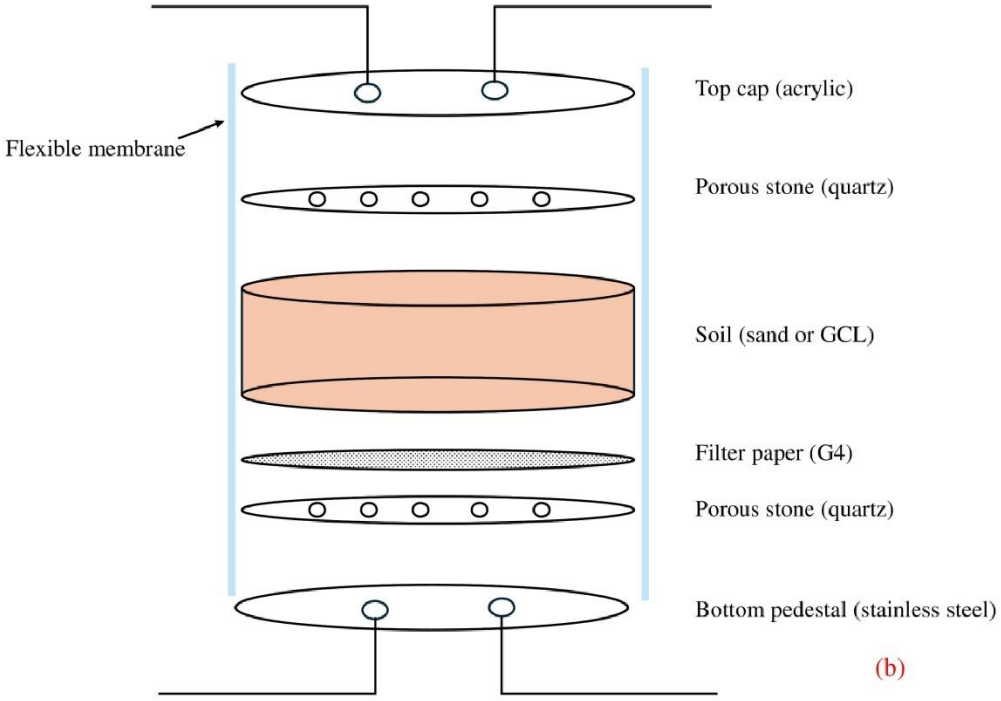

Figure 5.1. Conceptual diagram of (a) flexible wall permeameter (b) sample assembly used in this study (porous stone and filter paper were sandwiched by the top cap and bottom pedestal. The box with blue dashed line represents two modes of collection, mode 1 used for source and sink tests and mode 2 used during experiments with porous media.

Table 5.1. Source (Test Set 1) and sink (Test Set 2) experiment variables. The abbreviations G1, G4 and G42 represent Whatman® Grade 1, Grade 4, and Grade 42 filter papers, respectively. NFP means no filter paper.

test purpose (effect)	test descriptor	factor					
		MP size (µm)	MP concentration (mg/L)	permeant solution	porous stone	filter paper	pressure gradient (m/m)
Test Set 1 - Source Experiments							
base case	1a_base case	-	-	DI	quartz	G4	100
gradient	1b_i=60	-	-	DI	quartz	G4	▪ 60
	1b_i=250						▪ 250
porous stone type	1c_brass	-	-	DI	▪ brass	G4	100
	1c_bauxite				▪ bauxite		
filter paper type	1d_NFP	-	-	DI	quartz	▪ NFP	100
	1d_G1					▪ G1	
	1d_G42					▪ G42	
Test Set 2 - Sink Experiments (All tests used non-fluorescent MPs)							
base case	2a_base case	1	50	DI	quartz	G4	100
filter paper type	2b_G42	1	50	DI	quartz	▪ G42	100
	2b_G1					▪ G1	
	2b_NFP					▪ NFP	
porous stone type	2c_brass	1	50	DI	▪ brass	G4	100
	2c_bauxite				▪ bauxite		
gradient	2d_i=250	1	50	DI	quartz	G4	▪ 250
	2d_i=60						▪ 60
MP particle size	2e_0.5 µm	▪ 0.5	50	DI	quartz	G4	100
	2e_5 µm	▪ 5					
initial concentration	2f_25 mg/L	1	▪ 25	DI	quartz	G4	100
	2f_75 mg/L		▪ 75				
ionic strength	2g_0.03 M	1	50	▪ 0.03 M	quartz	G4	100
	2g_0.15 M			▪ 0.15 M			

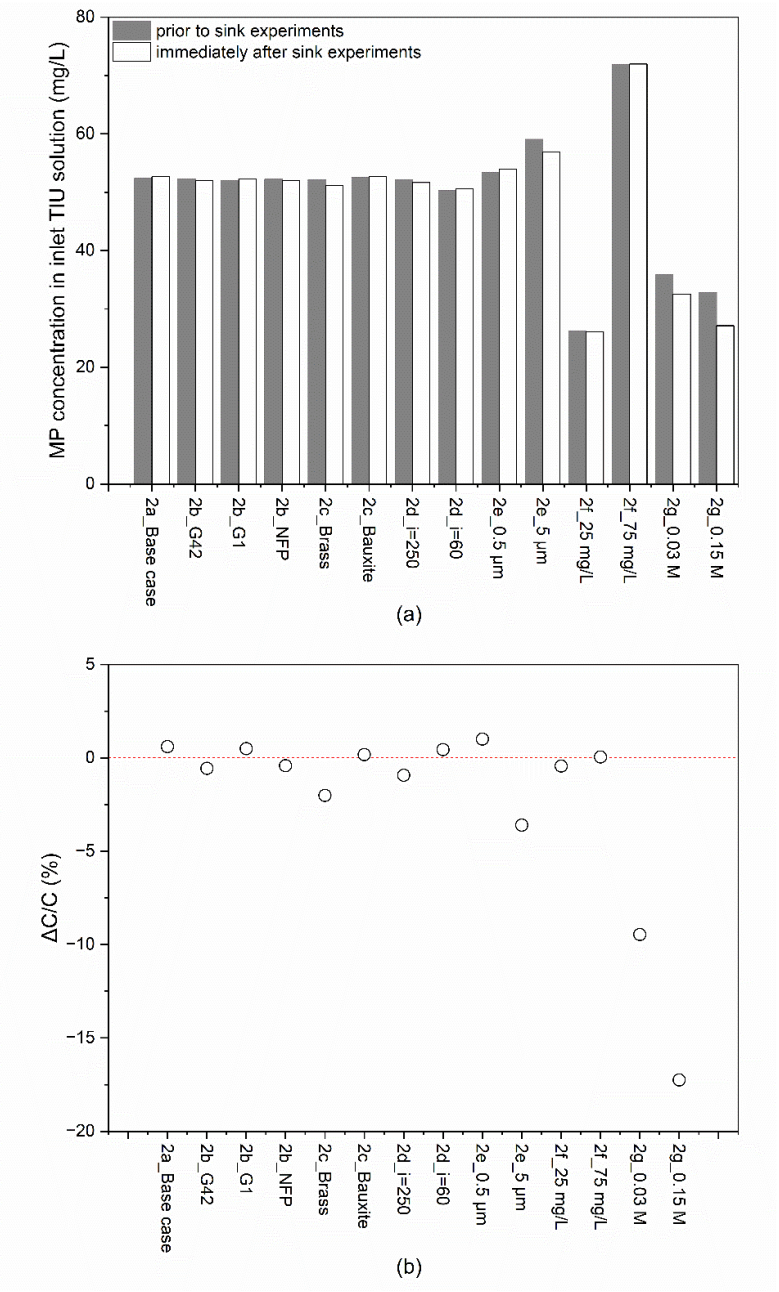

Figure 5.2. (a) MP concentrations in the inlet TIU measured immediately before and after Test Set 2: sink experiments, denoted C_{before} and C_{after}), and (b) the relative concentration change, $\Delta C/C_{before}$, where $\Delta C = C_{after}-C_{before}$, determined by UV-Vis spectroscopy. The red dotted line in (b) represents the ideal case ($C_{after}=C_{before}$), i.e., no change in MP concentration within the inlet TIU.

5.2.3 Testing Program

5.2.3.1 Test Set 1: "Source Experiments"- FWP as a Source of Particles

Source experiments were conducted to assess whether any particles or substances are

generated by the FWP that may interfere with UV-Vis measurements of MP concentrations. Tests were performed using a sample assembly consisting of filter paper and porous stones without any porous media. The effects of (a) FWP accessories (porous stones and filter papers) and (b) test conditions (pressure gradient) were tested (Table 5.1). Three commonly used cellulose filter papers (Whatman® Grades 1, 4, and 42, and referred to as G1, G4 and G42) and three types of porous stones (quartz, bauxite, and brass) were evaluated. Details of the filter papers and porous stones are provided in Table 5.2. For test conditions, three pressure gradients of 60, 100, and 250 were selected. In the base case, against which results from other test conditions were assessed, quartz porous stones, G4 filter paper, a pressure gradient of 100, and DI water as the permeant, were adopted. In each source experiment, one variable was changed relative to the base condition, resulting in a total of eight test cases.

For each test condition, DI water was placed in both inlet and outlet TIUs and a pressure gradient was applied across the assembly to generate flow between the two TIUs. The flow was maintained until the DI water in the inlet TIU ran out or the outlet TIU reached its volume capacity. At the end of every experiment, samples were collected from both inlet and outlet TIUs in glass vials, sealed and stored below 4 °C until UV-Vis spectra was measured. In addition, Raman spectroscopy was conducted on outlet TIU samples to identify any chemical changes in the permeant after testing (spectroscopy details given in Appendix X3).

Table 5.2. Description of materials used in the study.

No.	Material				Source
1.	DI water (resistivity = 18.2 MΩ·cm @ 25 °C)				Milli-Q ultrapure water purification system, University of Sydney
2.	$CaCl_2$ powder				Sigma Aldrich, Australia
3.	Polystyrene microplastics (500 nm)				
4.	Polystyrene microplastics (5 µm)				
5.	Polystyrene microplastics (1 µm)				Bioscientific Pty. Ltd., Australia
6.	**Material**	**Type**	**Pore size**	**Thickness**	Sigma-Aldrich, Australia
	Filter paper	G1	11 µm	180 µm	
		G4	20 - 25 µm	210 µm	
		G42	2.5 µm	200 µm	
7.	**Material**	**Type**	**Pore size**	**Thickness**	
	Porous stone	Quartz	250 - 550 µm	6.50 mm	Shanghai Wechance Industrial Co., Ltd, China

	Bauxite	179 μm	6.00 mm	GDS Instrument, UK
	Brass	30 μm	3.35 mm	Soil lab, University of Sydney

5.2.3.2 Test Set 2: "Sink Experiments"- FWP as Sink of Particles

Sink experiments were conducted to evaluate the extent of MP retention within the FWP apparatus. The experimental setup was similar to that used in the source experiments, except that both inlet and outlet TIUs contained MP suspensions with known initial concentrations, $C_{initial}$ [$M.L^{-3}$]. Changes in MP concentration within the TIUs were used to infer MP mass loss to the apparatus.

The effects of three groups of variables were assessed: (a) FWP accessories (porous stone and filter paper type), (b) test conditions (pressure gradient and ionic strength of solution), and (c) MP characteristics (size and concentration). Porous stones, filter papers, and pressure gradients were chosen to match the source experiments. Other commonly available hydrophilic filter materials such as glass fibre and nylon membranes were not selected because they typically have small pore sizes (<5-10 μm), which were not suitable for this study given that the MPs tested were up to 5 μm in size.

Filter paper was used selectively depending on the experimental objective. In the instrument validation experiments (Task 2 in Chapter 3), filter papers were placed both above and below the specimen to assess potential particle retention associated with the filter-porous stone assembly under a symmetric configuration. This configuration is considered conservative, as it maximises the potential for MP capture within the filter assembly. The absence of significant retention under these conditions therefore provides an upper-bound estimate of filter-related losses.

Two ionic strengths of 0.03 M and 0.15 M were prepared using $CaCl_2$. MP characteristics included three particle sizes (PS0.5, PS1, and PS5) and three concentrations (25, 50, and 75 mg/L). As with the source experiment, a base condition was established, consisting of quartz porous stones, G4 filter paper, a pressure gradient of 100, and PS1 at 50 mg/L in DI water. From this base case, each of six variables was altered one at a time. A detailed description of the test variables can be found in Table 5.1.

The sink experiments were conducted in a similar fashion to Test Set 1. In addition, after each sink experiment, porous stones and filter papers were removed, immersed in

100 mL DI water, and ultrasonicated for 10 minutes to extract retained MPs. The sonicated solution was transferred to glass vials for UV-Vis analysis to quantify MPs recovered from these components. Filter papers were air-dried in petri dishes, and a small piece from the centre of filter paper was prepared for SEM imaging (Appendix X2).

For ionic strength cases of 0.03 M and 0.15 M, given a higher risk of MP aggregation, the Teflon tubing connecting the inlet TIU to the permeameter inlet was flushed with 10 mL DI water after testing, and the flushed solution was measured to quantify MPs retained in the tubing. Although surfactants could have reduced MP aggregation, their use was intentionally excluded, as they are not standard in similar transport studies and may alter the baseline retention behaviour.

Two assessments of MP mass loss were made. First, MP concentrations in the inlet TIU were measured before ($C_{inlet\text{-}initial}$ [$M.L^{-3}$]) and after ($C_{inlet\text{-}final}$ [$M.L^{-3}$]) the experiment to detect losses within the inlet TIU (e.g., aggregation or settlement during the test). In most cases, differences between the two concentrations were very small (as discussed in the results section). The influent MP concentration leaving the inlet TIU with a volume of $V_{influent}$ was given by:

$$C_{influent} = \frac{C_{inlet-initial} + C_{inlet-final}}{2} \tag{5.1}$$

Second, a MP mass conservation statement in the outlet TIU was written as:

$$\begin{aligned} &C_{outlet-final} \times V_{outlet-final} \\ &= C_{outlet-initial} \times V_{outlet-initial} + C_{effluent} \times V_{effluent} \end{aligned} \tag{5.2}$$

where $C_{outlet\text{-}initial}$ [$M.L^{-3}$] and $C_{outlet\text{-}final}$ [$M.L^{-3}$] are the MP concentration in the outlet TIU before and after the test, respectively, $C_{effluent}$ [$M.L^{-3}$] is the average MP concentration in the effluent, $V_{outlet\text{-}initial}$ [L^3] and $V_{outlet\text{-}final}$ [L^3] are the solution volumes in the outlet TIU before and after the test, respectively, and $V_{effluent}$ [L^3] is the volume of effluent entering the outlet TIU during the test. Clearly, where the alternative modus operandi was used (no outlet TIU and no outlet pressure controller as described in section 5.2.2), $C_{effluent}$ was measured directly, and no back-calculation was needed.

$C_{effluent}$ was then used to calculate a MP mass recovery ratio:

$$\alpha_m = \frac{C_{effluent} \times V_{effluent}}{C_{influent} \times V_{influent}} \times 100\% \quad (5.3)$$

whereby a mass recovery ratio of 1 would indicate no MP retained in any of the FWP components. In addition, the ratio $V_{effluent}/V_{influent}$ for all the sink experiments was observed to be close to 1, confirming hydraulic steady state had been achieved and no appreciable leakage was present in the tests.

All source and sink experiments were conducted twice, referred to as original and repeat tests, using two identical FWP devices to assess reproducibility. For the base condition, both original and repeat tests were each performed three times to evaluate repeatability. Since the number of tests was insufficient to support detailed statistical analysis across conditions, statistical significance was not evaluated.

5.2.3.3 Test Set 3: MP Transport Experiments through Porous Media

The source and sink experiments (Test Sets 1 and 2) were conducted without a soil specimen. Test Set 3 was conducted to demonstrate the use of the FWP as a soil column with representative porous media (Table 5.3).

5.2.3.3.1 Sand-1 Column

A well-sorted, non-reactive sand (Sand-1) was chosen to minimize the likelihood of irreversible attachment of MPs to collector surfaces. This allowed MP mass recovery calculations based on effluent concentrations to be made, without having to separate MP from soil after the test. Cleaned Sand-1 was mixed with 5% DI water to increase its cohesiveness for ease of filling into the sample mould of dimensions of 50 mm diameter and 42 mm height. The porosity of the soil column was 0.40±0.01.

The FWP was set up under base case conditions of 1a and 2a shown in Table 5.1 (DI water, quartz porous stone, G4 filter paper), except that the hydraulic gradient was adjusted for flow-through transport. Effluent was collected directly at atmosphere pressure (direct collection mode in section 5.2.2).

In total, three MP transport tests were conducted. The first test used 20 mg/L PS1 with G4 filter paper. The second test used 50 mg/L PS1 under identical conditions. The third

test repeated the second one but removed the filter paper. The details of test conditions are provided in Table 5.3. In each test, the specimen was first flushed with DI water for ~4 PV to achieve fully saturated conditions. The MP suspension (20 or 50 mg/L PS1) was then permeated for 5 PV, followed by DI water elution for another 5 PV. Flow rate was maintained at 10 mL/min using a pressure controller. Effluent was collected at regular intervals and measured by UV-Vis spectroscopy.

5.2.3.3.2 Sand-2 and Sand-Clay Mixtures

A second series of transport tests was performed on Sand-2 and sand-clay mixtures to examine MP transport in more reactive and finer porous media. Sand-2 and the sand-feldspar-bentonite mixtures (50 mm diameter, 17 or 42 mm height) were prepared by mixing with DI water to 5% gravimetric water content, sealing and equilibrating overnight. Cylindrical specimens were then compacted to an average void ratio of 0.36±0.2 and installed between quartz porous stones (nominal pore size 250-550 μm). A single G4 filter paper (nominal pore size 20-25 μm) was placed beneath the specimen (between the lower porous stone and the specimen) to retain detached fines, while no filter paper was placed on top of the specimen. A cell pressure of 50 kPa was applied to provide confinement (Weerasinghe et al., 2021).

Given the particle size distributions of Sand-2 and powdered bentonite (section 3.2.2), there is a pronounced size gap between approximately 5 and 53 μm. Preliminary tests on Sand-2 and 1% bentonite mixtures exhibited significant leaching of fine particles during permeation. To address this internal instability, 5% feldspar was introduced as an intermediate-sized filler to bridge the gradation gap. Further tests confirmed that particle loss from the Sand 2-feldspar-bentonite mixture was greatest within the first PV, declining rapidly afterwards, with a total soil loss of ~ 45 mg out of the total ~142 g of soil sample. Assuming that all leached particles are bentonite, this loss was still only around 3.2% of the added clay, which shows that the addition of feldspar effectively promoted retention of bentonite within the sand skeleton, allowing the formation of a more stable soil matrix.

Five tests were conducted: Sand-2 only (with one repeat), Sand-2 and feldspar (with one repeat), and sand, feldspar and 1% bentonite. For Sand-2 only and Sand-2 and feldspar (no bentonite), flow was controlled at 4.17 mm^3/s (0.25 mL/min) using a pressure controller. When 1% bentonite was included, a constant head of 30 kPa was applied due to the much

lower hydraulic conductivity. Sand-2 only and sand-feldspar mixture specimens had a height of 42 mm, whereas the sand-feldspar-bentonite specimen height was reduced to 17 mm.

The smaller height for the bentonite-containing specimen was adopted to reduce interruptions associated with TIU refilling. Given the slower times of transport, a larger PV number of MP influent was applied in order to observe the breakthrough more clearly. Because the TIU capacity was 200 mL, the influent MP suspension had to be refilled periodically, during which flow was temporarily stopped and then restarted by increasing inlet pressure to the target value of 30 kPa. When the TIU ran dry overnight, the system remained pressurised at 30 kPa at the top, but no flow occurred until the TIU was refilled, and the test was restarted the following day. A smaller specimen height resulted in a smaller pore volume, thereby increasing the number of PV delivered per TIU filling and reducing the frequency of interruptions (three interruptions over the test duration), minimising their influence on the observed BTCs.

5.2.3.3.3 GCL Columns

GCL-1 specimens were selected as representative low-permeability porous media. Two pretreatment conditions were applied: (1) pre-hydration in DI water for seven days, and (2) two wet-dry cycles, each involving immersion in 0.1 M $CaCl_2$ followed by air drying, with each cycle lasting seven days. After cycling, specimens were rehydrated in $CaCl_2$ for three days prior to MP transport testing in the FWP. The gravimetric water contents after pretreatment were 163% (DI water-hydrated) and 96% ($CaCl_2$-hydrated), with corresponding void ratios of 0.90 and 0.73. The direct collection mode of effluents was adopted (see section 5.2.2 above for details).

MP transport tests were conducted using PS0.5 to increase the likelihood of breakthrough. A concentration of 50 mg/L PS0.5 was used in both tests. G4 filter paper was placed only beneath the GCL (between the specimen and the FWP pedestal). Test conditions are provided in Table 5.3. For the DI-hydrated specimen, 3 PV of PS0.5 suspension was permeated under a constant top pressure of 30 kPa. For the $CaCl_2$-hydrated specimen, the test began with 20 PV of DI water, followed by ~ 10 PV of PS0.5 suspension, and eluted by an additional 7 PV of DI water. A constant flow rate of 15 mL/hour was maintained, with top pressure not exceeding 30 kPa.

Table 5.3. Experimental program of Test Set 3 (MP transport experiments through porous media).

test descriptor		factor					
		sample height (mm)	**MP type & size**	**MP concentration (mg/L)**	**permeant solution**	**porous stone**	**filter paper**
Sand-1	wet-mixed with DI water	44.75	PS1	20	DI	quartz	G4
		44.48		50			G4
		44.49		50			NFP
Sand-2	wet-mixed with DI water	44.43	f-PS0.5	25	DI	quartz	G4
		44.33					
Sand-2 and feldspar mixture	5% feldspar wet-mixed with DI water	40.64	f-PS0.5	25	DI	quartz	G4
		41.71					
Sand-2, feldspar and BT mixture	5% feldspar, 1% BT wet-mixed with DI water	17.52	f-PS0.5	25	DI	quartz	G4
DI-water hydrated GCL	DI water pre-hydrated	10.76	PS-0.5	50	DI	quartz	G4
$CaCl_2$-hydrated GCL	0.1 M $CaCl_2$ pre-hydrated and air-dried in two cycles	6.58	PS-0.5	50	DI	quartz	G4

5.3 Results and Discussion

5.3.1 Test Set 1: Source Experiments

Source experiments were conducted to evaluate potential particle leaching that could interfere with the assessment of MP particles. Figure 5.3 shows the UV-Vis spectra of samples collected from solutions in pre- and post-experiment inlet and outlet TIUs. In all cases, there was negligible absorbance at wavelengths exceeding 340 nm. However, a significant increase in absorbance was observed at wavelengths below 340 nm for all source experiments (Figure 5.3). The increases in absorbance value are likely attributable to solutes/suspended particles leaching from the device. Notably, UV-Vis spectra of samples collected from the inlet TIU yielded similar results, suggesting that the modified composition of the solution is predominantly due to leaching from the TIU, rather than from

other permeameter components such as Teflon tubing, porous stone, or filter paper. For further confirmation, the liquid samples in outlet TIU were analysed using Raman spectroscopy, which revealed no visible evidence of identifiable plastic particles (Figure 5.4).

The UV-Vis spectra of PS0.5, PS1 and PS5 exhibited peaks at 279, 438 and 246 nm, respectively (Figure 5.5). This meant that the increase in absorbance at wavelengths below 340 nm, noted from the source experiment, could cause interference with concentration measurements of PS0.5 and PS5. To overcome this issue, alternate wavelengths above 340 nm were selected for PS0.5 and PS5. A 754 nm wavelength was selected for PS5 as it has a similar absorbance intensity as that of 246 nm. The UV-Vis spectra of PS0.5 showed two absorbance peaks (Figure 5.5), but both were affected by TIU. An alternate 438 nm wavelength was selected to measure concentration. The selection of wavelength at non-peak absorbance has been used in a previous study which have been shown to be effective (Tan et al., 2011). This adjustment did not compromise accuracy, as the sensitivities (slopes of the calibration curves) remained comparable (Figure 3.7).

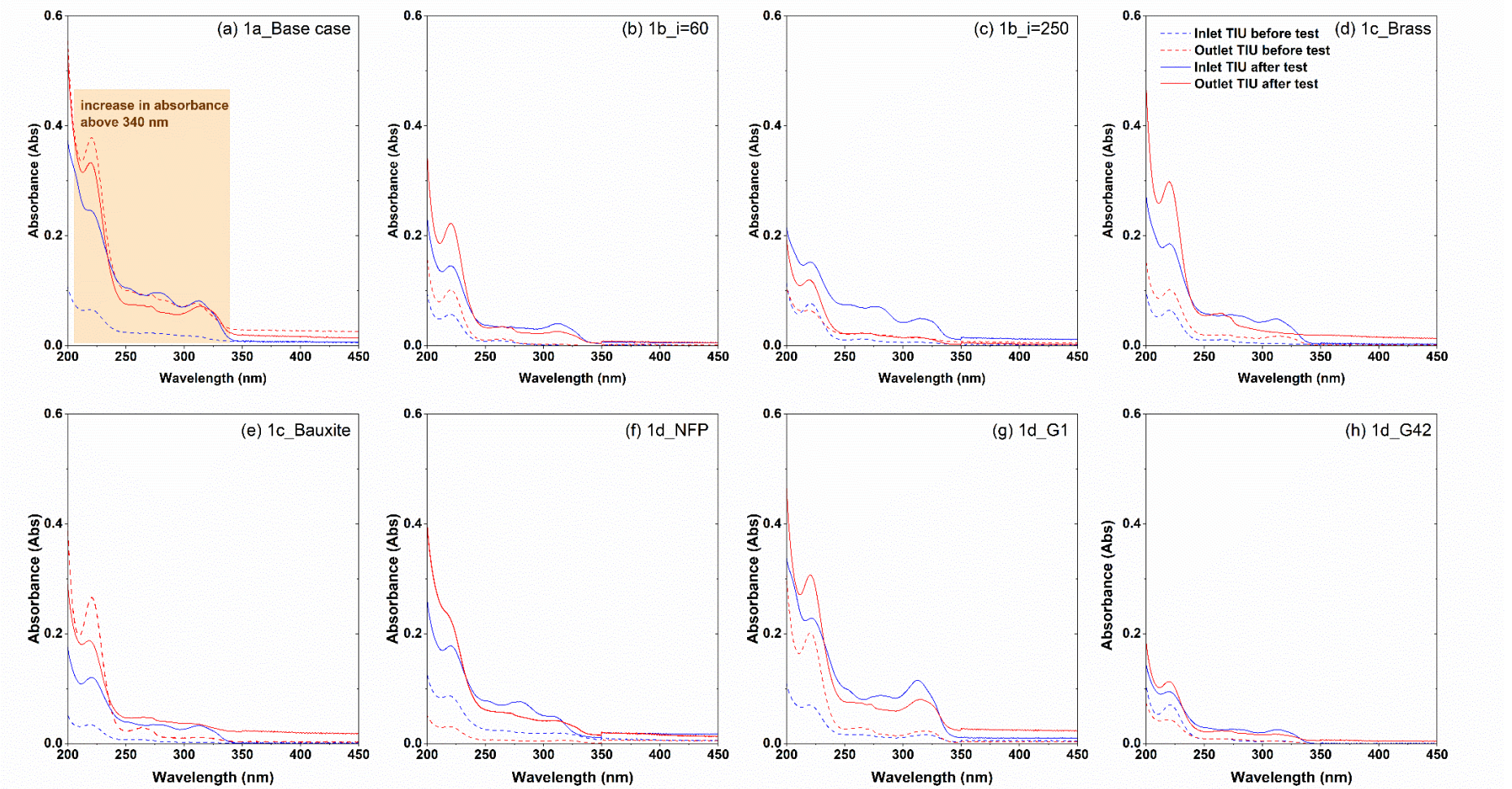

Figure 5.3. UV-Vis spectra illustrating the variation in absorbance values with wavelength for solutions collected from inlet (blue) and outlet (red) TIUs post-experiment of Test Set 1: source experiments (a) 1a_base case (b) 1b_i=60 (c) 1b_i=250 (d) 1c_Brass (e) 1c_Bauxite (f) 1d_NFP (g) 1d_G1 (h) 1d_G42. The dotted lines represent the changes in the absorbance spectra before DI water permeation.

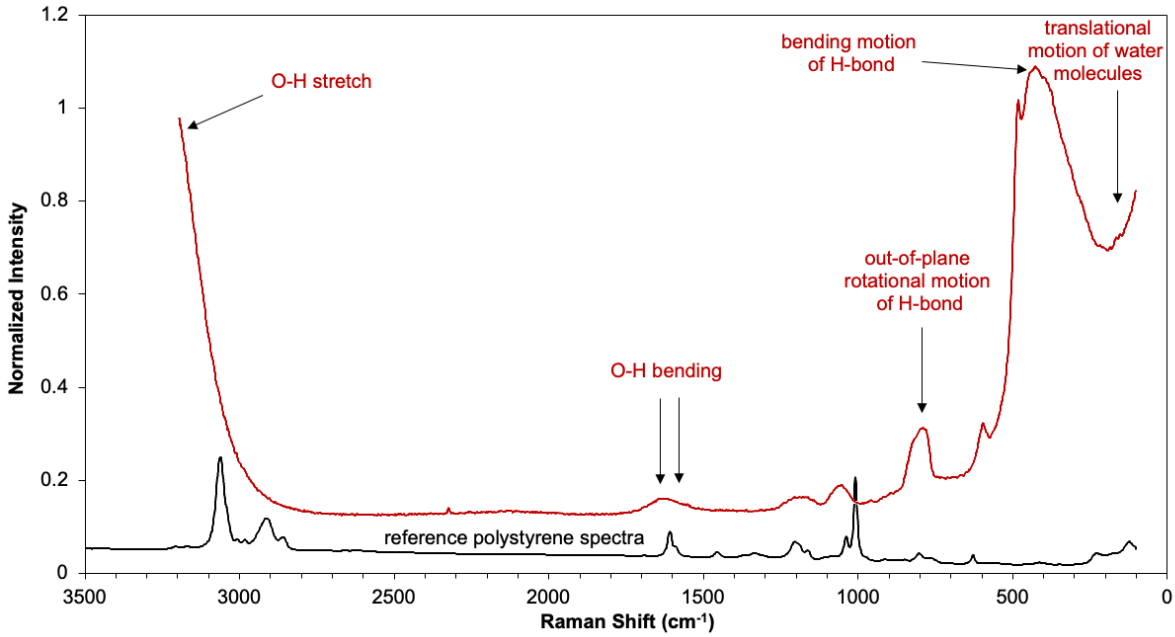

Figure 5.4. Raman spectra (in red lines) of samples collected from the outlet TIU of the source experiment (Test Set 1): 1a_base case. The spectra of a polystyrene standard (black line) is included as a reference for comparison with the Raman spectra from the sample in outlet TIU.

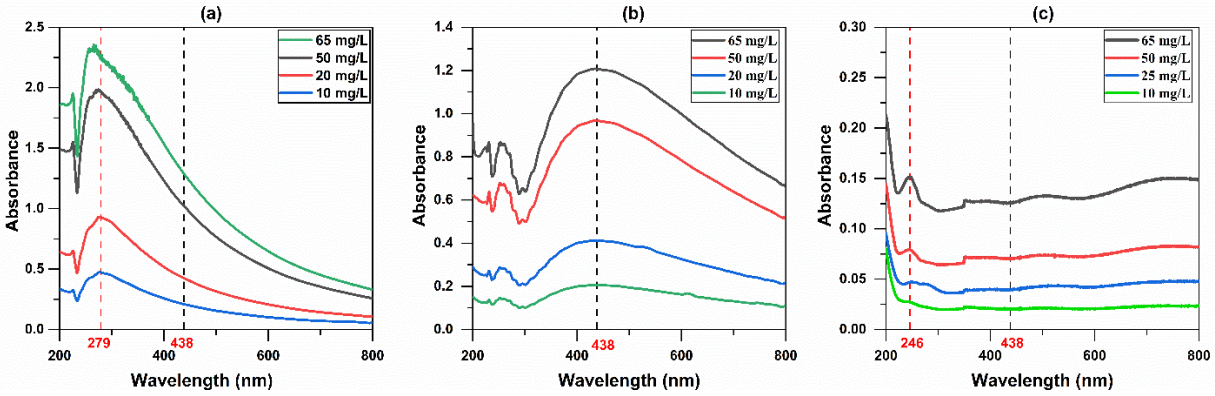

Figure 5.5. UV-Vis spectra of (a) PS0.5, (b) PS1, and (c) PS5.

5.3.2 Test Set 2: Sink Experiments

5.3.2.1 Repeatability and Base Case

Table 5.4 and Figure 5.6 present the mass recoveries, mass losses and mass recovery ratios α_m for various sink experiments. Figure 5.6 shows good repeatability, with two exceptions related to G42 filter paper (Figure 5.6a) and ionic strengths of 0.03 M and 0.15 M (Figure

5.6f) which will be discussed further below. In the base case, 80% mass recovery of MP was achieved in the effluent as shown in Figure 5.6a (average of two repeats), with 62% of lost MP extracted from the filter paper and porous stone after the test by sonication (Table 5.4). Given that very little MP was found in the washout solution of tubes, it is likely that at least part of the unaccounted-for lost MP may have settled in the inlet and/or outlet TIUs and hence was not captured by concentration measurements. The effects of different variables are discussed next.

5.3.2.2 Effects of Filter Paper

Figure 5.6a demonstrates that, in the best scenario, up to 10% of MP mass in 2a_Base case was likely held by the G4 filter paper (20-25 μm pore size), since the experiment without filter paper had yielded 91% mass recovery in the effluent. The observed average α_m of the original and repeat tests were 29% for G42, 76% for G1, and 80% for G4. Figure 5.7 shows SEM images of the G4 filter paper used in sink experiment 2a_Base case after ultrasonication in DI water. Given that the nominal pore sizes of G42, G1 and G4 filter papers are significantly larger than PS1 particles (Table 5.2), the reduction in mass recoveries is likely attributable to physical straining rather than electrostatically induced attachment. This is because the filter material is cellulose which is hydrophilic and becomes slightly negatively charged when in contact with water at neutral pH (Herrington and Petzold, 1992). The MPs used in this study had a zeta potential of approximately -30 mV, making electrostatic attractions unlikely. Further investigations focusing on filter papers are recommended to differentiate between physical straining and electrostatic adsorption to better elucidate the dominant mechanisms governing MP retention by filter paper and possibly develop ways of mitigating them.

Table 5.4. Retained and recovered mass of MP in Test Set 2: sink experiments (the values for "2a_base case" are the average values from three repeat tests with standard deviation shown in brackets).

	A	B	C	D	E	F	G
test number	MP mass transported from inlet TIU through the sample during the test (mg)	total MP mass recovered in the effluent (mg)	total MP mass retained in FWP (A-B) (mg)	MP mass "lost" (aggregated and/or settled) in the inlet TIU (mg)	MP mass extracted from porous stone and filter paper by ultrasonication after the test (mg)	percentage of total MP mass recovered in the effluent relative to total mass passing through permeameter (B/A) (%)	percentage of MP mass extracted from porous stone and filter paper by ultrasonication after the test relative to total mass retained in the permeameter (E/C) (%)
2a_base case	7.50 (±0.086)	5.99 (±0.33)	1.51 (±0.24)	0.00 (±0.005)	0.94 (±0.49)	80	62
2b_G42	7.36	1.48	5.88	0.03	2.42	20	41
2b_G1	7.85	5.59	2.26	0.00	0.90	71	40
2b_NFP	7.98	7.31	0.67	0.02	0.32	92	48
2c_brass	7.62	6.53	1.09	0.11	0.45	86	41
2c_bauxite	8.34	6.92	1.42	0.00	1.10	83	77
2d_i=250	8.15	7.11	1.04	0.05	0.58	87	56
2d_i=60	7.90	6.67	1.23	0.00	0.38	84	31
2e_0.5 µm	8.29	7.19	1.10	0.00	0.57	87	52
2e_5 µm	8.99	1.45	7.54	0.23	2.86	16	38
2f_25 mg/L	4.14	3.04	1.10	0.01	0.30	74	27
2f_75 mg/L	10.99	9.39	1.60	0.00	0.90	86	56
2g_0.03 M	5.18	0.26	4.92	0.37	1.25	5	25
2g_0.15 M	4.69	0.20	4.49	0.58	1.10	4	25

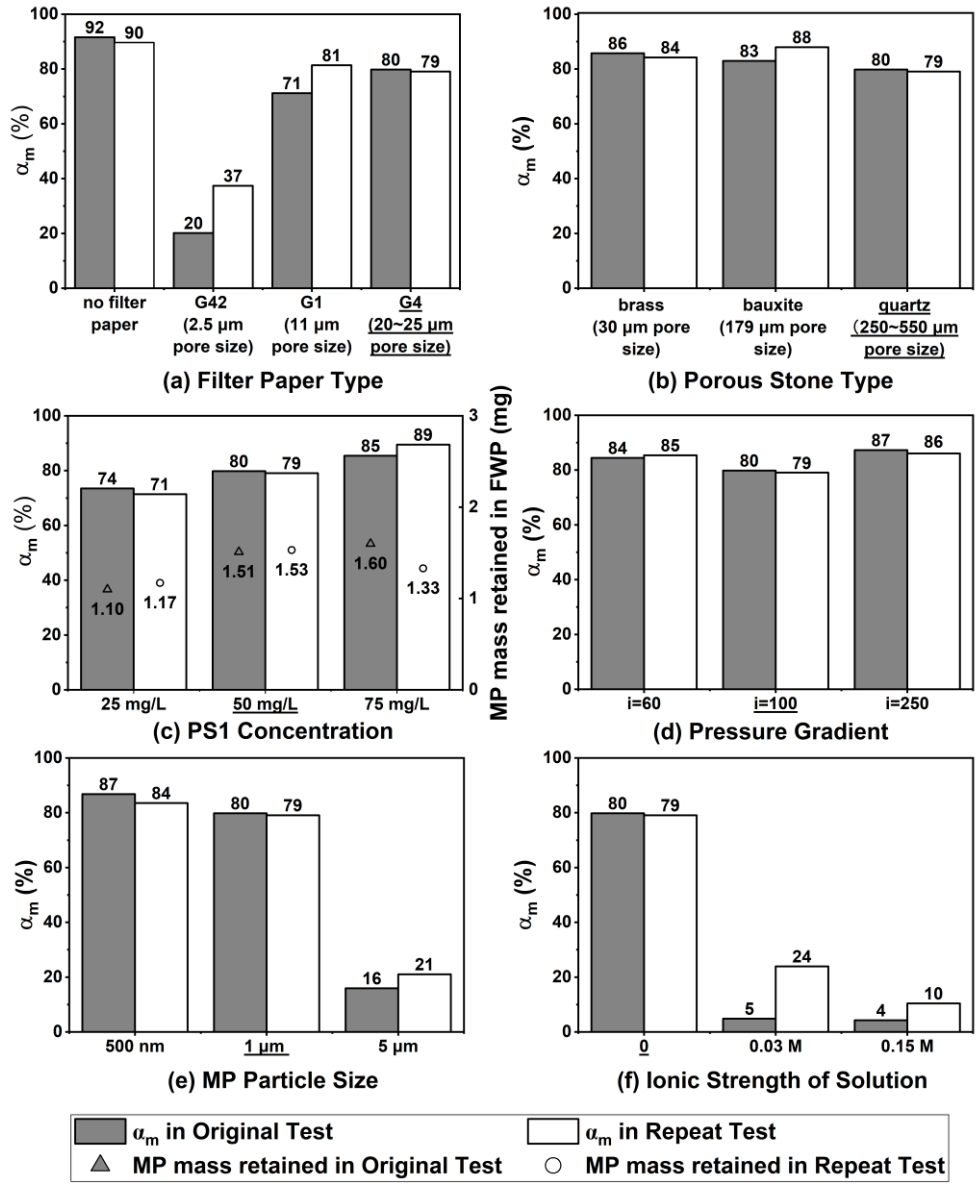

Figure 5.6. Mass recovery ratio α_m for Test Set 2: sink experiments: effects of (a) filter paper type (b) porous stone type (c) MP concentration (d) pressure gradient (e) MP size (f) ionic strength of solution (the original and repeat tests were conducted using the same procedures and materials in two separate but identical FWP devices acquired at the same time from the same manufacturer; the underlined factor on the x-axis in each image represents the variable in base case).

5.3.2.3 Effects of Porous Stone Type

Figure 5.6b shows the effects of different types of porous stone on α_m. In the base case, a quartz porous stone is used, yielding α_m =80%, compared to 85% and 86% for brass and bauxite, respectively. This relative similarity in recoveries was observed despite the fact that the pore sizes of bauxite and quartz were approximately 5-10 times larger than those of brass. Porous stones are essential components in FWP, helping to prevent large particles from escaping, maintain structural integrity of the test sample and to evenly distribute flow through the specimen (Zeng et al., 2024). Appropriate porous stone type needs to be considered for various porous media. The last column in Table 5.4 shows that extracted MP mass from filter paper and porous stone accounted for 62%, 86% and 83% of the total MP mass in the influent in cases 2a_Base case, 2c_Brass and 2c_Bauxite, respectively. This is because the ultrasonication process is not capable of extracting all MP particles as demonstrated by Figure 5.7.

5.3.2.4 Effects of Initial MP Concentration

Figure 5.6c shows the effect of initial MP concentration on mass recovery ratio. Total mass recovered in the effluent, is shown here, in addition to α_m, because, in this case the denominator of equation 5.3 is different for each of the three different cases owing to different initial concentrations. Figure 5.6c shows a clear trend of increasing α_m with increasing concentration (73%, 80%, 87% for influent concentrations of 25, 50 and 75 mg/L, respectively). The trend is reversed for total MP mass retained in the FWP (right-hand side vertical axis of Figure 5.6c) (except for test 2f_75mg/L of the repeat test). This is reasonable because a higher concentration introduces a larger number of MP particles into the device, increasing the likelihood of particle collisions during migration and their retention within the FWP compartments, even if they remain lower as a percentage of total mass travelling through the system. The concentrated MP solutions have the potential to promote agglomeration and settlement, resulting in the straining of MP particles in the pore spaces of porous media (Yu et al., 2022). On the other hand, using a higher initial concentration in column experiments could produce a UV-Vis spectrum with a greater signal-to-noise ratio, hence yielding more accurate results.

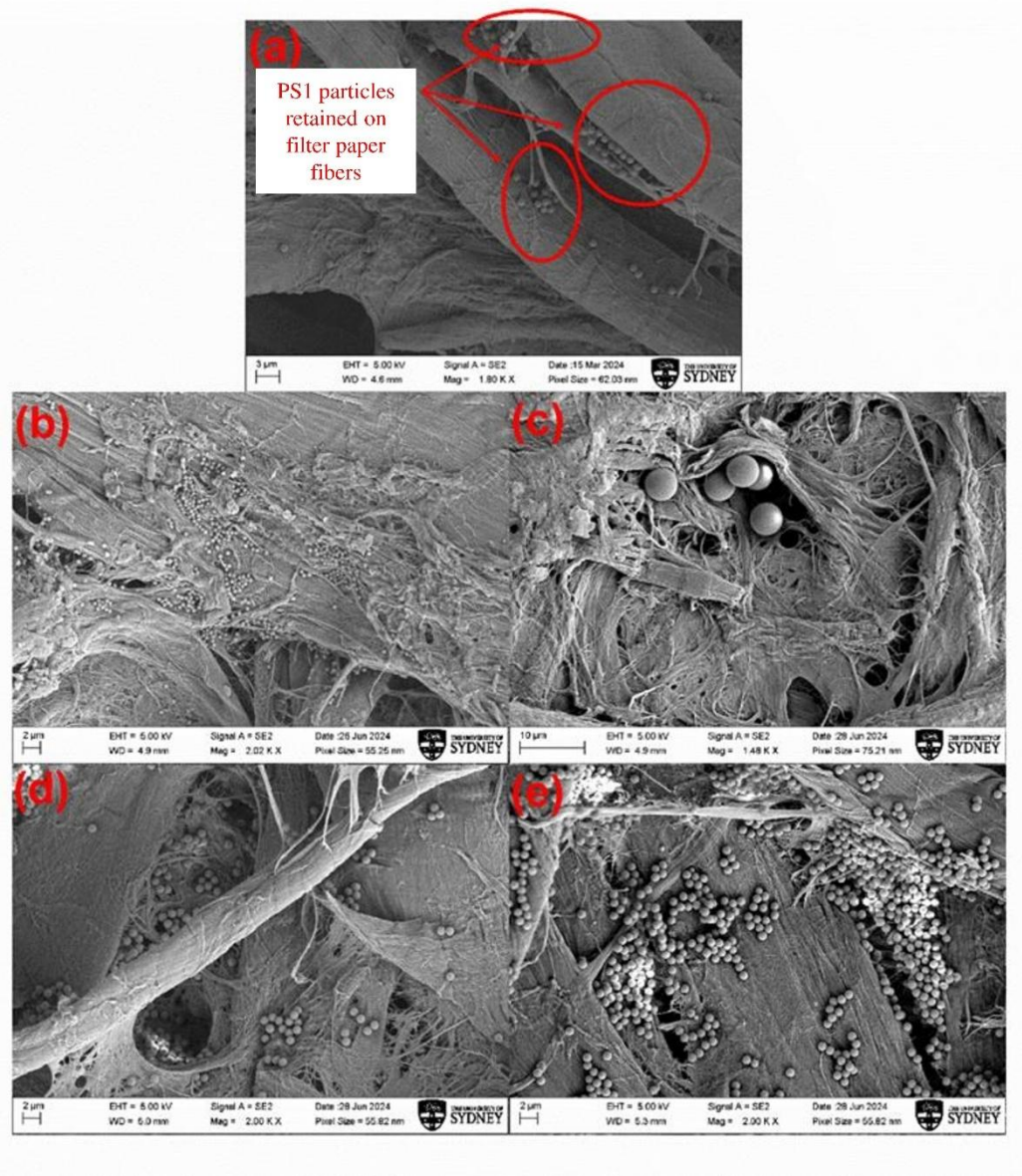

Figure 5.7. SEM images of the G4 filter paper in the Test Set 2: sink experiments under the test conditions of (a) 2a_base case (b) 2e_0.5 µm (c) 2e_5 µm (d) 2g_0.03 M (e) 2g_0.15 M. The images show unextracted MP particles in the filter paper by ultrasonication after sink experiment.

5.3.2.5 Effects of Pressure Gradient

In low-permeability soils, small poorly connected pore networks, capillary forces and adsorption to particle surfaces can resist water movement. Experimentation with such soil often requires high pressure gradients to facilitate movement of water and thereby enhance advective transport of MPs. Figure 5.6d shows α_m under three different pressure gradients

using quartz porous stone and G4 filter paper. The results indicate no significant variation in mass recovery ratios, which ranged from 80% to 87%. Due to the absence of soil between the porous stone and filter paper assembly, the flow rate remained high, even at the lowest gradient used (60). The findings suggest that approximately 15% to 20% of MP were lost within the FWP device, a loss that cannot be mitigated solely by increasing the pressure gradient. Conversely, a low-pressure gradient can lead to a slow flow rate, causing potential MP settlement and/or retention in the Teflon tubing of FWP. This is one of the reasons why careful mass balance assessment, similar to the sink/source experiments reported here, needs to be made under the specific conditions of the material and test scenario under consideration.

5.3.2.6 Effects of MP Particle Size

The sink experiment (Test Set 2) using PS0.5 achieved the highest α_m at 85% among the three tested sizes, followed by 80% for PS1 and 18% for PS5 (Figure 5.6e). It was observed that 38% of the total retained particles were extracted from the quartz porous stone and G4 filter paper for PS5 (Table 5.4). The significant reduction in α_m for PS5 can be attributed to their larger size, which leads to MP settlement in inlet TIU (column D of Table 5.4 and Figure 5.8) and retention at the pore mouths of the filter paper (Figure 5.7c). In addition, the density of MP particles is 1.05 g/cm^3, only slightly greater than DI water. Despite having similar specific gravity, larger MP particles tend to settle faster than smaller particles (Zhao et al., 2022), contributing to increased MP loss in the FWP system, especially in the inlet and outlet TIUs.

5.3.2.7 Effects of Ionic Strength

As stated above, smaller concentrations than the prepared value (50 mg/L) were obtained at 35.9 and 32.8 mg/L for 0.03 M and 0.15 M ionic strength (IS) based on UV-Vis measurement, respectively. The increase in IS leads to particle aggregation and increase in particle size, resulting in fewer particles at the same mass concentration and thus less absorbance of visible light. This trend was confirmed by the UV-Vis measurements of particles of different sizes at the same concentration (Figure 5.8).

The results indicated mass recoveries below 20% for both 0.03 M and 0.15 M IS, likely due to two factors, namely a) agglomeration and settlement of MP particles in the inlet and outlet TIUs during the tests and b) agglomerated MP particles blocking preferential pathways in the filter paper and porous stones (Figure 5.7). However, very little amount of MP was observed in the tubing (0.24% and 0.08% for 0.03 M and 0.15 M cases in the Test Set 2: sink experiment), demonstrating that the tubing does not seem to contribute the MP loss in the FWP device even under high IS of solution. In addition, significant variability in α_m was observed across repeated experiments under 0.03 M and 0.15 M IS. In these cases, secondary phenomena such as aggregation and/or settling were evident, both of which are time-dependent processes. Variations in the duration of the experiments and the time elapsed before analysis likely contributed to the observed variability. One way to overcome this issue is to use surfactants which can be helpful to stabilize the suspended MP particles and provided they do not interfere with the experimental outcomes (Sun et al., 2022). The other approach to deal with the issue is to find alternative concentration measurement methods that can measure different MP sizes concurrently.

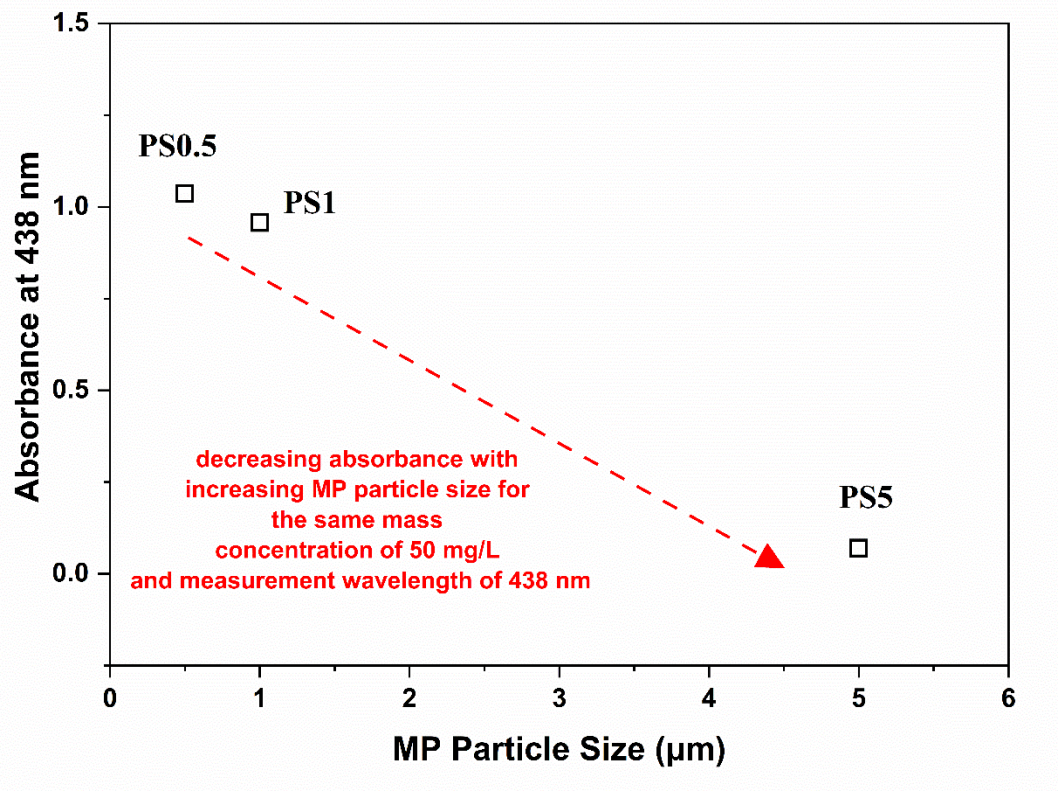

Figure 5.8. Effects of MP size on UV-Vis absorbance.

5.3.3 Test Set 3: MP Transport Experiments through Porous Media

5.3.3.1 Sand-1 Column

In the two tests in which filter paper was included, a spike in effluent MP concentration is observed at the beginning of the second stage of the experiment when MP-solution is ceased, and DI water is introduced (Figure 5.9). This is most likely due to the flushing of MP particles previously held by the filter paper upon application of DI water. This hypothesis is supported by the third test in which no filter paper is used, and no such spike observed.

The mass recovery ratios from the three tests are calculated as 80%, 71% and 99%, respectively. This is broadly consistent with results from the sink tests and confirms that a) FWP appears to be suitable for conducting soil column experiments on small MP and NP and b) even large-porosity filter papers can hold a non-negligible mass of small MPs. Finally, given that no outlet TIU has been used in this case, the high recovery rate in the third test, when no filter paper is used, indicates that a proportion of MP during the sink experiments may have settled in the outlet TIU and was hence not captured in measurements of MP concentration in effluent samples.

5.3.3.2 Sand-2 and Sand-Clay Mixtures

For Sand-2 only specimens, the normalised BTCs (Figure 5.10a) exhibited rapid breakthrough and relatively high effluent concentrations. C/C_0 increased to ~0.93 and remained near this plateau for approximately one PV. DI water flushing commenced at 2.71 and 2.51 PV for the original and repeat tests, respectively, after which concentrations declined during the elution stage. The two BTCs are in good agreement, demonstrating good repeatability of MP transport response in the coarse-grained Sand-2 under the applied hydraulic conditions. The relatively high plateau suggests limited MP retention.

Introducing 5% feldspar produced a modest but consistent change in breakthrough behaviour (Figure 5.10b). Peak C/C_0 values decreased to ~0.65, indicating enhanced MP retention and retardation relative to Sand-2 only. Duplicate experiments were again closely aligned, suggesting that the sand-feldspar mixture remained structurally stable during permeation. These results imply that the added feldspar likely created a more tortuous pore network and provided additional surface area for MP attachment. Despite this enhanced

retention, flow remained relatively unimpeded with hydraulic conductivity remaining on the order of 10^{-7} m/s.

Adding a small amount of bentonite (1% by dry mass) to the sand-feldspar mixture produced a much stronger reduction in MP mobility. Under this condition, the specimen height was reduced to 17 mm, and the hydraulic conductivity was very low (~2×10^{-9} m/s). Breakthrough was highly retarded, and effluent concentrations were strongly attenuated (Figure 5.11). C/C_0 remained below 0.12 throughout the test (Figure 5.11 inset). These results indicate that even a low bentonite dosage can significantly enhance MP retention under low-permeability conditions.

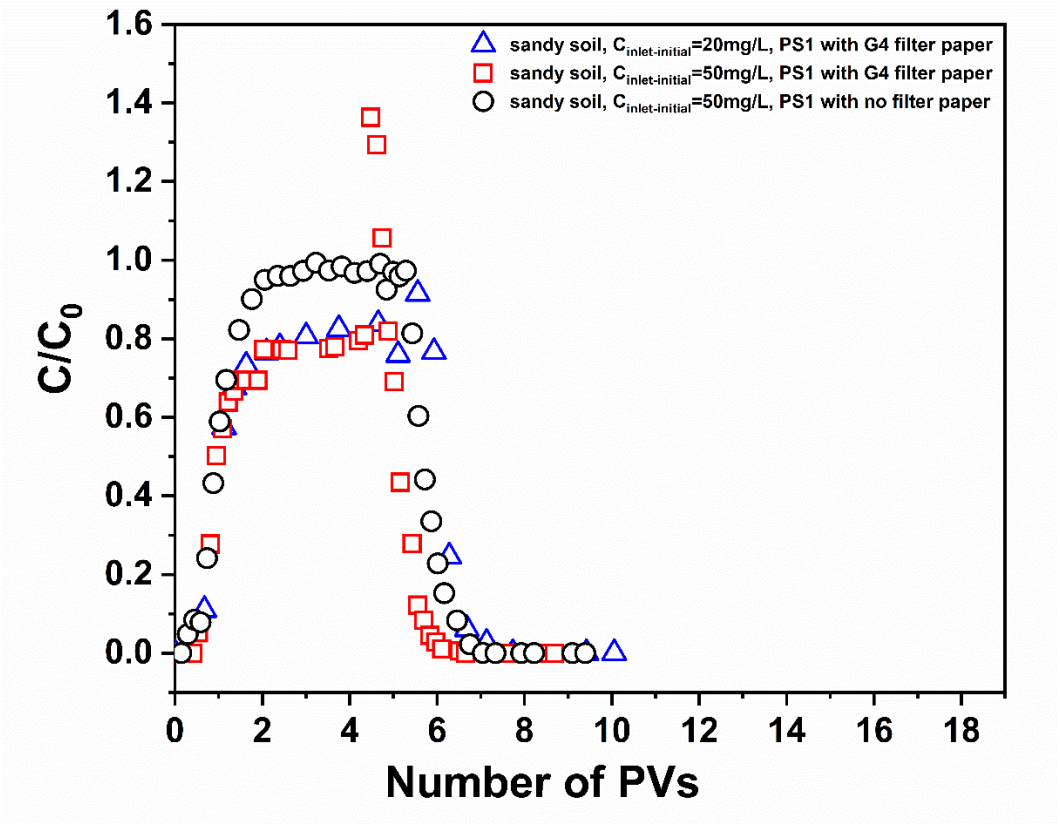

Figure 5.9. Change in normalized PS1 concentration with the number of PV in Sand-1 obtained from Test Set 3. The PS1 suspension was flushed through each sample for 5 PV, followed by permeation with DI water for another 5 PV. Flow rate throughout the test was constant at 10 mL/min.

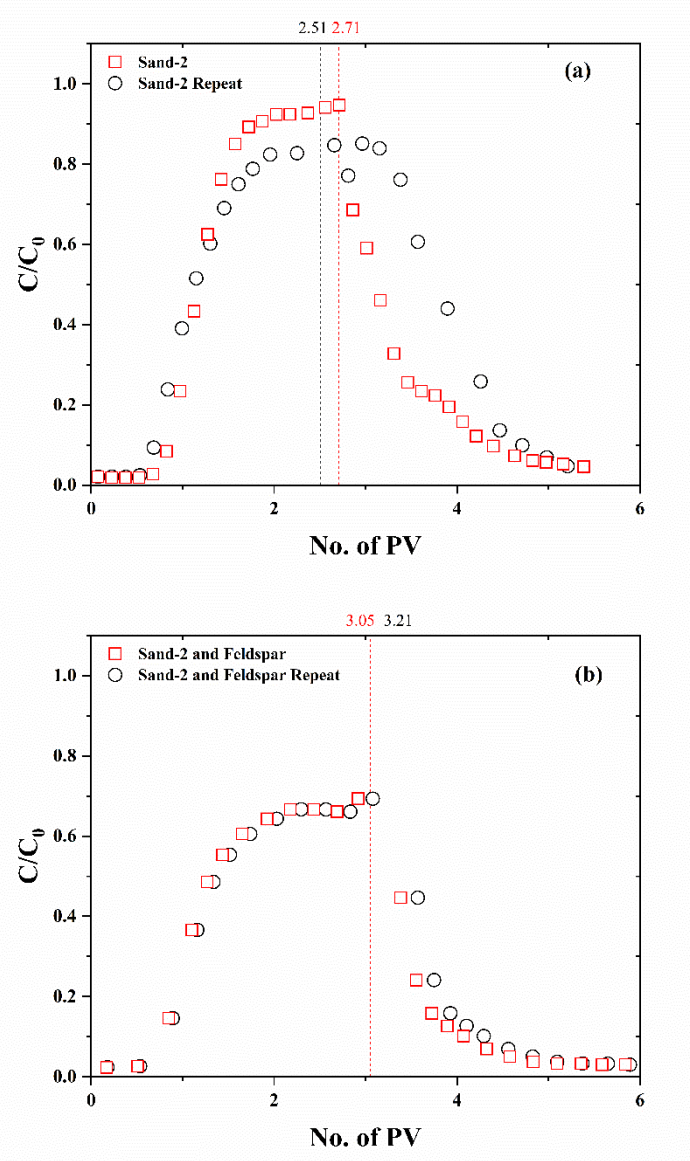

Figure 5.10. BTCs for (a) Sand-2 (duplicate tests) and (b) Sand-2 with 5% feldspar (duplicate tests) showing normalised effluent concentration (C/C_0) versus the number of PV. Vertical dashed lines indicate the transition from MP influent to DI water.

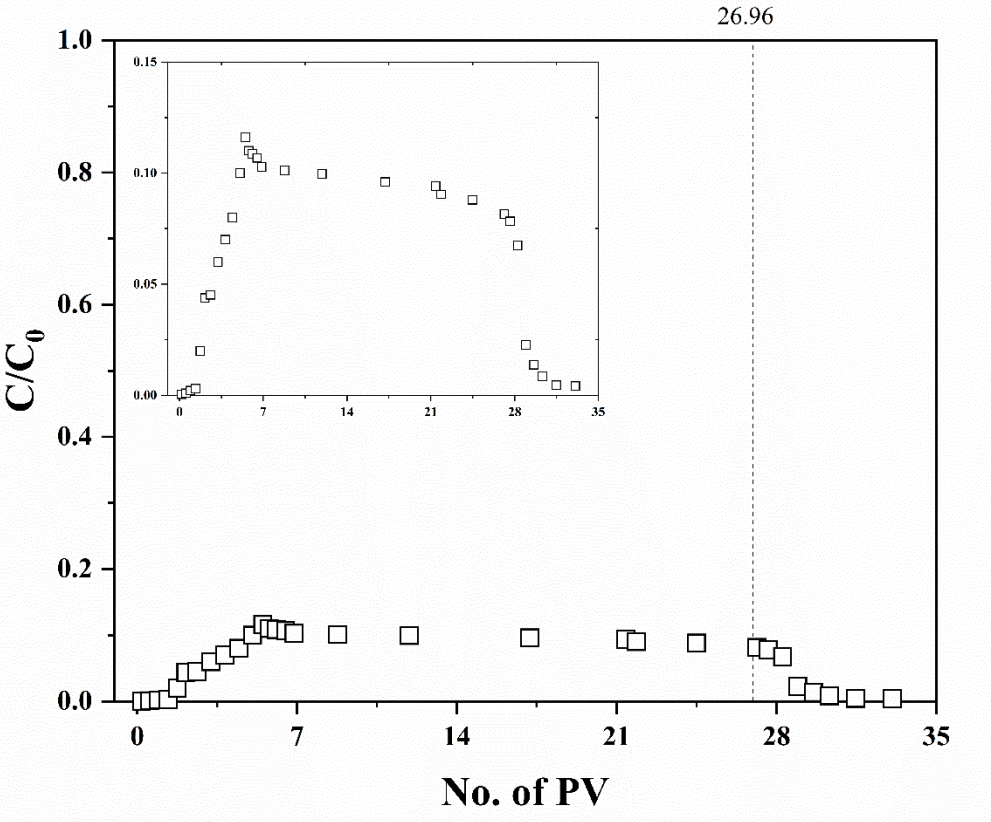

Figure 5.11. BTC for Sand-2 with 5% feldspar and 1% bentonite with reduced specimen height of 17 mm. The inset shows an expanded view of the low-concentration region ($C/C_0 \leq 0.15$) to highlight breakthrough behaviour and tailing. The vertical dashed line at 26.96 PV indicates the end of MP injection (i.e. the start of the DI water elution stage).

5.3.3.3 Geosynthetic Clay Liners

Soil column tests with DI-hydrated GCL, effluent concentrations remained below detection limit by UV-Vis, after 3 PV. The hydraulic conductivity was measured at 8.5×10^{-9} cm/s, confirming its effective performance as barrier under ideal DI pre-hydration. The GCL likely restricted MP migration by reducing pore connectivity and enhancing particle retention (Wan et al., 2022).

In contrast, the $CaCl_2$-hydrated GCL sample exhibited observable breakthrough with stable C/C_0 plateau around 0.4 and a noticeable spike upon transition from MP solution to DI water, similar to that observed in tests on sandy soil (Figure 5.12). These results confirm the ability of the FWP to operate as a soil column for investigating MP transport through clay-rich porous media. Note that this test is reported here only to confirm the ability of

FWP to generate BTCs with bentonite-based GCLs. The next chapter reports in far more detail an extensive program of FWP column studies on MP transport through GCLs.

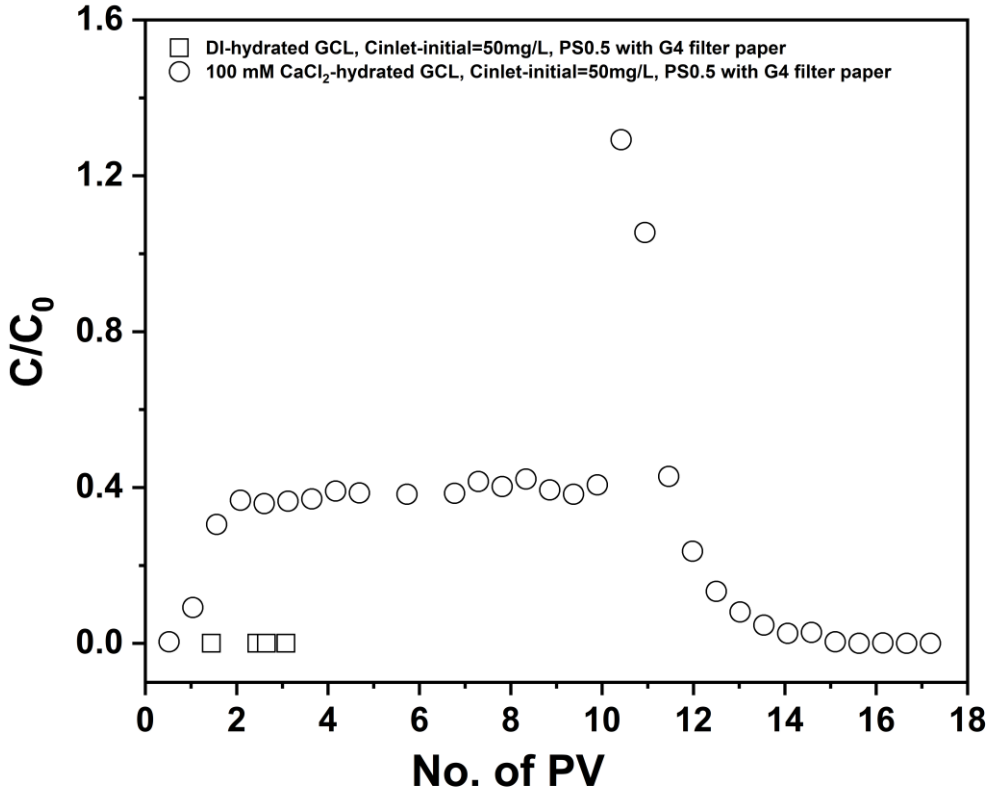

Figure 5.12. Change in normalized PS0.5 concentration with the number of PV in GCL obtained from Test Set 3. For DI water-hydrated GCL, PS0.5 suspension was flushed through the sample for 3 PV. For $CaCl_2$-hydrated GCL, PS0.5 suspension was flushed through the sample for 10 PV, followed by DI water permeation for 8 PV.

5.4 Constraints in Using FWP as Column for MP Transport Research

The FWPs have proven effective for MP transport studies; however, important factors require careful consideration. Beyond the well-documented limitations of FWPs such as their unsuitability for field conditions with minimal overburden pressure and their high cost, additional factors warrant attention.

First, careful consideration is required when selecting the sample collection method. This study demonstrates two modes of effluent collection: the conventional mode, which

uses TIUs at both the inlet and outlet, and the direct collection mode, which uses a single TIU at the inlet with samples collected at an open-to-atmosphere outlet. The choice between these modes depends on experimental priorities. If time-series sampling is critical and precise control over effective stress is not required, the direct collection mode is preferable due to its simplicity and to avoid 'dilution error' (Mazzieri et al., 2015). Conversely, the conventional mode is more suitable for experiments requiring precise control over effective stress, gradient measurement, and flow rates, although time-series sampling in this setup can be cumbersome due to the need for frequent refills. In addition, the conventional mode could introduce complexities when working with soil samples containing high clay content. As the TIUs remain sealed during the experiment, effluent accumulation carrying co-ions and nano-clay particles from the soil matrix may affect MP concentrations. MPs are particularly sensitive to changes in ionic strength and tend to attach to clay particles, leading to aggregation. This aggregation can result in larger particle sizes that settle out of the solution, which may alter concentration measurements by UV-Vis and transport parameters. As an ensemble method, UV-Vis measurements rely on a calibration curve developed using a pure MP solution. Therefore, any changes in MP size or the composition of the surrounding solution can introduce errors in the measurements. If the use of the outlet TIU is necessary, alternative techniques such as nanoparticle tracking analysis, flow cytometry, or time-resolved laser particle sizing should be considered.

Furthermore, the use of filter paper and ionic strength presents additional challenges. This study demonstrates that filter paper and use of relatively high IS leads to more MP retention and settlement. However, omitting filter paper is not always feasible, particularly with soil samples where there is risk of larger particles escaping the system. Moreover, a certain degree of MP loss appears to be inherent to such experiments; even in setups without filter paper, losses of up to ~7% were observed, likely due to the suspended nature of MPs in porous media. Similarly, under high IS conditions, particle aggregation contributed to underestimation of concentrations, partly due to the limitations of UV-Vis spectroscopy and delays in sample analysis. While this study examined a more extreme scenario, such conditions are unlikely in surface water, rainfall or groundwater-based investigations, where IS typically ranges from 0.03 to 11.6 mM (Salve et al., 2008; Rapant et al., 2017). However, in more concentrated systems such as landfill leachate, which can reach up to 90 mM, some baseline retention may occur (Kjeldsen et al., 2002). Therefore, care must be taken to

stabilize MP solutions in monodisperse experiments, or to use methods able to quantify aggregated particle concentrations.

Importantly, these factors are not exclusive to FWP systems and almost certainly affect conventional RWC setups. As such, these observations reflect broader methodological challenges associated with MP transport studies, rather than limitations unique to the FWP approach. Future studies should consider conducting baseline retention assessments, as demonstrated in this work, to quantify and account for inherent losses in mass balance calculations. Ultimately, the choice of components such as filter paper or IS of influent solutions should be guided by the specific research context, with an understanding of how these parameters may influence experimental outcomes.

5.5 Conclusion

This chapter evaluated the suitability of FWPs for investigating MP transport in low-permeability materials and established the experimental framework adopted for the subsequent GCL transport study. The validation experiments showed that reliable MP transport measurements can be achieved when appropriate apparatus components, hydraulic conditions, and sampling procedures are employed.

The results showed that porous stone type, filter configuration, tubing arrangement, ionic strength, and particle size all influence MP recovery and transport behaviour. Quartz porous stones (250-550 μm), a single Whatman® Grade 4 filter paper placed beneath the specimen, chemically inert tubing, and direct vented outlet collection were identified as the most suitable configuration for the transport experiments conducted in this thesis. Under these conditions, blank tests and sand reference columns yielded recoveries of approximately 90-98%, indicating satisfactory mass balance and limited retention artefacts.

The study further demonstrated that some degree of MP loss is unavoidable in particulate transport experiments, particularly under conditions promoting aggregation or filtration. These effects became more pronounced under elevated ionic strength conditions, where particle aggregation and settling may influence both measured concentrations and transport behaviour. These methodological challenges are not unique to FWPs and are also likely to affect conventional rigid-wall column systems.

Overall, the validated FWP configuration established in this chapter provided stable hydraulic control and reliable sampling conditions for the GCL transport experiments presented in Chapter 6. The methodology developed here therefore forms the basis for investigating the effects of pre-hydration chemistry, GCL type, and MP properties on MP breakthrough and retention under controlled stress conditions.

Chapter 6 Barrier Performance of GCL against Microplastic Migration

6.1 Introduction

GCLs are widely used as low-permeability components of composite landfill liner systems to limit leachate flux and attenuate dissolved contaminants. As reviewed in Chapter 2, landfills are now recognised as long-term reservoirs and potential sources of MPs, while the polymeric geosynthetics that comprise liner systems, including GMBs and geotextiles can themselves generate secondary MPs through chemical, thermal, ultraviolet, and mechanical degradation. Despite these emerging concerns, most research on clay-based liner performance has focused on dissolved inorganic and organic contaminants. Evidence on particulate retention remains limited, with mechanistic insights drawn mainly from ENP transport studies rather than MPs.

This chapter reports an experimental investigation of MP transport through two commercially available GCLs under idealised and chemically impacted hydration conditions (Task 3 in Chapter 3). Specimens were pre-hydrated with deionized (DI) water or $CaCl_2$ solution and, where specified, subjected to wet-dry cycling to represent chemically aggressive and cyclic moisture exposure relevant to field service. BTCs were generated using FWPs to quantify MP mobility and evaluate effluent mass recovery. Derjaguin–Landau–Verwey–Overbeek (DLVO) interaction energy profiles were calculated to help interpret experimental breakthrough and retention behaviour. Specifically, this chapter addresses the following questions:

(1) To what extent do GCLs attenuate the migration of small MPs under DI water and $CaCl_2$ pre-hydration, and what retention processes dominate?

(2) How do GCL bentonite type and MP attributes (polymer type and particle size) influence breakthrough behaviour and mass recovery?

6.2 Materials and Methods

6.2.1 Materials

This chapter used the GCLs and MP suspensions described in Section 3.2. Two commercially manufactured GCLs (GCL-1 and GCL-2) were used as barrier materials. Fluorescent MPs consisted of monodisperse PS microspheres with nominal diameters of 0.2, 0.5 and 1 μm (f-PS0.2, f-PS0.5 and f-PS1) and PE microspheres with a mean diameter of ~0.5 μm (f-PE0.5). Working influent suspensions (50 mg/L) were prepared by diluting stock dispersions with DI water. Immediately prior to injection, suspensions were gently agitated and briefly ultrasonicated to re-disperse any aggregates.

6.2.2 Methods

MP transport testing through GCLs was conducted in three stages:

1. Pre-hydration of GCL under different conditions representative of ideal and chemically aggressive site scenarios.
2. Columns test to quantify MP transport through the pre-hydrated GCLs.
3. Post-test dye elution and SEM imaging of recovered GCL components.

Details of the three steps are described next.

6.2.2.1 Pre-hydration of GCLs under Different Chemical Conditions

Pre-hydration of GCL has a well-documented effect on its performance, with cation exchange suppressing bentonite swelling and leading to significant increases in hydraulic conductivity (Chen et al., 2018b; AbdelRazek and Rowe, 2019b). Hence, two pre-hydration states were targeted in the tests conducted here: an ideal DI water condition and a chemically impacted condition. To select a suitable $CaCl_2$ concentration for the latter, a "critical" concentration was defined as the point at which the swell index (SI) of the extracted bentonite fell below 10 mL/2 g (ASTM D5890, 2019). This choice is consistent with forensic studies on exhumed, Ca^{2+}/Mg^{2+}-exchanged GCL bentonites in landfill covers and composite liners, where SI values of ~7-14 mL/2 g have been reported alongside hydraulic conductivities several orders of magnitude higher than those of virgin sodium bentonite

(Meer and Benson, 2007; Bradshaw et al., 2013; Scalia IV et al., 2018). Hence, preliminary SI tests were conducted to establish the relationship between $CaCl_2$ concentration in the hydration solution and SI for each GCL.

SI tests followed ASTM D5890 (2019), with a minor adaptation to specimen preparation. Bentonite recovered from pre-conditioned GCL specimens was oven-dried overnight, cooled in a sealed container, and gently crushed to its original powdered or granular form. For each test, 2 g of bentonite was incrementally sprinkled (<0.10 g per addition at ~10 minutes intervals) into 70-80 mL of DI water in a 100 mL graduated cylinder without agitation to avoid clumping and air entrapment. After the full 2 g was added, DI water was added to the 100 mL mark. The cylinder was left undisturbed for at least 16 hours, after which the gel volume was read to the nearest millilitre and reported as SI (mL/2 g). The resulting SI versus $CaCl_2$ concentration relationships (Figure 6.1) showed that $CaCl_2$ concentrations of 100 mM (GCL-1) and 300 mM (GCL-2) reduced SI below 10 mL/2 g and were therefore adopted as "chemically aggressive" hydration conditions. A concentration of 10 mM $CaCl_2$ was used to represent moderate concentration.

All GCL specimens underwent one of the two pre-conditioning protocols before MP transport testing. Under the DI-hydration protocol (ideal condition), GCL discs were placed in an oedometer and hydrated with DI water for 7 days under a vertical seating load of 1 kPa. Under the chemically impacted protocol, GCL discs were hydrated in $CaCl_2$ solution for 3 days, air-dried for 3 days, and the wet-dry cycle was repeated twice. A third 3-day $CaCl_2$ hydration was then applied immediately prior to installation in the FWP. No confining stress was applied during drying. After preconditioning, specimen mass and thickness were recorded to 0.01 g and 0.01 mm, respectively. Water contents were ~100% in most cases, except for GCL-2 hydrated in 10 mM $CaCl_2$, which reached ~200%. A target water content near 100% is consistent with values reported for side-slope conditions in chemically impacted and thermally cycled liners (Gates et al., 2018).

Macroscopic specimen appearance varied with conditioning (Figure 6.2). GCL-1 hydrated in DI water exhibited pronounced swelling, rounded edges, and a gel-rich surface consistent with extensive hydration. In contrast, GCL-1 conditioned in 100 mM $CaCl_2$ with two wet-dry cycling appeared thinner and showed a mottled surface, suggesting reduced swelling. Under the same $CaCl_2$ cycling, GCL-2 retained a smoother and more uniform surface than GCL-1. These observations align with chemistry-induced reductions in

interlayer swelling and the effects of wet-dry cycling on gel development (Alziyadi and Denton, 2021).

To assess the effect of different modes of pre-hydration on bentonite microstructure, bentonite was recovered from GCL specimens that had been preconditioned by DI water and $CaCl_2$ solutions. After carefully separating cover and carrier geotextiles, the bentonite core was gently scraped free of fibres and trimmed into 5 mm× 5 mm × 5 mm pieces. Samples were freeze-dried using the protocol in section 6.2.2.3. Pore-structure characterization was performed using Mercury Intrusion Porosimetry (MIP; AutoPore IV 9500, Micromeritics). Mercury intrusion curves were used to derive cumulative and differential pore-size distributions, enabling comparison of micro- and meso-pore domains between hydration conditions.

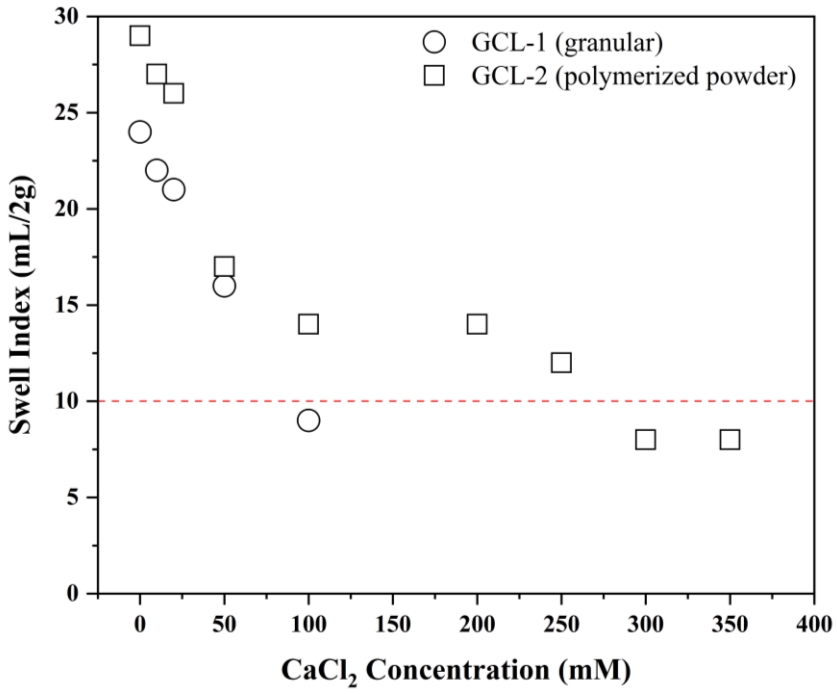

Figure 6.1. SI of bentonite extracted from GCL-1 (granular Na-bentonite) and GCL-2 (polymer-amended powder Na-bentonite) as a function of $CaCl_2$ concentration. The red dotted line shows the critical $CaCl_2$ concentrations at which the swell index drops below 10 mL/2 g, identified here as 100 mM for GCL-1 and 300 mM for GCL-2, and are used to define chemically aggressive conditions for subsequent transport tests.

Figure 6.2. Representative photographs of GCL specimens after conditioning: (a) GCL-1 hydrated in DI water; (b) GCL-1 hydrated in 100 mM $CaCl_2$ and subjected to two wet-dry cycles; (c) GCL-2 hydrated in 100 mM $CaCl_2$ and subjected to two wet-dry cycles.

6.2.2.2 MP Transport Column Experiments

MP transport tests were conducted in a laboratory FWP as described in section 5.2.2. Departing from the standard hydraulic conductivity setup that uses TIUs at both the inlet and outlet, a single inlet TIU served as the MP-rich influent reservoir (identical to the direct collection mode for Test Set 3 in section 5.2.3.3). The outlet was vented to atmosphere and routed directly into pre-weighed glass vials for time-resolved sampling, thereby avoiding potential dilution and retention effects in a downstream TIU and enabling continuous effluent collection.

Each GCL disc was sandwiched between quartz porous stones (nominal pore size 250-550 µm) to minimize end-platen filtration and improve effluent mass recovery (Figure 6.3). To reduce fluorescence interference from detached fines (e.g., bentonite particles or geotextile fibres), a single Whatman® 4 filter paper (nominal pore size 20-25 µm) was placed beneath the specimen, between the carrier geotextile and the lower porous stone (Sujathan and El-Zein, 2025). No filter paper was installed above the specimen because flow was applied top-to-bottom and to avoid introducing an upstream retention element that could bias influent MP delivery. All wetted tubing and fittings were Teflon or stainless steel (nominal 1/8-inch). Preliminary tests indicated negligible MP losses in Teflon lines under the test conditions (Gao et al., 2025).

To suppress MP settling and agglomeration within the inlet reservoir, the TIU was mounted on an orbital shaker operating at 160 rpm, which maintained mixing without introducing flow pulsation (i.e., stopping the experiment while re-fill the TIU with fresh

suspensions). Influent MP concentration in the inlet TIU was monitored and remained reasonably constant throughout the experiments, as evidenced in section 5.2.2.

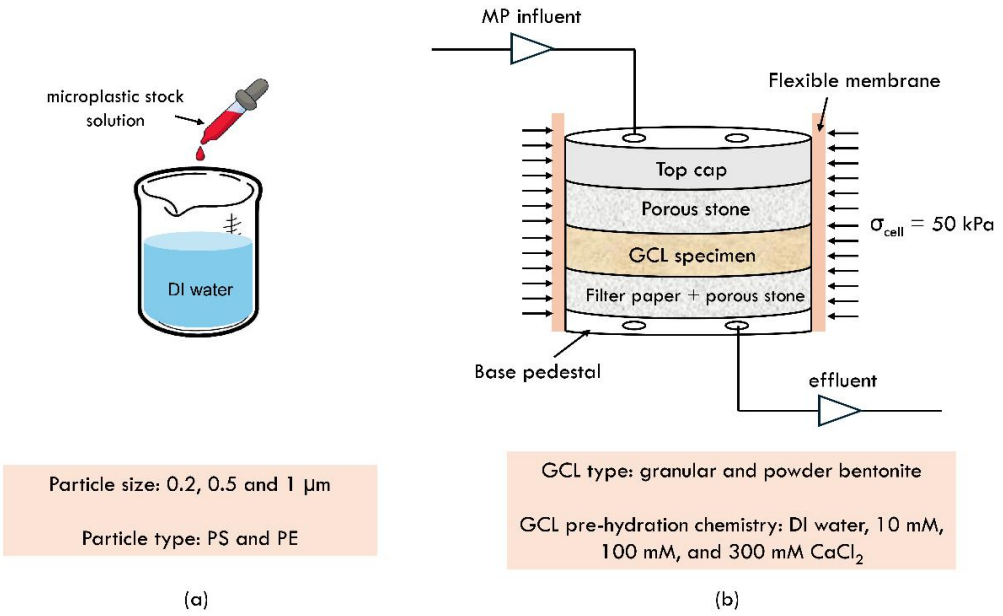

Figure 6.3. Schematic of testing scenarios for MP transport through GCLs (a) preparation of MP stock suspensions in DI water using f-PS and f-PE particles with nominal diameters of 0.2, 0.5 and 1.0 µm, (b) Column configuration within the FWP: a GCL specimen is sandwiched between porous stones and a filter paper, with MP influent applied from the top and effluent collected at the base. Tested variables include GCL type and pre-hydration chemistry.

Prior to specimen installation, a thin layer of bentonite paste was smeared around the specimen perimeter to reduce potential sidewall flow (Scalia and Benson, 2010; Benson et al., 2022). The specimen assembly (GCL + filter paper + porous stones) was positioned on the base pedestal, with an O-ring used to seat the flexible membrane. The setup employed a single filter paper beneath the specimen only, to avoid introducing an upstream retention interface that could affect influent MP concentrations. An acrylic top cap was installed, and a second O-ring was used to complete the membrane seal. The permeameter chamber was then filled with tap water and gently tapped to release trapped air bubbles. The system was visually inspected to confirm the absence of air in the cell fluid and tubing before commencing hydration and flow.

Tests were conducted either in constant-head (effective stress of 35 kPa) or constant-

flow mode (effective stress of 45-49 kPa) using automated controllers. Controller volumes/pressures were logged in GDSLAB v2.8.4 (GDS Instrument, UK). Inflow rate was obtained from the controller, whereas outflow was determined gravimetrically from effluent mass and collection time. Following ASTM D5084 (2016), hydraulic steady state was considered achieved when the inflow/outflow ratio remained within 0.75-1.25 for a sustained period.

Table 6.1 shows the series of tests conducted, aiming to assess the effects of pre-hydration regimes, MP size and polymer type, and GCL product type on breakthrough behaviour and mass recovery.

Table 6.1. Testing program of GCL experiments.

test number	test description: variable relative to base case	MP type	MP size	C_0 (mg/L)	porosity (-)	PV (cm^3)	water content before MP loading (%)
Set 1: GCL-1 hydrated in 100 mM $CaCl_2$ and subjected to 2 wet-dry cycles							
1	base case (with 4 repeats)	PS	0.5 µm	48.8	0.73	9.21	99.2
2				51.0	0.75	11.2	91.2
3				50.0	0.74	9.36	107.1
4				55.9	0.72	9.79	90.1
5				55.1	0.74	9.60	99.1
6	MP size (with 1 repeat)	PS	0.2 µm	49.5	0.71	8.83	96.8
7				48.1	0.74	9.77	97.4
8	MP size (with 2 repeats)	PS	1 µm	53.3	0.72	9.68	91.8
9				53.2	0.73	8.80	107.2
10				46.4	0.73	9.33	97.6
11	MP type	PE	0.5 µm	56.4	0.74	9.45	101.6
Set 2: GCL-1 hydrated in 10 mM $CaCl_2$ and subjected to 2 wet-dry cycles							
12	Hydration chemistry	PS	1 µm	50.1	0.78	17.8	123.7
Set 3: GCL-1 hydrated in DI water							
13	Hydration chemistry	PS	1 µm	51.1	0.90	19.1	163.5
Set 4: GCL-2 hydrated in 300 mM $CaCl_2$ and subjected to 2 wet-dry cycles							
14	GCL type	PS	0.5 µm	50.1	0.82	16.13	94.6
Set 5: GCL-2 hydrated in 10 mM $CaCl_2$ and subjected to 2 wet-dry cycles							
15	GCL type	PS	0.5 µm	51.3	0.94	24.19	203.1
Set 6: GCL-2 hydrated in DI water							
16	GCL type	PS	0.5 µm	52.3	0.93	22.46	205.7

After pre-hydration, specimens were mounted between porous stones as described in Section 6.2.2. For Test Set 1, an ion-elution step was first performed by percolating DI water (~20 PV) until the effluent electrical conductivity (EC) stabilized at 50-100 µS/cm for two consecutive fractions. The stabilised EC values indicate substantial removal of mobile porewater ions from the advective flow domain. However, the chemical and microstructural evolution of the bentonite during the transition from high ionic strength $CaCl_2$ hydration to DI-water permeation was not characterised directly. Residual Ca^{2+} may have remained within low-permeability or poorly connected pore regions, and partial re-swelling or microstructural reorganisation of the bentonite may have occurred during flushing. The MP-injection phase then commenced by switching the inlet TIU to a 50 mg/L working suspension while maintaining a 50 kPa confining pressure. A constant flow rate of 4.17 mm^3/s was imposed for Test Set 1, whereas a constant pressure head of 30 kPa was applied for Test Sets 2-6 (Table 6.2). The difference in hydraulic specifications is due to the much lower hydraulic conductivities of specimens in Test Sets 2-6 compared to Test Set 1. Under low hydraulic conductivity conditions, constant head control provides a more stable and practical boundary condition. For the same reason, effluent was collected up to 10 PV for Test Set 1 but only up to 4 PV for Test Sets 2-6. For Test Set 1, a post-injection DI water flush of ~10 PV was also conducted. MP concentrations in all effluent fractions were quantified by fluorescence spectrophotometry using calibration curves established in Chapter 3.

BTCs were expressed as C/C_0 versus the number of PV, where C_0 is the influent concentration. Using the number of PV rather than elapsed time as the independent variable allows comparison across specimens with different thicknesses and void ratios. The following BTC metrics were used (Table 6.2):

- C_{max}/C_0: peak (or plateau) value, indicating the extent of MP transmission (lower values imply stronger filtration).
- $PV_{initial\ breakthrough}$: PV at which C/C_0 first reaches 0.1, used as an early-arrival indicator (larger values imply delayed breakthrough).
- $PV_{0.5}$: PV at which C/C_0 reaches half of C_{max}/C_0 (used as descriptive breakthrough indicators rather than uniquely defined retardation parameters).
- PV_s: PV at which C/C_0 first reaches C_{max}/C_0 (often less sensitive to curve shape than $PV_{0.5}$).
- $M_{MP\text{-}feed}$: cumulative MP mass fed per unit area (mg/m^2).

- $M_{MP\text{-}effluent}$: cumulative MP mass eluted per unit area (mg/m^2).
- γ: transmission coefficient, defined as $\gamma = M_{MP\text{-}effluent}/M_{MP\text{-}feed}$. Note that 1- γ quantifies overall retention by the barrier.

Table 6.2. Analysis of breakthrough curve.

Parameter	Description	Formulation
C_{max}/C_0	Maximum normalized concentration (plateau or peak)	$(\frac{C}{C_0})_{max}$
$PV_{initial\ breakthrough}$	Pore volumes at initial breakthrough when C/C_0 exceeds 0.1	$PV_{initial\ breakthrough}=PV(C/C_0=0.1C_0)$ (linear interpolation)
$PV_{0.5}$	Pore volumes at half-maximum	$PV_{0.5}=PV(C/C_0=0.5C_{max}/C_0)$ (linear interpolation)
PV_s	Pore volumes to reach maximum (plateau)	Observed from breakthrough curve
$M_{MP\text{-}feed}$ (mg/m^2)	Cumulative MP mass feed per unit area	$M_{MP\text{-}feed}=\frac{1}{A}\int_0^{t_{end}} C_0 Q_{in}(t)dt \approx \frac{C_0 V_{in,total}}{A}$
$M_{MP\text{-}effluent}$ (mg/m^2)	Cumulative transmitted MP mass per unit area	$M_{MP\text{-}effluent}=\frac{1}{A}\sum_i C_i \Delta V_i$ (sum over effluent fractions)
γ (-)	Overall transmission efficiency	$\gamma=\frac{M_{MP-effluent}}{M_{MP-feed}}$

A is the specimen area (for a disc, $A=\pi d^2/4$). C_0 is the influent concentration at the inlet TIU. $V_{in,\ total}$ is the total influent volume delivered to the specimen.

6.2.2.3 Post-test GCL Characterization by Scanning Electron Microscopy & Dyeing

To visualize MPs associated with the bentonite matrix and geotextile fibres, small bentonite fragments and geotextile coupons were recovered from selected specimens after transport tests. For GCL-1 pre-hydrated with 100 mM $CaCl_2$ (Test 1), bentonite was sampled separately from the centre and edge of the specimen. For GCL-2 pre-hydrated with 300 mM $CaCl_2$ (test 14), bentonite and cover geotextile were sampled from the centre of the specimen.

In a freeze-drier, samples were subjected to -57 °C for 24 h followed by 24 h of drying under a vacuum of 0.10 mbar to remove pore water while minimizing soil solid fabric collapse. Dried material was stored in sealed containers with desiccant until analysis. For SEM, samples were mounted on aluminium stubs using conductive carbon tape and gold sputter-coated with a ~10 nm gold layer. Imaging was performed using a field-emission

SEM (Sigma HD, Zeiss) at an accelerating voltage of 5 kV and a working distance of ~5 mm. Images were acquired to highlight surface morphology and microscale contacts between MPs, bentonite, and geotextile fibres.

To visualise preferential flow paths within the GCL, a post-transport dye-tracing test was performed on the specimen from test 10 (see Table 6.1). After completion of MP injection and the DI water flush, a fluorescent red dye (item No. EW-00298-06, Cole Parmer) was introduced at the inlet using the same hydraulic configuration as the transport test. Injection continued until dye was first detected in the effluent. The specimen was then removed and split longitudinally into two halves using a clean, sharp blade. The freshly exposed internal faces were photographed immediately to document stained pathways along fibres, interfaces, and within the bentonite matrix.

6.2.2.4 DLVO Interaction Energy

Interaction energy profiles between MPs and bentonite were calculated using classical DLVO theory, as summarized in section 2.3.2.3. The collector (soil grain) surface was idealised as a flat plate and the MP particle as a sphere (sphere-plate geometry) (Ye et al., 2022b). The total interaction energy, ξ_{tot}(d), was expressed as the sum of van der Waals attraction and electrostatic double-layer interaction terms and evaluated as a function of separation distance, d. Interaction energies were normalised by thermal energy, K_BT, where K_B is the Boltzmann constant and T is the absolute temperature, and reported as the dimensionless profile ξ_{tot}(d)/(K_BT). pH was not adjusted during the experiments, and effluent pH values measured during testing were within the range of 7.5-8.5.

Table 6.3. Parameters used in DLVO interaction energy calculations.

r_p	The radius of MPs (f-PS0.2, f-PS0.5, f-PS1 and f-PE0.5) (m).
λ_c*	The "characteristic wavelength" of the interaction, assumed to be 100 nm.
A_{132}#	Effective Hamaker constant for interaction between subject 1 (MP, Hamaker constant A_{11}) and subject 3 (clay, Hamaker constant A_{33}) in the medium 2 (DI water, Hamaker constant A_{22}), computed as $A_{123} = (\sqrt{A_{11}} - \sqrt{A_{22}})(\sqrt{A_{33}} - \sqrt{A_{22}})$

	with A_{11}=6.06×10^{-20} J (PS) and 6.88×10^{-20} J (PE), A_{22}= 3.70×10^{-20} J (water), and A_{33}=7.81×10^{-20} J (montmorillonite)
η_p	Zeta potential of MP particles (V) with -48.0 mV (f-PS0.2), -45.7 mV (f-PS0.5), -46.0 (f-PS1), and -54.7 mV (f-PE0.5).
η_c	Zeta potential of bentonite particles (-35.0 mV).
d	The separation distance between two interacting particles (m).
κ	The inverse Debye length (m^{-1}) defined as $\kappa = \sqrt{\frac{2N_A e^2 IS}{\varepsilon_r \varepsilon_0 K_B T}}$
IS	Ionic strength (mol/m^3)
N_A	Avogadro's number, 6.02×10^{23} mol^{-1}.
e	Unit charge of electron, 1.602×10^{-19} C.
ε_0*	The vacuum dielectric constant, 8.845×10^{-12} C/V/m.
ε_r*	The dielectric constant of water, 78.5 (dimensionless).
K_B	Boltzmann constant, 1.38×10^{-23} J/K.
T	The absolute temperature, 298 K.

* Data based on Ye et al. (2022b).

Data based on Wang et al. (2015).

6.3 Results and Discussion

6.3.1 Effects of Pre-hydration Conditions on Hydraulic Conductivity of GCLs

Hydraulic conductivity, *k*, was monitored throughout the MP transport tests. For GCL-1, Figure 6.4a compares specimens pre-hydrated in DI water with those subjected to 10 mM $CaCl_2$ and two wet-dry cycles. Under DI hydration, GCL-1 maintained a low *k* value over the test duration, consistent with the expected performance of sodium bentonite GCLs. Pre-hydrating with 10 mM $CaCl_2$ (with wet-dry cycling) did not produce a discernible degradation in hydraulic performance, and measured *k* remained within the same order of magnitude as the DI baseline. These observations suggest that moderate ionic strength and limited wet-dry exposure did not substantially compromise the hydraulic barrier performance of the granular Na-bentonite product. Similar results are reported in previous studies (Lee and Shackelford, 2005).

In contrast, when GCL-1 was hydrated with 100 mM $CaCl_2$ and wet-dry cycling, k increased by approximately one to two orders of magnitude relative to the DI and 10 mM cases once steady-state flow was reached (Figure 6.5). This trend is consistent with the well-established sensitivity of sodium bentonite to divalent cation exchange and diffuse double layer compression, which reduce swelling and increase pore connectivity (Mitchell and Soga, 2005). In geotechnical practice, GCLs are commonly considered to have lost low-permeability performance when k exceeds 1×10^{-9} m/s, a benchmark widely used for the mineral component of composite liners (Rowe and Brachman, 2004). Under the 100 mM $CaCl_2$ regime, GCL-1 exceeded this benchmark, whereas DI and 10 mM $CaCl_2$ conditions maintained k within a low-permeability range.

For GCL-2, Figure 6.4b shows that k remained low following DI and 10 mM $CaCl_2$ hydration and, notably, stayed in the order of 10^{-10} m/s even after conditioning with 300 mM $CaCl_2$ and wet-dry cycling. A gradual decrease in k was observed for the 300 mM $CaCl_2$ condition after approximately 75 hours of permeation (Figure 6.4b), potentially due to self-sealing of the polymer-amended bentonite (El-Zein et al., 2021). This behaviour indicates that GCL-2 exhibited greater chemical resistance than GCL-1, maintaining low hydraulic conductivity even under high $CaCl_2$ concentration and cyclic wetting and drying.

Gravimetric water content of GCL-1 in Test Set 1 increased sharply during each wetting phase to ~100-110%, and subsequently decreased to ~15-25% during drying, indicating that the wet-dry protocol effectively cycled the bentonite between quasi-dry and hydrated states (Figure 6.6a). Despite these swings in water content, specimen thickness remained comparatively stable at ~6.7-7.3 mm (Figure 6.6b) and no significant net volumetric swelling was recorded. In comparison, GCL-2 specimens pre-hydrated with DI water and 10 mM $CaCl_2$ showed substantially higher water contents (>200%). The difference reflects the combined influence of hydration chemistry, bentonite type and bentonite mass per unit area.

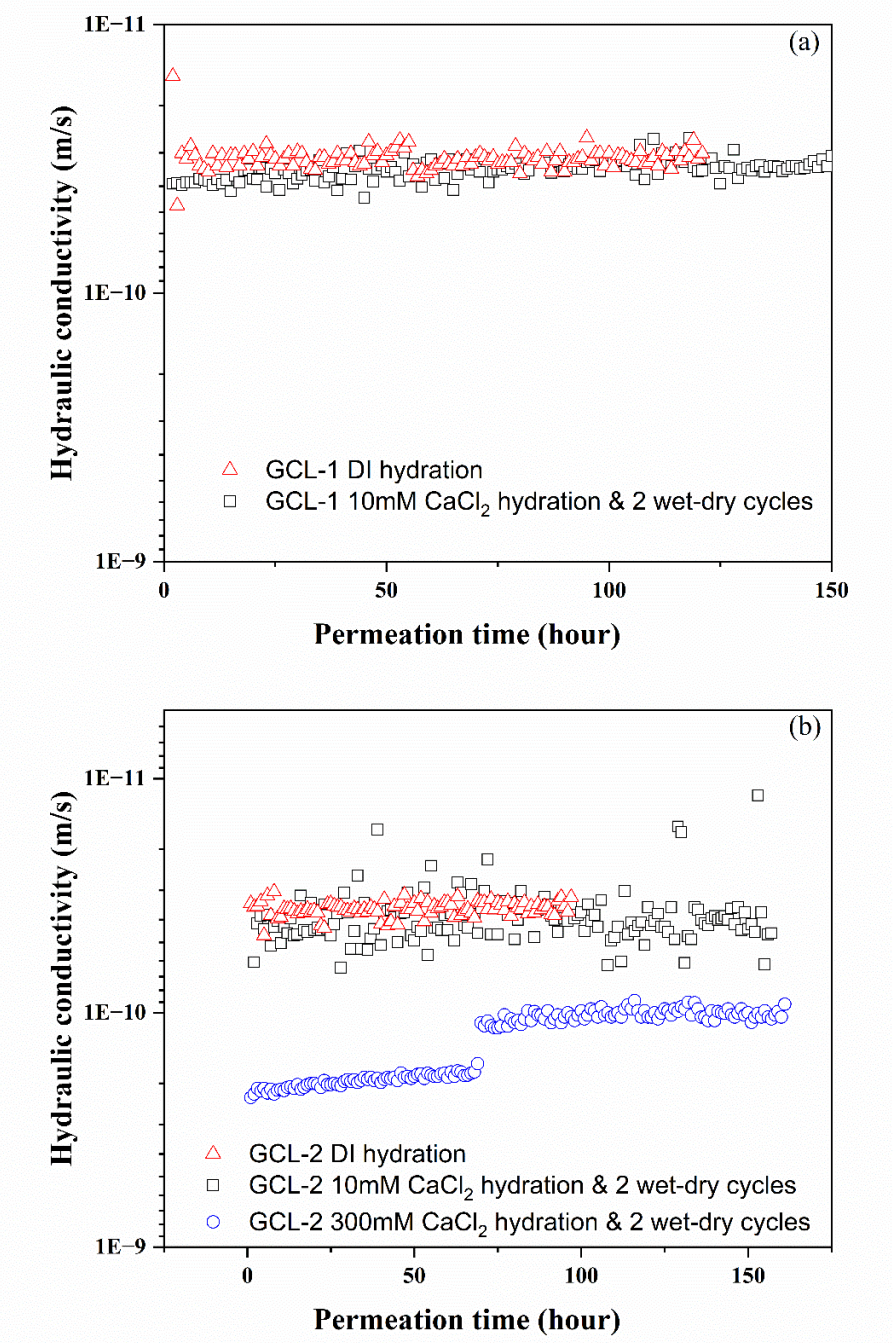

Figure 6.4. Hydraulic conductivity *k* versus permeation time for (a) GCL-1 and (b) GCL-2 under different pre-hydration conditions (DI water in red, 10 mM $CaCl_2$ hydration with wet-dry cycling in black, and 300mM $CaCl_2$ with wet-dry cycling in blue. The vertical axis is plotted on a logarithm scale.

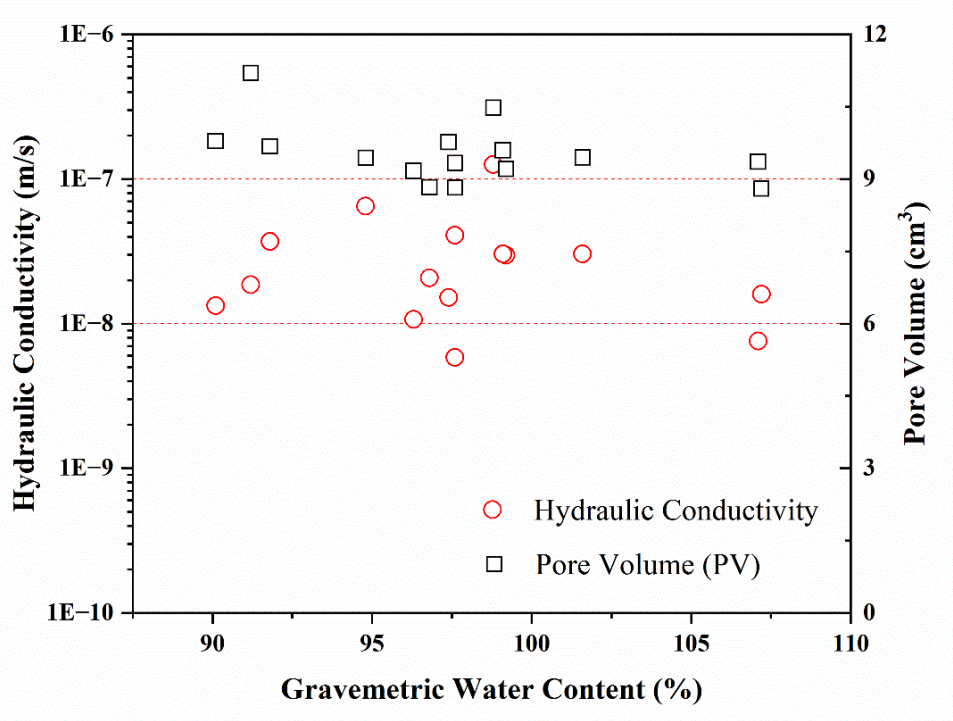

Figure 6.5. Hydraulic conductivity and pore volume of GCL-1 specimens hydrated in 100 mM $CaCl_2$ with two wet-dry cycles (Test Set 1).

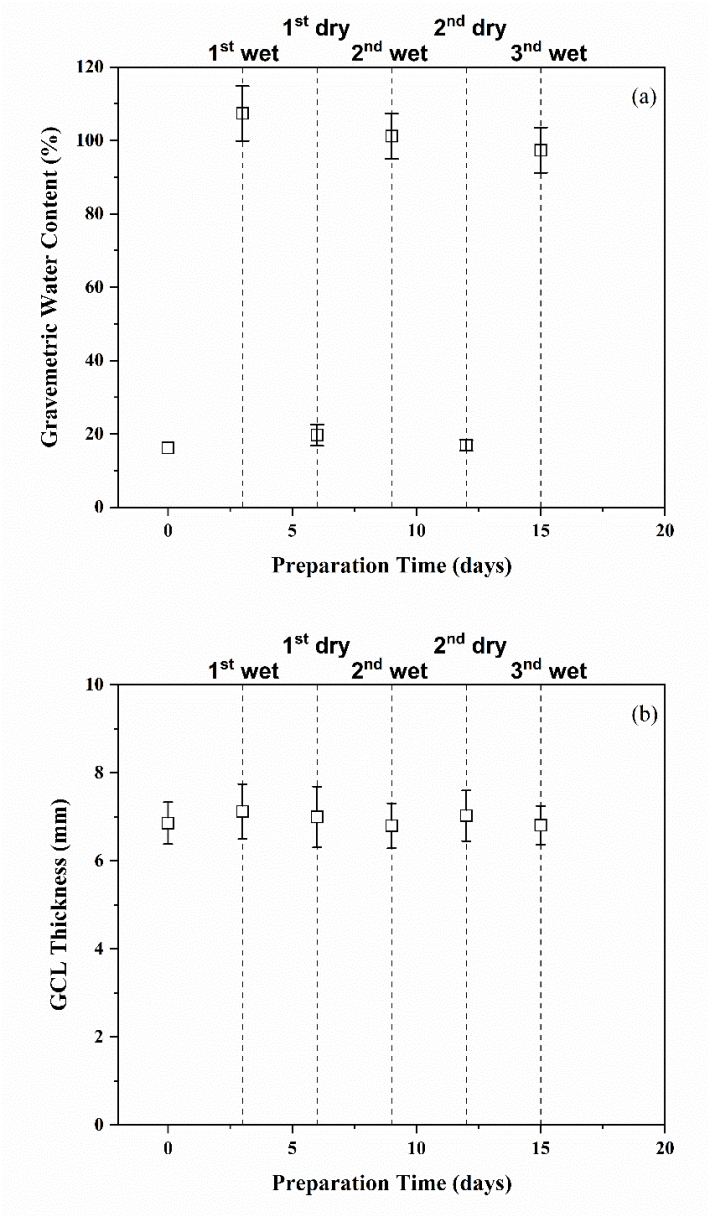

Figure 6.6. (a) Gravimetric water content and (b) specimen thickness of GCL-1 during preconditioning in Test Set 1 (100 mM $CaCl_2$ and two wet-dry cycles). Vertical dashed lines indicate the end of each drying step (1st dry, 2nd dry) and the start of the subsequent wetting (2nd wet, 3rd wet). Error bars show the standard deviation from five repeat tests.

6.3.2 MIP Microstructural Analysis of the Effect of Pre-hydration Conditions

The bentonite microstructure in GCL-1 and GCL-2 was evaluated by MIP after pre-hydration with (a) DI water and (b) 100 mM $CaCl_2$ with two wet-dry cycles (Figure 6.7). Duplicate tests for GCL-1 under the 100 mM $CaCl_2$ condition showed only minor discrepancies in the log-differential intrusion curves, with maximum cumulative intrusion values of 0.167-0.173 mL/g. For both GCL types, cumulative intrusion was higher after 100

mM $CaCl_2$ hydration than after DI hydration, indicating greater mercury-accessible void volume (i.e., a more open pore structure) when swelling is chemically suppressed.

The log-differential intrusion curves (Figure 6.7b, d) span entrance radii of roughly 5-100 μm and display clear shifts in the location and amplitude of dominant peaks. For GCL-1, $CaCl_2$ pre-hydration increases contributions in the ~20-40 μm range, whereas the DI-hydrated specimen shows a dominant contribution near ~11 μm. For GCL-2, $CaCl_2$ shifts the distribution toward larger pores of ~60-100 μm, while the DI-hydrated specimen shows higher contributions in the ~8-15 μm range, with a broader shoulder near ~100 μm. Under $CaCl_2$ hydration, the pore size distribution of GCL-1 remains bimodal, whereas GCL-2 becomes closer to unimodal, dominated by a single peak mode.

Microstructural studies on $CaCl_2$-treated bentonite have shown that Ca^{2+} can promote highly aggregated structures with cohesive clusters and fewer voids, reducing the separation between distinct pore families (Ahmed et al., 2025). This interpretation is qualitatively consistent with the unimodal pore size distribution observed for GCL-1 (Figure 6.7b). In comparison, Li et al. (2025c) reported that a biopolymer-amended GCL exhibited lower cumulative intrusion and a reduced macropore fraction in 12.5 mM $CaCl_2$ compared with DI water, attributed to partial collapse of macropores and an increased proportion of mesopores (3-30 μm). Their study also suggests that polymer amendments can increase the macropore volume fraction under certain chemistries. In the present study, MIP results for the polymer-amended GCL-2 hydrated in 100 mM $CaCl_2$ show a shift of the peak location and an increase in cumulative intrusion, indicating increased microporosity relative to the DI-hydrated state.

Overall, the increase in cumulative intrusion and the shift of dominant peaks towards larger entrance radii after Ca^{2+} exposure are consistent with established behaviour of Na-bentonite under cation exchange and wet-dry cycling, caused by compression of the diffuse double layer and reduced interlayer swelling, which open larger transport pathways (Jo et al., 2004; Sun et al., 2019; He et al., 2022; Li et al., 2025a).

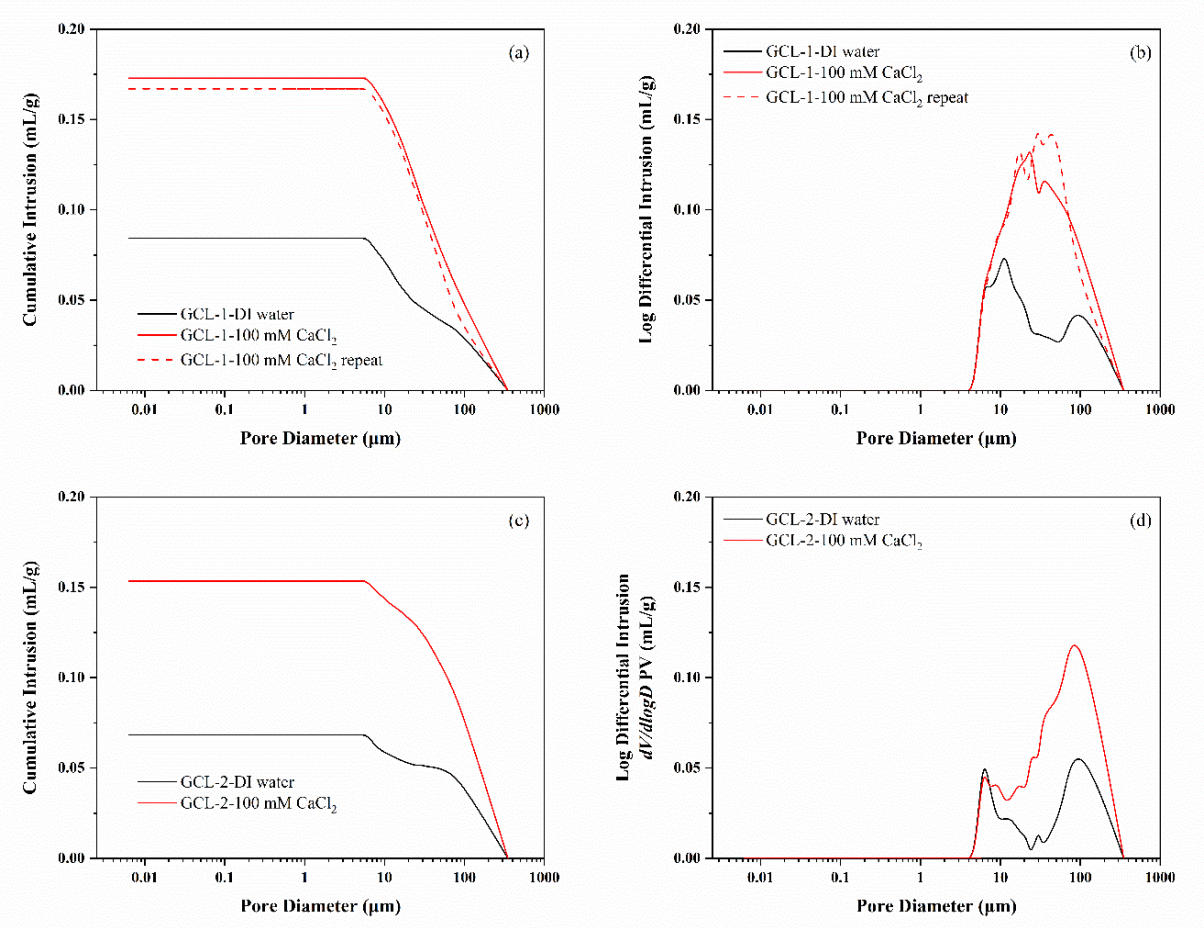

Figure 6.7. MIP results for DI-hydrated (black) and 100 mM $CaCl_2$-hydrated (red) specimens: (a and b) GCL-1 and (c and d) GCL-2. A repeat test for GCL-1 at 100 mM $CaCl_2$ is plotted as a red dashed line.

6.3.3 MP Transport through GCL: Results of Column Tests

6.3.3.1 Test Sets 2-6: Low Hydraulic Conductivity and No Breakthrough Observed

All experiments in Test Sets 2-6 exhibited very low hydraulic conductivity ($<1\times10^{-10}$ m/s) and correspondingly low flow rates (Figure 6.4). Each test was operated for approximately 30-60 days, generating up to 4 PV of effluent. Throughout this experimental duration, no detectable MP breakthrough was observed, and effluent MP concentrations remained below the analytical detection limit.

The interpretation of "no breakthrough" should be considered within the temporal and hydraulic limits of the experiments conducted. For specimens with hydraulic conductivity below approximately 5×10^{-10} m/s, only limited pore volumes could be

generated within practical laboratory timescales. Consequently, breakthrough at longer times or higher pore volumes cannot be excluded. The present results therefore suggest no detectable breakthrough within up to 4 PV and 60-day duration examined in this study, rather than definitive evidence of permanent or long-term containment.

The absence of detectable breakthrough under these conditions is consistent with the low hydraulic conductivity of the hydrated bentonite systems, which limited advective transport during the experimental timeframe. Restricted pore accessibility within the hydrated bentonite matrix and retention at the geotextile-bentonite interface also likely contributed to the observed behaviour.

Accordingly, extrapolation of these findings to field-scale landfill performance requires caution because long-term behaviour will also depend on factors such as hydration state, chemical exposure, hydraulic gradients, and temporal evolution of bentonite microstructure. Nevertheless, the results demonstrate that, under the controlled conditions investigated here, well-hydrated low-permeability GCL systems can substantially restrict short-term advective migration of small MPs.

6.3.3.2 Test Set 1: GCL-1 Pre-hydrated in 100 mM $CaCl_2$

Test Set 1, which used the granular sodium bentonite GCL (GCL-1) pre-hydrated in 100 mM $CaCl_2$ with two wet-dry cycles, exhibited extensive MP breakthrough. Summary statistics for the 11 tests in this set are presented in Table 6.4. In what follows, the base case and the effects of MP particle size and polymer type on their transport are discussed.

It is important to note that some variability in hydraulic conductivity was observed even among repeat tests conducted under pre-hydration conditions designed to be identical to each other. Measured k values in the base-case tests varied by approximately a factor of four (7.6×10^{-9} to 3.0×10^{-8} m/s), likely reflecting specimen-scale heterogeneity associated with bentonite distribution, needle-punch reinforcement, manufacturing variability, and differences in microstructural rearrangement during chemical conditioning and wet-dry cycling. Consequently, hydraulic conductivity became a *de facto* experimental variable in the series of test that is considered in the analyses below. As a result, differences in breakthrough behaviour cannot be attributed solely to MP properties, and interpretation of particle size and polymer effects must also consider the influence of concurrent variation in

k. Accordingly, breakthrough trends are interpreted comparatively with reference to hydraulic conductivity where appropriate.

6.3.3.2.1 Base Case

Figure 6.8 compares BTCs for the base case at two ranges of hydraulic conductivity. For the pair with $k \approx 3.0 \times 10^{-8}$ m/s (Tests 1 and 5), both curves exhibit a gradual rise to C_{max}/C_0 of 0.80±0.01 at 9.6-9.8 PV. For the second pair (Figure 6.8b), where *k* differed modestly (1.9×10^{-8} vs 1.3×10^{-8} m/s), the peak was reached earlier (7.5 PV for Test 2 and 5.6 PV for Test 4) with similar maxima (~0.62-0.65). In comparison, Test 3, which had the lowest conductivity (7.6×10^{-9} m/s), yielded the lowest peak (C_{max}/C_0=0.51).

Within each conductivity range, peak locations and magnitudes agree closely, indicating good repeatability under the chemically aggressive pre-hydration protocol. Minor test-to-test differences in PV_s (e.g., 9.8 vs 9.6 PV for Tests 1 and 5; Table 6.4) are plausible attributable to pore-scale heterogeneity, minor differences in microstructural configuration after preconditioning, and fluctuations near the plateau. The similarity of the tailing limbs suggests comparable degrees of reversible retention (Ryan and Elimelech, 1996). No substantial progressive reduction in hydraulic conductivity was observed during the experiments. This suggests that the BTC plateauing behaviour was controlled primarily by retention processes rather than progressive blockage during MP injection, although localised pore constriction at preferential retention locations cannot be excluded. In the following sections, MP type and size are varied and results are compared to those of the base case, as a reference.

Table 6.4. Summary of analysis of MP breakthrough in Test Set 1.

Test number	Test description	k (m/s)	PV No. of influent	C_{max}/C_0 (-)	$PV_{initial\ breakthrough}$ (-)	$PV_{0.5}$ (-)	PV_s (-)	$M_{MP\text{-}feed}$ (mg/m^2)	$M_{MP\text{-}effluent}$ (mg/m^2)	γ (-)
Set 1: GCL-1 hydrated in 100 mM $CaCl_2$ and subjected to 2 wet-dry cycles										
1	base case (PS 0.5 μm)	3.0×10^{-8}	9.8	0.81	1.2	2.0	9.8	2235	1550	0.69
2		1.9×10^{-8}	7.6	0.65	1.0	1.4	7.6	2254	1236	0.55
3		7.6×10^{-9}	9.6	0.51	1.4	2.1	6.4	2292	734	0.32
4		1.3×10^{-8}	9.5	0.62	1.2	1.9	5.6	2633	1384	0.53
5		3.0×10^{-8}	9.6	0.79	1.2	1.8	9.6	2598	1757	0.68
6	MP size (0.2 μm)	2.1×10^{-8}	10.7	0.71	1.3	2.0	9.0	2382	1652	0.69
7		1.5×10^{-8}	9.2	0.67	1.4	2.4	6.9	2161	1339	0.62
8	MP size (1 μm)	3.7×10^{-8}	9.3	0.47	1.4	2.3	8.0	2443	951	0.39
9		1.6×10^{-8}	9.5	0.48	1.3	1.8	5.7	2370	995	0.42
10		5.9×10^{-9}	8.6	0.37	1.4	1.6	3.8	1897	723	0.38
11	MP type (PE)	3.0×10^{-8}	8.8	0.64	1.1	1.5	6.4	2379	1326	0.56

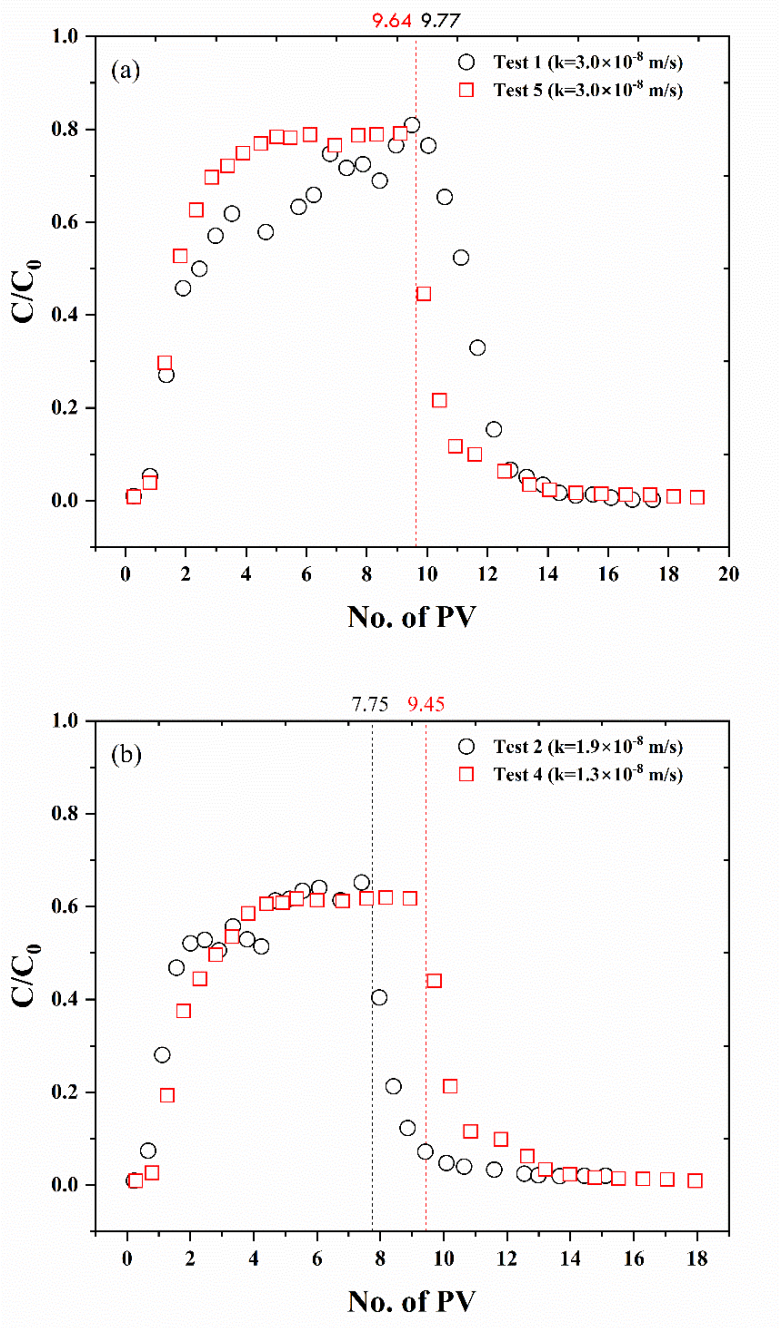

Figure 6.8. Comparison of BTCs for the Test Set 1 base case at comparable hydraulic conductivity: (a) Tests 1 and 5 with k of 3.0×10^{-8} m/s; (b) Tests 2 and 4 with k of 1.9×10^{-8} and 1.3×10^{-8} m/s. Numbers above dashed lines represent the PV number of MP influent. Circles and squares denote separate tests.

6.3.3.2.2 Effect of Particle Size

Figure 6.9 compares BTCs for three particle sizes under identical pre-hydration conditions for GCL-1 (100 mM $CaCl_2$ and two wet-dry cycles). Increasing PS size from 0.2 µm to 1.0 µm reduced both the breakthrough peak and the transmitted mass ratio. The peak normalised

concentrations (C_{max}/C_0) declined from 0.71 (0.2 μm) to 0.65 (0.5 μm) and 0.48 (1.0 μm). Consistently, the cumulative eluted mass per unit area ($M_{MP\text{-}effluent}$) decreased from 1652 mg/m^2 (0.2 μm) to 995 mg/m^2 (1.0 μm), and the transmission efficiency γ declined from 0.69 to 0.42. These trends indicate progressively stronger retention with increasing particle size.

BTC shapes were broadly similar across sizes. The PV at which C/C_0 reached its maximum (PV_s) decreased monotonically with size (9.0, 7.6 and 5.7 PV for 0.2, 0.5 and 1.0 μm, respectively), although PV_s is less robust for quantitative comparison due to fluctuations near the plateau. Small differences in hydraulic conductivity among these tests (2.1×10^{-8}, 1.9×10^{-8}, 1.6×10^{-8} m/s in Figure 6.9) likely contributed to shifts in peak location by altering residence time. Early-arrival metrics were relatively clustered, with $PV_{initial\ breakthrough}$=0.9-1.3 and $PV_{0.5}$=1.4-2.0.

A transient decrease in C/C_0 at approximately 5.4 PV for f-PS1 occurred while MP influent loading continued. This behaviour is consistent with ripening, in which deposited particles become secondary collectors and increase capture rates with time, temporarily lowering effluent concentrations (Pradel et al., 2024). Relative to 0.2 and 0.5 μm PS, the 1.0 μm particles exhibited the strongest retention, reflected in lower C_{max}/C_0, lower $M_{MP\text{-}effluent}$, and smaller γ. This size dependence is consistent with the increased likelihood of pore-scale interception as the particle-to-pore size ratio increases, together with increased contact efficiency at geotextile interfaces and within the bentonite-dominated flow networks (Lin et al., 2021; Wu et al., 2023).

A substantial body of work on colloidal transport in coarse-grained media suggests that straining is likely to be small or negligible when the straining ratio d_c/D_{50} falls below an empirical threshold of ~0.008 (Xu et al., 2006), where d_c is colloid diameter and D_{50} is the median soil grain diameter. Although the criterion was developed for sand and is not directly applicable to bentonite clay, it can serve as a broad screening reference. The granular bentonite in GCL-1 has D_{50} of ~1 mm (Tan et al., 2024), therefore its straining ratio is less than the threshold of 0.008, which means straining is unlikely to occur in this case. Furthermore, MIP results discussed earlier show that dominant pore sizes in all studied cases were greater than 10 μm, at least one order of magnitude greater than the largest MP particle studied here. Hence, if straining is occurring, it was likely associated with secondary processes such as aggregation and/or bridging of particles.

DLVO interaction energy profiles between MPs and bentonite (Figure 6.10) were calculated using measured zeta potentials and a low background ionic strength representative of the low electrical conductivity of the effluent after DI flushing and prior to MP loading (as described in section 6.2.2.2). For comparison, interaction energies were also calculated at ionic strengths of 10 mM and 50 mM. At very low ionic strength (0.1 mM, Figure 6.10a), all three PS sizes and PE MPs exhibit a large primary maximum (~400-2000 kT) at separation distances of 1-5 nm and no evident secondary minimum over the range 0.2-100 nm. Such energy barriers correspond to highly unfavourable attachment on ideal, smooth surfaces. Previous DLVO analyses indicate that Brownian collisions can overcome energy barriers of order <10 kT with appreciable probability, whereas much larger barriers lead to negligible primary minimum attachment (Bradford et al., 2011). Accordingly, most collisions between MPs and bentonite are not expected to overcome the barrier and do not result in strong attachment (Hahn and O'Melia, 2004). At higher ionic strengths (10 mM and 50 mM, Figure 6.10b, c), compression of the electrical double layer reduces the height of the primary maximum and produces shallow secondary minima at separations of tens of nanometres, indicating weak, potentially reversible secondary-minimum attachment under more saline conditions.

However, substantial retention was observed experimentally under the low ionic strength conditions corresponding to Figure 6.10a, despite the strongly repulsive interaction energies predicted by classical DLVO theory. This discrepancy demonstrates that DLVO theory alone is insufficient to quantitatively explain MP retention behaviour in the present GCL system. The assumptions underlying classical DLVO analysis, including chemically homogeneous and hydraulically smooth surfaces, are not representative of hydrated bentonite-geotextile systems, which exhibit pore-scale heterogeneity, surface roughness, fibre-clay contacts, and evolving microstructure.

Although the calculated DLVO barrier for f-PS1 is higher than that for the smaller PS particles on an idealised smooth surface, the pronounced ripening behaviour for f-PS1 indicates that an increasing fraction of the larger particles may become immobilised during continued loading. This behaviour is compatible with deposition at a limited number of favourable retention locations where local surface conditions differ from those assumed in classical DLVO theory. Possible mechanisms include surface roughness, charge heterogeneity, fibre-clay contacts, and nano-scale patches, all of which may reduce energy barriers and promote particle retention.

The DLVO calculations presented here are interpreted primarily as a qualitative indication that electrostatic interactions alone cannot account for the observed breakthrough and retention behaviour. The calculations are sensitive to assumptions regarding zeta potential, pH, surface chemistry and interaction geometry, and therefore represent approximate descriptions of MP-bentonite interactions under the tested chemical conditions. Nevertheless, across reasonable ranges of pH and zeta potential, the calculations predict strongly repulsive interaction conditions at low ionic strength. Interpretation of MP transport is therefore based on the experimental BTC characteristics. In particular, the ripening behaviour observed for f-PS1 suggests that retention was controlled by a limited number of high-affinity retention locations associated with pore-scale heterogeneity or localised physical interception rather than secondary-minimum attachment alone. The larger collision cross-section of f-PS1 may also have increased the probability of interaction with these retention sites despite the overall repulsive interaction energy profile predicted by the DLVO calculations.

However, these mechanisms cannot be confirmed conclusively from the present experiments because retention profiles and direct measurements of attached MP distributions were not available. The proposed mechanisms should be interpreted as plausible explanations consistent with the observed BTC behaviour rather than definitive proof of the dominant retention process.

The BTCs in Figure 6.9 were obtained under the low ionic strength conditions represented by Figure 6.10a and show sustained breakthrough during MP injection (C_{max}/C_0 ≈0.5-0.7), followed by a rapid decline towards zero during the MP-free DI water flush. This pattern indicates that a large fraction of MPs remained mobile during loading, consistent with a repulsive interaction at very low ionic strength. In contrast, under DI pre-hydration, no detectable breakthrough was observed, and hydraulic conductivities remained extremely low. These results suggest that the absence of breakthrough in DI-hydrated specimens is controlled primarily by microstructural factors such as enhanced swelling, reduced pore sizes, and low hydraulic conductivity. Whether MPs can migrate through the bentonite therefore depends fundamentally on the relationship between MP particle size and the size of hydraulically accessible pore spaces. In contrast, the elevated conductivity and altered pore network of Ca^{2+}-hydrated GCL-1 allowed significant MP transmission, with retention arising from a combination of pore-scale interception and localised high-affinity attachment rather than classical secondary-minimum attraction alone.

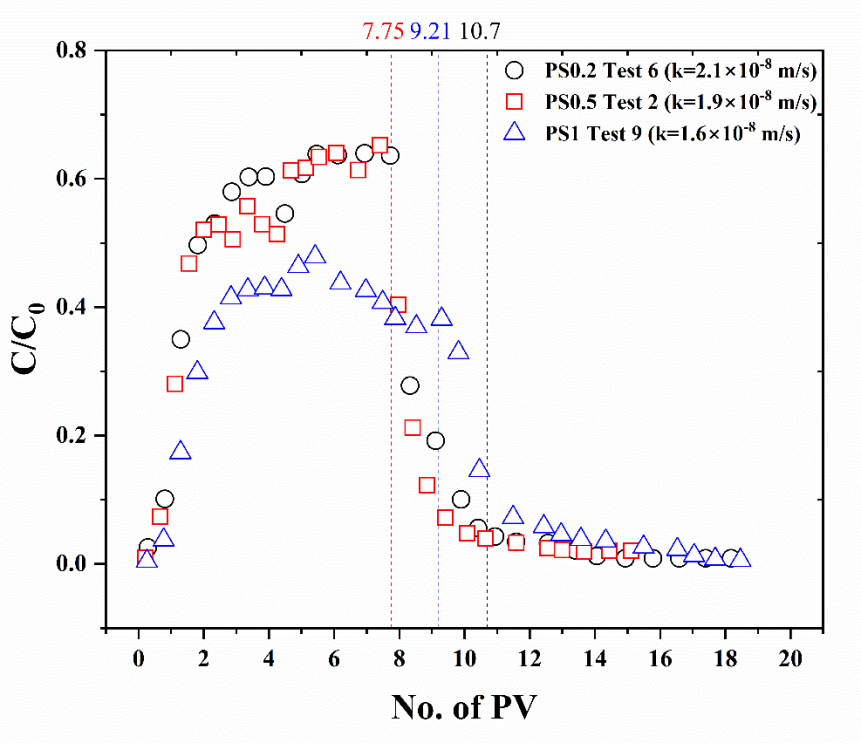

Figure 6.9. BTCs for f-PS0.2 (Test 6), f-PS0.5 (Test 2) and f-PS1 (Test 9) through GCL-1 at 100 mM $CaCl_2$ after two wet-dry cycles. Numbers above dashed lines represent the PV number during which MP was injected into the column and beyond which MP-free DI solution was eluted. Reported *k* values are shown in the legend.

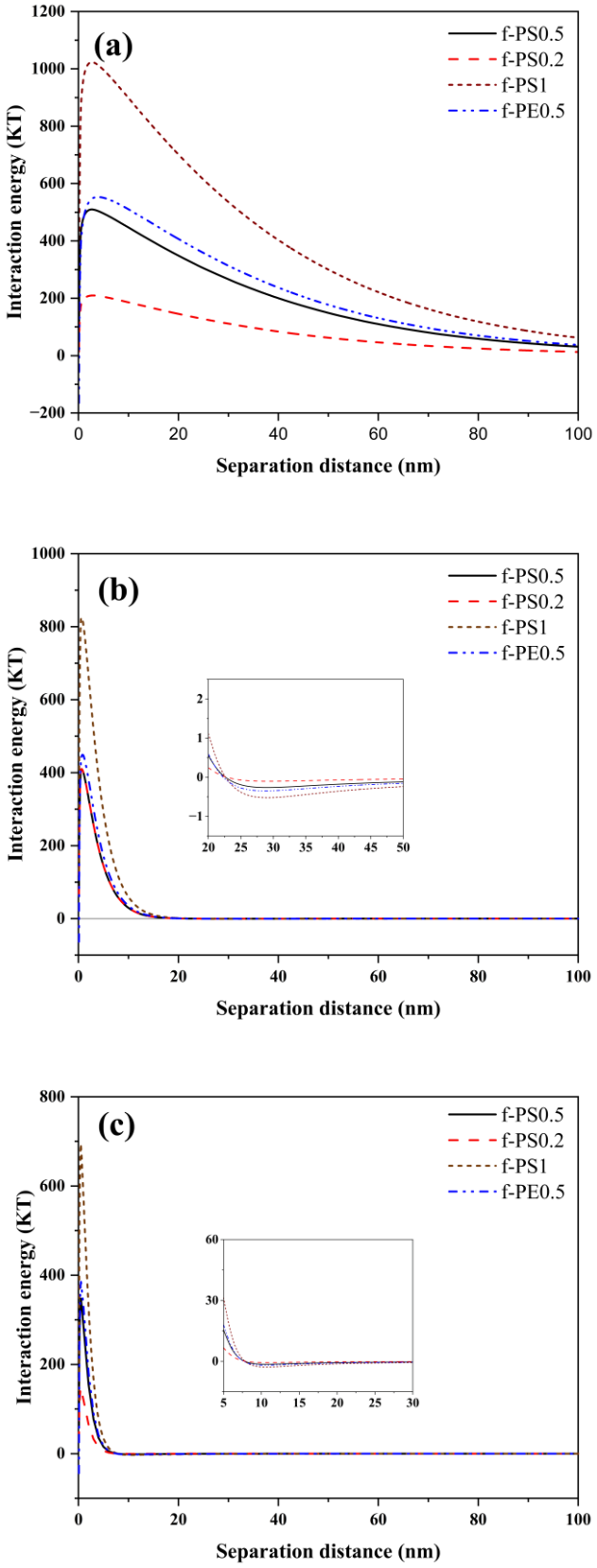

Figure 6.10. DLVO interaction energy profiles between MPs and bentonite at (a) extremely low ionic strength (~0.1 mM), (b) 10 mM, and (c) 50 mM.

6.3.3.2.3 Effect of Particle Type

Figure 6.11 compares BTCs for f-PS0.5 and f-PE0.5, under identical pre-hydration conditions for GCL-1 (100 mM $CaCl_2$ and two wet-dry cycles) and closely matched hydraulic conductivity (both k $\approx 3.0\times10^{-8}$ m/s). Under these conditions, f-PS0.5 (Test 5) rose gradually to a peak C_{max}/C_0 of 0.79 at 9.6 PV, whereas f-PE0.5 (Test 11) reached its peak earlier at 6.4 PV with a lower plateau of 0.64. Consistent with the lower peak, the transmitted mass per unit area $M_{MP\text{-}effluent}$ decreased from 1757 to 1326 mg/m^2, and the transmission coefficient γ dropped from 0.68 to 0.56 (Table 6.4), suggesting weaker retention of f-PS0.5 than f-PE0.5 at comparable nominal size.

A repeat f-PS0.5 test (Test 2) conducted at a lower hydraulic conductivity (k $=1.9\times10^{-8}$ m/s) yielded a lower peak and transmitted mass (C_{max}/C_0=0.65, $M_{MP\text{-}effluent}$=1236 mg/m^2, and γ=0.55), consistent with the sensitivity of breakthrough magnitude to hydraulic conductivity observed elsewhere in this test set.

Several factors may contribute to the stronger retention observed for f-PE0.5. First, f-PE0.5 exhibits broader size distributions than f-PS0.5 (see Figure 3.8e), which likely introduces larger particles and aggregates in the influent. Even a modest fraction of larger particles can increase the possibility of pore-throat straining (Auset and Keller, 2006). Second, polymer-specific surface properties may alter interactions at geotextile and clay interfaces. Stronger hydrophobic interactions between PE and geotextile fibres may strengthen retention relative to PS particles (Bîrleanu et al., 2023). Third, higher surface heterogeneity of f-PE0.5 may enhance effective contact area and mechanical interlocking (Torkzaban and Bradford, 2016). These mechanisms are not mutually exclusive and may act concurrently.

DLVO interaction profiles calculated at low ionic strength (Figure 6.10a) show that f-PE0.5 has a slightly higher primary energy barrier than f-PS05, implying more repulsive interactions with an idealised smooth bentonite surface. The stronger observed retention of f-PE0.5 therefore suggests that non-DLVO processes (e.g., hydrophobic interactions with geotextile fibres) may play a dominant role in controlling MP retention in GCL-1 for different polymer types.

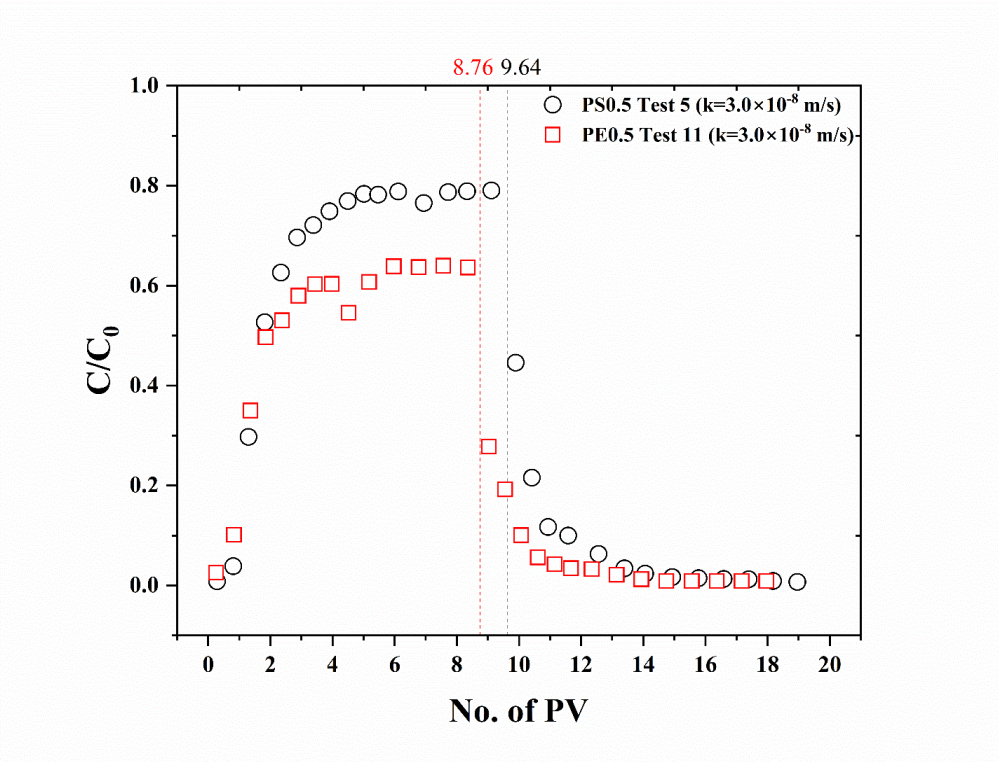

Figure 6.11. Polymer-type effect on MP breakthrough (f-PS0.5 and f-PE0.5) in GCL-1 at 100 mM $CaCl_2$ with wet-dry cycling. Numbers above dashed lines represent the PV number of MP influent. Reported *k* values are shown in the legend.

6.3.3.2.4 Effect of Hydraulic Conductivity

As shown in section 6.3.1, $CaCl_2$-hydrated GCL-1 specimens yielded a range of hydraulic conductivities despite identical pre-hydration protocols, likely due to variations in bentonite distribution and gel development arising from manufacturing and handling variability (e.g., panel-to-panel variability and needle-punched density, and minor edge or cutting effects that alter effective bentonite mass per unit area). This variability provides an opportunity to assess how hydraulic conductivity influences MP transport.

Figure 6.12 summarises the relationships between hydraulic conductivity and both the peak normalised concentration and overall transmission for Test Set 1. As *k* increases, breakthrough peaks for PS particles rise. At comparable *k*, f-PS1 attains lower C_{max}/C_0 than f-PS0.2 and f-PS0.5, whereas f-PS0.2 and f-PS0.5 show no significant difference. For a fixed size (0.5 μm), f-PS exhibits higher C_{max}/C_0 than f-PE, implying stronger retention of PE than PS under the same chemical conditions. Collectively, these results indicate that $CaCl_2$-induced increase in *k* strongly influences breakthrough magnitude, while particle size and polymer type modulate the response vertically at a given *k*.

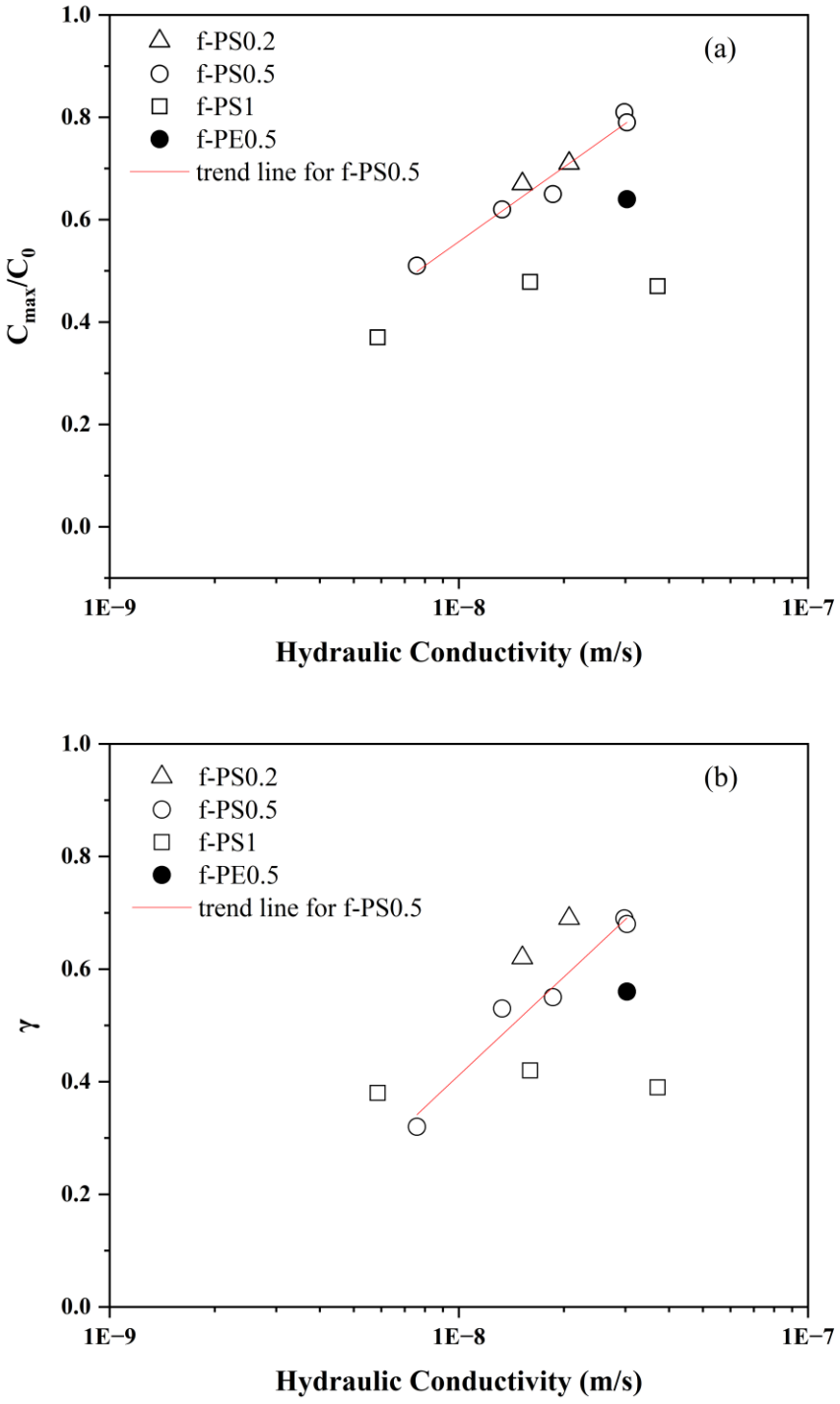

Figure 6.12. Relationship between hydraulic conductivity and (a) maximum normalized concentration (C/C_0); and (b) overall transmission coefficient γ from Test Set 1 for GCL-1 hydration with 100 mM $CaCl_2$ solution.

6.3.3.2.5 Interpretation of Plateau Behaviour

The plateauing behaviour of the BTCs provides insight into MP retention within the GCL specimens. In the experiments with MP breakthrough, effluent concentrations generally stabilised at C/C_0 values below 1 rather than approaching complete breakthrough. This behaviour suggests that only part of the injected MP mass remained mobile during transport, while another fraction continued to be retained within the GCL structure during the experiments.

The BTCs also suggest the coexistence of reversible and irreversible retention processes. During DI-water flushing, effluent concentrations declined relatively rapidly, indicating that part of the retained MP mass was weakly retained and could be remobilised under low ionic strength conditions. At the same time, incomplete mass recovery indicates that a proportion of MPs remained retained within the GCL specimens over the duration of the experiments.

These observations are consistent with the MIP results presented previously, which showed increased volumes of larger accessible pores in the chemically impacted GCLs following $CaCl_2$ exposure and wet-dry cycling. Enlargement of pore throats and reduction in bentonite swelling would be expected to reduce physical straining and increase MP mobility. However, retention could still occur at localised pore constrictions, bentonite surfaces, and fibre-clay interfaces within the damaged structure.

From an engineering perspective, the breakthrough observed in the chemically impacted GCLs represents a substantial reduction in barrier performance relative to the well-hydrated specimens, which showed no detectable MP breakthrough within the testing duration. Nevertheless, even under chemically aggressive conditions, a considerable fraction of the injected MPs remained retained within the GCL system over the duration of the tests, indicating that partial attenuation capacity was maintained despite the increase in hydraulic conductivity.

6.3.4 Scanning Electron Microscopy and Dyeing Test

Figure 6.13 shows SEM images obtained from Test 1 (GCL-1 pre-hydrated with 100 mM $CaCl_2$), Test 13 (GCL-1 pre-hydrated with DI water), and Test 14 (GCL-2 pre-hydrated with 300 mM $CaCl_2$). In Test 1, distinct f-PS0.5 particles were visible on bentonite surfaces after DI water flushing (Figure 6.13a, b), indicating particle deposition and likely irreversible attachment within the bentonite matrix. In contrast, as discussed in section 6.3.3.1, no MP breakthrough was detected for GCL-2 even after pre-hydration with 300 mM $CaCl_2$ and wet-dry cycling. SEM assessment of bentonite recovered from the interior of GCL-2 specimen did not reveal MPs within the imaged fields (Figure 6.13d). However, MPs were evident on the cover geotextile fibres (Figure 6.13c). A similar pattern was observed for DI-hydrated GCL-1 (Figure 6.13e), where MPs were clearly observed on the cover geotextile but not within the bentonite. These observations suggest that the cover geotextile can capture a substantial fraction of MPs, while the low-permeability bentonite gel limits particle penetration, promoting retention at or near the cover geotextile-bentonite interface.

These SEM observations qualitatively align with the conceptual framework proposed by Bordoloi et al. (2022), which distinguishes between physical straining of few-micrometre MPs within intra-aggregate pore spaces and surface attachment of weathered-nanoscale particles onto mineral surfaces. In the present study, direct evidence of straining within bentonite pores was not observed in the SEM fields examined, whereas particle attachment to bentonite surfaces (in $CaCl_2$-hydrated GCL-1) and interception by geotextile fibres (in DI-hydrated GCL-1 and $CaCl_2$-hydrated GCL-2) were apparent, suggesting that surface deposition and geotextile filtration are the primary retention pathways under the tested conditions.

It should be noted that SEM analysis provides only limited spatial coverage of the specimen and examines relatively small fields of view. Consequently, sparse or spatially heterogeneous MP distributions within the bentonite matrix may not have been captured in the imaged regions. The SEM observations presented here should be interpreted as indicative evidence of preferential retention near the cover geotextile-bentonite interface. More systematic spatial sampling, retention profiling, or complementary imaging techniques would be required to quantitatively resolve MP distributions throughout the GCL structure.

Post-test dyeing images indicate a non-uniform flow field influenced by the needle-punched reinforcement (Figure 6.14). In the plan view (Figure 6.14a), two darker patches coincide with the footprints of needle-punched fibre bundles, implying locally higher through-flow. The faint pink ring at the perimeter is dye wicking in the support paper rather than edge leakage. The absence of pronounced staining at the specimen perimeter is consistent with negligible sidewall flow in the FWP.

After peeling the cover geotextile (Figure 6.14d), an exposed bundle is seen embedded in bentonite. The needle-punched bundles may act as preferential flow pathways that promote early arrival of the solution. However, in the present dye tracing experiment, no significant staining was observed directly along the bundle interfaces. Taken together with the MIP results (Figure 6.7), which show macropore development in GCL-1 after 100 mM $CaCl_2$ conditioning, these observations suggest that under chemically impacted states, macropores may provide the dominant preferential paths, with bundle-adjacent interfaces acting as secondary conduits.

It should also be noted that dye tracing was conducted for a single specimen only, and therefore variability in local flow behaviour between specimens could not be systematically evaluated. Consequently, the role of needle-punched bundles in promoting preferential flow remains uncertain and should be interpreted cautiously. More extensive replicated dye tracing or spatial flow visualisation studies would be required to conclusively assess the influence of bundle-related interfaces on MP transport behaviour.

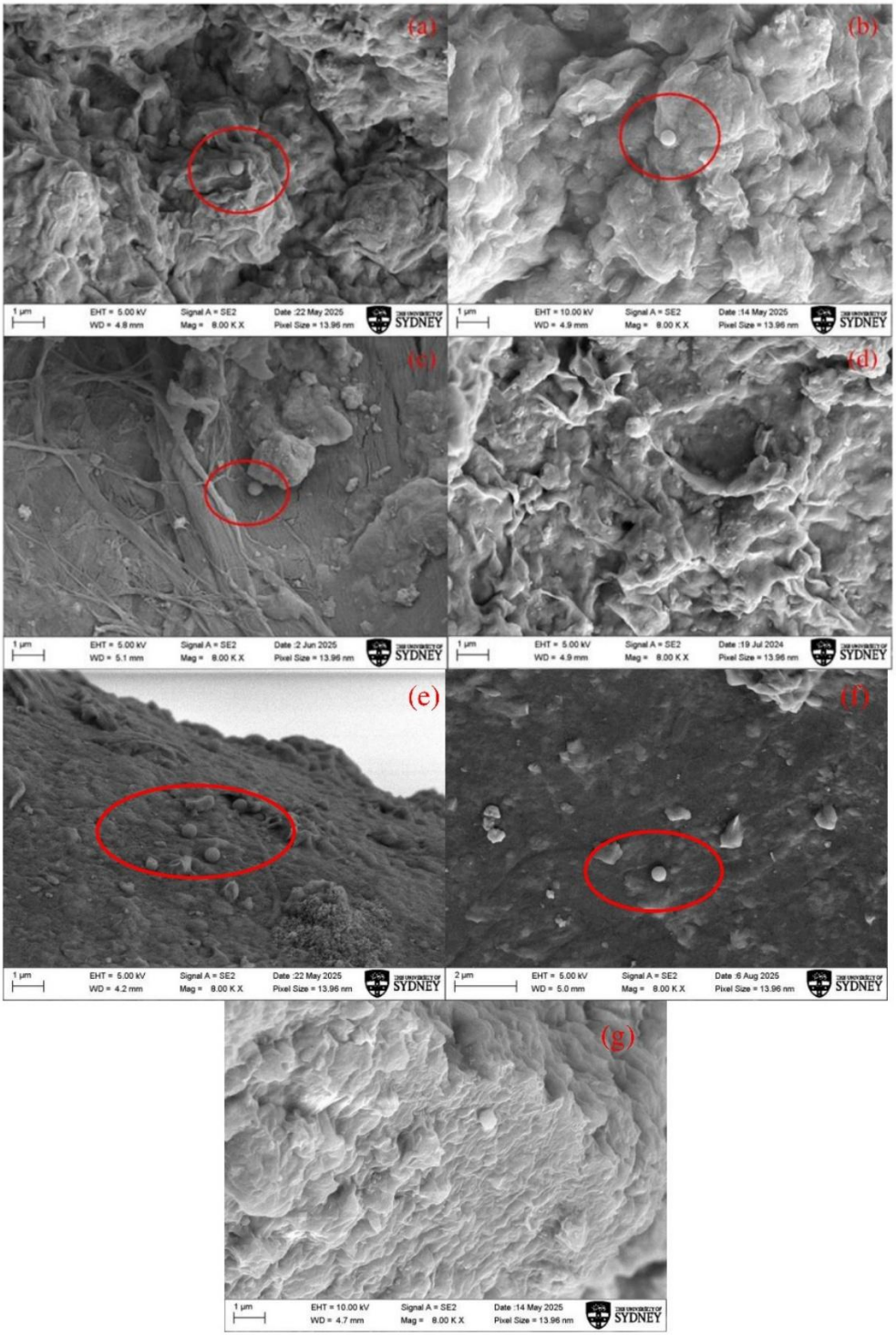

Figure 6.13. SEM images (8000×, scale bar =1 μm, SE2 detector) showing deposition and entrapment of f-PS0.5 within GCL components: (a) centre bentonite region after Test 1; (b) edge bentonite region after Test 1; (c) cover geotextile after Test 14; (d) bentonite from Test 14 showing surface features in the absence of obvious f-PS0.5; (e) cover geotextile after Test 13; (f) cover geotextile after Test 1; and (g) centre bentonite region after Test 13. Red circles denote MP particles.

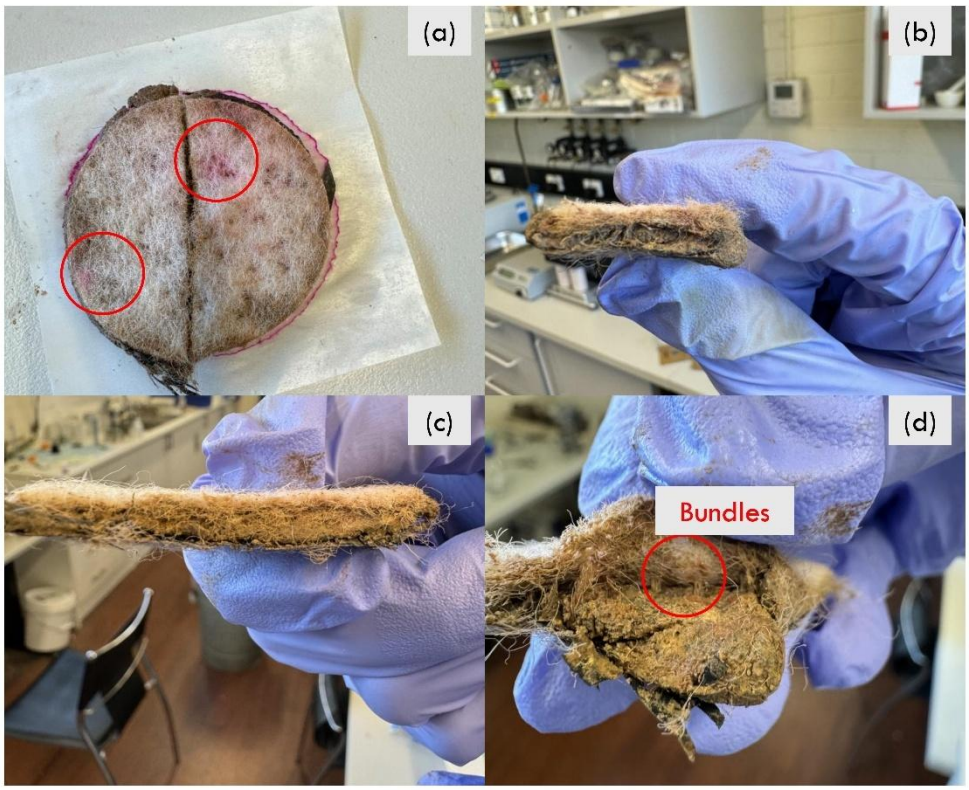

Figure 6.14. Post-test photographs of the GCL specimen from Test 10 following MP transport and DI water elution under top-to-bottom flow: (a) plan view; (b) side view; (c) cross-section through the specimen; and (d) specimen after peeling the cover geotextile.

6.4 Conclusions

This study examined the transport of sub-micrometre MPs (PS, PE) through two commercial GCLs: a granular sodium bentonite GCL (GCL-1) and a polymer-amended powdered sodium bentonite GCL (GCL-2) under controlled hydration chemistries using FWPs. Swelling index testing identified the $CaCl_2$ concentration that reduce bentonite swelling below 10 mL/2 g, namely 100 mM for GCL-1 and 300 mM for GCL-2, reflecting the greater chemical tolerance of the polymer-amended bentonite. Under deionized hydration, hydraulic conductivities remained low and neither GCL (with powder or granular bentonite) exhibited measurable breakthrough within the experimental duration.

In contrast, pre-hydrating GCL-1 with 100 mM $CaCl_2$ under wet-dry cycling increased hydraulic conductivity by approximately one to two orders of magnitude and produced measurable breakthrough of sub-micrometre MPs. However, GCL-2 maintained k in the 10^{-10} m/s range and showed no detectable breakthrough even after 300 mM $CaCl_2$

hydration with wet-dry cycling, indicating preserved sealing capacity under aggressive chemistry, within the experimental duration of the tests (up to 4 PV). More generally, at low hydraulic conductivities ($<5\times10^{-10}$ m/s), no breakthrough was detected after around 4 PV, consistent with diffusion-limited penetration and geometric size exclusion in hydrated bentonite and geotextiles.

Size and type of MP particles moderately affected the response of 100 mM $CaCl_2$-hydrated GCL-1, but breakthrough continued to occur under all cases considered. Specifically, increasing particle size from 0.2 μm to 1.0 μm reduced C_{max}/C_0, $M_{MP\text{-}effluent}$, and γ, while at fixed size (0.5 μm), PE showed stronger retention than PS, likely reflecting polymer-specific surface properties and PE's broader size distribution. Replication for the 0.2 μm and 1.0 μm particle sizes was limited, and these differences should therefore be interpreted as indicative trends rather than statistically robust relationships.

These mechanistic interpretations are conditional on the chemically degraded test conditions under which breakthrough was observed and may not be directly transferable to well-hydrated or well-maintained GCL conditions exhibiting substantially lower hydraulic conductivity and negligible breakthrough within the experimental duration. It should also be noted that mass balance analysis in this study is conducted with measuring effluent recovery, but without explicit partitioning of retained MPs among individual components (e.g. geotextiles, bentonite, and porous stones). Accordingly, retention behaviour is interpreted in terms of overall system response rather than component-specific mechanisms. Quantitative resolution of MP distribution within GCL components would require targeted extraction or imaging approaches and represents an area for future investigation.

These findings indicate that, within the limits of experimental methods used in this thesis, properly hydrated GCLs, can act as effective barriers to sub-micrometre MPs. They underscore the importance of pre-hydration chemistry control, avoidance of early exposure to divalent-rich leachates and desiccation cycles, and design practices that pair conductivity targets with flux-based leakage assessments under site-specific heads and defect scenarios. To strengthen field applicability of these findings, future work should extend monitoring durations, vary hydraulic gradients, pair conservative tracers with MPs to better quantify dispersivity and tortuosity, and conduct column studies with actual landfill leachate.

Chapter 7 Numerical Modelling of Microplastic Breakthrough in GCLs

7.1 Introduction

Chapter 6 presented experimental data on MP breakthrough and mass retention in two commercially available GCLs using a FWP under different hydration chemistries and wet-dry cycling. The results showed significant increases in hydraulic conductivity and MP transmission for GCLs with granular sodium bentonite pre-hydrated with 100 mM $CaCl_2$ with wet-dry cycling. Qualitative interpretation of BTCs, supported by DLVO calculations and SEM analyses, suggested the presence of both mobile and strongly retained MP fractions with multiple retention processes likely involved (e.g., reversible and irreversible attachment, and capacity-limited blocking).

In this chapter, predictions of first-order kinetic ADR models are backfitted to the BTCs from these tests in order to quantitatively infer possible mechanisms governing transport and retention of MPs in GCLs. Specifically, the following two research questions are addressed: (a) to what extent can one- and two-site kinetic ADR models with time- or depth-dependent blocking terms reproduce the observed BTCs, and (b) what do the fitted parameters reveal about the dominant MP retention mechanisms?

Experimental observations from Chapter 6 indicate that MP retention likely occurred through several mechanisms at different locations within the GCL structure. In the no-breakthrough tests, SEM observations suggest that front-end interception near the carrier geotextile and limited pore accessibility contributed substantially to retention. In contrast, the breakthrough experiments suggest that additional retention processes occurred within the chemically impacted bentonite structure and preferential flow regions. The relative importance of these retention mechanisms likely varies depending on hydraulic conductivity, hydration condition, and the extent of MP breakthrough.

The ADR modelling framework adopted in this chapter represents the entire GCL specimen as a single equivalent one-dimensional transport domain. The modelling does not distinguish explicitly between retention occurring at the geotextile interfaces and retention occurring within the bentonite layer. Consequently, the fitted attachment and retention parameters represent the overall retention behaviour of the composite GCL system rather than retention processes associated with a specific component.

7.2 Methods: Backfitting ADR Equations to BTCs

The breakthrough behaviour was interpreted using a one-dimensional ADR model in which the aqueous MP concentration, $C(x,t)$, is coupled to one or two solid-phase reservoirs of retained mass, $S_1(x,t)$ and $S_2(x,t)$. The aqueous-phase mass balance follows the ADR equation given in section 2.3.2. Within this framework, reversible retention refers to first-order attachment to, and detachment from, a solid-phase site, whereas irreversible retention refers to first-order attachment with no detachment term.

First-order kinetics were adopted throughout. Attachment rate coefficients to sites 1 and 2 are k_{a1} and k_{a2} [T^{-1}], and the detachment rate coefficient from the reversible site is k_{d2} [T^{-1}]. Finite retention capacity is represented by a maximum solid-phase capacity, $S_{\max}$ [$M.M^{-1}$], such that attachment is progressively reduced as retained mass accumulates.

Two modifiers were used to allow attachment rates to evolve during transport:

- Time-dependent blocking modifier:

$$\psi(t) = 1 - \frac{S}{S_{max}}$$

  As deposited mass S grows, ψ decreases from 1 toward 0, reducing the effective attachment rate.

- Depth-dependent modifier:

$$\psi(x) = \left(\frac{d_c + x}{d_c}\right)^{-\beta}$$

  where x is distance from the inlet, d_c is the median grain size, and β is the shape parameter of colloid.

In addition to blocking, ripening was represented using an attachment enhancement factor ψ that increases with retained mass, reflecting formation of secondary collectors and increasing interception probability as deposition proceeds. Although both blocking and ripening modify the effective attachment rate during transport, they represent different types of retention behaviour. Blocking describes progressive occupation of a finite number of retention sites, whereas ripening reflects conditions in which previously retained particles promote additional deposition through particle clustering, surface roughening, or formation of secondary collectors.

In the present study, blocking is consistent with the gradual reduction in retention efficiency observed during continued MP transport through chemically impacted GCLs, where finite retention sites may become progressively occupied. Ripening is more consistent with the BTC behaviour observed for f-PS1, where retention increased during continued loading, suggesting that previously retained particles may have promoted additional capture through particle clustering or secondary collector formation near preferential flow paths.

Dispersivity was not measured independently using a conservative tracer. Instead, dispersivity and the kinetic retention parameters were estimated simultaneously through inverse fitting of the BTCs. The fitted dispersivity values should therefore be regarded as effective fitting parameters within the adopted modelling framework rather than uniquely defined physical properties of the GCL system. Since the modelling relied solely on BTC data, without independent hydrodynamic constraints, some overlap between dispersive transport effects and kinetic retention behaviour is unavoidable. Consequently, different combinations of dispersivity and retention parameters, and in some cases different model structures, were able to reproduce similar BTC responses. This issue is particularly important for tests exhibiting incomplete breakthrough, where dispersive spreading and retention effects cannot be separated from the available data.

Table 7.1 lists the kinetic options evaluated. Models 1-5 are single-site irreversible formulations, optionally with time- and/or depth-dependent blocking or ripening. These models assume that irreversible processes are dominant (e.g., strong retention or effectively irreversible capture over the test duration). Models 6-11 are two-site formulations that combine an irreversible site and a reversible site (with detachment). Time- and/or depth-dependent blocking or ripening were applied on the irreversible site (including Model 11,

in which modifiers may act on both sites). For each model, the corresponding first-order kinetic expressions for S_1 and S_2 are given in columns B and D of Table 7.1.

Table 7.1. Eleven variants of blocking functions that used in the ADR framework.

A	B	C	D	E	F
Model No.	**Site No. (n=1)**		**Site No. (n=2)**		**Retention Description**
	Site One	**Blocking Function at first site (ψ_1)**	**Site Two**	**Blocking Function at second site (ψ_2)**	
1	$\frac{\rho}{\theta}\frac{\partial S_1}{\partial t} = k_{a1}\psi_1 C$	1	Not Relevant		Irreversible
2		$\left(1-\frac{S_1}{S_{max,1}}\right)$			Irreversible with time-dependent blocking
3		$\left(\frac{d_c+x}{d_c}\right)^{-\beta}$			Irreversible with depth-dependent blocking
4		$\left(1-\frac{S_1}{S_{max,1}}\right)\left(\frac{d_c+x}{d_c}\right)^{-\beta}$			Irreversible with both time- and depth-dependent blocking
5		$\max(1, S^{S_{max,1}})$			Irreversible with ripening
6	$\frac{\rho}{\theta}\frac{\partial S_1}{\partial t} = k_{a1}\psi_1 C$	1	$\frac{\rho}{\theta}\frac{\partial S_2}{\partial t} = k_{a2}\psi_2 C - \frac{k_{d2}\rho S_2}{\theta}$	1	Irreversible and reversible
7		$\left(1-\frac{S_1}{S_{max,1}}\right)$		1	Irreversible and reversible with time-dependent blocking for the irreversible retention
8		$\left(\frac{d_c+x}{d_c}\right)^{-\beta}$		1	Irreversible and reversible with depth-dependent blocking for the irreversible retention
9		$\left(1-\frac{S_1}{S_{max,1}}\right)\left(\frac{d_c+x}{d_c}\right)^{-\beta}$		1	Irreversible and reversible with both time- and depth-dependent blocking for the irreversible retention
10		$\max(1, S^{S_{max,1}})$		1	Irreversible and reversible with ripening for the irreversible retention
11		$\left(1-\frac{S_1}{S_{max,1}}\right)$		$\left(1-\frac{S_2}{S_{max,2}}\right)$	Irreversible and reversible with time-dependent blocking for both types of retention

A customised inverse solver (Duncan and El-Zein, 2026) was used to backfit kinetic parameters for each of the eleven ADR variants considered in this chapter, including attachment rate coefficients (k_{a1},k_{a2}), a detachment rate coefficient for the reversible site (k_{d2}), and lumped capacity terms ($S_{max,1}$, $S_{max,2}$) where applicable. To select the model with the best ability to capture observed behaviour, two complementary metrics were used: the coefficient of determination (R^2, descriptive goodness-of-fit) and the small-sample corrected Akaike Information Criterion (AIC) with Akaike weights (comparative model selection) (Duncan and El-Zein, 2026).

The coefficient of determination, R^2, summarises the fraction of variance in the observations explained by a fitted curve, with higher values closer to 1 indicating closer match between predictions and data. However, because R^2 does not penalise model complexity, it is not sufficient on its own for comparing models with different numbers of fitted parameters.

Hence, competing ADR formulations were further ranked using AIC (Guo and Fei, 2023), which balances lack-of-fit against model parsimony:

$$AIC_i = n\ \log\left(\frac{SSQ}{n}\right) + 2p + \frac{2p^2+2p}{n-p-1} \tag{7.1}$$

where n is the number of data points in the fitted curves, p is the number of fitted parameters, i is an index indicating the model, and SSQ is the normalised sum of squared residuals.

In this chapter, only BTC data were available, so SSQ was computed as:

$$SSQ = \frac{\sum(Y_{obs,BTC}-Y_{pred,BTC})^2}{\sum(Y_{obs,BTC}-\overline{Y_{obs,BTC}})^2} \tag{7.2}$$

where $Y_{obs,BTC}$ and $Y_{pred,BTC}$ are the observed BTC vector and the corresponding model predictions, respectively. The overbar denotes the sample mean of the observed BTC. This normalisation renders SSQ dimensionless.

For interpretation, AIC values were converted to Akaike weights w_i, which quantify the relative likelihood that a model is best performing within the candidate set:

$$w_i = \frac{\exp\{-\frac{1}{2}(AIC_i-\min(AIC)\}}{\sum_{i=1}^{I}\exp\{-\frac{1}{2}(AIC_i-\min AIC)\}} \tag{7.3}$$

where I is the total number of candidate models (I=1-11). Following Duncan and El-Zein (2026), this chapter interprets $w_i \geq 0.70$ as strong support for model i. Sensitivity checks using thresholds of 0.50, 0.60, 0.80, 0.90 and 0.95 did not change the rankings or overall

conclusions, therefore results are reported for the 0.70 criterion (Duncan and El-Zein, 2026). Note that $w_i \geq 0.7$ implies odds of at least $w_i/(1- w_i) \geq 2.3$ in favour of the top-ranked model over all alternatives combined, since any single runner-up necessarily has $w_i \leq 0.30$.

7.3 Results and Discussion

7.3.1 Best Model Selection for Tests 1-11 (Breakthrough Observed)

For all experiments in which measurable breakthrough occurred (Tests 1-11 in Table 6.1), predictions from the eleven candidate models listed in Table 7.1 were backfitted to the BTCs. Model performance was ranked using the AIC, and Akaike weights w_i were computed for each model to quantify relative support within the candidate set. Table 7.2 summarises, for each experiment, the three models with the largest w_i values. Detailed modelling plots are shown in Figures X2-X12.

To keep the table concise while retaining the models most supported by the data, the following reporting rule was applied. If the best-ranked model satisfies $w_i \geq 0.70$, only that model is reported (in the third column of Table 7.2). Otherwise, up to three highest-ranking models are shown in such a way that the total Akaike weight of the three models is 0.7 or more. Table 7.3 lists the fitted parameter values for the models shown in Table 7.2 (i.e., those with high Akaike weights up to a total greater than 0.7). Where multiple parameter sets are reported for a given experiment, these correspond to alternative candidate model formulations identified through the AIC-based model selection procedure rather than replicate experiments. Differences between parameter sets for the same test reflect model-selection uncertainty and parameter identifiability limitations, rather than experimental variability.

The key objective of this model-selection exercise is to identify the dominant transport and retention processes that could explain the BTCs, rather than to argue for a single “best” functional form. Several qualitative features of the BTCs, such as tailing, incomplete breakthrough, and ripening-like behaviour, are evident from visual inspection. However, the ADR modelling provides a quantitative framework for evaluating whether simpler transport formulations are sufficient to reproduce the observations. In particular, comparison across multiple model structures allows assessment of whether processes such as blocking, reversible attachment, or ripening are consistently required to reproduce the

BTC shapes. The modelling therefore serves primarily as a consistency check on the conceptual interpretation of the experiments and as a means of excluding simpler model classes that cannot adequately capture the observed transport behaviour.

Table 7.2. Well-fitted model selections for Tests 1-11 (Model numbers refer to the model definitions in Table 7.1; up to three models are shown with sum of Akaike weight > 0.7).

Test number	Test description	Max Akaike weight (Model No., R^2)	Second-max Akaike weight (Model No., R^2)	Third-max Akaike weight (Model No., R^2)
1	base case (PS 0.5 μm)	0.798 (7, 0.980)	/	/
2		0.470 (3, 0.923)	0.245 (1, 0.919)	/
3		0.255 (1, 0.778)	0.241 (8, 0.803)	0.231 (3, 0.776)
4		0.676 (7, 0.919)	0.196 (6, 0.905)	/
5		0.311 (1, 0.885)	0.221 (3, 0.882)	0.095 (4, 0.883)
6	MP size (0.2 μm)	0.911 (8, 0.933)	/	/
7		0.935 (2, 0.807)	/	/
8	MP size (1 μm)	0.999 (8, 0.926)	/	/
9		0.946 (11, 0.974)	/	/
10		0.842 (10, 0.688)	/	/
11	MP type (PE)	0.671 (10, 0.930)	0.130 (7, 0.921)	/

For Tests 1-7 (base case and f- PS0.2 on GCL-1), the models receiving the strongest overall support across the experiments are Models 2, 3, 7 and 8, whereas the single-site Model 1 (irreversible attachment) appears only as a secondary option or with relatively low w_i. What Models 2, 3, 7 and 8 have in common is the presence of blocking functions (time- or depth-dependent), which reduce the availability of retention sites as attachment progresses. The consistent preference for models incorporating blocking suggests that finite retention capacity and progressive site occupation may be important features of MP transport in GCL-1 pre-hydrated with 100 mM $CaCl_2$. In other words, the BTCs cannot be reproduced satisfactorily by assuming a single, uniform population of attachment sites with constant capacity. Instead, the data require a description in which accessible sites are gradually exhausted as MPs accumulate.

It is important to note that model selection was not fully consistent across the base-case experiments (Tests 1-5), with different models receiving the highest Akaike weights in different tests. This variability likely reflects both experimental heterogeneities, particularly differences in hydraulic conductivity between specimens, and model equifinality, whereby

different ADR formulations can reproduce similar BTC behaviour using alternative combinations of dispersive and kinetic parameters. Accordingly, the model-selection results should not be interpreted as evidence of a single unique transport mechanism for each experiment. Instead, interpretation focuses on transport characteristics that appeared consistently across several plausible models and experiments, including blocking, finite retention capacity, and the presence of reversible-irreversible retention behaviour.

The models performing best for Tests 8-11, which involve the largest PS size (1 μm) and the PE MPs, introduce further complexity. For Tests 8 and 9 (f-PS1), models that incorporate blocking on the irreversible retention site (and, in some cases, also on the reversible site) are overwhelmingly preferred, implying that finite-capacity effects and progressive site saturation are important. Tests 10 and 11 favour Model 10, which combines ripening on the irreversible site with a reversible attachment domain.

The irreversible attachment rate k_{a1} generally varies between 0.0016 min^{-1} and 0.2575 min^{-1}. The only exception is in the calculations of Model 10 for Test 11 (f-PE0.5) which yielded outliers for k_{a1}. On the other hand, k_{a2}, k_{d2} and $S_{max,1}$ have wider variabilities spanning three or more orders of magnitude.

A discrepancy also exists between the DLVO interaction energy calculations presented in Chapter 6 and the fitted kinetic attachment coefficients obtained from the ADR modelling in this chapter. The DLVO analysis predicted strongly unfavourable attachment under low ionic strength conditions, with large primary energy barriers (~400-2000 kT) and no evident secondary minima for idealised smooth surfaces. In contrast, the ADR backfitting yielded non-negligible effective attachment coefficients for both reversible and irreversible retention domains. These observations are not directly comparable because the fitted kinetic coefficients represent transport parameters derived from BTC behaviour rather than direct physicochemical attachment probabilities.

The fitted attachment coefficients therefore likely incorporate the combined influence of multiple unresolved retention processes beyond classical DLVO interactions. In addition, the assumptions underlying classical DLVO theory, including smooth and chemically homogeneous collector surfaces, are unlikely to fully represent the heterogeneous pore structure and evolving microfabric of chemically impacted bentonite.

Overall, given the higher Akaike values for two-site models (Table 7.2) and the fact that both k_{a1} and k_{a2} for these models are non-negligible, results in Table 7.3 are consistent

with the earlier conclusion that a combination of reversible and irreversible attachment best explains observed experimental behaviour.

Table 7.3. Parameter output for the eleven formulations of ADR equations.

Test No.	Model No.	Calculated Parameters based on Backfitting to Experimental BTCs						
		Dispersivity (cm)	k_{a1} (min^{-1}) (irreversible attachment rate)	k_{a2} (min^{-1}) (reversible attachment rate)	k_{d2} (min^{-1}) (detachment rate)	S_{max1} (g/g) (capacity)	S_{max2} (g/g) (capacity)
1	7	0.3032	0.0299	10	5.0119	2.25×10^{-4}	N/A
2	3	0.1031	0.0170	N/A	N/A	N/A	N/A
	1	0.0793	0.0766	N/A	N/A	N/A	N/A
3	1	0.0205	0.1370	N/A	N/A	N/A	N/A
	8	0.2808	0.2575	0.0621	0.0314	N/A	N/A
	3	0.0197	0.0350	N/A	N/A	N/A	N/A
4	7	0.0688	0.0368	0.0127	2.63×10^{-5}	3.34×10^{-5}	N/A
	6	0.3539	0.0222	0.1146	0.0539	N/A	N/A
5	1	0.0633	0.0512	N/A	N/A	N/A	N/A
	3	0.1156	0.0112	N/A	N/A	N/A	N/A
	4	0.0549	0.0116	N/A	N/A	4.28×10^{-6}	N/A
6	8	0.0010	0.0378	0.0724	0.0863	N/A	N/A
7	2	0.0558	0.0441	N/A	N/A	1.12×10^{-4}	N/A
8	8	0.2205	0.1629	0.7426	0.2561	N/A	N/A
9	11	0.0257	0.0269	0.0433	0.0620	0.0178	0.26
10	10	0.0041	0.0016	0.0413	0.0014	2.73×10^{-7}	N/A
11	10	0.0389	1.5106	10	0.1075	1.00×10^{-7}	N/A
	7	0.1767	0.0533	0.0191	1.21×10^{-4}	2.07×10^{-5}	N/A

7.3.2 Effects of Experimental Variables on Fitting Parameters

Different tests favoured different ADR models according to the AIC-based selection (Table 7.2), so direct comparison of fitted parameters across all eleven tests is not straightforward. Instead, for each subset of experiments designed to investigate the effect of a specific variable (base-case repetitions, particle size, and polymer type), a representative model was selected for comparative interpretation within each subset. These selections do not imply that alternative models are invalid, but rather provide a consistent basis for examining relative trends in fitted parameters across experiments. Given the observed model variability in hydraulic conductivity between specimens, the parameter comparisons presented below should therefore be interpreted as indicative trends rather than unique mechanistic descriptors.

Model selection within each subset was based on both the maximum and the mean Akaike weights obtained for that model across the relevant tests. On this basis, Model 7 was adopted for Tests 1-5, Model 8 for Tests 6 and 8, and Model 10 for Tests 10 and 11. Figure 7.1 to Figure 7.4 present the corresponding sets of backfitted transport and retention parameters.

Figure 7.1 and Figure **7.*2*** show the parameters estimated for Tests 1-5 under Model 7, plotted against the measured hydraulic conductivity k and the overall transmission efficiency γ, respectively. The fitted dispersivity and kinetic coefficients (k_{a1}, k_{a2}, k_{d2}) span several orders of magnitude. There is no strictly monotonic trend with k, whereas tests with higher hydraulic conductivity tend to require larger dispersivity values and faster kinetic rates. The maximum retention capacity $S_{\max,1}$ tends to decrease with increasing k, indicating that increased permeability is associated with a reduced ability of the GCL to retain MPs. When parameters are plotted against γ, tests exhibiting higher transmission efficiencies tend to exhibit combinations of higher dispersivity and/or higher detachment rates together with lower $S_{\max}$, consistent with enhanced breakthrough through a less retentive barrier.

The influence of particle size is examined in Figure 7.3, which presents parameters obtained using Model 8 for Tests 2, 6 and 8 (PS particle diameters of 0.5, 0.2 and 1.0 μm, respectively). The fitted dispersivity increases with MP particle size, suggesting that larger particles experience greater effective spreading during transport through the GCL. Size-dependent variations in fitted dispersivity have also been reported in particulate transport studies (Chrysikopoulos and Katzourakis, 2015; Li et al., 2024d). However, this trend is not fully consistent with classical colloid transport theory, in which smaller particles may exhibit greater diffusion-enhanced spreading due to Brownian motion. In the present study, dispersivity should therefore be interpreted as an effective parameter reflecting not only hydrodynamic dispersion, but also unresolved transport heterogeneity and retention-related processes embedded within the ADR fitting framework.

For example, larger MPs may experience more spatially variable interactions with preferential flow pathways, pore constrictions, or localised retention sites, leading to increased dispersion. Given the parameter identifiability limitations discussed previously, the fitted dispersivity trends should therefore be interpreted cautiously and not as direct measurements of physical dispersion alone. The irreversible attachment rate k_{a1} also increases with particle size, implying that larger particles are more prone to irreversible

retention. In contrast, the second-site attachment and detachment rates (k_{a2}, k_{d2}) display a non-monotonic behaviour, with relatively low values for the intermediate size (0.5 μm).

Figure 7.4 compares fitted parameters for PS and PE suspensions (Tests 5 and 11) using Model 10. For PE, the fitted dispersivity and kinetic rate coefficients (k_{a1}, k_{a2}, k_{d2}) are one to two orders of magnitude higher than those obtained for PS, while the estimated maximum retention capacity $S_{\max,1}$ is substantially lower. However, given the limited number of experiments on which this observation is based, it is not possible to draw any definite conclusions from the PS-PE comparison.

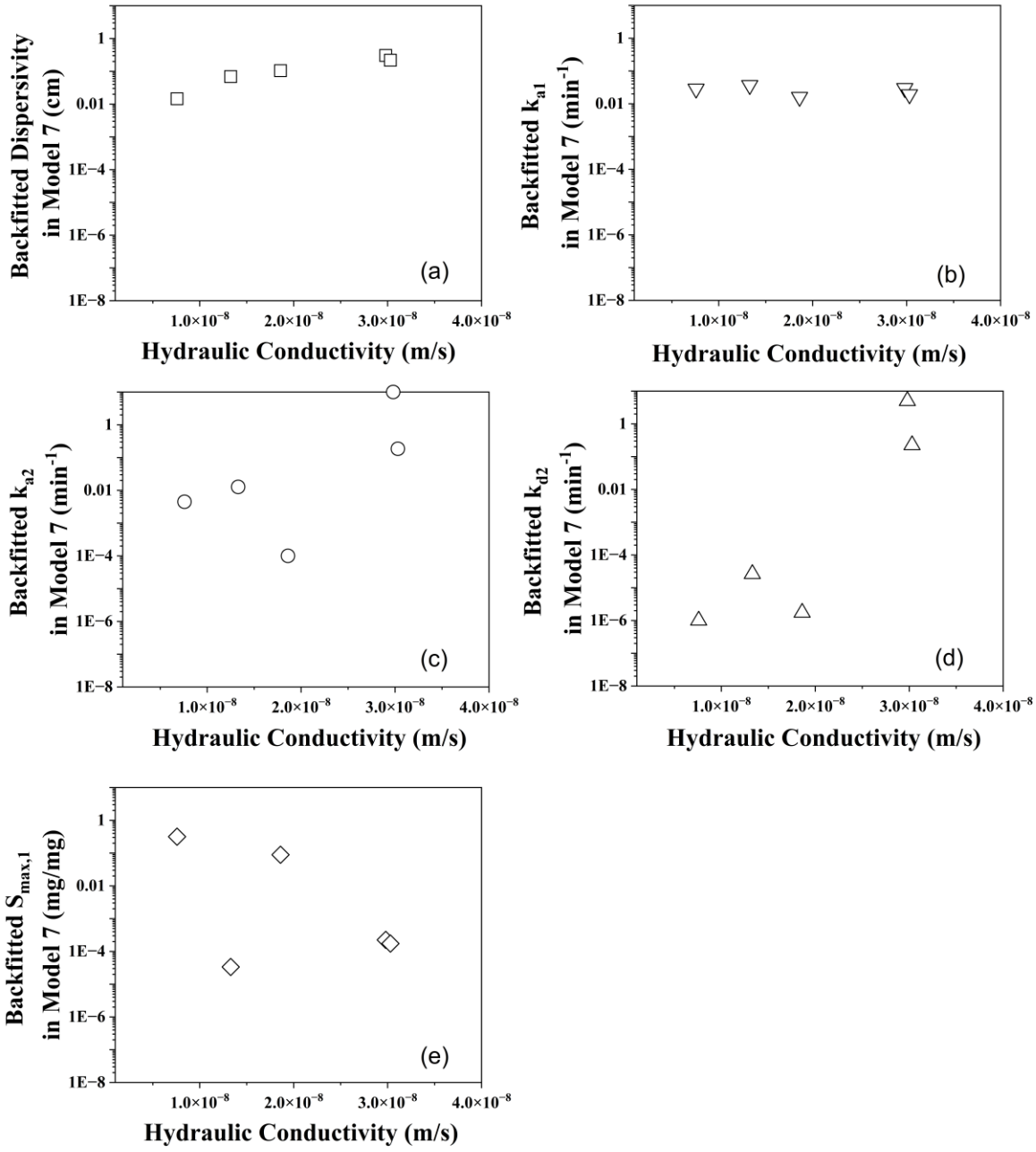

Figure 7.1. Backfitted parameters for Tests 1-5 under Model 7 as a function of hydraulic conductivity.

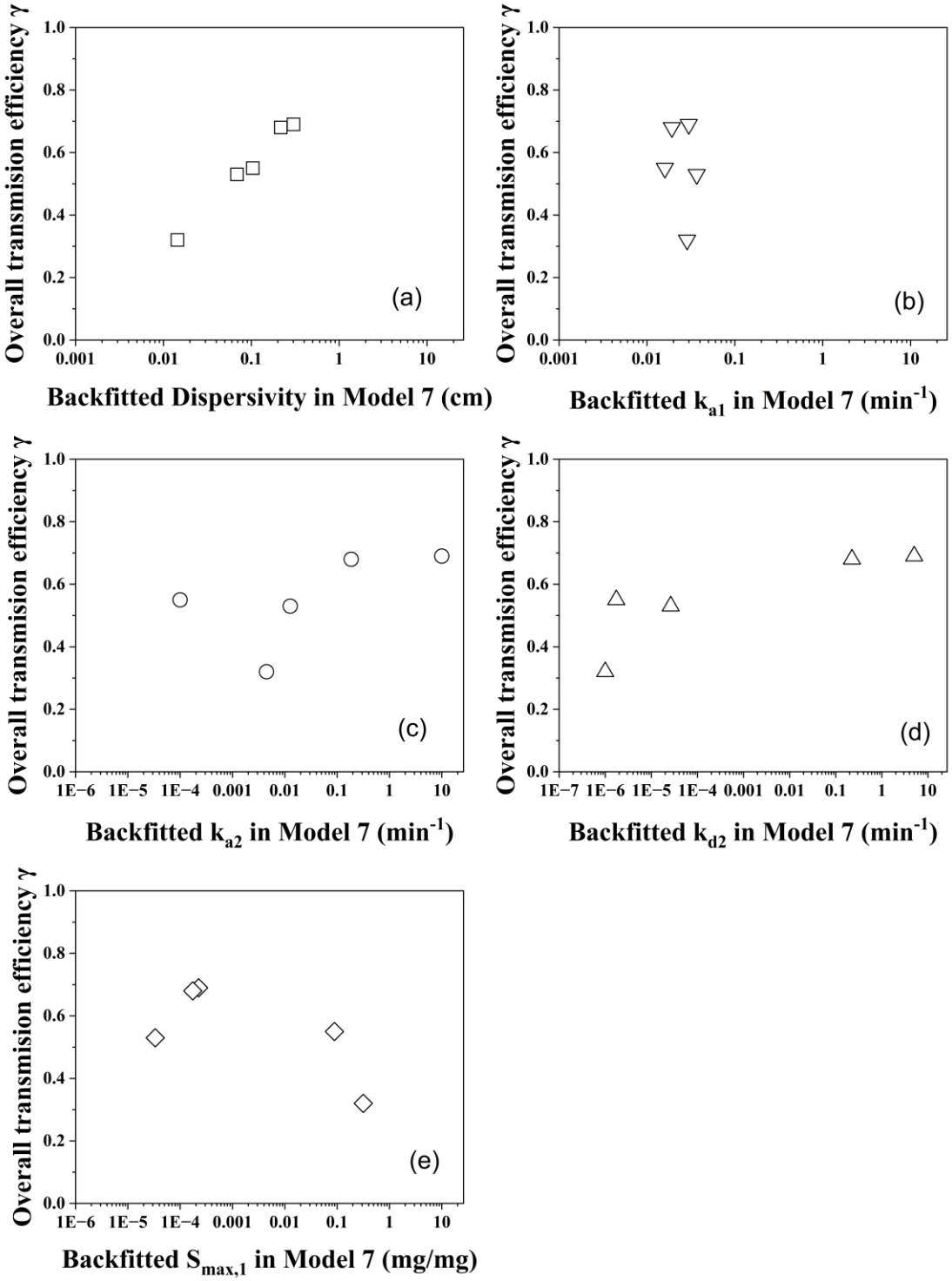

Figure 7.2. Overall transmission efficiency γ of Tests 1-5 under Model 7 as a function of backfitted parameters.

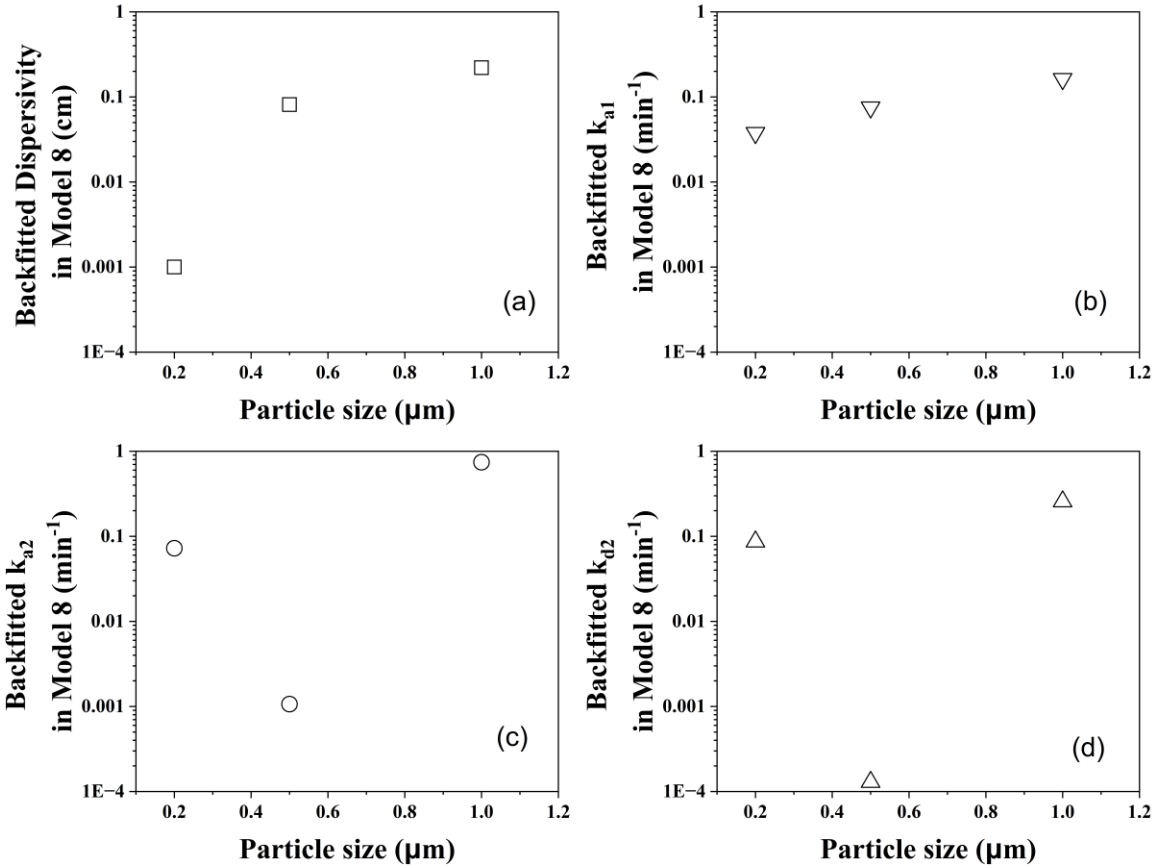

Figure 7.3. Backfitted parameters for Tests 2, 6 and 8 under Model 8 as a function of particle size.

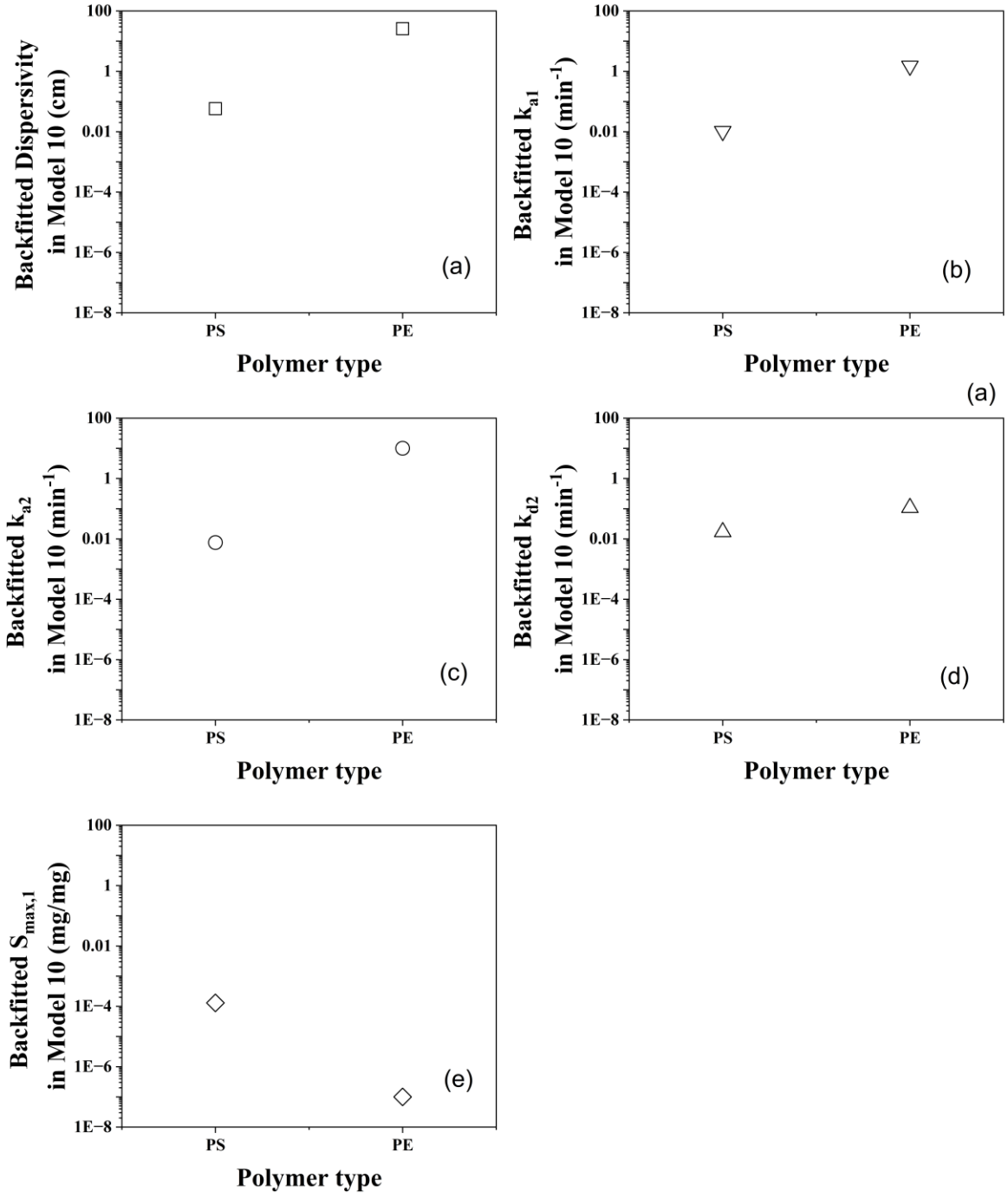

Figure 7.4. Backfitted parameters for Tests 5 and 11 under Model 10 as a function of polymer type (PS and PE).

7.4 Limitations and Conclusions

This chapter applied eleven one- and two-site kinetic ADR formulations to the MP BTCs measured in chemically impacted GCL-1, in order to identify the main transport and retention processes. For experiments with different MP sizes and polymer types, models with blocking (time- and/or depth-dependent) were most strongly supported, while the simple single-site irreversible model rarely ranked highest. This pattern suggests that finite retention capacity and progressive occupation of retention sites may be essential features of MP transport in the tested, chemically impacted GCL, and that a single, spatially uniform attachment domain with constant capacity is insufficient to reproduce the observed BTCs.

For experiments with 1 μm PS and PE, the most strongly supported models additionally required a reversible retention site and, in several cases, ripening on the irreversible site. The fitted parameters imply coexisting reversibly and irreversibly retained fractions, with capacity limitation acting on the irreversible retention site. Trends across tests show that higher hydraulic conductivity, larger particle size and PE polymer all tend to be associated with higher dispersivity and faster kinetic rates, and in some cases lower fitted maximum capacities, consistent with the stronger breakthrough observed experimentally. Overall, the ADR modelling corroborates the experimental evidence that MP transport in GCLs is governed by a combination of finite-capacity irreversible capture and reversible attachment-detachment, moderated by particle size and polymer type.

However, the absence of a single consistently preferred model across similar experiments indicates that model discrimination remained imperfect under the present experimental conditions. Variability in hydraulic conductivity between specimens and the absence of independent conservative tracer constraints likely contributed to equifinality between dispersive transport and kinetic retention processes. Consequently, different ADR formulations were often capable of reproducing similar BTC behaviour with alternative parameter combinations. The principal conclusions of this chapter should be interpreted in terms of transport features consistently supported across multiple plausible model structures, including blocking behaviour, finite retention capacity, and the coexistence of reversible and irreversible retention domains, rather than selection of a unique “best” model.

A key limitation is that ADR backfitting is only applicable when measurable breakthrough occurs. Accordingly, ADR fitting was not attempted for low-permeability GCL conditions in which no breakthrough was observed within the experimental duration.

Nevertheless, these non-breakthrough outcomes remain informative: they provide an upper bound on MP mobility under the tested hydraulic conditions and, when contrasted with the breakthrough cases in chemically impacted GCL-1, reinforce the conclusion that reductions in pore accessibility and advective flux can significantly suppress MP transmission through the GCL.

A further limitation is that the fitted parameters reported in Table 7.3 are presented as single best-fit values without formal uncertainty ranges. Although Akaike weights provide a measure of relative support for competing model structures, they do not quantify uncertainty associated with individual fitted parameters. Consequently, differences in fitted parameters between tests or models should be interpreted cautiously, particularly because multiple parameter combinations were often capable of reproducing similar BTC behaviour. This limitation is related to the model equifinality discussed above and is further complicated by the absence of independent conservative tracer data or retention profile measurements to constrain the fitting process. Accordingly, the fitted parameters are interpreted primarily as effective descriptors of transport behaviour under the tested conditions. Future studies could improve parameter identifiability and uncertainty assessment through sensitivity analysis, conservative tracer testing, and additional measurements such as retention profiles or spatially resolved MP distributions.

Another limitation is that the fitted kinetic and transport parameters were not evaluated independently against physical constraints or external benchmarks from the colloid transport literature. Because the parameters were derived from BTC fitting in heterogeneous GCL specimens, some fitted values may partly compensate for unresolved transport processes or limitations in the adopted model structures. The fitted kinetic parameters should be interpreted primarily as effective descriptors of the observed BTC behaviour within the present modelling framework rather than uniquely defined physical quantities.

Future experimental studies should incorporate conservative non-reactive tracer tests conducted under identical hydraulic and chemical conditions, together with independent measurements of retention profiles or spatially resolved retained MP distributions. Independent estimation of pore-water velocity and dispersivity prior to MP transport modelling would reduce equifinality between hydrodynamic and kinetic retention parameters, while retention-profile measurements would provide additional constraints on

attachment processes and improve confidence in model discrimination and mechanistic interpretation.

Chapter 8 Conclusion

8.1 Research Summary

MPs are emerging contaminants that threaten environmental and human health. Landfills act as long-term reservoirs of plastic waste and potential sources of MPs to surrounding soils and waters. Modern landfill lining systems typically contain a geomembrane over either a GCL or a CCL, designed to contain leachate and prevent the transmission of contaminants into the subsurface. Bentonite is the principal component in GCL-based barriers, and its performance relies on hydration-induced swelling and the resulting low hydraulic conductivity. However, bentonite performance is sensitive to chemically aggressive conditions (e.g., increased ionic strength and divalent cations) and wet-dry cycling. While the efficacy of GCLs against dissolved contaminants and engineered nanoparticles has been well documented, their ability to contain MPs, particularly sub- and few-micrometre particles, remains under-researched. This thesis addressed four key research questions:

1) Does exposure to suspended MPs during hydration alter the swelling capacity of bentonite?

2) Can a FWP serve as a reliable instrument for MP transport studies in low permeability soils?

3) To what extent do GCLs limit MP migration under ideal hydration (DI water) and chemically impacted conditions (e.g., $CaCl_2$ with wet-dry cycling)?

4) Can one- or two-site kinetic ADR equations with time and/or depth-dependent blocking terms reproduce experimental MP BTCs in GCLs?

To answer these questions, two natural sands and two commercially available GCLs were tested under controlled effective stress conditions. The experimental programme

included bentonite swell index and oedometer swell-strain tests, an evaluation of FWP suitability for MP transport, MIP, extensive soil column testing of MP transport in GCLs, fluorescence/UV-Vis quantification, SEM, and one-dimensional ADR modelling with one-site and two-site kinetic terms to account for attachment and detachment. Taken together, these methods provide a coherent experimental-modelling framework for evaluating MP migration and retention in barrier-relevant materials and conditions.

8.2 Main Research Findings

The principal findings of this thesis are synthesised below. Table 8.1 summarised the key quantitative findings associated with reference to the research questions posed in Chapter 3 and their corresponding interpretations.

In Task 1, exposure to suspended MPs during hydration was found to have a negligible effect on the swelling behaviour of sodium bentonite within the range of particle sizes (1 μm) and concentrations (50-100 mg/L) investigated. Free swell index (SI) measurements required ~10 days to equilibrate, exceeding the ASTM standard, but were repeatable within measurement uncertainty (0.5 mL flask readability). Under distilled water hydration, the addition of 1 μm PS up to a bentonite:MP mass ratio of ~200:1 (0.5 wt%) did not produce a measurable change in SI. Similarly, oedometer swell-strain tests indicated hydration chemistry exerted the dominant control on swelling behaviour, with $CaCl_2$ reducing swell strain relative to distilled water, while MP addition resulted in only minor and inconsistent variations. SEM observations further identified MPs on bentonite sampled near specimen edges and on bentonite aggregates adhering to the carrier geotextile, but not within the core bentonite in the fields examined, suggesting limited penetration and preferential retention at cover geotextile or possibly external clay surfaces. Overall, within the tested particle size (1 μm) and concentration (≤100 mg/L) range, calcium-induced suppression of swelling dominated, and the influence of MPs on GCL swelling was negligible.

In Task 2, the suitability of flexible-wall permeameters (FWPs) for MP transport studies in low-permeability materials was confirmed through a series of validation tests. Appropriate selection of system components, including quartz porous stones (250-550 μm pore size), a single Whatman® Grade 4 filter paper beneath the specimen, and chemically inert tubing, minimised artefacts associated with particle retention and effluent analysis. The

inlet TIU was gently orbital shaken to suppress settling and agglomeration. System blanks and sand reference columns yielded recoveries of ~90-98%, establishing reasonable mass balance. Two outlet configurations were examined: (a) an outlet toxic interface unit (TIU), used to monitor hydraulics and effluent concentration trends; and (b) a vented outlet routed directly to pre-weighed glass vials, adopted for soil column experiments to avoid dilution and retention effect in downstream compartments and to enable uninterrupted effluent collection. Collectively, the configuration provided stable hydraulics and robust sampling relative to RWCs, supporting the suitability of FWPs for MP transport studies in both granular and very low-permeability (clay-based) media.

In Task 3, the extent to which GCLs limit MP migration was found to depend strongly on hydration chemistry and material condition. Under ideal DI water pre-hydration, both GCLs maintained extremely low hydraulic conductivity and showed no detectable MP breakthrough within the test durations (up to ~4 PV over 1-2 months). SEM observations support a mechanistic interpretation in which MP migration is prevented by a combination of filtration by the cover geotextile and limited pore accessibility within a well-hydrated, low-permeability bentonite gel. MPs were observed primarily on the cover geotextile, with no clear evidence of deep penetration into the bentonite core, consistent with "front-end" interception at or near the cover geotextile bentonite interface. It is note, however, that the mass balance is resolved at the system level, and the distribution of retained MPs among individual components (e.g., geotextiles, bentonite, and porous stone) cannot be explicitly quantified.

When GCL-1 (granular bentonite) was chemically impacted, MP breakthrough became measurable. Pre-hydration in 100 mM $CaCl_2$ with wet-dry cycling suppressed swelling, increased hydraulic conductivity, and produced higher peak normalized concentrations (C_{max}/C_0), with sub-micron MP particles showing the most pronounced transmission. Post-test dye tracing indicated no preferential flow features aligned with the needle-punched bundles, while the absence of perimeter staining corroborated minimal sidewall leakage in the FWP. Together with MIP evidence, these results indicate that chemistry-induced pore opening and macro-pore development contributed to breakthrough. In contrast, the polymer-enhanced GCL-2 showed superior chemical resistance, maintaining low hydraulic conductivity and exhibiting no measurable breakthrough even after 300 mM $CaCl_2$ pre-hydration over the test duration.

In Task 4, for cases in which measurable breakthrough curves were obtained, MP transport behaviour was interpreted using first-order kinetic ADR models incorporating both irreversible and reversible attachment processes. Finite-capacity effects were represented through time- or depth-dependent blocking terms. The consistent preference for two-site formulations over simple single-site irreversible models tentatively suggests that transport is governed by a coupled process of (i) progressive occupation of a limited set of retention sites and (ii) reversible attachment-detachment that contributes to MP release.

Classical DLVO calculations conducted under low ionic strength conditions predicted highly unfavourable attachment on ideal smooth surfaces, characterised by large primary energy barriers and the absence of secondary minima. This prediction is inconsistent with the experimentally observed retention behaviour, demonstrating that classical DLVO theory alone is insufficient to explain MP retention and breakthrough in chemically impacted GCL specimens. The results therefore highlight the importance of non-DLVO interactions and surface heterogeneity, including short-range acid-base and hydrophobic interactions, roughness- and charge-related effects, and physical retention within evolving pore networks.

Overall, the transport experiments suggest that MP migration through GCLs is negligible under well-hydrated, low-permeability conditions, but can become significant when chemical exposure and hydro-mechanical degradation reduce swelling and generate preferential flow pathways. The observed breakthrough behaviour appears to be governed by a combination of reversible retention, finite-capacity irreversible capture, and non-DLVO or heterogeneous interactions operating within the bentonite and geotextile system.

Table 8.1. Summary of principal findings of this thesis.

Task	Topic	Principal Findings	Key Interpretation
1	Effect of MPs on bentonite swelling index	Swell index equilibrated after ~10 days. Addition of 1 μm PS at ≤100 mg/L (0.5 wt% bentonite:MP ratio) did not measurably alter SI.	MP exposure had negligible influence on bentonite swelling under low ionic strength conditions. Hydration chemistry dominated swelling behaviour.
1	Oedometer swell-strain behaviour	$CaCl_2$ hydration reduced swell strain relative to DI water, whereas MP addition produced only minor and inconsistent changes.	Divalent cation effects controlled swelling suppression more strongly than MP presence.
2	Validation of FWP methodology	System blanks and sand reference columns yielded MP recoveries of ~90-98%.	FWPs provided acceptable mass balance and stable

2	Instrument configuration	Quartz porous stones (250-550 μm), single G4 filter beneath the specimen, and direct vented outlet collection minimised retention artefacts.	hydraulic control for MP transport testing. Appropriate system configuration is critical for reliable MP transport measurements in low-permeability media.
3	DI-hydrated GCL behaviour	Both GCLs maintained very low hydraulic conductivity ($<5\times10^{-10}$ m/s) and exhibited no detectable breakthrough up to ~4 PV over 2 months.	Well-hydrated GCLs acted as effective barriers to sub-micrometre MPs over the experimental duration.
3	Chemically impacted GCL-1	Pre-hydration in 100 mM $CaCl_2$ with wet-dry cycling increased GCL-1 hydraulic conductivity by approximately 1-2 orders of magnitude and produced measurable breakthrough.	Chemical degradation reduced swelling and increased pore connectivity, enabling MP migration.
3	GCL-2 chemical resistance	Polymer-amended GCL-2 maintained hydraulic conductivity in the order of 10^{-10} m/s and exhibited no detectable breakthrough even after 300 mM $CaCl_2$ conditioning.	Polymer-amended bentonite significantly improved chemical resistance and MP containment performance.
3	Particle size effect	Increasing particle size from 0.2 μm to 1.0 μm reduced C_{max}/C_0 and MP mass recovery in effluent.	Larger particles exhibited stronger retention, consistent with enhanced physical interception and finite-capacity retention behaviour.
3	Polymer type effect	At fixed size (0.5 μm), PE particles exhibited stronger retention than PS particles.	Transport behaviour was influenced by polymer-specific surface properties and particle size distribution.
4	ADR modelling	Two-site kinetic ADR formulations consistently provided improved agreement with BTCs relative to single-site irreversible models.	MP transport behaviour is governed by coupled reversible and irreversible retention processes.
4	DLVO interpretation	DLVO calculations predicted highly unfavourable attachment under low ionic strength conditions (large energy barriers; no secondary minima), inconsistent with observed retention.	Classical DLVO theory alone is insufficient to explain MP retention in GCL systems; non-DLVO interactions and pore-scale heterogeneity are important.

8.3 Novelty Contributions of this Thesis

This thesis makes several original contributions to the understanding of MP migration in engineered landfill barrier systems, particularly geosynthetic clay liners (GCLs), under controlled hydraulic and chemical conditions.

Firstly, the thesis provides one of the first experimental investigations into the influence of small MPs on the swelling behaviour of sodium bentonite relevant to GCL applications. Through combined swell index and oedometer swell-strain testing, the study demonstrates that, within the concentration range investigated, MP exposure does not

measurably alter bentonite swelling under low ionic strength conditions, whereas hydration chemistry exerts the dominant control on swelling behaviour.

Secondly, the thesis develops and validates a flexible-wall permeameter (FWP) methodology for MP transport studies in low-permeability materials. Validation experiments systematically evaluated the effects of porous stone type, filter configuration, tubing arrangement, pressure gradients, ionic strength, and particle size on MP recovery and transport behaviour. The study demonstrates that FWPs can provide stable hydraulic control and satisfactory system-level mass balance for particulate transport studies in both granular and clay-based media.

Thirdly, this thesis presents one of the first controlled studies of small MP transport through commercially available GCLs under both ideal and chemically degraded hydration conditions. The results demonstrate that MP migration is strongly governed by hydration chemistry and bentonite microstructure. Under deionized hydration, both GCLs maintained low hydraulic conductivity and exhibited no measurable breakthrough within the experimental duration. In contrast, chemically aggressive conditions involving $CaCl_2$ exposure and wet-dry cycling increased hydraulic conductivity and enabled measurable MP breakthrough in granular bentonite GCLs.

Fourthly, the study demonstrates the enhanced chemical resistance of polymer-amended bentonite GCLs with respect to MP containment. Compared with conventional granular sodium bentonite GCLs, the polymer-amended product maintained low hydraulic conductivity and prevented detectable MP breakthrough even under elevated ionic strength conditions, highlighting the importance of bentonite modification in maintaining barrier performance under chemically aggressive environments.

Fifthly, the thesis applies one-dimensional kinetic advection-dispersion-reaction (ADR) modelling to interpret MP transport behaviour in GCL systems. One- and two-site kinetic formulations incorporating reversible and irreversible attachment processes and finite-capacity blocking terms were evaluated against experimentally measured breakthrough curves. The results indicate that two-site formulations provide improved agreement with experimental observations, suggesting that MP transport is governed by coupled reversible retention and progressive occupation of limited retention sites.

Finally, by comparing experimental observations with DLVO interaction energy calculations, the thesis demonstrates that classical DLVO theory alone is insufficient to

explain MP retention behaviour in GCL systems. The results highlight the importance of pore-scale heterogeneity, surface roughness, and non-DLVO interactions in governing MP attachment and retention within hydrated bentonite structures.

Collectively, these contributions advance the understanding of MP migration in engineered landfill barrier systems and provide an experimental and modelling framework for evaluating MP transport under both ideal and chemically degraded conditions.

8.4 Limitations of the Study

Several limitations should be considered when interpreting the findings and implications of this thesis. These limitations mainly relate to the experimental scope, the representativeness of the chemical and physical conditions, the range of MP types and properties investigated, the duration of breakthrough monitoring, and the idealised nature of the transport modelling.

First, MP-exposure swelling experiments were conducted only in distilled water and at a single salt concentration (10 mM $CaCl_2$), with a limited number of GCL types and replicates. Consequently, potential effects associated with ionic strength and more complex interactions between salt concentration, MP concentration, size, type and aging on bentonite swelling could not be resolved with high confidence. In addition, the small number of tests does not allow determination of whether observed differences in swelling response are statistically significant.

Second, MP transport experiments in Chapter 6 were constrained to idealised DI water and simple $CaCl_2$ electrolyte solutions at a limited set of ionic strengths, with wet-dry cycling applied only to $CaCl_2$-hydrated GCLs. The $CaCl_2$ solutions used in this study should therefore be interpreted as simplified chemical analogues intended to isolate the effects of divalent cation exposure, rather than direct representations of specific landfill leachates. In contrast, real landfill leachates contain complex mixtures of inorganic salts, dissolved organic matter, surfactants, colloids and variable pH, all of which can influence bentonite properties and MP surface chemistry. Other environmental factors such as temperature, confining stress, hydraulic gradient, and long-term chemical evolution of leachate were also not explored. In addition, pH was not monitored during the transport experiments. Although the study investigated the effects of ionic strength associated with $CaCl_2$ solutions, pH may also influence bentonite swelling behaviour, MP surface charge, and interfacial interactions

relevant to retention and transport. Consequently, some of the effects attributed to ionic strength may also include coupled pH-related influences. Future work should therefore incorporate buffered solutions and systematic pH monitoring to better separate ionic-strength effects from coupled chemical effects on MP transport behaviour.

Third, the MPs investigated were restricted to well-characterised, near-spherical PS and PE in a relatively narrow size range (0.2-5 μm), and the particles were used in pristine (unweathered) form. This omits common MP morphologies encountered in landfills and soils, such as fibres, films, and irregular fragments, which may experience different hydrodynamic force, orientation effects and mechanical entanglement within pore networks. Likewise, surface ageing, oxidation and the presence of additives or sorbed contaminants were not considered, nor were other polymers with different densities and surface chemistries. The findings in this study therefore primarily characterise the behaviour of idealised, laboratory-grade MPs rather than the full diversity of MPs present in real waste streams. In addition, cover and base carrier geotextiles of the GCL, as well as the GMB, may also constitute a secondary source of MPs, which was not studied in this thesis but may be important.

Fourth, breakthrough observation durations were necessarily limited, especially for GCLs hydrated with DI water where hydraulic conductivity was extremely low. Under these conditions, tests typically were conducted for several weeks but reached up to 4 PV, which may be insufficient to capture very slow breakthrough or long-term changes in barrier performance, such as microstructural rearrangement, gradual clogging, or delayed MP release from reversible attachment domains. Thus, the conclusions regarding “no breakthrough” in low-permeability cases should be interpreted as evidence of strong short-term retention under the tested conditions, rather than definitive proof of long-term containment.

An additional limitation is that the potential long-term coupling between MP accumulation and bentonite swelling behaviour was not investigated directly. Chapter 4 showed that exposure to MPs at concentrations up to approximately 0.5 wt% did not measurably alter bentonite swelling under the short-term laboratory conditions examined. In contrast, the retained MP masses observed during the transport experiments in Chapter 6 were substantially lower, typically corresponding to only a small fraction of the bentonite mass. These observations suggest that the levels of MP retention achieved during the present experiments were likely too low to measurably influence swelling behaviour. However, over

long operational timescales relevant to landfill barriers, gradual accumulation of MPs within bentonite pores or at fibre-clay interfaces could potentially alter microstructure, pore connectivity, or hydration behaviour. Such long-term coupled effects remain uncertain and were beyond the scope of the present study. Extended-duration experiments incorporating repeated MP loading and long-term hydration monitoring would therefore be required to evaluate whether progressive MP accumulation could eventually influence swelling or hydraulic performance of GCL systems.

Another limitation relates to the use of different MP types across the experimental programme. The swelling experiments in Chapter 4 used non-fluorescent PS particles, whereas the transport experiments in Chapters 5-7 primarily used fluorescently labelled PS particles to enable concentration quantification and visualisation. Although the measured zeta potentials of fluorescent and non-fluorescent PS particles were similar under the tested conditions (Figure 3.8), fluorescent labelling may alter other surface properties, including acid–base interactions, hydrophobicity, or steric behaviour. Consequently, some differences in particle–bentonite interactions between the swelling and transport experiments cannot be completely excluded. However, given the similar electrokinetic behaviour observed and the relatively limited effect of MPs on bentonite swelling under the tested conditions, fluorescent labelling is not expected to qualitatively alter the principal conclusions of this thesis. Further work directly comparing fluorescent and non-fluorescent MPs under identical conditions would nevertheless help clarify the influence of particle functionalisation on transport and retention behaviour.

In addition, no conservative tracer tests were performed. Consequently, independent quantification of hydrodynamic dispersion and retardation behaviour was not possible, and parameters derived from breakthrough curve interpretation cannot be regarded as uniquely constrained transport descriptors.

Finally, the ADR formulations employed were restricted to first-order kinetic attachment-detachment with optional time- and depth-dependent blocking functions and a ripening factor. It inevitably simplifies the complexity of MP-soil interactions and does not explicitly represent processes such as straining in evolving pore networks, or heterogeneous flow paths. Parameter identifiability is also imperfect given that model fitting relied solely on BTCs because no RPs or independent measurements of attached MP mass were available to constrain the solution.

Some of the limitations mentioned here reflect the relatively recent nature of research on MP transport in soil generally, combined with well-established complexities of experimentally investigating long-term transport processes in clay materials. For example, questions about limited representability of MPs in mono-disperse solutions and the limited consideration of the effect of aging and other environmental variables in studies of MP transport have only recently begun to be tackled.

Despite these limitations, it is important to emphasize that, to the best of the authors' knowledge, this study is the first to (i) examine bentonite swelling under MP-rich solution during hydration, (ii) rigorously validate a FWP for MP mass balance studies in porous media including clay-based materials, and (iii) investigate MP transport through GCLs in combination with numerical ADR modelling. Its findings are therefore a significant step towards better understanding how plastics in landfills interact with clay-based barriers and impact the surrounding environment.

8.5 Implications for the Management of Plastics in Landfills

The results of this thesis have several implications for the design, operation and long-term management of landfills as sources and sinks of MPs. First, the swelling tests indicate that, within the tested size and concentration ranges, suspended MPs do not significantly reduce bentonite swelling compared with the strong effect of divalent cations. This suggests that, for well-hydrated GCLs exposed to dilute MP suspensions, hydraulic performance is likely controlled primarily by pore-water chemistry (e.g., Ca^{2+} concentration) rather than MP loading per se. Practically, this reinforces current guidance that prioritises control of leachate chemistry and protection of GCLs from early exposure to high ionic strength solutions, while indicating that the presence of small MPs in leachate does not, by itself, pose an additional swelling-related threat to GCL integrity under the conditions studied.

Second, the validation of the FWP as a tool for MP mass-balance studies provides a practical framework for evaluating barrier materials under controlled effective stress and realistic hydraulic boundary conditions. This offers regulators, consultants, and operators a laboratory methodology for testing GCL products, clay amendments and alternative barrier configurations for their ability to retain MPs, and for generating data that can be incorporated into design criteria and risk assessments. Over time, such testing could support the development of performance-based specifications that explicitly address MP

containment alongside more traditional metrics such as hydraulic conductivity and chemical compatibility.

Third, the column experiments demonstrate that MP containment performance is highly sensitive to both GCL type and hydro-chemo-mechanical environment. Findings indicate that best-practice in base-liner design and operation, aimed at minimizing contamination by dissolved organic and inorganic contaminants, seem to be equally relevant to the small MPs. Hence, under ideal DI hydration, both GCLs provided effective short-term barriers with no detectable MP breakthrough within the experimental duration. In contrast, $CaCl_2$ pre-hydration combined with wet-dry cycling substantially increased hydraulic conductivity and MP transmission in GCL-1, especially for sub-micron particles.

A particularly important finding is the markedly different response of the polymer-amended GCL-2 under chemically aggressive conditions. Despite pre-hydration with 300 mM $CaCl_2$ and wet-dry cycling, GCL-2 maintained hydraulic conductivity in the order of 10^{-10} m/s and exhibited no detectable MP breakthrough during the test period. This behaviour contrasts strongly with the granular sodium bentonite GCL (GCL-1), which exhibited measurable breakthrough after conditioning with 100 mM $CaCl_2$. These results demonstrate that polymer amendment can substantially improve the chemical resistance and MP containment performance of GCL systems under elevated ionic strength conditions.

From landfill design and operational perspective, these results support specifying GCLs that maintain low hydraulic conductivity under elevated ionic strength and limiting desiccation through appropriate cover design, liquid management and construction scheduling.

Fourth, the ADR modelling results underscore the importance of considering both reversible and irreversible retention processes in assessing MP transport from waste to subsoils and groundwater. Performance assessments and risk evaluations should explicitly account for particulate transport and retention processes, including the potential for long-term release from reversibly attached domains.

8.6 Future Research

8.6.1 Critical Near-Term Research

A critical knowledge gap identified in this thesis is the limited understanding of the concentration, size distribution and polymer composition of small MPs (<10 μm) in landfill leachate. As discussed in Chapter 2, existing field datasets are constrained by methodological limitations in sampling, filtration, separation and analytical detection, resulting in datasets that are strongly biased towards larger particles. Addressing this limitation requires dedicated field monitoring programs that combine size-fractionated sampling, including sub-micron fractions, together with validated analytical workflows (e.g., micro-FTIR and Raman spectroscopy) (Rathore et al., 2023; Liu et al., 2024; Utecht et al., 2025). Establishing robust and site-comparable inventories of small MPs in landfill leachate is essential for defining environmentally realistic influent concentrations for laboratory studies, quantifying exposure of barrier systems, and identifying conditions under which MP transport may become significant.

Future transport experiments should also extend beyond idealised DI water and simple $CaCl_2$ solutions to include synthetic and real landfill leachates containing mixed electrolytes, dissolved organic matter, surfactants, variable pH, and MPs with different sizes, shapes, morphologies, polymer types, and aging states (Chamanee et al., 2023; Kabir et al., 2023). Such studies are required to evaluate the influence of complex leachate chemistry on bentonite microstructure and MP mobility under more realistic environmental conditions.

Longer-duration transport experiments are required, particularly for low-permeability GCLs in which no measurable breakthrough was observed within the ~3-4 pore volumes investigated in this thesis. Extended testing would allow evaluation of delayed breakthrough, long-term retention behaviour, clogging effects, and potential structural evolution of the bentonite matrix. Future experiments should also incorporate 3-5 pore volumes of conservative tracers prior to MP injection to better constrain hydrodynamic transport processes and improve interpretation of breakthrough behaviour.

8.6.2 Important Medium-Term Research

Additional experimental work is required to generalise the swelling and transport findings beyond the conditions investigated in this thesis. A more extensive experimental study covering wider ranges of ionic strength, salt composition, MP concentration, and GCL product type, together with increased replication, would enable more rigorous statistical assessment of bentonite swelling and MP transport behaviour. Systematic variation of MP size, polymer type, and concentration would also help clarify the relative importance of physicochemical and geometric retention mechanisms (Kolstad et al., 2004; Dong et al., 2025).

Future studies should further examine the effects of additional environmental variables relevant to landfill conditions, including elevated temperature, higher confining stresses, variable hydraulic gradients, and repeated wet-dry cycling under different chemical environments. Investigation of a broader range of MP morphologies, including fibres, films, and irregular fragments, as well as aged MPs and particles carrying sorbed contaminants or additives, would improve understanding of transport behaviour under environmentally realistic conditions.

Quantitative resolution of retained MP distribution within GCL systems also remains an important research need. In the present study, retention was assessed for the entire GCL assembly, without explicit partitioning among geotextiles, bentonite, porous stones, or tubing. Future work employing targeted extraction procedures, destructive sampling, or high-resolution imaging techniques would enable more detailed identification of retention locations and mechanisms.

8.6.3 Longer-Term Aspirational Research

An additional long-term research direction concerns the potential generation of MPs from geosynthetic components used in landfill liner systems. Modern base liners commonly incorporate polymeric materials including HDPE geomembranes, PET/PP geotextiles, geonets and perforated drainage pipes (Bai et al., 2022; Gustavsson et al., 2022). As these materials undergo mechanical, chemical, and thermal degradation, they may themselves become secondary sources of MPs within landfill environments. Although research in this area remains limited, emerging evidence suggests that degradation of geosynthetic

components may contribute microplastic fragments and fibres to leachate and adjacent soils (Bai et al., 2022; Gustavsson et al., 2022; Krishnendu and Varghese, 2025). Further investigation is therefore required to quantify MP generation rates, identify dominant degradation mechanisms, and evaluate the implications for long-term liner system performance. From a modelling perspective, future work should aim to overcome the simplifying assumptions adopted in this thesis. Coupling continuum-scale transport formulations with pore-scale network models could provide a more physically grounded representation of MP migration in heterogeneous bentonite structures (Lim et al., 2023). Integration of retention profiles obtained through destructive sampling, imaging, or tracer techniques alongside breakthrough curve analysis would further improve parameter identifiability and enable more rigorous validation of transport models. Collectively, these developments would contribute to a more comprehensive predictive framework for assessing MP migration through engineered landfill barrier systems under realistic field conditions.

Appendix

X1. Critical Review of MP Effects on Soil Physical and Hydraulic Properties

Soil contamination by microplastics (MPs) is sometimes operationally defined as concentrations exceeding 0.1 wt% of soil dry mass (Wang et al., 2019a; Wang et al., 2019b), although no consensus definition exists. Landfills represent a major reservoir of MPs, with reported concentrations of up to 3.57×10^6 particles/kg in topsoil (0-0.5 m) adjacent to landfill reservoir areas (Guo et al., 2024). Polypropylene (PP) and polyethylene (PE) commonly dominate polymer compositions in landfill-adjacent soils (Kim et al., 2023; Mahesh et al., 2023; Saengchut et al., 2024; Ma et al., 2025a). MPs may enter soils through multiple pathways, including leachate percolation, surface runoff, wind dispersion and bioturbation (Sajjad et al., 2022; Wojnowska-Baryła et al., 2022; Abbasi et al., 2023; Luo et al., 2024), with leachate transport being particularly important in landfill environments due to the potential for bypass through leakage, defects or overflow events (Rowe, 2009; Rowe et al., 2023).

Once present, MPs can persist for decades and may alter key soil engineering properties, including structure, bulk density, porosity, hydraulic conductivity, and water retention. However, reported effects vary widely across studies due to differences in particle characteristics (e.g. MP size, morphology, polymer type), soil properties, chemical conditions, and experimental design. In particular, many studies are based on homogenised MP-soil mixtures under controlled laboratory conditions, often at elevated MP concentrations, which limits their direct applicability to field scenarios where MPs are transported through intact soils under advective flow. The following sections therefore provide a critical synthesis of published studies for each soil property, as summarized in Table X.1.

X1.1 Soil Structure

Soil structure describes the arrangement of mineral particles and organic matter into aggregates together with the pore spaces that govern water flow, aeration, and mechanical stability (Bonetti et al., 2021; Wang et al., 2022b). MPs can become embedded within soil aggregates, where they may act either as rigid inclusions that weaken interparticle bonding or as bridging elements that modify aggregate stability (Ingraffia et al., 2021; Lehmann et al., 2021).

Experimental evidence indicates that MPs are frequently associated with soil aggregates. Zhang and Liu (2018) reported that approximately 72% of MPs in contaminated soils were bound within aggregates, while the remaining fraction remained dispersed. Fibrous MPs were found to preferentially occur in micro-aggregates (Zhang and Liu, 2018).

Laboratory studies generally show that MP effects on soil aggregation depend strongly on particle morphology, size and concentration, as well as on soil properties such as texture and organic matter content (Lehmann et al., 2019; Solly et al., 2020; Li et al., 2025b). Fibrous and foam-like MPs tend to reduce aggregate stability due to their high aspect ratio and wedging effects, whereas fragments and films often have weaker impacts (Lehmann et al., 2019). For example, Ingraffia et al. (2021) showed that polyester (PES) fibres at 0.5 wt% reduced the formation of new macroaggregates without significantly affecting the stability of pre-existing ones. Consistent with this trend, Li et al. (2025b) reported that PE reduced the proportion of aggregates larger than 2 mm by 77%. Likewise, Han et al. (2024) observed reductions in macroaggregate fraction and mean aggregate size following the addition of large PE particles. In addition, small MPs at high concentrations (≥1 wt%) can be readily trapped within aggregates, resulting in weaker soil structure (Fang et al., 2024).

However, reported effects are not consistent across studies. Some investigations report substantial reductions in macroaggregate stability, while others observe limited or negligible changes. These discrepancies likely reflect differences in MP morphology, loading, soil texture, and organic matter content. For example, higher organic carbon content may partially offset MP-induced weakening of soil structure through microbial binding agents and polyvalent-cation bridging at particle contacts (Solly et al., 2020; Zhang et al., 2023b). Zhang et al. (2019) reported greater stability of larger than 2 mm aggregates at higher organic matter contents. Soil texture and clay mineralogy also play a role. Fine-

textured soils with higher specific surface area may favour MP occlusion within aggregates, whereas coarse soils tend to exhibit greater reductions in aggregation (Guo et al., 2022).

A key limitation is that most studies are conducted on homogenised MP-soil mixtures under controlled laboratory conditions, often at concentrations exceeding those typically observed in the field. Such conditions may exaggerate structural effects and do not represent scenarios in which MPs are transported through intact soil structures.

Overall, while there is general agreement that MPs can modify soil aggregation and pore connectivity, the magnitude and direction of these effects remain variable. Importantly, the implications of these structural changes for MP mobility under advective transport conditions remain unclear, particularly in low-permeability barrier systems.

X1.2 Bulk Density

Bulk density, defined as the dry mass of soil per unit volume, is a critical indicator of soil packing, porosity, and compaction state (Håkansson and Lipiec, 2000; Walter et al., 2016; Topa et al., 2021). MPs can influence bulk density primarily through density contrasts with mineral soil particles and through disruption of soil packing (Wang et al., 2022b). Most studies report a reduction in bulk density following MP addition, particularly for low-density polymers such as PP and PE (0.90-0.96 g/cm^3) relative to mineral soils (~2.60-2.70 g/cm^3) (Wang et al., 2022b). This effect is more pronounced for fibrous or elongated fragments, which interfere with particle packing and increase void space (Liang et al., 2021).

However, the magnitude of bulk density change varies widely. Minimal effects are often observed at low MP concentrations (<0.5 wt%), whereas more substantial reductions occur at higher loadings or in fine-grained soils (Zhang et al., 2019; Qi et al., 2020; Ingraffia et al., 2021). Differences between studies are likely attributable to variations in particle morphology, concentration, and soil texture. In particular, fibrous MPs can induce changes at lower concentrations than granular MP particles due to their greater influence on packing structure (Yu et al., 2023).

These findings are subject to important limitations. Most experiments involve uniformly mixed MPs within soil matrices, which differs from environmental conditions where MPs are introduced progressively and transported by flow. As a result, observed bulk density changes may not be representative of in situ conditions (Ke et al., 2022).

In summary, there is general agreement that MPs tend to reduce bulk density, especially at higher concentrations and for fibrous particles. However, the relevance of these changes to MP transport processes is uncertain, as bulk density variations observed in static mixtures may not directly translate to flow-through systems.

X1.3 Porosity

Porosity represents the fraction of soil volume occupied by voids and governs fluid storage and flow. MPs can influence porosity by modifying pore structure through clogging, filling, or aggregate formation.

Experimental studies report both increases and decreases in porosity depending on MP characteristics and soil type (Wang et al., 2022b; Yu et al., 2022). Fine particles and fibres (~150 μm) may increase porosity by promoting aggregation and generating new voids, whereas larger particles (~950 μm) often reduce porosity by occupying existing pore spaces (Wang et al., 2023). Dual effects of PES fibres (<5 μm) in clay loam soils have also been observed, with reductions in micropores (<30 μm) due to clogging and concurrent increase in macropores (>30 μm) due to fibre entanglement that promoted aggregate formation (Zhang et al., 2019).

Contradictory findings across studies are likely driven by differences in particle size distribution, morphology, and soil texture. For example, fine-textured soils may favour MP retention within aggregates, while coarse soils (e.g., sandy and loamy soils) are more sensitive to pore blockage or filling effects (Guo et al., 2022; Wang et al., 2023). Polymer-specific interactions, including hydrophobic and electrostatic forces, further complicate these responses (Wang et al., 2022b; Yu et al., 2022).

A major limitation is that porosity measurements are typically obtained under static conditions, without accounting for dynamic flow processes. In addition, the use of homogenised mixtures may obscure preferential flow pathways and heterogeneity present in natural systems.

Overall, MP effects on porosity are highly variable and controlled by multiple interacting factors. While these changes may influence fluid flow behaviour, their implications for MP transport under advective conditions remain insufficiently constrained.

X1.4 Hydraulic Conductivity

Saturated hydraulic conductivity (k_{sat}) quantifies the capacity of soil to transmit water and is a key parameter in engineered barrier system performance (Yu et al., 2020). Reported MP effects on k_{sat} are highly variable and depend on soil texture, polymer type, particle size, concentration, and morphology.

Zhang et al. (2019) observed no detectable change in k_{sat} when PES fibres (<5 μm diameter, 2.65 mm length) were present at 0.1-0.3 wt%, suggesting that low MP doses may not significantly affect water flow in fine-grained soils. Qi et al. (2020) likewise reported no significant change at 0.5 wt% for MP sizes of 0.05-5 mm in sandy soils. At higher loadings (1-2 wt%), larger biodegradable polymer microfibres (Bio-PMFs) produced higher k_{sat} than smaller fibres (Qi et al., 2020). For low-density polyethylene (LDPE), the effect depended on both MP dose and size. At 0.5 wt%, larger particles led to a reduced k_{sat}, whereas at 2.0 wt% larger particles increased it (Qi et al., 2020). Increasing the LDPE concentration beyond 2 wt% produced little further change in k_{sat}. Increases in k_{sat} are commonly attributed to macropore formation by large inclusions (Herath et al., 2013). In contrast, Shafea et al. (2023) observed decreases in k_{sat} for polystyrene (PS) and polyethylene terephthalate (PET) (>0.6 mm) at 0.5-2 wt%, as shown in Figure X.1. These contrasting results can be explained by competing mechanisms. Pore blocking tends to dominate when MP size is comparable to pore throat size, whereas structural disruption and macropore formation become more important for larger particles or higher loadings.

Soil texture further modulates these effects. Guo et al. (2022) reported monotonic k_{sat} reductions with increasing MP concentration across loam, clay and sand, with the greatest decreases in sandy soils. Hossain et al. (2025) found that adding PET at very low concentrations (0.001-0.005 wt%) increased k_{sat} in loam soils, whereas an opposite trend occurred in sand. For polyvinyl chloride (PVC), k_{sat} increased at low concentration in sand but decreased in loam (Hossain et al., 2025).

Despite extensive laboratory data, most studies are based on homogenised mixtures under simplified chemical conditions, limiting their relevance to field-scale systems. In landfill environments, hydraulic behaviour is influenced by intact structure, chemical gradients, and low-permeability conditions that are not captured in many experimental designs.

In summary, no clear consensus exists on the direction of MP-induced changes in k_{sat}. The variability reflects competing mechanisms and experimental conditions. Critically, the applicability of these findings to MP transport through engineered barrier systems remains uncertain, particularly under low-permeability and advective flow conditions.

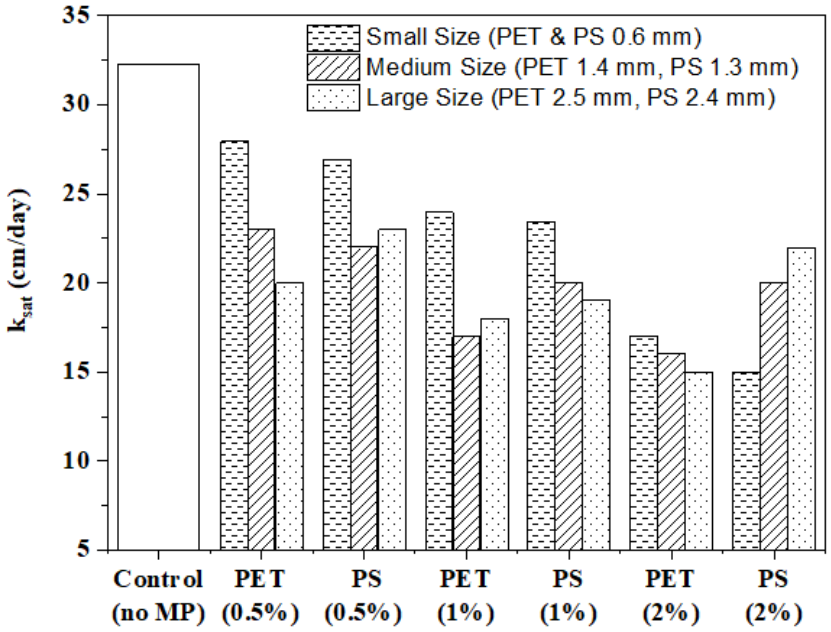

Figure X.1. Effect of MP size, type and concentration on saturated hydraulic conductivity (k_{sat}) with adding small-, modest- and large-sized PS and PET to topsoil. Based on data from Shafea et al. (2023).

X1.5 Water Retention Capacity (WRC)

Soil water retention describes the relationship between water content and matric suction and is fundamental to understand unsaturated soil behaviour (Ghavam-Nasiri et al., 2019). High water-holding capacity is particularly important in barrier-system soils, where it helps maintain moisture, reduces the risk of desiccation cracking, and supports low permeability (Bordoloi et al., 2018; Xie et al., 2024b). The presence of MPs can alter WRC by modifying micropore abundance and connectivity, effective surface area, and wettability (Wang et al., 2023; Wang et al., 2024).

Experimental results show both increases and decreases in WRC depending on MP characteristics. For example, Qi et al. (2020) reported that Bio-PMFs increased WRC at 1-2 wt% in sandy soils, whereas LDPE decreased WRC at 2 wt%. In comparison, at 0.5 wt%,

neither polymer had a significant effect (Qi et al., 2020). Shafea et al. (2023) found that PET and PS particles (0.6-2.5 mm) at 0.5-2 wt% consistently reduced WRC in loess topsoil, attributing the decline to MPs occupying water-storing pores and acting as hydrophobic, non-absorbent inclusions that diminish fine-pore retention.

Conversely, some conditions yielded enhanced WRC. Bakhshaee et al. (2025) found that small additions (0.01 wt%) of high-density polyethylene (HDPE) fragments increased WRC by 15-36%, with stronger effects for irregular fragments and larger sizes, while fibres and films produced more modest increases. Jazaei et al. (2022) similarly observed that fibrous MPs increased water retention in sandy soils, whereas pellet- and strand-shaped MPs reduced it, highlighting the importance of particle shape.

These contrasting outcomes are primarily governed by particle size, shape, polymer type, concentration, and soil texture. Fine-grained soils (e.g., clays) are more susceptible to reductions in WRC due to disruption of micropores, whereas coarse-grained soils may exhibit increased retention when fibrous MPs enhance pore heterogeneity (Guo et al., 2022). Changes in wettability, particularly for hydrophobic polymers such as PE and PP, further influence water retention behaviour (Cramer et al., 2023).

However, most studies rely on static laboratory measurements and homogenised mixtures, which may not represent conditions in which MPs are transported through soils under hydraulic gradients. In addition, the effects of chemical conditions and long-term evolution of soil structure are rarely considered.

Overall, MP effects on WRC are highly variable and system specific. While these changes may influence hydraulic behaviour, their relevance to MP transport and retention in barrier systems remains poorly understood, highlighting the need for studies under advective flow conditions.

Table X.1. Summary of effects of MPs on soil physical properties. Studies are presented in chronological order by publication year and alphabetically by the first author's surname within year.

Soil Property	Soil Type	MP Type	MP Size	MP Dose (w/w %)	Summary of Observed Effects	Reference
Soil structure	Sandy clay loam soil	PE, PLA	Not specified	0.1	Significant decrease in macro-aggregates (>2000 µm) and changes in soil aggregate profiles.	Boots et al. (2019)
	Clay loam soil	PES	Diameter <5 µm; length =2.65 mm	0.1, 0.3	Increase in pot experiment (40% clay); no significant effect in the field experiment (35% clay). Higher clay content in pot experiments promoted MP-soil contact, enhancing entanglement and formation of larger aggregates.	Zhang et al. (2019)
	Vertisol, Entisol, Alfisol	PES	Diameter ~2.87 mm	0.5	Decrease in the new aggregate formation.	Ingraffia et al. (2021)
	Sandy silt soil	Fibers (PA, PES, PP) Films (PET, PP, PE) Foams (PE, EPP, PU) Particles (PC, PET, PP)	<5 mm	0.1	Fibers: inhibited new macroaggregate formation (>2 mm) and destabilized structure. Films: fewer large aggregates formed but higher water stability. Foams: decreased new aggregate formation and stability. Particles: reduced >2 mm aggregates, no stability effect.	Lehmann et al. (2021)
	Silty loam; clay loam soil	PE	<35, <125, <500 µm	0.1, 1, 10	Higher MP concentration and smaller size decreased aggregate formation.	Fang et al. (2024)
	Silty loam soil	PE, PLA	50, 150, 300 µm	0.5	Reduced formation and stability of large aggregates due to loss of adhesive agents.	Han et al. (2024)
	Fluvisol (aquic)	PE, PLA	15 µm	1	Promoted formation of small-sized aggregates (0.25-1 mm).	Li et al. (2024c)
	Loam soil	PE and PP (fragments/powder)	9 µm	1	Severe destabilization of aggregates. PE reduced large macro-aggregates (>2 mm) by ~77%. PE and PP both reduced 0.5-1 mm aggregate by ~21%.	Li et al. (2025b)
Bulk density	Clay loam soil	PES	Diameter: <5 µm; length =2.65 mm	0.1, 0.3	No significant effects observed.	Zhang et al. (2019)

	Sandy soil	LDPE, Bio-PMF	50-1000 µm, 5 mm	0.5, 1, 2	No significant effect at 0.5%. At ≥1% MP, bulk density dropped significantly. LDPE (lower-density polymer) caused greater bulk density reduction than the heavier biodegradable plastic. Larger fragments led to more pronounced bulk density declines than finer particles.	Qi et al. (2020)
	Vertisol, Entisol and Alfisol	PES	Diameter =2.87 mm	0.5	Significant decrease in clay-rich Vertisol; slight or negligible change in loose soils.	Ingraffia et al. (2021)
	Silt loam soil	PES fibres, PP granules	Fibres: diameter =8 µm and length =5 mm; Granules: 53-125 µm	up to 0.5 (fibers); 2 (granules)	Bulk density decreased at high MP doses, no change at low doses. Significant reductions occurred beyond threshold concentrations (~0.5% for fibers, ~2% for granules). Polyester fibers induced a stronger bulk density decline.	Yu et al. (2023)
	Urban agricultural topsoil	PP straw fragments (rigid, irregular); Synthetic microfibres (70% PES, 30% PA)	Fragments <2.36 mm; Microfibers: ~4 mm	0.4, 1, 2	Largest decline (~7.3%) observed at 2% mixed MPs (PP + fibers). Lower doses caused smaller decreases (2-5%), and 0.4% fibers had negligible impact.	Das and Alam (2024)
Porosity	Clay loam soil	PES	Diameter: <5 µm; length =2.65 mm	0.1, 0.3	Decrease in volume of pores <30 µm. Increase in volume of pores >30 µm.	Zhang et al. (2019)
	Sandy soil	LDPE, Bio-PMF	50-1000 µm, 5 mm	0.5, 1, 2	No significant effect with 0.5% content.	Qi et al. (2020)
	Loam, clay, sand	PP	<20, <200, <500 µm	0.5, 1, 2, 4, 6	Significant decrease in macropore number with higher MP content.	Guo et al. (2022)
	Sandy soil; loamy soil	PE	150,550, 950 µm	0.5, 1, 2	Increase in porosity with 2% small PE (150 µm). Decrease in porosity with 2% large PE (950 µm).	Wang et al. (2023)
	Lean clay	PE	48, 150, 550 µm	0.5, 1, 2, 3, 5	Decrease in inter-aggregate pores. Increase in intra-aggregate pores.	Guo et al. (2025a)
Saturated hydraulic conductivity (k_s)	Clay loam soil	PES	Diameter: <5 µm; length =2.65 mm	0.1, 0.3	No detectable change in k_s at tested doses.	Zhang et al. (2019)
	Sandy soil	LDPE, Bio-PMF	50-1000 µm, 5 mm	0.5, 1, 2	No significant effect at 0.5% content. Increase in k_s with larger Bio-PMF sizes at 1-2% concentrations; increase in k_s with higher MP content at 0.5-1%, but no significant difference at higher content	Qi et al. (2020)

					Decrease in k_s for small-sized LDPE compared to Bio-PMF at 0.5% content.	
	Loam, clay, sand	PP	<20, <200, <500 µm	0.5, 1, 2, 4, 6	Decrease in k_s up to ~70-96%; stronger decline with smaller MPs; coarse soils most affected.	Guo et al. (2022)
	Loess Luvisol (topsoil)	PET, PS	0.6-2.5 mm	0.5, 1, 2	Decrease in k_s in all MP types, sizes and concentrations.	Shafea et al. (2023)
	Lean clay	PE	48, 150, 550 µm	0.5, 1, 2, 3, 5	Decrease in k_s for compacted soil.	Guo et al. (2025a)
Water retention	Sandy soil	LDPE, Bio-PMF	50-1000 µm, 5 mm	0.5, 1, 2	No significant effect at 0.5% MP content. Increase in water retention for Bio-PMF at 1-2% Decrease in water retention for LDPE at 2%.	Qi et al. (2020)
	Loam, clay, sand	PP	<20, <200, <500 µm	0.5, 1, 2, 4, 6	Decrease in water retention with MPs, with a greater reduction in clay compared to loam and sand.	Guo et al. (2022)
	Sandy soil; loamy soil	PE	150,550, 950 µm	0.5, 1, 2	No significant effect at 0.5% content. Increase in water retention for 2% 150 µm PE in loamy soil. Decrease in water retention for 2% 950 µm PE in sandy soil.	Wang et al. (2023)
	Loess Luvisol (topsoil)	PET, PS	0.6-2.5 mm	0.5, 1, 2	Decrease in soil water retention in all MP-treatments.	Shafea et al. (2023)
	Lean clay	PE	48, 150, 550 µm	0.5, 1, 2, 3, 5	Increase in water retention and water stability of compacted soil.	Guo et al. (2025a)

Note: PA = polyamide; PES = polyester; PP = polypropylene; PE = polyethylene; PET = polyethylene terephthalate; PLA = polylactic acid; EPP = expandable polypropylene; PU = polyurethane; PC = polycarbonate; LDPE = low-density polyethylene; Bio PMF = biodegradable plastic mulch film.

X2. Review of Experimental Apparatus for MP Transport Studies

X2.1 Rigid Wall Column (RWCs)

Rigid-wall columns (RWCs) are widely used in laboratory studies of contaminant and microplastic (MP) transport due to their simplicity, low cost, and ease of replication. They are typically constructed from glass, acrylic, or PVC, and operated under constant head or constant flow conditions.

However, several limitations affect their suitability for MP transport studies, particularly in low-permeability soils. First, hydraulic state of the specimen is often insufficiently controlled or reported. Although columns are typically prepared at a target water content and subsequently flushed, key parameters such as degree of saturation S_r, *B*-value or void ratio are rarely measured. This makes it difficult to determine whether experiments are conducted under saturated or unsaturated conditions, limiting reproducibility and interpretation. For example, Waldschläger and Schüttrumpf (2020) visualised MP transport in unsaturated glass beads but did not report saturation evolution, whereas Tehrani et al. (2025) employed instrumentation to monitor in-situ water content and suction, enabling more rigorous analysis.

Second, RWCs typically do not allow control confining stress, which is critical for simulating field conditions in landfill barriers and fine-grained soils (AbdelRazek and Rowe, 2019b). The absence of confinement can lead to gap formation between the soil and column wall, promoting preferential flow paths and biasing transport behaviour.

Third, sidewall leakage is a well-documented artefact in RWCs, particularly in low-permeability or highly swelling materials. Preferential flow along the wall can result in premature breakthrough and overestimation of MP mobility (Daniel et al., 1984). In addition, pump-induced pulsation may introduce pressure fluctuations at the inlet boundary, leading to variability in breakthrough curves (BTCs) (Guo and Fei, 2023).

To mitigate edge effects, some studies adopt a double-ring design (ASTM D2434, 2022), in which an outer ring provides hydraulic buffering to reduce lateral flow and an inner ring is used to measure infiltration into the soil (Xie et al., 2024a). Typical setups are ~25-50 cm high with different diameters for the two rings, and water is applied under constant head to both. Matching the outer-ring water head to the inner-ring infiltration rate prevents bypass flowing along the inner wall. However, this design is essentially an

infiltration rig and is not well-suited to contaminant transport studies. In its common form, it uses a single water reservoir for both rings, so it cannot impose a well-defined, inner-ring-only inlet MP concentration to the porous medium. It also does not control effective stress, limiting realistic simulation of landfill liner conditions. Moreover, lateral exchange between rings complicates real-time effluent collection for BTCs and mass balance.

Overall, RWCs are suitable for comparative and exploratory studies but have significant limitations for investigating MP transport in low-permeability and stress-dependent systems. In particular, lack of stress control, uncertain saturation conditions, and sidewall leakage introduce artefacts that can lead to overestimation of MP mobility and limit applicability to field barrier systems.

X2.2 Geotechnical Centrifuge

Geotechnical centrifuges have been adapted for contaminant transport studies in geomaterials by increasing gravitational acceleration, thereby accelerating advective transport processes in low-permeability media (Savvidou and Culligan, 1998; Sharma et al., 2008; Huang et al., 2025). By operating at elevated g-levels (e.g. up to ~200 g), centrifuge tests can simulate long-term transport behaviour within practical laboratory timescales while accommodating relatively large specimens, improving boundary realism and reducing edge effects. Centrifuge experiment also accommodates large-scale specimens, improving boundary realism and reducing edge effects (Savvidou and Culligan, 1998).

For example, Huang et al. (2025) investigated chloride migration through a sand-bentonite (SB) cutoff wall using a customised centrifuge model representing a landfill system. An underlying unweathered rock layer served as an impermeable aquitard, and the SB wall was installed downgradient of the landfill. The setup was partitioned into three sections with two 8 mm-thick perforated acrylic baffles: a head water reservoir, an aquifer, and a tailwater reservoir maintained a constant head during testing. The SB cutoff wall and the adjacent soil deposits were contained within the aquifer zone (Huang et al., 2025). Experiments were conducted at 100 g (gravity force) for 36 hours, corresponding to ~41 years of prototype transport time. This study reported that SB walls with high sand fractions developed preferential flow along the interface between the aquitard and the SB wall, suggesting the importance of material selection and construction details in barrier performance.

Despite these advantages, centrifuge testing presents several challenges for MP transport studies. Flow control is more challenging in the rotating frame, and experimental complexity increases compared with conventional column tests. More importantly, particle-scale physicochemical interactions governing MP transport, such as Brownian motion, electrostatic interactions, and surface forces, do not scale with gravitational acceleration (Sharma et al., 2008; Huang and Zhang, 2022). Consequently, while advective transport can be accelerated, retention and attachment processes may not be accurately represented.

Centrifuge testing is a powerful tool for accelerating advective transport and investigating large-scale boundary effects. However, its applicability to MP transport is limited by the mismatch between scaled hydraulic processes and unscaled particle-scale interactions. Consequently, interpretation of MP retention and attachment mechanisms requires caution.

X3. Laser Diffraction Particle Size Measurement

Particle size distributions of MP stock suspensions were measured using a laser diffraction analyser (Mastersizer 3000, Malvern, UK). Measurements were conducted using a Hydro-series wet dispersion cell. Prior to each analysis, the wet dispersion unit was cleaned by draining and refilling with DI water at least three times, after which it was filled with the dispersant.

Background measurements were acquired for 10 seconds, and each sample analysis consisted of five consecutive measurements. The target obscuration range was maintained between 5% and 10%. MP stock suspensions were ultrasonicated and introduced dropwise into the dispersion unit until the desired obscuration was achieved. Particle size measurements were conducted after the dispersant and MP suspension had stabilized.

X4. Scanning Electron Microscopy

The surface morphology of both fluorescent and non-fluorescent MP particles was characterized by scanning electron microscopy (Sigma HD VP, Zeiss). A small aliquot of each MP stock suspension was deposited onto an SEM pin stub and allowed to air-dry. Dried samples were sputter-coated with a 10 nm gold layer prior to imaging. Specimens were then

loaded into the SEM chamber and imaged at an accelerating voltage of 5 kV using a 30 µm standard aperture. A working distance of ~5 mm was used.

For the sink experiments in Chapter 5 (Test Set 2), filter papers collected after sonication in DI water were air-dried. A representative section of each filter paper was cut, mounted on a pin stub, sputter-coated with gold, and analysed using the same SEM settings described above.

X5. Raman Spectroscopy

Raman measurements were obtained with a Renishaw inVia Qontor microscope (Renishaw plc., Wotton-under-Edge, UK) fitted with an air-cooled CCD detector. Liquid specimens collected from the outlet TIU for the 1a_base case (Test Set 1: source experiment) were transferred to 4 mL standard quartz cuvettes, filled to eliminate headspace, sealed, and mounted horizontally on the microscope stage. Excitation employed a 532 nm laser with a 1200 lines/mm visible grating, focused through a 50× objective (NA 0.75) and a live video for sample viewing. Instrument control and data acquisition were performed in Renishaw WiRE™ v5.6.

Spectra were recorded from 200 to 3200 cm^{-1} using 10-second exposure, 100% laser power at the source, and three accumulations per spectrum. Wavenumber calibration was verified against the silicon internal standard before data collection. All parameter choices were selected to maximise signal while maintaining spectral fidelity and enabling consistent comparison across samples.

X6. Fitted breakthrough curves of Tests 1-11 in Chapter 6

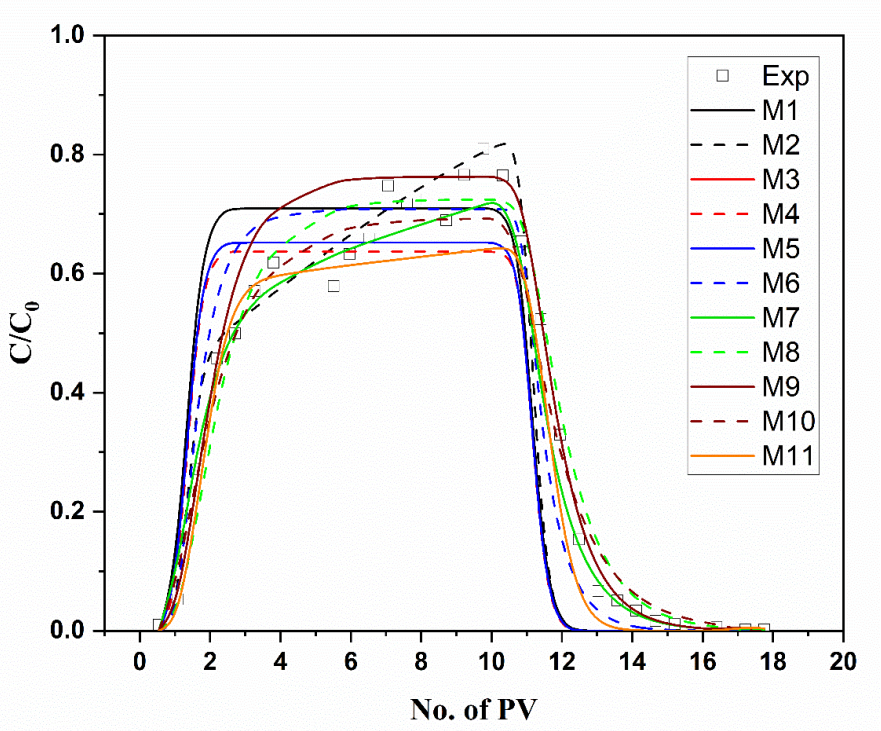

Figure X.2. Fitted curve of Test 1 in Table 6.1 (the letter "M" in the legend denotes the model number).

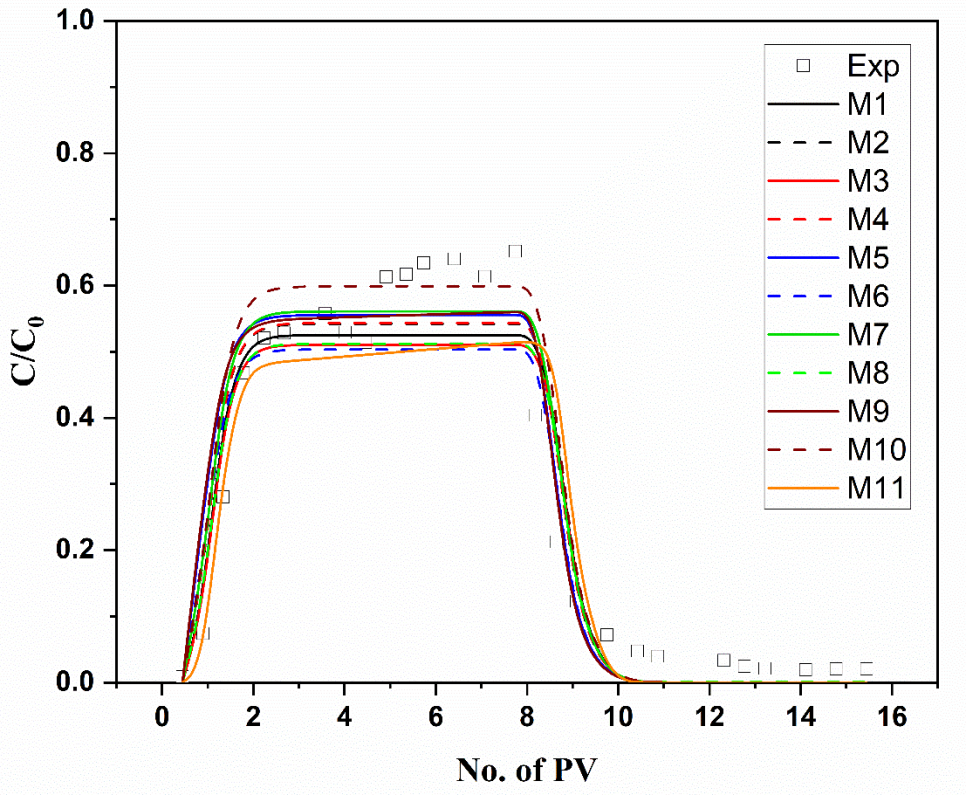

Figure X.3. Fitted curve of Test 2 in Table 6.1.

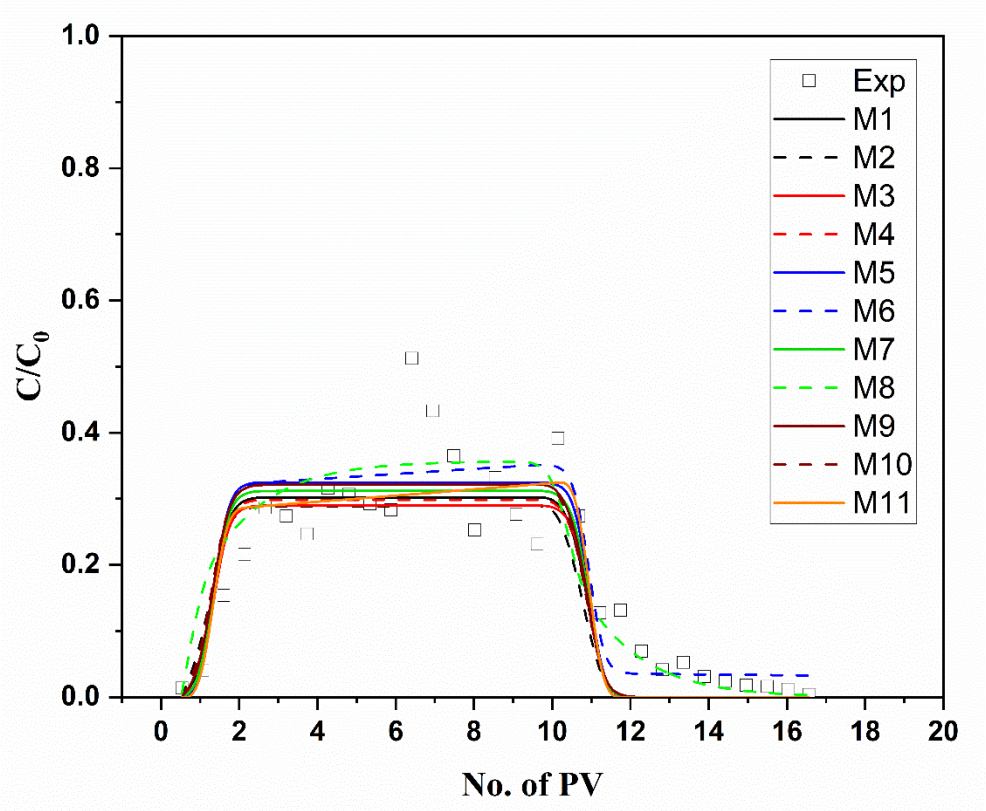

Figure X.4. Fitted curve of Test 3 in Table 6.1.

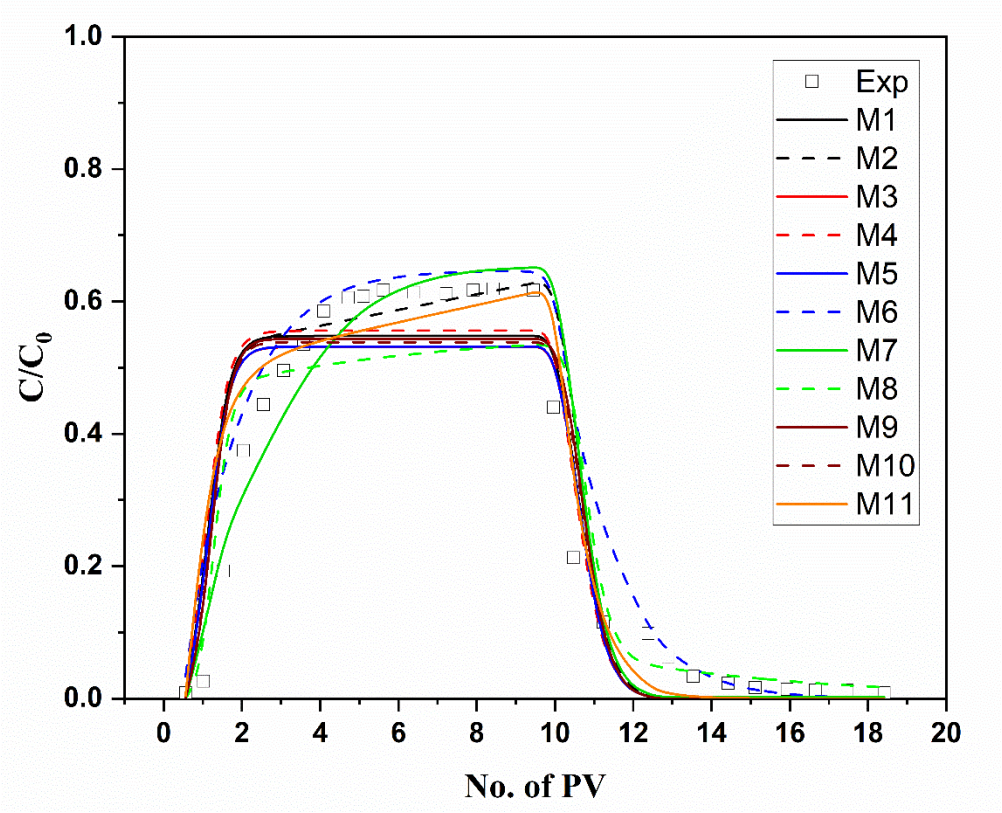

Figure X.5. Fitted curve of Test 4 in Table 6.1.

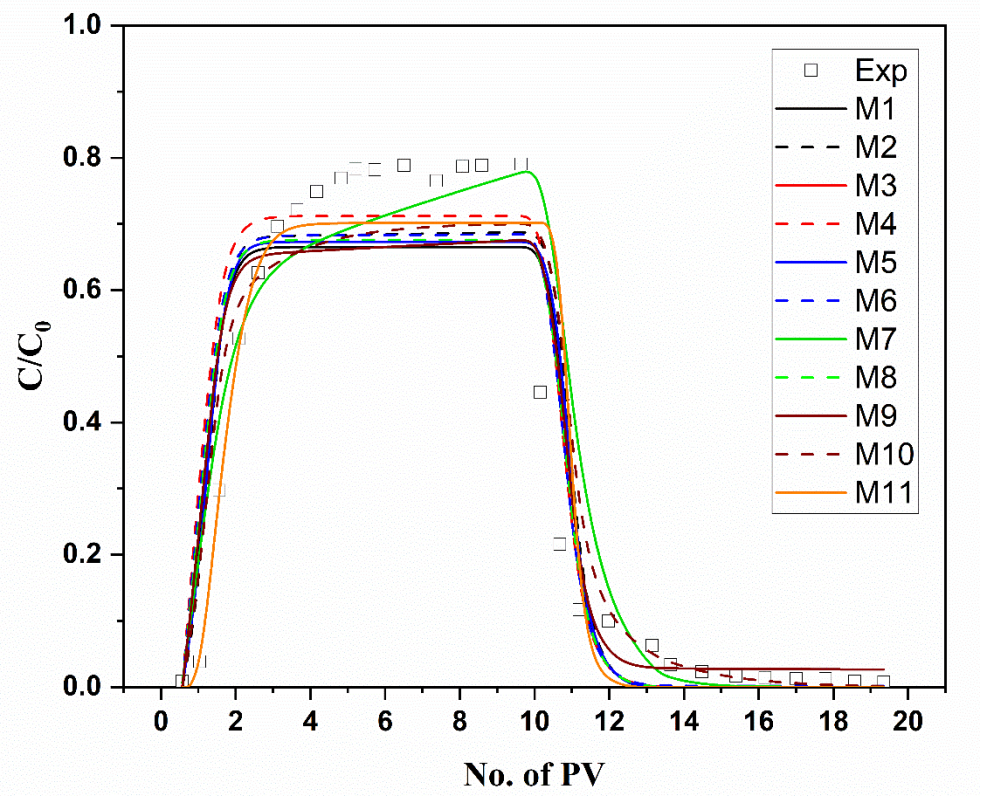

Figure X.6. Fitted curve of Test 5 in Table 6.1.

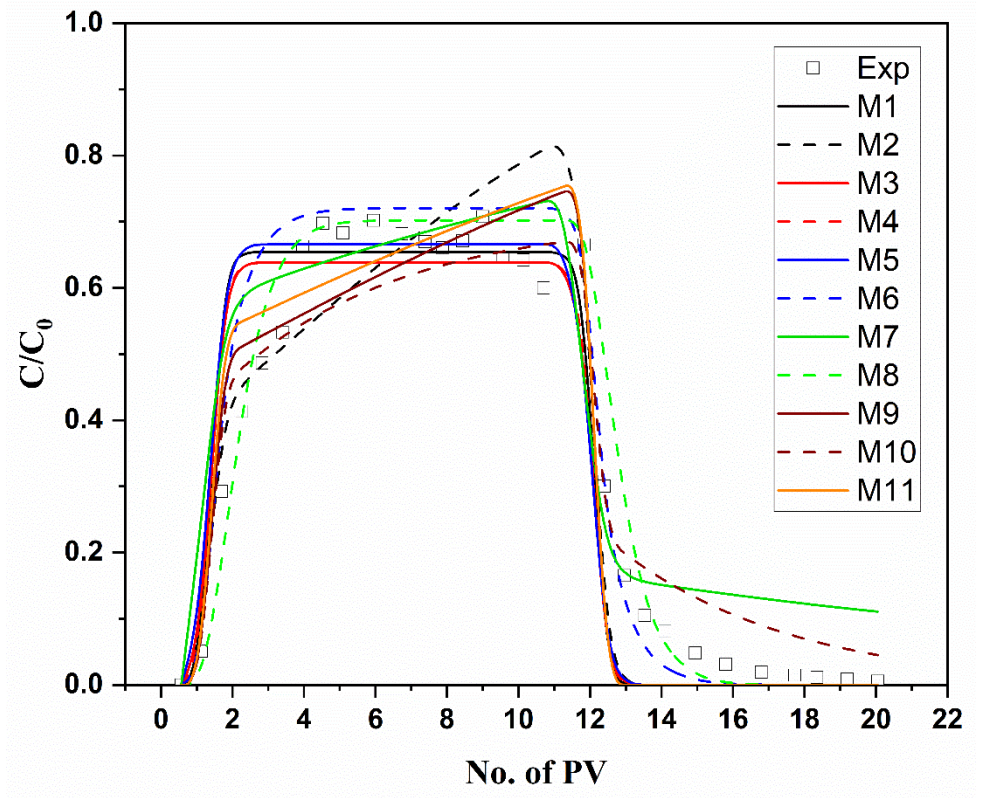

Figure X.7. Fitted curve of Test 6 in Table 6.1.

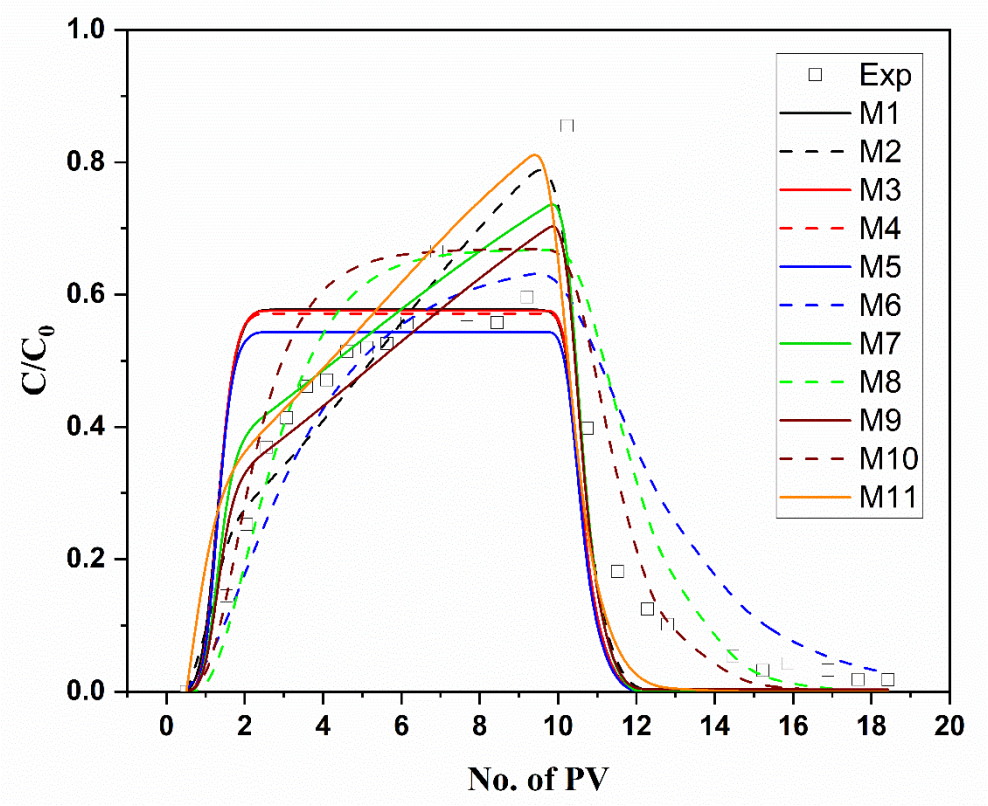

Figure X.8. Fitted curve of Test 7 in Table 6.1.

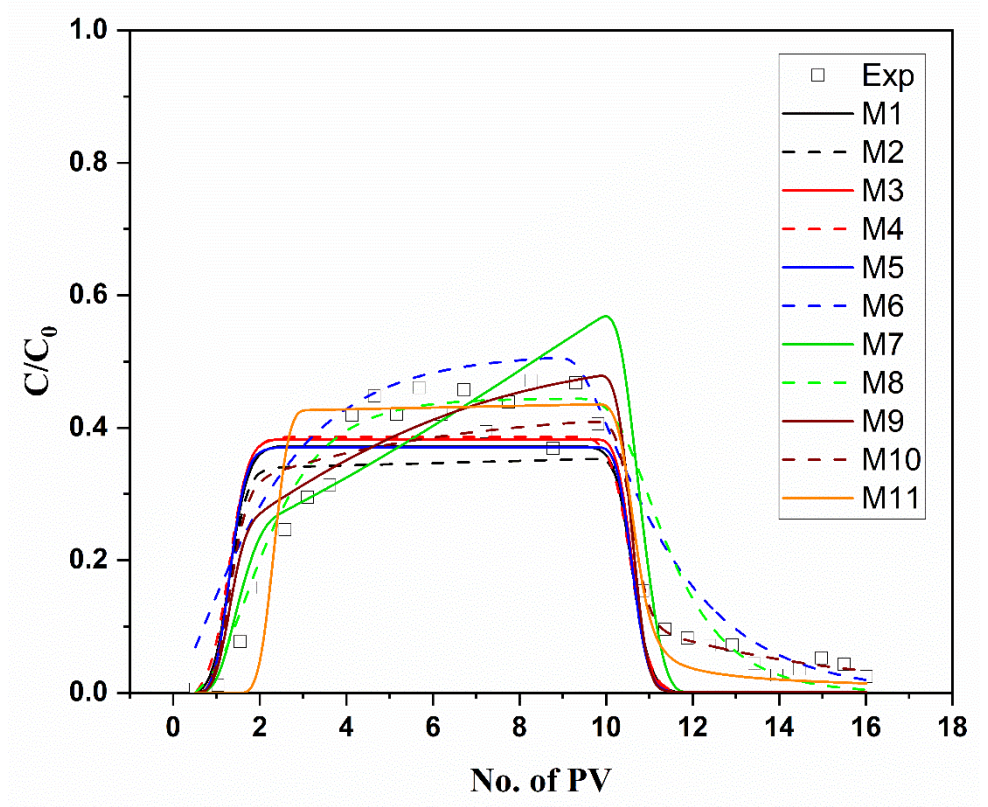

Figure X.9. Fitted curve of Test 8 in Table 6.1.

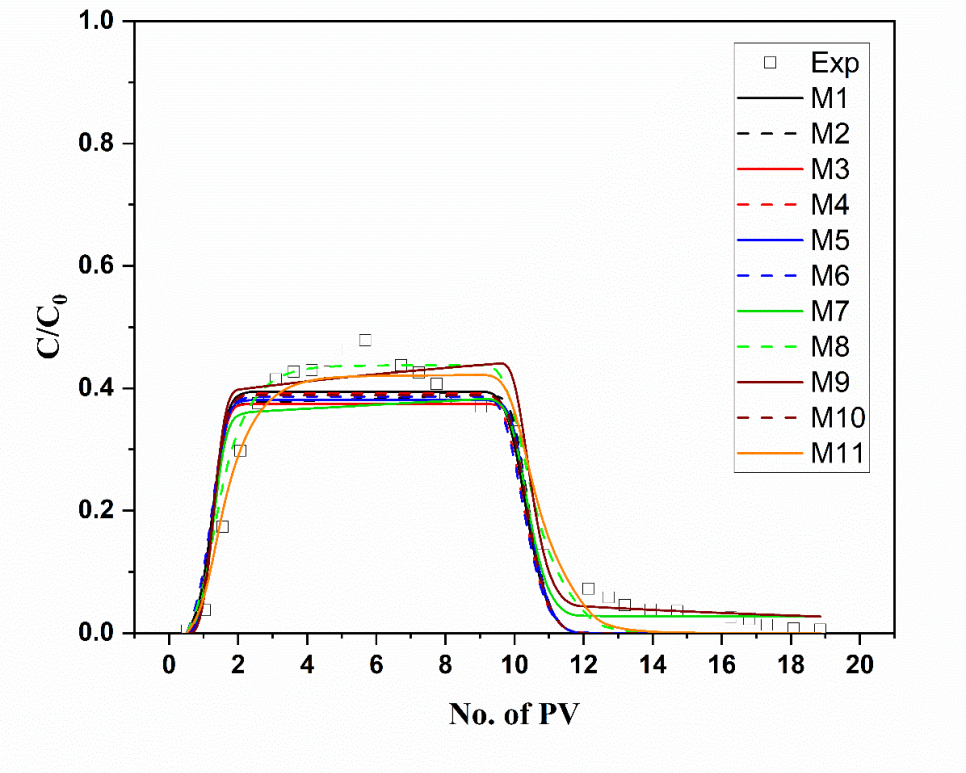

Figure X.10. Fitted curve of Test 9 in Table 6.1.

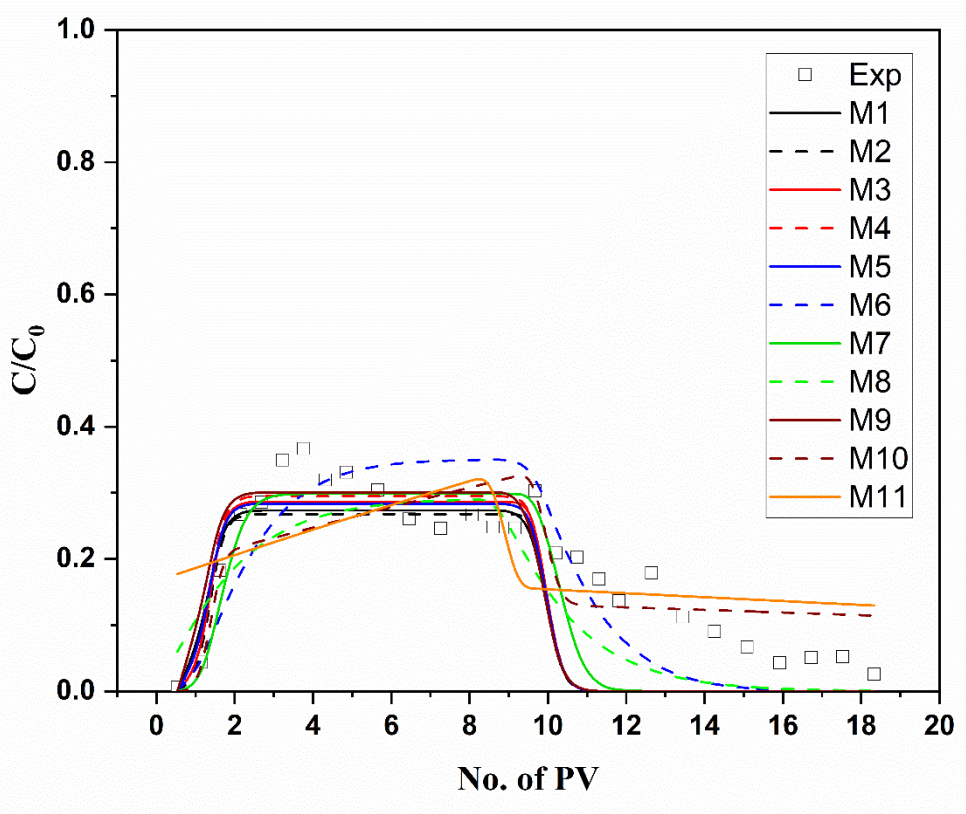

Figure X.11. Fitted curve of Test 10 in Table 6.1.

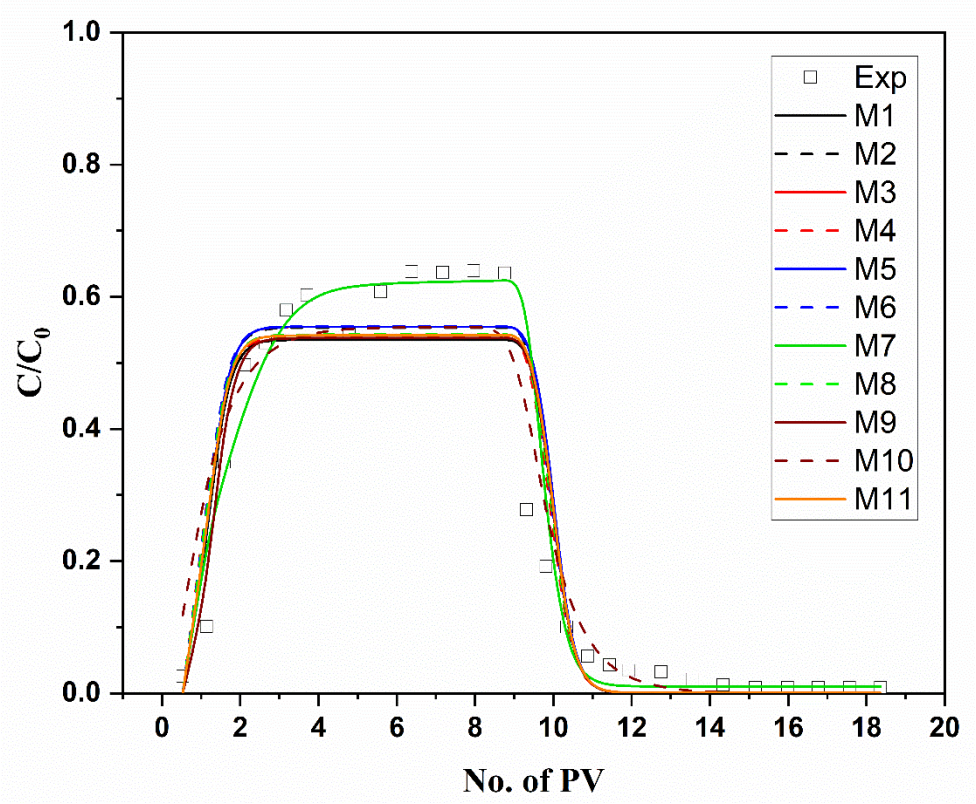

Figure X.12. Fitted curve of Test 11 in Table 6.1.

References

Abbasi, S., Rezaei, M., Mina, M., Sameni, A., Oleszczuk, P., Turner, A., & Ritsema, C. (2023). Entrainment and horizontal atmospheric transport of microplastics from soil. *Chemosphere, 322*, 138150, https://doi.org/10.1016/j.chemosphere.2023.138150.

Abdelfatah, E., Kang, K., Pournik, M., Shiau, B. J. B., & Harwell, J. (2017). Mechanistic study of nanoparticles deposition and release in porous media. *Journal of Petroleum Science and Engineering, 157*, 816-832, https://doi.org/10.1016/j.petrol.2017.08.003.

AbdelRazek, A. Y., & Rowe, R. K. (2019a). Interface transmissivity of conventional and multicomponent GCLs for three permeants. *Geotextiles and Geomembranes, 47*(1), 60-74, https://doi.org/10.1016/j.geotexmem.2018.10.001.

AbdelRazek, A. Y., & Rowe, R. K. (2019b). Performance of GCLs in high salinity impoundment applications. *Geosynthetics International, 26*(6), 611-628, https://doi.org/10.1680/jgein.19.00043.

Ahmed, H., Zhang, K. N., Zhu, K. F., & Ishfaque, M. (2025). Hydro-chemical influence on soil-water characteristic behavior of laterite-bentonite mixture. *Results in Engineering, 25*, 103698, https://doi.org/10.1016/j.rineng.2024.103698.

AL-Bazali, T. (2022). Insight into Debye Hückel length (κ−1): Smart gravimetric and swelling techniques reveals discrepancy of diffuse double layer theory at high ionic concentrations. *Journal of Petroleum Exploration and Production Technology, 12*(2), 461-471, https://doi.org/10.1007/s13202-021-01380-2.

Aldaeef, A. A., & Rayhani, M. T. (2014). Hydraulic performance of Compacted Clay Liners (CCLs) under combined temperature and leachate exposures. *Waste Management, 34*(12), 2548-2560, https://doi.org/10.1016/j.wasman.2014.08.007.

Alzamel, M., Fall, M., & Haruna, S. (2022). Swelling ability and behaviour of bentonite-based materials for deep repository engineered barrier systems: Influence of physical, chemical and thermal factors. *Journal of Rock Mechanics and Geotechnical Engineering, 14*(3), 689-702, https://doi.org/10.1016/j.jrmge.2021.11.009.

Alziyadi, M. O., & Denton, A. R. (2021). Osmotic pressure and swelling behavior of ionic microcapsules. *The Journal of Chemical Physics, 155*(2), 214904, https://doi.org/10.1063/5.0064282.

Andrady, A. L., Barnes, P. W., Bornman, J. F., Gouin, T., Madronich, S., White, C. C., . . . Jansen, M. (2022). Oxidation and fragmentation of plastics in a changing environment; from UV-radiation to biological degradation. *Science of the Total Environment, 851*, 158022, https://doi.org/10.1016/j.scitotenv.2022.158022.

Anik, A. H., Oishy, M. N., Murshed, M. F., Abdullah, R. B., & Khan, M. R. (2025). Distribution and health impacts of micro-and nanoplastics (MNPs) in human organs: Accumulation, translocation, and toxicity – A systematic review of current evidence. *Journal of Hazardous Materials: Plastics, 1*, 100002, https://doi.org/10.1016/j.hazmp.2025.100002.

ASTM D2434-22 (2022). Standard test methods for measurement of hydraulic conductivity of coarse-grained soils. ASTM International.
ASTM D4546-21 (2021). Standard test methods for one-dimensional swell or collapse of soils. ASTM International.
ASTM D5084-16 (2016). Standard test methods for measurement of hydraulic conductivity of saturated porous materials using a flexible wall permeameter. ASTM International.
ASTM D5890-19 (2019). Standard test method for swell index of clay mineral component of geosynthetic clay liners. ASTM International.
ASTM D6913-04(2009)e1 Standard Test Methods for Particle-Size Distribution (Gradation) of Soils Using Sieve Analysis. ASTM International.
Auset, M., & Keller, A. A. (2006). Pore-scale visualization of colloid straining and filtration in saturated porous media using micromodels. *Water Resources Research, 42*(12), W12S02, https://doi.org/10.1029%2F2005WR004639.
Bai, X., Li, F., Ma, L., & Li, C. (2022). Weathering of geotextiles under ultraviolet exposure: A neglected source of microfibers from coastal reclamation. *Science of the Total Environment, 804*, 150168, https://doi.org/10.1016/j.scitotenv.2021.150168.
Bakhshaee, A., Babakhani, P., Ashiq, M. M., Bell, K., Salehi, M., & Jazaei, F. (2025). Potential impacts of microplastic pollution on soil–water–plant dynamics. *Scientific Reports, 15*(1), 9784, https://doi.org/10.1038/s41598-025-93668-0.
Batchelor, G. K. (1976). Brownian diffusion of particles with hydrodynamic interaction. *Journal of Fluid Mechanics, 74*(1), 1-29, https://doi.org/10.1017/s0022112076001663.
Beck, A., Kramer, E., & Smith, M. (2008). *Specifications for Moisture Content of GCL to Perform Electrical Leak Location Surveys.* Paper presented at the EuroGeo4, Scotland.
Benson, C. H., Tan, Y., Youngblood, J., & Bradshaw, S. (2022). *Bentonite-polymer composite geosynthetic clay liners for heap leach liners.* Paper presented at the 5th International Conference on Heap Leach Mining Solutions, Sparks, USA.
Benson, C. H., & Yesiller, N. (2016). Variability of saturated hydraulic conductivity measurements made using a flexible-wall permeameter. *Geotechnical Testing Journal, 39*(3), 476-491, https://doi.org/10.1520/GTJ20150138.
Bhattacharjee, S., Chen, J. Y., & Elimelech, M. (2000). DLVO interaction energy between spheroidal particles and a flat surface. *Colloids and Surfaces A: Physicochemical and Engineering Aspects, 165*(1-3), 143-156, https://doi.org/10.1016/S0927-7757(99)00448-3.
Bi, Y., Qian, J., Jia, X., Hao, Y., & Lu, D. (2025). Mechanism of Surface Particle Exfoliation and Its Impact on Water Flow in Shale Nanopores. *Langmuir, 41*(32), 21525-21534, https://doi.org/10.1021/acs.langmuir.5c02295.
Bi, Y. Z., Fu, X. L., Zhou, S. J., Ni, J., & Du, Y. J. (2022). Field investigation of effect of plants on cracks of compacted clay covers at a contaminated site. *International Journal of Environmental Research and Public Health, 19*(12), 7248, https://doi.org/10.3390/ijerph19127248.
Bîrleanu, E., Mihăilă, I., Topală, I., Borcia, C., & Borcia, G. (2023). Adhesion properties and stability of non-polar polymers treated by air atmospheric-pressure plasma. *Polymers, 15*(11), 2443, https://doi.org/10.3390/polym15112443.
Bohnhoff, G. L., & Shackelford, C. D. (2013). Improving membrane performance via bentonite polymer nanocomposite. *Applied Clay Science, 86*, 83-98, https://doi.org/10.1016/j.clay.2013.09.017.
Bohnhoff, G. L., & Shackelford, C. D. (2014). Hydraulic conductivity of polymerized bentonite-amended backfills. *Journal of Geotechnical and Geoenvironmental Engineering, 140*(3), 04013028, https://doi.org/10.1061/(ASCE)GT.1943-5606.0001034.

Bohnhoff, G. L., Shackelford, C. D., & Sample-Lord, K. M. (2014). Calcium-resistant membrane behavior of polymerized bentonite. *Journal of Geotechnical and Geoenvironmental Engineering, 140*(3), 04013029, https://doi.org/10.1061/(ASCE)GT.1943-5606.0001042.

Bonetti, S., Wei, Z., & Or, D. (2021). A framework for quantifying hydrologic effects of soil structure across scales. *Communications Earth & Environment, 2*(1), 107, https://doi.org/10.1038/s43247-021-00180-0.

Boots, B., Russell, C. W., & Green, D. S. (2019). Effects of microplastics in soil ecosystems: above and below ground. *Environmental Science and Technology, 53*(19), 11496-11506, https://doi.org/10.1021/acs.est.9b03304.

Bordoloi, S., Garg, A., Sreedeep, S., Lin, P., & Mei, G. (2018). Investigation of cracking and water availability of soil-biochar composite synthesized from invasive weed water hyacinth. *Bioresource Technology, 263*, 665-677, https://doi.org/10.1016/j.biortech.2018.05.011.

Bordoloi, S., Gupt, C. B., & Sarmah, A. K. (2022). Exploring the theoretical effects of landfill based microplastic accumulation on the hydro-mechanical properties of porous soil media. *Current Opinion in Environmental Science & Health, 26*, 100332, https://doi.org/10.1016/j.coesh.2022.100332.

Born, M. P., & Brüll, C. (2022). From model to nature - A review on the transferability of marine (micro-) plastic fragmentation studies. *Science of the Total Environment, 811*, 151389, https://doi.org/10.1016/j.scitotenv.2021.151389.

Bouazza, A., & Gates, W. P. (2014). Overview of performance compatibility issues of GCLs with respect to leachates of extreme chemistry. *Geosynthetics International, 21*(2), 151-167, https://doi.org/10.1680/gein.14.00006.

Brachman, R. W., Gudina, S., Rowe, R. K., & Take, W. A. (2010). *Adhesion from supplemental bentonite placed at GCL overlaps.* Paper presented at the Proceedings of the 63rd Canadian Geotechnical Conference, Calgary, Alta.

Bradford, S. A., & Torkzaban, S. (2008). Colloid transport and retention in unsaturated porous media: A review of interface-, collector-, and pore-scale processes and models. *Vadose Zone Journal, 7*(2), 667-681, https://doi.org/10.2136/vzj2007.0092.

Bradford, S. A., Torkzaban, S., & Simunek, J. (2011). Modeling colloid transport and retention in saturated porous media under unfavorable attachment conditions. *Water Resources Research, 47*(10), W10503, https://doi.org/10.1029/2011WR010812.

Bradford, S. A., Torkzaban, S., & Walker, S. L. (2007). Coupling of physical and chemical mechanisms of colloid straining in saturated porous media. *Water Research, 41*(13), 3012-3024, https://doi.org/10.1016/j.watres.2007.03.030.

Bradshaw, S. L., Benson, C. H., & Scalia IV, J. (2013). Hydration and cation exchange during subgrade hydration and effect on hydraulic conductivity of geosynthetic clay liners. *Journal of Geotechnical and Geoenvironmental Engineering, 139*(4), 526-538, https://doi.org/10.1061/(ASCE)GT.1943-5606.0000793.

Browning, S., Beymer-Farris, B., & Seay, J. R. (2021). Addressing the challenges associated with plastic waste disposal and management in developing countries. *Current Opinion in Chemical Engineering, 32*, 100682, https://doi.org/10.1016/j.coche.2021.100682.

Cao, S., Dong, S., Wang, L., Suakollie, E. B., Wu, H., & Yu, Y. (2023). Transport of polypropylene, polyvinyl chloride, polyethylene terephthalate and polymethyl methacrylate microplastics in porous media under gradient ionic strength. *Environmental Pollutants and Bioavailability, 35*(1), 2269315, https://doi.org/10.1080/26395940.2023.2269315.

Cen, W., Wang, L., Sheng, X., & Yan, J. (2025). Leakage behavior of defective geomembrane on different underliners: Experimental and modeling studies. *KSCE Journal of Civil Engineering, 29*(5), 100078, https://doi.org/10.1016/j.kscej.2024.100078.

Chamanee, G., Sewwandi, M., Wijesekara, H., & Vithanage, M. (2023). Global perspective on microplastics in landfill leachate; Occurrence, abundance, characteristics, and environmental impact. *Waste Management, 171*, 10-25, https://doi.org/10.1016/j.wasman.2023.08.011.

Chamanee, G., Sewwandi, M., Wijesekara, H., & Vithanage, M. (2024). Occurrence and abundance of microplastics and plasticizers in landfill leachate from open dumpsites in Sri Lanka. *Environmental Pollution, 350*, 123944, https://doi.org/10.1016/j.envpol.2024.123944.

Chappel, M. J., Rowe, R. K., Brachman, R. W. I., & Take, W. A. (2012). A comparison of geomembrane wrinkles for nine field cases. *Geosynthetics International, 19*(6), 453-469, https://doi.org/10.1680/gein.12.00030.

Chaudhary, E., Swami, D., Joshi, N., & Reddy, K. R. (2024). Flow and contaminant transport dynamics in clay-amended barriers through flushing experiments and multi-porosity-based modeling. *Environmental Pollution, 355*, 124138, https://doi.org/10.1016/j.envpol.2024.124138.

Chen, C., Liu, K., & Shang, J. (2018a). Effects of ionic strength, electrolyte type, pH, and flow rate on transport and retention of atmospheric deposition particles in saturated porous media. *Journal of Soils and Sediments, 18*(3), 1066-1075, https://doi.org/10.1007/s11368-017-1826-x.

Chen, J. N., Benson, C. H., & Edil, T. B. (2018b). Hydraulic conductivity of geosynthetic clay liners with sodium bentonite to coal combustion product leachates. *Journal of Geotechnical and Geoenvironmental Engineering, 144*(3), 04018008, https://doi.org/10.1061/(ASCE)GT.1943-5606.0001844.

Chen, X., Wan, Y., Jia, J., Qiang, X., & Wu, C. (2023). Transport of micron-sized polyethylene particles in confined aquifer: effects of size, aging, and confining pressure. *Heliyon, 9*(8), 1-8, https://doi.org/10.1016/j.heliyon.2023.e18464.

Chowdhury, A. I., O'Carroll, D. M., Xu, Y., & Sleep, B. E. (2012). Electrophoresis enhanced transport of nano-scale zero valent iron. *Advances in Water Resources, 40*, 71-82, https://doi.org/10.1016/j.advwatres.2012.01.014.

Chowdhury, I., Duch, M. C., Mansukhani, N. D., Hersam, M. C., & Bouchard, D. (2014). Deposition and release of graphene oxide nanomaterials using a quartz crystal microbalance. *Environmental Science & Technology, 48*(2), 961-969, https://doi.org/10.1021/es403247k.

Chrysikopoulos, C. V., & Katzourakis, V. E. (2015). Colloid particle size-dependent dispersivity. *Water Resources Research, 51*(6), 4668-4683, https://doi.org/10.1002/2014WR016094.

Chu, X., Li, T., Li, Z., Yan, A., & Shen, C. (2019). Transport of microplastic particles in saturated porous media. *Water, 11*(12), 2474, https://doi.org/10.3390/w11122474.

Cordova, M. R., & Riani, E. (2021). Micro-and mesoplastics release from the Indonesian municipal solid waste landfill leachate to the aquatic environment: Case study in Galuga Landfill Area, Indonesia. *Marine Pollution Bulletin, 163*, 111986, https://doi.org/10.1016/j.marpolbul.2021.111986.

Dagwar, P. P., & Dutta, D. (2024). Landfill leachate a potential challenge towards sustainable environmental management. *Science of the Total Environment*, 171668, https://doi.org/10.1016/j.scitotenv.2024.171668.

Daniel, D. E., Anderson, D. C., & Boynton, S. S. (1985). Fixed-Wall Versus Flexible-Wall Permeameters. In A. I. Johnson et al. (Eds.), *Hydraulic Barriers in Soil and Rock, ASTM STP 874* (pp. 107-126). American Society for Testing and Materials.

Daniel, D. E., Trautwein, S. J., Boynton, S. S., & Foreman, D. E. (1984). Permeability testing with flexible-wall permeameters. *Geotechnical Testing Journal, 7*(3), 113-122, https://doi.org/10.1520/GTJ10487J.

Das, E. J., & Alam, A. R. (2024). Effects of microplastics polluted soil on the growth of Solanum lycopersicum L. *Environmental Systems Research, 13*(1), 36, https://doi.org/10.1186/s40068-024-00367-2.

Das, P., & Bharat, T. V. (2022). Assessment of clay mineral attenuation capacity for human viral pathogens. *Journal of Hazardous, Toxic, Radioactive Waste, 26*(1), 04021040, https://doi.org/10.1061/(ASCE)HZ.2153-5515.0000643.

Dehal, A., Prajapati, A., P. Patil, M., & Kumar, A. R. (2024). A review on microplastics in landfill leachate: formation, occurrence, detection, and removal techniques. *Chemistry Ecology, 40*(1), 65-101, https://doi.org/10.1080/02757540.2023.2290183.

Deng, H., Wei, R., Luo, W., Hu, L., Li, B., & Shi, H. (2020). Microplastic pollution in water and sediment in a textile industrial area. *Environmental Pollution, 258*, 113658, https://doi.org/10.1016/j.envpol.2019.113658.

Dey, S., Sen, K., Saha, N. C., & Saha, S. (2025). Analytical approaches for quantifying and characterizing microplastics: environmental impacts and bioaccumulation in aquatic Systems. *Green Analytical Chemistry, 12*, 100191, https://doi.org/10.1016/j.greeac.2024.100191.

Dong, S., Xia, J., Sheng, L., Wang, W., Liu, H., & Gao, B. (2021). Transport characteristics of fragmental polyethylene glycol terephthalate (PET) microplastics in porous media under various chemical conditions. *Chemosphere, 276*, 130214, https://doi.org/10.1016/j.chemosphere.2021.130214.

Dong, S., Zhou, M., Su, X., Xia, J., Wang, L., Wu, H., . . . Wang, D. (2022). Transport and retention patterns of fragmental microplastics in saturated and unsaturated porous media: A real-time pore-scale visualization. *Water Research, 214*, 118195, https://doi.org/10.1016/j.watres.2022.118195.

Dong, Y., Ren, L., Jia, X., Liao, X., Huang, L., Zhang, X., . . . Xu, L. (2025). Microplastics decrease soil compressibility but have no major impact on soil physical properties. *Soil and Tillage Research, 253*, Soil and Tillage Research, https://doi.org/10.1016/j.still.2025.106688.

Dong, Z., Qiu, Y., Zhang, W., Yang, Z., & Wei, L. (2018). Size-dependent transport and retention of micron-sized plastic spheres in natural sand saturated with seawater. *Water research, 143*, 518-526., https://doi.org/10.1016/j.watres.2018.07.007.

Dong, Z., Zhu, L., Zhang, W., Huang, R., Lv, X., Jing, X., . . . Qiu, Y. (2019). Role of surface functionalities of nanoplastics on their transport in seawater-saturated sea sand. *Environmental Pollution, 255*, 113177, https://doi.org/10.1016/j.envpol.2019.113177.

Duncan, L., & El-Zein, A. (2026). Continuum-Scale Analysis of Micro- and Nano-Plastic Retention Mechanisms in Porous Media. *Nature Communications. (Under review)*.

Ebina, T., Minja, R. J., Nagase, T., Onodera, Y., & Chatterjee, A. (2004). Correlation of hydraulic conductivity of clay–sand compacted specimens with clay properties. *Applied Clay Science, 26*(1-4), 3-12, https://doi.org/10.1016/j.clay.2003.09.010.

El-Zein, A., Airey, D., Yu, B., Esgandani, G. A., Proust, G., Dias-da-Costa, D., . . . Chen, S. (2021). Self-repair of cracks and defects in clay: a review of evidence, mechanisms, theories and nomenclature. *Acta Geotechnica, 16*(12), 3741-3760, https://doi.org/10.1007/s11440-021-01382-8.

Eun, J., Tinjum, J. M., Benson, C. H., & Edil, T. B. (2017). Comparison of volatile organic compound transport in composite liners with HDPE and ethylene-vinyl alcohol co-extruded geomembranes. *Journal of Geotechnical and Geoenvironmental Engineering, 143*(6), 04017010, https://doi.org/10.1061/(ASCE)GT.1943-5606.0001484.

Fan, R. D., Du, Y. J., Reddy, K. R., Liu, S. Y., & Yang, Y. L. (2014). Compressibility and hydraulic conductivity of clayey soil mixed with calcium bentonite for slurry wall backfill: Initial assessment. *Applied Clay Science, 101*, 119-127, https://doi.org/10.1016/j.clay.2014.07.026.

Fang, Z., Sallach, J. B., & Hodson, M. E. (2024). Size-and concentration-dependent effects of microplastics on soil aggregate formation and properties. *Journal of Hazardous Materials, 465*, 133395, https://doi.org/10.1016/j.jhazmat.2023.133395.

Fei, J., Xie, H., Zhao, Y., Zhou, X., Sun, H., Wang, N., . . . Yin, X. (2022). Transport of degradable/nondegradable and aged microplastics in porous media: Effects of physicochemical factors. *Science of the Total Environment, 851*, 158099, https://doi.org/10.1016/j.scitotenv.2022.158099.

Filiciotto, L., & Rothenberg, G. (2021). Biodegradable plastics: Standards, policies, and impacts. *Chemistry Sustainability Energy Materials, 14*(1), 56-72, https://doi.org/10.1002/cssc.202002044.

Fu, X., Jiang, Z., Wang, M., Ni, H., & Du, Y. (2025a). Enhancing containment performance of geosynthetic clay liner to bauxite liquor via composite polymer amendment. *Engineering Geology, 354*, 108189, https://doi.org/10.1016/j.enggeo.2025.108189.

Fu, Y., Wang, H., Yang, Z., Liu, L., Jin, X., Huang, Y., . . . Dang, Z. (2025b). Deposition and release of clay colloids on alumina and natural organic matter surfaces via heterogeneous pathways. *Applied Clay Science, 274*, 107856, https://doi.org/10.1016/j.clay.2025.107856.

Gao, J., Pan, S., Li, P., Wang, L., Hou, R., Wu, W., . . . Hou, D. (2021). Vertical migration of microplastics in porous media: Multiple controlling factors under wet-dry cycling. *Journal of Hazardous Materials, 419*, 126413., https://doi.org/10.1016/j.jhazmat.2021.126413.

García-Romero, E., Lorenzo, A., García-Vicente, A., Morales, J., García-Rivas, J., & Suárez, M. (2021). On the structural formula of smectites: a review and new data on the influence of exchangeable cations. *Applied Crystallography, 54*(1), 251-262, https://doi.org/10.1107/S1600576720016040.

Gates, W. P., Gibbs, D., & Amstberg, M. (2018). *Resilience of Australian polymer-modified powdered sodium bentonite geosynthetic clay liners to downslope bentonite erosion.* Paper presented at the The International Congress on Environmental Geotechnics, Singapore.

Geyer, R., Jambeck, J. R., & Law, K. L. (2017). Production, use, and fate of all plastics ever made. *Science Advances, 3*(7), e1700782, https://www.science.org/doi/10.1126/sciadv.1700782.

Ghavam-Nasiri, A., El-Zein, A., Airey, D., & Rowe, R. K. (2019). Water retention of geosynthetics clay liners: Dependence on void ratio and temperature. *Geotextiles and Geomembranes, 47*(2), 255-268, https://doi.org/10.1016/j.geotexmem.2018.12.014.

Ghazizade, M. J., & Safari, E. (2017). Analysis of desiccation crack depth in three compacted clay liners exposed to annual cycle of atmospheric conditions with and without a geotextile cover. *Journal of Geotechnical and Geoenvironmental Engineering, 143*(3), 06016024, https://doi.org/10.1061/(ASCE)GT.1943-5606.0001607.

Gigault, J., El Hadri, H., Nguyen, B., Grassl, B., Rowenczyk, L., Tufenkji, N., . . . Wiesner, M. (2021). Nanoplastics are neither microplastics nor engineered nanoparticles. *Nature nanotechnology, 16*(5), 501-507, https://doi.org/10.1038/s41565-021-00886-4.

Gilbert, B., Comolli, L. R., Tinnacher, R. M., Kunz, M., & Banfield, J. F. (2015). Formation and restacking of disordered smectite osmotic hydrates. *Clays and Clay Minerals, 63*(6), 432-442, https://doi.org/10.1346/CCMN.2015.0630602.

Gómez-Espina, R., & Villar, M. V. (2010). Geochemical and mineralogical changes in compacted MX-80 bentonite submitted to heat and water gradients. *Applied Clay Science, 47*(3-4), 400-408, https://doi.org/10.1016/j.clay.2009.12.004.

Grim, R. E., & Guven, N. (2011). *Bentonites: geology, mineralogy, properties and uses* (Vol. 24): Elsevier.

Guo, L., Xu, X., Wang, Q., Park, J., Zhou, L., Lei, H., & Wang, X. (2025a). Effects of microplastics on the hydraulic properties and pore characteristics of compacted soil. *Soil and Tillage Research, 254*, 106742, https://doi.org/10.1016/j.still.2025.106742.

Guo, S., Wu, Z., Li, X., Shen, D., Shentu, J., Lu, L., . . . Long, Y. (2024). Microplastic, a possible trigger of landfill sulfate reduction process. *Science of the Total Environment, 906*, 167662, https://doi.org/10.1016/j.scitotenv.2023.167662.

Guo, Y., & Fei, X. (2023). Insights on experimental methodologies and theoretical models for microplastics transport in soils and sediments based on meta-analysis. *Acta Geotechnica, 18*(8), 4477-4492, https://doi.org/10.1007/s11440-022-01767-3.

Guo, Y., Zhao, B., She, Q., Fu, X., & Fei, X. (2025b). Transport Mechanisms of Microplastics in Clean Sand under Cyclic Hydraulic Gradients. *Journal of Geotechnical and Geoenvironmental Engineering, 151*(5), 04025021, https://doi.org/10.1061/JGGEFK.GTENG-13047.

Guo, Z., Li, P., Yang, X., Wang, Z., Lu, B., Chen, W., . . . Xue, S. (2022). Soil texture is an important factor determining how microplastics affect soil hydraulic characteristics. *Environment International, 165*, 107293, https://doi.org/10.1016/j.envint.2022.107293.

Gustavsson, N., Bylund, A., Grabo, L., Grönholdt Palm, J., Nordzell, H., & Snöbohm, S. (2022). *Geotextiles and microplastics in Sweden-an assessment* (No. from

Hahn, M. W., Abadzic, D., & O'Melia, C. R. (2004). Aquasols: On the role of secondary minima. *Environmental Science & Technology, 38*(22), 5915-5924, https://doi.org/10.1021/es049746d.

Hahn, M. W., & O'Melia, C. R. (2004). Deposition and reentrainment of Brownian particles in porous media under unfavorable chemical conditions: Some concepts and applications. *Environmental Science & Technology, 38*(1), 210-220, https://doi.org/10.1021/es030416n.

Håkansson, I., & Lipiec, J. (2000). A review of the usefulness of relative bulk density values in studies of soil structure and compaction. *Soil and Tillage Research, 53*(2), 71-85, https://doi.org/10.1016/S0167-1987(99)00095-1.

Han, L., Chen, L., Feng, Y., Kuzyakov, Y., Chen, Q., Zhang, S., . . . Sun, K. (2024). Microplastics alter soil structure and microbial community composition. *Environment International, 185*, 108508, https://doi.org/10.1016/j.envint.2024.108508.

Haque, F., & Fan, C. (2023). Fate of microplastics under the influence of climate change. *Iscience, 26*(9), 107649, https://doi.org/10.1016/j.isci.2023.107649.

Hartini, E., & Warsito, B. (2025). Distribution and ecological risk of microplastics in soil at the Jatibarang landfill in Semarang, Indonesia. *Journal of Ecological Engineering, 26*(2), https://doi.org/10.12911/22998993/197043.

He, F., Zhang, M., Qian, T., & Zhao, D. (2009). Transport of carboxymethyl cellulose stabilized iron nanoparticles in porous media: Column experiments and modeling. *Journal of Colloid and Interface Science, 334*(1), 96-102, https://doi.org/10.1016/j.jcis.2009.02.058.

He, P., Chen, L., Shao, L., Zhang, H., & Lü, F. (2019). Municipal solid waste (MSW) landfill: A source of microplastics?-Evidence of microplastics in landfill leachate. *Water Research, 159*, 38-45, https://doi.org/10.1016/j.watres.2019.04.060.

He, Y., Lu, P. H., Ye, W. M., Chen, Y. G., & Zhang, K. N. (2022). Coupled chemo-hydro-mechanical effects on volume change behaviour of compacted bentonite used as buffer/backfill material in high-level radioactive waste repository. *Journal of Nuclear Science and Technology, 59*(10), 1207-1231, https://doi.org/10.1080/00223131.2022.2044930.

Hedley, J. G., Berthoumieux, H., & Kornyshev, A. A. (2023). The dramatic effect of water structure on hydration forces and the electrical double layer. *The Journal of Physical Chemistry C, 127*(18), 8429-8447, https://doi.org/10.1021/acs.jpcc.3c00262.

Herath, H. M. S. K., Camps-Arbestain, M., & Hedley, M. (2013). Effect of biochar on soil physical properties in two contrasting soils: an Alfisol and an Andisol. *Geoderma, 209*, 188-197, https://doi.org/10.1016/j.geoderma.2013.06.016.

Herrington, T. M., & Petzold, J. C. (1992). An investigation into the nature of charge on the surface of papermaking woodpulps 1. Charge/pH isotherms. *Colloids and surfaces, 64*(2), 97-108, https://doi.org/10.1016/0166-6622(92)80088-J.

Horton, A. A., Cross, R. K., Read, D. S., Jürgens, M. D., Ball, H. L., Svendsen, C., . . . Johnson, A. C. (2021). Semi-automated analysis of microplastics in complex wastewater samples. *Environmental Pollution, 268*, 115841, https://doi.org/10.1016/j.envpol.2020.115841.

Hosney, M. S., & Rowe, R. K. (2014). Performance of three GCLs used for covering gold mine tailings for 4 years under field and laboratory exposure conditions. *Geosynthetics International, 21*(3), 197-212, https://doi.org/10.1680/gein.14.00009.

Hossain, R., Hakim, A., Roy, S., Tanu, F. Z., & Akhtaruzzaman, M. (2025). Saturated hydraulic conductivity in microplastics incorporated soils: Effects of soil texture, polymer type, particle size, and concentration. *Discover Polymers, 2*(1), 11, https://doi.org/10.1007/s44347-025-00022-8.

Hotton, C., Bizien, T., Hamon, C., Ferrage, E., & Paineau, E. (2025). Bridging the Gap between Osmotic and Crystalline Swelling in 2D Layered Materials Using Levitated Droplets. *Nano Micro Small, 21*(33), 2505038, https://doi.org/10.1002/smll.202505038.

Hou, J., Xu, X., Lan, L., Miao, L., Xu, Y., You, G., & Liu, Z. (2020). Transport behavior of micro polyethylene particles in saturated quartz sand: Impacts of input concentration and physicochemical factors. *Environmental Pollution, 263*, 114499, https://doi.org/10.1016/j.envpol.2020.114499.

Hu, E., Shang, S., Fu, Z., Zhao, X., Nan, X., Du, Y., & Chen, X. (2020). Cotransport of naphthalene with polystyrene nanoplastics (PSNP) in saturated porous media: Effects of PSNP/naphthalene ratio and ionic strength. *Chemosphere, 245*, 125602, https://doi.org/10.1016/j.chemosphere.2019.125602.

Hu, K., Zhou, P., Yang, Y., Hall, T., Nie, G., Yao, Y., . . . Wang, S. (2021). Degradation of microplastics by a thermal Fenton reaction. *Environmental Science & Technology Engineering, 2*(1), 110-120, https://doi.org/10.1021/acsestengg.1c00323.

Huang, B., Cao, L., Guo, J., Xu, C., & Li, Y. (2025). Centrifuge modeling of contaminant transport in keyed sand-bentonite cutoff walls. *Journal of Zhejiang University-SCIENCE A, 26*(6), 573-584, https://doi.org/10.1631/jzus.A2400148.

Huang, S., Wang, H., Ahmad, W., Ahmad, A., Ivanovich Vatin, N., Mohamed, A. M., . . . Mehmood, I. (2022). Plastic waste management strategies and their environmental aspects: A scientometric analysis and comprehensive review. *International Journal of Environmental Research Public Health, 19*(8), 4556, https://doi.org/10.3390/ijerph19084556.

Huang, Y., Liu, Q., Jia, W., Yan, C., & Wang, J. (2020). Agricultural plastic mulching as a source of microplastics in the terrestrial environment. *Environmental Pollution, 260*, 114096, https://doi.org/10.1016/j.envpol.2020.114096.

Huang, Y., & Zhang, B. (2022). Review on key issues in centrifuge modeling of flow-structure interaction. *European Journal of Environmental and Civil Engineering, 26*(6), 2354-2370, https://doi.org/10.1080/19648189.2020.1762751.

Hüffer, T., Praetorius, A., Wagner, S., Von der Kammer, F., & Hofmann, T. (2017). Microplastic exposure assessment in aquatic environments: learning from similarities and differences to engineered nanoparticles. *Environmental Science & Technology, 51*(5), 2499-2507, https://doi.org/10.1021/acs.est.6b04054.

Huysmans, M., & Dassargues, A. (2005). Review of the use of Péclet numbers to determine the relative importance of advection and diffusion in low permeability environments. *Hydrogeology Journal, 13*(5), 895-904, https://doi.org/10.1007/s10040-004-0387-4.

Ingraffia, R., Amato, G., Bagarello, V., Carollo, F. G., Giambalvo, D., Iovino, M., . . . Frenda, A. S. (2021). Polyester microplastic fibers affect soil physical properties and erosion as a function of soil type. *Soil Discussions, 2021*, 1-22, https://doi.org/10.5194/soil-8-421-2022.

Jazaei, F., Chy, T. J., & Salehi, M. (2022). Can microplastic pollution change soil-water dynamics? Results from controlled laboratory experiments. *Water, 14*(21), 3430, https://doi.org/10.3390/w14213430.

Jo, H. Y., Benson, C. H., & Edil, T. B. (2004). Hydraulic conductivity and cation exchange in non-prehydrated and prehydrated bentonite permeated with weak inorganic salt solutions. *Clays and Clay Minerals, 52*(6), 661-679, https://doi.org/10.1346/CCMN.2004.0520601.

Jo, H. Y., Benson, C. H., Shackelford, C. D., Lee, J. M., & Edil, T. B. (2005). Long-term hydraulic conductivity of a geosynthetic clay liner permeated with inorganic salt solutions. *Journal of Geotechnical and Geoenvironmental Engineering, 131*(4), 405-417, https://doi.org/10.1061/(ASCE)1090-0241(2005)131:4(405).

Jørgensen, P. R., Urup, J., Helstrup, T., Jensen, M. B., Eiland, F., & Vinther, F. P. (2004). Transport and reduction of nitrate in clayey till underneath forest and arable land. *Journal of Contaminant Hydrology, 73*(1-4), 207-226, https://doi.org/10.1016/j.jconhyd.2004.01.005.

Kabir, M. S., Wang, H., Luster-Teasley, S., Zhang, L., & Zhao, R. (2023). Microplastics in landfill leachate: Sources, detection, occurrence, and removal. *Environmental Science and Ecotechnology, 16*, 100256, https://doi.org/10.1016/j.ese.2023.100256.

Kamai, T., Nassar, M. K., Nelson, K. E., & Ginn, T. R. (2015). Colloid filtration prediction by mapping the correlation-equation parameters from transport experiments in porous media. *Water Resources Research, 51*(11), 8995-9012, https://doi.org/10.1002/2015WR017403.

Kamon, M., Zhang, H., Katsumi, T., & Sawa, N. (2002). Redox effect on the hydraulic conductivity of clay liner. *Soils and Foundations, 42*(6), 79-91, https://doi.org/10.3208/sandf.42.6_79.

Kang, J., & Shackelford, C. D. (2009). Clay membrane testing using a flexible-wall cell under closed-system boundary conditions. *Applied Clay Science, 44*(1-2), 43-58, https://doi.org/10.1016/j.clay.2009.01.006.

Kang, J., & Shackelford, C. D. (2011). Consolidation enhanced membrane behavior of a geosynthetic clay liner. *Geotextiles and Geomembranes, 29*(6), 544-556, https://doi.org/10.1016/j.geotexmem.2011.07.002.

Kara, N., Sari Erkan, H., & Onkal Engin, G. (2023). Characterization and removal of microplastics in landfill leachate treatment plants in Istanbul, Turkey. *Analytical Letters, 56*(9), 1535-1548, https://doi.org/10.1080/00032719.2022.2137808.

Kasanin-Grubin, M. (2013). Clay mineralogy as a crucial factor in badland hillslope processes. *Catena, 106*, 54-67, https://doi.org/10.1016/j.catena.2012.08.008.

Kasel, D., Bradford, S. A., Šimůnek, J., Heggen, M., Vereecken, H., & Klumpp, E. (2013). Transport and retention of multi-walled carbon nanotubes in saturated porous media: effects of input concentration and grain size. *Water Research, 47*(2), 933-944, https://doi.org/10.1016/j.watres.2012.11.019.

Katzourakis, V. E., & Chrysikopoulos, C. V. (2024). Aggregating nanoparticle transport with nonlinear attachment: Modeling and experimental validation. *Advances in Water Resources, 193*, 104819, https://doi.org/10.1016/j.advwatres.2024.104819.

Kaufhold, S., Dohrmann, R. B., Ufer, K., & Meyer, F. M. (2002). Comparison of methods for the quantification of montmorillonite in bentonites. *Applied Clay Science, 22*(3), 145-151, https://doi.org/10.1016/S0169-1317(02)00131-X.

Ke, H., Liu, Y., Hu, J., Qin, R., Xu, X. B., & Chen, Y. M. (2022). Experimental study on anisotropy of hydraulic conductivity for municipal solid waste. *Waste Management, 137*, 39-49, https://doi.org/10.1016/j.wasman.2021.10.030.

Keller, A. A., Sirivithayapakorn, S., & Chrysikopoulos, C. V. (2004). Early breakthrough of colloids and bacteriophage MS2 in a water-saturated sand column. *Water Resources Research, 40*(8), W08304, https://doi.org/10.1029/2003WR002676.

Kilponen, J. (2016). *Microplastics and harmful substances in urban runoffs and landfill leachates: possible emission sources to marine environment.* (Retrieved from https://www.theseus.fi/bitstream/handle/10024/114539/Kilponen_Juho.pdf?s)

Kim, W. K., Park, H., Ishii, K., & Ham, G. (2023). Investigation on Microplastics in Soil near Landfills in the Republic of Korea. *Sustainability, 15*(15), 12057, https://doi.org/10.3390/su151512057.

Kjeldsen, P., Barlaz, M. A., Rooker, A. P., Baun, A., Ledin, A., & Christensen, T. H. (2002). Present and long-term composition of MSW landfill leachate: a review. *Critical Reviews in Environmental Science and Technology, 32*(4), 297-336, https://doi.org/10.1080/10643380290813462.

Kolstad, D. C., Benson, C. H., & Edil, T. B. (2004). Hydraulic conductivity and swell of nonprehydrated geosynthetic clay liners permeated with multispecies inorganic solutions. *Journal of Geotechnical and Geoenvironmental Engineering, 130*(12), 1236-1249, https://doi.org/10.1061/(ASCE)1090-0241(2004)130:12(1236).

Krishnendu, S. A., & Varghese, G. K. (2025). Landfill liners as a source of microplastics: Do the guards guard themselves? *Journal of Environmental Management, 391*, 126522, https://doi.org/10.1016/j.jenvman.2025.126522.

Kushwaha, M., Shankar, S., Goel, D., Singh, S., Rahul, J., Rachna, K., & Singh, J. (2024). Microplastics pollution in the marine environment: A review of sources, impacts and mitigation. *Marine Pollution Bulletin, 209*, 117109, https://doi.org/10.1016/j.marpolbul.2024.117109.

Lalrinfela, P., Vanlalsangi, R., Lalrinzuali, K., & Babu, P. J. (2024). Microplastics: Their effects on the environment, human health, and plant ecosystems. *Environmental Pollution and Management, 1*, 248-259, https://doi.org/10.1016/j.epm.2024.11.004.

Lange, K., Rowe, R. K., & Jamieson, H. (2010). The potential role of geosynthetic clay liners in mine water treatment systems. *Geotextiles and Geomembranes, 28*(2), 199-205, https://doi.org/10.1016/j.geotexmem.2009.10.003.

Laskar, N., & Kumar, U. (2019). Plastics and microplastics: A threat to environment. *Environmental Technology Innovation, 14*, 100352, https://doi.org/10.1016/j.eti.2019.100352.

Ledieu, L., Phuong, N., Flahaut, B., Radigois, P., Papin, J., Le Guern, C., . . . Gasperi, J. (2023). May a former municipal landfill contaminate groundwater in microplastics? First investigations from the "prairie de mauves site" (Nantes, France). *Microplastics, 2*(1), 93-106, https://doi.org/10.3390/microplastics2010007.

Lee, J. M., & Shackelford, C. D. (2005). Impact of bentonite quality on hydraulic conductivity of geosynthetic clay liners. *Journal of Geotechnical and Geoenvironmental Engineering, 131*(1), 64-77, https://doi.org/10.1061/(ASCE)1090-0241(2005)131:1(64).

Lee, Y. S., Kim, Y. M., Lee, J., & Kim, J. Y. (2021). Evaluation of silver nanoparticles (AgNPs) penetration through a clay liner in landfills. *Journal of Hazardous Materials, 404*, 124098, https://doi.org/10.1016/j.jhazmat.2020.124098.

Lehmann, A., Fitschen, K., & Rillig, M. C. (2019). Abiotic and biotic factors influencing the effect of microplastic on soil aggregation. *Soil Systems, 3*(1), 21, https://doi.org/10.3390/soilsystems3010021.

Lehmann, A., Leifheit, E. F., Gerdawischke, M., & Rillig, M. C. (2021). Microplastics have shape-and polymer-dependent effects on soil aggregation and organic matter loss–an experimental and meta-analytical approach. *Microplastics and Nanoplastics, 1*(1), 7, https://doi.org/10.1186/s43591-021-00007-x.

Li, B., Li, C., Gui, Y., Zhan, H., Gu, Y., Yu, M., & Rowe, R. K. (2024a). Understanding structural anisotropy and mechanical properties of Na-montmorillonite with crystalline swelling and uniaxial deformation under different hydration degrees. *Computers and Geotechnics, 169*, 106200., https://doi.org/10.1016/j.compgeo.2024.106200.

Li, F., Huang, D., Wang, G., Cheng, M., Chen, H., Zhou, W., . . . Xu, W. (2024b). Microplastics/nanoplastics in porous media: Key factors controlling their transport and retention behaviors. *Science of the Total Environment, 926*, 171658, https://doi.org/10.1016/j.scitotenv.2024.171658.

Li, H., Liu, L., & Li, C. (2024c). Small-size polyethylene and polylactic microplastic alterations on soil aggregate formation with soil sterilization. *Chemosphere, 364*, 143158, https://doi.org/10.1016/j.chemosphere.2024.143158.

Li, H., Lu, Y., & Zhang, H. (2025a). Swelling deformation and model calculation of Mg/Ca-bentonite under the influence of salt solution. *PLoS One, 20*(5), e0323021, https://doi.org/10.1371/journal.pone.0323021.

Li, H., Yang, L., Luo, C., Liu, L., Li, C., Wang, J., . . . Zhong, H. (2025b). Soil aggregation alterations under soil microplastic and biochar addition and aging process. *Environmental Pollution, 367*, 125655, https://doi.org/10.1016/j.envpol.2025.125655.

Li, M., & Fannin, R. J. (2008). Comparison of two criteria for internal stability of granular soil. *Canadian Geotechnical Journal, 45*(9), 1303-1309, https://doi.org/10.1139/T08-046.

Li, M., & Fannin, R. J. (2022). Internal erosion: critical hydraulic gradient in one-dimensional vertical seepage and its relation to soil gradation. *Canadian Geotechnical Journal, 59*(5), 769-772, https://doi.org/10.1139/cgj-2021-0238.

Li, W., Brunetti, G., Bolshakova, A., & Stumpp, C. (2024d). Effect of particle density on microplastics transport in artificial and natural porous media. *Science of the Total Environment, 935*, 173429, https://doi.org/10.1016/j.scitotenv.2024.173429.

Li, W., Brunetti, G., Zafiu, C., Kunaschk, M., Debreczeby, M., & Stumpp, C. (2024e). Experimental and simulated microplastics transport in saturated natural sediments: impact of grain size and particle size. *Journal of Hazardous Materials, 468*, 133772, https://doi.org/10.1016/j.jhazmat.2024.133772.

Li, Y. C., Yao, S. Y., Chen, C., Chen, Y. M., Chen, G. N., & Zhang, R. H. (2023). A solution for calculating the leakage rate through GMB/CCL composite liners with long defects. *Computers and Geotechnics, 163*, 105770, https://doi.org/10.1016/j.compgeo.2023.105770.

Li, Y. Z., Zhuang, H., Fan, J. Y., Xia, W. Y., Wan, J. L., Che, C., & Du, Y. J. (2025c). Biopolymer-amended geosynthetic clay liners for landfills and contaminated sites: gas/hydraulic performance. *Environmental Research, 278*, 121714, https://doi.org/10.1016/j.envres.2025.121714.

Liang, A., Liu, C., & Branicio, P. S. (2024a). Colloid transport in bicontinuous nanoporous media. *Langmuir, 40*(21), 10868-10883, https://doi.org/10.1021/acs.langmuir.4c00037.

Liang, S., Chen, X., Chen, J., Peng, D., Wang, Z., & Meng, C. (2024b). Hydraulic conductivity of polymer-enhanced bentonite geosynthetic clay liners to coal gangue leachate. *Environmental Technology & Innovation, 34*, 103574, https://doi.org/10.1016/j.eti.2024.103574.

Liang, Y., Lehmann, A., Yang, G., Leifheit, E. F., & Rillig, M. C. (2021). Effects of microplastic fibers on soil aggregation and enzyme activities are organic matter dependent. *Frontiers in Environmental Science, 9*, 650155, https://doi.org/10.3389/fenvs.2021.650155.

Liang, Y., Zhou, J., Dong, Y., Klumpp, E., Šimůnek, J., & Bradford, S. A. (2020). Evidence for the critical role of nanoscale surface roughness on the retention and release of silver nanoparticles in porous media. *Environmental Pollution, 258*, 113803, https://doi.org/10.1016/j.envpol.2019.113803.

Lim, S. J., Seo, J., Hwang, M., Kim, H. C., Kim, E. J., Lee, J., . . . Chung, J. (2023). A multi-scale framework for modeling transport of microplastics during sand filtration: bridging from pore to continuum. *Journal of Hazardous Materials, 443*, 130219., https://doi.org/10.1016/j.jhazmat.2022.130219.

Lin, D., Hu, L., Bradford, S. A., Zhang, X., & Lo, I. M. (2021). Pore-network modeling of colloid transport and retention considering surface deposition, hydrodynamic bridging, and straining. *Journal of Hydrology, 603*, 127020, https://doi.org/10.1016/j.jhydrol.2021.127020.

Liu, G., Zhong, H., Ahmad, Z., Yang, X., & Huo, L. (2020). Transport of engineered nanoparticles in porous media and its enhancement for remediation of contaminated groundwater. *Critical Reviews in Environmental Science and Technology, 50*(22), 2301-2378, https://doi.org/10.1080/10643389.2019.1694823.

Liu, G., Zhu, Z., Yang, Y., Sun, Y., Yu, F., & Ma, J. (2019a). Sorption behavior and mechanism of hydrophilic organic chemicals to virgin and aged microplastics in freshwater and seawater. *Environmental Pollution, 246*, 26-33, https://doi.org/10.1016/j.envpol.2018.11.100.

Liu, J., Ma, Y., Zhu, D., Xia, T., Qi, Y., Yao, Y., . . . Chen, W. (2018). Polystyrene nanoplastics-enhanced contaminant transport: role of irreversible adsorption in glassy polymeric domain. *Environmental Science & Technology, 52*(5), 2677-2685, https://doi.org/10.1021/acs.est.7b05211.

Liu, J., Zhang, T., Tian, L., Liu, X., Qi, Z., Ma, Y., . . . Chen, W. (2019b). Aging significantly affects mobility and contaminant-mobilizing ability of nanoplastics in saturated loamy sand. *Environmental Science & Technology,, 53*(10), 5805-5815, https://doi.org/10.1021/acs.est.9b00787.

Liu, P. (2021). *Microstructure, Rheology and Thixotropy of Composite Clay Gels.* (Doctor of Philosophy, the University of Western Australia, Retrieved from https://api.research-repository.uwa.edu.au/ws/portalfiles/portal/181415713/THESIS_DOCTOR_OF_PHILOSOPHY_LIU_Pengfei_2021_2.pdf)

Liu, S., Shikhov, I., Cui, Y., & Arns, C. H. (2023). Pore-scale morphology effects on colloid deposition by trajectory tracking simulations. *Geoenergy Science and Engineering, 227*, 211772, https://doi.org/10.1016/j.geoen.2023.211772.

Liu, X., Cai, G., Liu, L., Liu, S., & Puppala, A. J. (2019c). Thermo-hydro-mechanical properties of bentonite-sand-graphite-polypropylene fiber mixtures as buffer materials for a high-level radioactive waste repository. *Int J Heat Mass Transf, 141*, 981-994.

Liu, Y., & Jiang, T. (2024). Effects of Temperature, Ionic Strength and Humic Acid on the Transport of Graphene Oxide Nanoparticles in Geosynthetic Clay Liner. *Materials, 17*(9), 2082, https://doi.org/10.3390/ma17092082.

Liu, Y., Lüttjohann, S., Vianello, A., Lorenz, C., Liu, F., & Vollertsen, J. (2024). Detecting small microplastics down to 1.3 µm using large area ATR-FTIR. *Marine Pollution Bulletin, 198*, 115795, https://doi.org/10.1016/j.marpolbul.2023.115795.

Lodh, A., Shafi, M., & Goel, S. (2025). Microplastics in municipal solid waste landfill leachate and their removal in treatment units: A perspective of controlled and uncontrolled landfills. *Environmental Pollution*, 125853, https://doi.org/10.1016/j.envpol.2025.125853.

Lu, T., Gilfedder, B. S., Peng, H., Niu, G., & Frei, S. (2021a). Effects of clay minerals on the transport of nanoplastics through water-saturated porous media. *Science of the Total Environment, 796*, 148982, https://doi.org/10.1016/j.scitotenv.2021.148982.

Lu, T., Gilfedder, B. S., Peng, H., Peiffer, S., Papastavrou, G., Ottermann, K., & Frei, S. (2021b). Relevance of iron oxyhydroxide and pore water chemistry on the mobility of nanoplastic particles in water-saturated porous media environments. *Water, Air, & Soil Pollution, 232*(5), 168, https://doi.org/10.1007/s11270-021-05125-z.

Luo, H., Chang, L., Ju, T., & Li, Y. (2024). Factors Influencing the Vertical Migration of Microplastics up and down the Soil Profile. *ACS omega, 9*(51), 50064-50077, https://doi.org/10.1021/acsomega.4c04083.

Ma, J., Ma, M., Li, J., Yang, Q., Wan, Y., Zhao, K., . . . Fei, X. (2025a). Distribution and characteristics of Microplastics in leachate and underneath soil of two informal landfills. *Waste Management, 195*, 155-166, https://doi.org/10.1016/j.wasman.2025.02.002.

Ma, Q., Sun, Y., Zhou, S., Yin, X., & Sun, H. (2025b). The transport of polystyrene microplastics in saturated porous media: Impacts of functional groups and solution chemistry. *Journal of Environmental Management, 377*, 124696., https://doi.org/10.1016/j.jenvman.2025.124696.

Mahesh, S., Gowda, N. K., & Mahesh, S. (2023). Identification of microplastics from urban informal solid waste landfill soil; MP associations with COD and chloride. *Water Science & Technology, 87*(1), 115-129, https://doi.org/10.2166/wst.2022.412.

Makusa, G. P., Bradshaw, S. L., Berns, E., Benson, C. H., & Knutsson, S. (2014). Freeze–thaw cycling concurrent with cation exchange and the hydraulic conductivity of geosynthetic clay liners. *Canadian Geotechnical Journal, 51*(6), 591-598, https://doi.org/10.1139/cgj-2013-0127.

Malusis, M. A., & Daniyarov, A. S. (2016). Membrane efficiency and diffusive tortuosity of a dense prehydrated geosynthetic clay liner. *Geotextiles and Geomembranes, 44*(5), 719-730, https://doi.org/10.1016/j.geotexmem.2016.05.006.

Malusis, M. A., Kang, J., & Shackelford, C. D. (2015). Restricted salt diffusion in a geosynthetic clay liner. *Environmental Geotechnics, 2*(2), 68-77, https://doi.org/10.1680/envgeo.13.00080.

Malusis, M. A., & Shackelford, C. D. (2002). Chemico-osmotic efficiency of a geosynthetic clay liner. *Journal of Geotechnical and Geoenvironmental Engineering, 128*(2), 97-106, https://doi.org/10.1061/(ASCE)1090-0241(2002)128:2(97).

Mao, R., Luo, X., Jiao, J. J., & Li, H. (2023). Molecular diffusion and pore-scale mechanical dispersion controls on time-variant travel time distribution in hillslope aquifers. *Journal of Hydrology, 616*, 128798, https://doi.org/10.1016/j.jhydrol.2022.128798.

Maqbool, A., Li, W., Stumpp, C., Soriano, M. A., & Gómez, J. A. (2025). Effect of Preferential Microplastics Leaching Through Macropores on Vertical Soil Particle Transport. *European Journal of Soil Science, 76*(3), e70140, https://doi.org/10.1111/ejss.70140.

Mazzieri, F., di Sante, M., & Fratalocchi, E. (2015). Dilution effect of the apparatus on contaminant transport parameters assessed by column testing. *Journal of Geotechnical and Geoenvironmental Engineering, 141*(9), 1-5.

Mbedzi, R., Cuthbert, R. N., Wasserman, R. J., Murungweni, F. M., & Dalu, T. (2020). Spatiotemporal variation in microplastic contamination along a subtropical reservoir shoreline. *Environmental Science and Pollution Research, 27*(19), 23880-23887, https://doi.org/10.1007/s11356-020-08640-4.

McCarthy, J. F., McKay, L. D., & Bruner, D. D. (2002). Influence of ionic strength and cation charge on transport of colloidal particles in fractured shale saprolite. *Environmental Science & Technology, 36*(17), 3735-3743, https://doi.org/10.1021/es025522o.

Meer, S. R., & Benson, C. H. (2007). Hydraulic conductivity of geosynthetic clay liners exhumed from landfill final covers. *Journal of Geotechnical and Geoenvironmental Engineering, 133*(5), 550-563, https://doi.org/10.1061/(ASCE)1090-0241(2007)133:5(550).

Miao, J., Huang, W., Pan, R., & Zhou, K. (2023). Research progress and hotspot analysis of soil microplastics: a bibliometrics-based review. *Frontiers in Environmental Science, 11*, 1297646, https://doi.org/10.3389/fenvs.2023.1297646.

Mitchell, J. K., & Soga, K. (2005). *Fundamentals of soil behavior* (Vol. 3). Hoboken, NJ: John Wiley & Sons.

Mitzel, M. R., Sand, S., Whalen, J. K., & Tufenkji, N. (2016). Hydrophobicity of biofilm coatings influences the transport dynamics of polystyrene nanoparticles in biofilm-coated sand. *Water Research, 92*, 113-120, https://doi.org/10.1016/j.watres.2016.01.026.

Mohammadi, A., Malakootian, M., Dobaradaran, S., Hashemi, M., & Jaafarzadeh, N. (2022). Occurrence, seasonal distribution, and ecological risk assessment of microplastics and phthalate esters in leachates of a landfill site located near the marine environment: Bushehr port, Iran as a case. *Science of the Total Environment, 842*, 156838, https://doi.org/10.1016/j.scitotenv.2022.156838.

Molz, F. (2015). Advection, dispersion, and confusion. *Ground Water, 53*(3), 348-353, https://doi.org/10.1111%2Fgwat.12338.

Mondol, M., Angon, P. B., & Roy, A. (2025). Effects of microplastics on soil physical, chemical and biological properties. *Natural Hazards Research, 5*(1), 14-20, https://doi.org/10.1016/j.nhres.2024.02.002.

Nagar, H., & Sharma, S. (2025). Role of surface functional groups in the adsorption behavior of microcystin-LR on graphene surfaces. *Chemosphere, 374*, 144169, https://doi.org/10.1016/j.chemosphere.2025.144169.

Nakayama, H., Fukuda, A., & Shimaoka, T. (2024). Microplastics in a solid waste landfill in Japan: concentrations in landfilled waste, cover soil, rainwater and leachate. *Journal of Material Cycles Waste Management, 26*(2), 792-799, https://doi.org/10.1007/s10163-024-01895-w.

Nandikes, G., Banerjee, O., Mirthipati, M., Bhargavi, A., Jones, H., & Pathak, P. (2024). Separation, Identification, and Quantification of Microplastics in Environmental Samples. In *Microplastic Pollutants in Biotic Systems: Environmental Impact and Remediation Techniques* (pp. 1-19): ACS Publications.

Narevski, A. C., Novaković, M. I., Petrović, M. Z., Mihajlović, I. J., Maoduš, N. B., & Vujić, G. V. (2021). Occurrence of bisphenol A and microplastics in landfill leachate: lessons from South East Europe. *Environmental Science Pollution Research, 28*, 42196-42203, https://doi.org/10.1007/s11356-021-13705-z.

Nath, H., Kabir, M. H., Kafy, A. A., Rahaman, Z. A., & Rahman, M. T. (2023). Geotechnical properties and applicability of bentonite-modified local soil as landfill and environmental sustainability liners. *Environmental and Sustainability Indicators, 18*, 100241, https://doi.org/10.1016/j.indic.2023.100241.

Nayahi, N. T., Ou, B., Liu, Y., & Janjaroen, D. (2022). Municipal solid waste sanitary and open landfills: Contrasting sources of microplastics and its fate in their respective treatment systems. *Journal of Cleaner Production, 380*, 135095, https://doi.org/10.1016/j.jclepro.2022.135095.

Nizzetto, L., Bussi, G., Futter, M. N., Butterfield, D., & Whitehead, P. G. (2016). A theoretical assessment of microplastic transport in river catchments and their retention by soils and river sediments. *Environmental Science: Processes & Impacts, 18*(8), 1050-1059, https://doi.org/10.1039/C6EM00206D.

Njie, C. E., Ling, K., Tomomewo, O., Fadairo, A. S., Nkok, L. Y., Jakaria, Md., . . . Marti, J. (2023). Pore-Throat Blocking Mechanisms in Tight Rocks by Colloidal Particles in Treated and Untreated Produced Water. *Journal of Petrochemical Engineering, 3*(2), 68-85, https://doi.org/10.36959/901/256.

Norris, A., Scalia IV, J., & Shackelford, C. D. (2023). Mechanisms controlling the hydraulic conductivity of anionic polymer-enhanced GCLs. *Geosynthetics International, 30*(6), 628-650, https://doi.org/10.1680/jgein.21.00051.

O'Connor, D., Pan, S., Shen, Z., Song, Y., Jin, Y., Wu, W., & Hou, D. (2019). Microplastics undergo accelerated vertical migration in sand soil due to small size and wet-dry cycles. *Environmental Pollution, 249*, 527-534, https://doi.org/10.1016/j.envpol.2019.03.092.

Ohshima, H. (2012). The Derjaguin-Landau-Verwey-Overbeek (DLVO) Theory of Colloid Stability. *Electrical Phenomena at Interfaces and Biointerfaces: Fundamentals and Applications in Nano-, Bio-, and Environmental Sciences*, 27-34.

Ören, A. H., & Akar, R. Ç. (2017). Swelling and hydraulic conductivity of bentonites permeated with landfill leachates. *Applied Clay Science, 142*, 81-89, https://doi.org/10.1016/j.clay.2016.09.029.

Pak, T., Archilha, N. L., Berg, S., & Butler, I. B. (2023). Design considerations for dynamic fluid flow in porous media experiments using X-ray computed micro tomography–a review. *Tomography of Materials and Structures, 3*, 100017, https://doi.org/10.1016/j.tmater.2023.100017.

Pedretti, D., & Bianchi, M. (2018). Reproducing tailing in breakthrough curves: are statistical models equally representative and predictive? *Advances in Water Resources, 113*, 236-248, https://doi.org/10.1016/j.advwatres.2018.01.023.

Peng, M., Feng, S., Chen, H., & Chen, Z. (2021). An analytical solution for organic pollutant diffusion in a triple-layer composite liner considering the coupling influence of thermal diffusion. *Computers and Geotechnics, 137*, 104283, https://doi.org/10.1016/j.compgeo.2021.104283.

Petrov, R.J., Rowe, R.K., & Quigley, R.M. (1997). Comparison of Laboratory-Measured GCL Hydraulic Conductivity Based on Three Permeameter Types. *Geotechnical Testing Journal, 20*(1), 49-62, https://doi.org/10.1520/GTJ11420J.

Pradel, A., El Hadri, H., Desmet, C., Ponti, J., Reynaud, S., Grassl, B., & Gigault, J. (2020). Deposition of environmentally relevant nanoplastic models in sand during transport experiments. *Chemosphere, 255*, 126912, https://doi.org/10.1016/j.chemosphere.2020.126912.

Prasad, D., Mitra, N., & Deb, K. (2023). Hydrogen and metal–ligand bonds in swelling of smectite clay minerals. *The Journal of Physical Chemistry C, 127*(42), 20823-20837., https://doi.org/10.1021/acs.jpcc.3c02916.

Proia, R., Salvatore, E., Croce, P., & Modoni, G. (2024). Compacted sand–bentonite mixtures for the confinement of waste landfills. *Acta Geotechnica*, 1-16, https://doi.org/10.1007/s11440-024-02335-7.

Puthcharoen, A., & Leungprasert, S. (2019). Determination of microplastics in soil and leachate from the landfills. *Thai Environmental Engineering Journal, 33*(3), 39-46.

Qi, S., Song, J., Shentu, J., Chen, Q., & Lin, K. (2022). Attachment and detachment of large microplastics in saturated porous media and its influencing factors. *Chemosphere, 305*, 135322, https://doi.org/10.1016/j.chemosphere.2022.135322.

Qi, Y., Beriot, N., Gort, G., Lwanga, E. H., Gooren, H., Yang, X., & Geissen, V. (2020). Impact of plastic mulch film debris on soil physicochemical and hydrological properties. *Environmental Pollution, 266*, 115097, https://doi.org/10.1016/j.envpol.2020.115097.

Qin, L., Zha, F., Xu, R., Liu, S., Bouazza, A., Huang, H., & Wang, Q. (2025). Experimental and numerical investigation of gas preferential flow through geosynthetic clay liner overlap joint in landfill final cover system. *Bulletin of Engineering Geology and the Environment, 84*(9), 423, https://doi.org/10.1007/s10064-025-04426-5.

Quevedo, I. R., & Tufenkji, N. (2012). Mobility of functionalized quantum dots and a model polystyrene nanoparticle in saturated quartz sand and loamy sand. *Environmental science & technology, 46*(8), 4449-4457, https://doi.org/10.1021/es2045458.

Rao, S. M., Thyagaraj, T., & Raghuveer Rao, P. (2013). Crystalline and osmotic swelling of an expansive clay inundated with sodium chloride solutions. *Geotechnical and Geological Engineering, 31*(4), 1399-1404, https://doi.org/10.1007/s10706-013-9629-3.

Rapant, S., Cvečková, V., Fajčíková, K., Sedláková, D., & Stehlíková, B. (2017). Impact of calcium and magnesium in groundwater and drinking water on the health of inhabitants of the Slovak Republic. *International Journal of Environmental Research and Public Health, 14*(3), 1-21, https://doi.org/10.3390/ijerph14030278.

Rathore, C., Saha, M., Gupta, P., Kumar, M., Naik, A., & de Boer, J. (2023). Standardization of micro-FTIR methods and applicability for the detection and identification of microplastics in environmental matrices. *Science of the Total Environment, 888*, 164157, https://doi.org/10.1016/j.scitotenv.2023.164157.

Ren, Z., Gui, X., Wei, Y., Chen, X., Xu, X., Zhao, L., . . . Cao, X. (2021). Chemical and photo-initiated aging enhances transport risk of microplastics in saturated soils: Key factors, mechanisms, and modeling. *Water Research, 202*, 117407, https://doi.org/10.1016/j.watres.2021.117407.

Rong, H., He, L., Li, M., Zhang, M., Yi, K., Han, P., & Tong, M. (2021). Different electrically charged proteins result in diverse transport behaviors of plastic particles with different surface charge in quartz sand. *Science of the Total Environment, 756*, 143837, https://doi.org/10.1016/j.scitotenv.2020.143837.

Rong, H., Li, M., He, L., Zhang, M., Hsieh, L., Wang, S., . . . Tong, M. (2022). Transport and deposition behaviors of microplastics in porous media: Co-impacts of N fertilizers and humic acid. *Journal of Hazardous Materials, 426*, 127787, https://doi.org/10.1016/j.jhazmat.2021.127787.

Rowe, R. K. (2009). *Long-term performance of leachate collections systems and geomembrane liners for MSW landfills.* Paper presented at the GIGSA GeoAfrica 2009, South Africa.

Rowe, R. K. (2011). Systems engineering: the design and operation of municipal solid waste landfills to minimize contamination of groundwater. *Geosynthetics International, 18*(6), 391-404, https://doi.org/10.1680/gein.2011.18.6.391.

Rowe, R. K. (2012). Short-and long-term leakage through composite liners. The 7th Arthur Casagrande Lecture. *Canadian Geotechnical Journal, 49*(2), 141-169, https://doi.org/10.1139/t11-092.
Rowe, R. K. (2014). Performance of GCLs in liners for landfill and mining applications. *Environmental Geotechnics, 1*(1), 3-21, http://dx.doi.org/10.1680/envgeo.13.00031.
Rowe, R. K., Ali, M. M., & Morsy, M. S. (2024). Long-term performance of textured HDPE geomembranes in municipal solid waste landfills. *Canadian Geotechnical Journal, 62*, 1-24, https://doi.org/10.1139/cgj-2024-0024.
Rowe, R. K., & Brachman, R. W. I. (2004). Assessment of equivalence of composite liners. *Geosynthetics International, 11*(4), 273-286, https://doi.org/10.1680/gein.2004.11.4.273.
Rowe, R. K., & Hamdan, S. (2021). Effect of wet-dry cycles on standard & polymer-amended GCLs in covers subjected to flow over the GCL. *Geotextiles and Geomembranes, 49*(5), 1165-1175, https://doi.org/10.1016/j.geotexmem.2021.03.010.
Rowe, R. K., & Hamdan, S. (2023). Performance of GCLs after long-term wet–dry cycles under a defect in GMB in a landfill. *Geosynthetics International, 30*(3), 225-246, https://doi.org/10.1680/jgein.21.00023a.
Rowe, R. K., & Hosney, M. S. (2015). Interface transmissivity and hydraulic conductivity of GCLs below poured concrete. *Geosynthetics International, 22*(1), 48-69, https://doi.org/10.1680/gein.14.00031.
Rowe, R. K., & Jabin, F. (2021). Effect of prehydration, permeant, and desiccation on GCL/Geomembrane interface transmissivity. *Geotextiles and Geomembranes, 49*(6), 1451-1469, https://doi.org/10.1016/j.geotexmem.2021.04.006.
Rowe, R. K., & Li, T. K. (2020). Self-healing of circular and slit defects in GCLs upon hydration from silty sand under applied stress. *Geotextiles and Geomembranes, 48*(5), 667-683, https://doi.org/10.1016/j.geotexmem.2020.05.001.
Rowe, R. K., & Li, T. K. (2021). Influence of pore water chemistry on GCL self-healing with hydration from silica sand. *Geotextiles and Geomembranes, 49*(4), 871-894, https://doi.org/10.1016/j.geotexmem.2020.12.007.
Rowe, R. K., Reinert, J., Li, Y., & Awad, R. (2023). The need to consider the service life of all components of a modern MSW landfill liner system. *Waste Management, 161*, 43-51, https://doi.org/10.1016/j.wasman.2023.02.004.
Ryan, J. N., & Elimelech, M. (1996). Colloid mobilization and transport in groundwater. *Colloids and Surfaces: A Physicochemical and Engineering Aspects, 107*, 1-56, https://doi.org/10.1016/0927-7757(95)03384-X.
Saengchut, P., Viriya, H., & Kongritti, N. (2024). Source apportionment of microplastics in environment from sanitary landfill–a case study of Muangpak Municipality Landfill, Thailand. *Journal of Ecological Engineering, 25*(1), 278-284, https://doi.org/10.12911/22998993/175410.
Sajjad, M., Huang, Q., Khan, S., Khan, M. A., Liu, Y., Wang, J., . . . Guo, G. (2022). Microplastics in the soil environment: A critical review. *Environmental Technology Innovation, 27*, 102408, https://doi.org/10.1016/j.eti.2022.102408.
Salikova, N. S., Rodrigo-Ilarri, J., Rodrigo-Clavero, M. E., Urazbayeva, S. E., Askarova, A. Z., & Magzhanov, K. M. (2023). Environmental assessment of microplastic pollution induced by solid waste landfills in the Akmola region (North Kazakhstan). *Water, 15*(16), 2889, https://doi.org/10.3390/w15162889.
Salve, P. R., Maurya, A., Wate, S. R., & Devotta, S. (2008). Chemical composition of major ions in rainwater. *Bulletin of Environmental Contamination and Toxicology, 80*(3), 242-246, https://doi.org/10.1007/s00128-007-9353-x.

Savino, I., Campanale, C., Trotti, P., Massarelli, C., Corriero, G., & Uricchio, V. F. (2022). Effects and impacts of different oxidative digestion treatments on virgin and aged microplastic particles. *Polymers, 14*(10), 1958, https://doi.org/10.3390/polym14101958.

Savvidou, C., & Culligan, P. J. (1998). The application of centrifuge modelling to geo-environmental problems. *Proceedings of the Institution of Civil Engineers-Geotechnical Engineering, 131*(3), 152-162, http://dx.doi.org/10.1680/igeng.1998.30471.

Scalia IV, J., Bohnhoff, G. L., Shackelford, C. D., Benson, C. H., Sample-Lord, K. M., Malusis, M. A., & Likos, W. J. (2018). Enhanced bentonites for containment of inorganic waste leachates by GCLs. *Geosynthetics International, 25*(4), 392-411, https://doi.org/10.1680/jgein.18.00024.

Scalia, J., & Benson, C. H. (2010). Effect of permeant water on the hydraulic conductivity of exhumed GCLs. *Geotech. Test. J., 33*(3), 201-211, https://doi.org/10.1520/GTJ102609.

Schijven, J. F., & Šimůnek, J. (2002). Kinetic modeling of virus transport at the field scale. *Journal of Contaminant Hydrology, 55*(1-2), 113-135, https://doi.org/10.1016/S0169-7722(01)00188-7.

Scholz, P., Putna-Nimane, I., Barda, I., Liepina-Leimane, I., Strode, E., Kileso, A., . . . Simon, F. G. (2021). Environmental impact of geosynthetics in coastal protection. *Materials, 14*(3), 634, https://doi.org/10.3390/ma14030634.

Sekar, V., & Sundaram, B. (2023). Preliminary evidence of microplastics in landfill leachate, Hyderabad, India. *Process Safety Environmental Protection, 175*, 369-376, https://doi.org/10.1016/j.psep.2023.05.070.

Sembiring, E., & Ramadan, A. H. (2024). *Microplastic pollution from active and inactive landfill in Indonesia: Case study in Leuwigajah and Sarimukti Landfill.* Paper presented at the E3S Web of Conferences.

Shackelford, C. D. (2021). *Fundamental considerations for column testing of engineered, clay-based barriers.* Paper presented at the Third International Symposium on Coupled Phenomena in Environmental Geotechnics.

Shackelford, C. D., Benson, C. H., Katsumi, T., Edil, T. B., & Lin, L. (2000). Evaluating the hydraulic conductivity of GCLs permeated with non-standard liquids. *Geotextiles and Geomembranes, 18*(2-4), 133-161, https://doi.org/10.1016/S0266-1144(99)00024-2.

Shackelford, C. D., & Hong, C. S. (2019). Comparative analyses of alternative breakthrough curves from cumulative mass column testing of soil–bentonite backfills. *Canadian Geotechnical Journal, 57*(8), 1197-1214, https://doi.org/10.1139/cgj-2019-0468.

Shackelford, C. D., & Lee, J. (2003). The destructive role of diffusion on clay membrane behavior. *Clays and Clay Minerals, 51*(2), 186-196, https://doi.org/10.1346/CCMN.2003.0510209.

Shackelford, C. D., Meier, A., & Sample-Lord, K. (2016). Limiting membrane and diffusion behavior of a geosynthetic clay liner. *Geotextiles and Geomembranes, 44*(5), 707-718, https://doi.org/10.1016/j.geotexmem.2016.05.009.

Shackelford, C. D., Sevick, G. W., & Eykholt, G. R. (2010). Hydraulic conductivity of geosynthetic clay liners to tailings impoundment solutions. *Geotextiles and Geomembranes, 28*(2), 149-162., https://doi.org/10.1016/j.geotexmem.2009.10.005.

Shafea, L., Felde, V. J., Woche, S. K., Bachmann, J., & Peth, S. (2023). Microplastics effects on wettability, pore sizes and saturated hydraulic conductivity of a loess topsoil. *Geoderma, 437*, 116566, https://doi.org/10.1016/j.geoderma.2023.116566.

Sharma, P., Flury, M., & Mattson, E. (2008). Studying colloid transport in porous media using a geocentrifuge. *Water Resources Research, 44*, 1-11, https://doi.org/10.1029/2007WR006456.

Shen, C., Huang, Y., Li, B., & Jin, Y. (2010). Predicting attachment efficiency of colloid deposition under unfavorable attachment conditions. *Water Resources Research, 46*(11), W11526, https://doi.org/10.1029/2010WR009218.

Shen, C., Wang, L. P., Li, B., Huang, Y., & Jin, Y. (2012). Role of surface roughness in chemical detachment of colloids deposited at primary energy minima. *Vadose Zone Journal, 11*(1), vzj2011-0057, https://doi.org/10.2136/vzj2011.0057.

Sholokhova, A., Denafas, G., Ceponkus, J., & Omelianenko, T. (2023). Microplastics in landfill bodies: abundance, spatial distribution and effect of landfill age. *Sustainability, 15*(6), 5017, https://doi.org/10.3390/su15065017.

Solly, E. F., Weber, V., Zimmermann, S., Walthert, L., Hagedorn, F., & Schmidt, M. W. (2020). A critical evaluation of the relationship between the effective cation exchange capacity and soil organic carbon content in Swiss forest soils. *Frontiers in Forests and Global Change, 3*, 98, https://doi.org/10.3389/ffgc.2020.00098.

Song, J., Wang, C., & Li, G. (2024). Defining primary and secondary microplastics: a connotation analysis. *ACS ES&T Water, 4*(6), 2330-2332, https://doi.org/10.1021/acsestwater.4c00316.

Sposito, G., & Prost, R. (1982). Structure of water adsorbed on smectites. *Chemical Reviews, 82*(6), 553-573.

Sterpi, D. (2015). Effect of freeze–thaw cycles on the hydraulic conductivity of a compacted clayey silt and influence of the compaction energy. *Soils and Foundations, 55*(5), 1326-1332, https://doi.org/10.1016/j.sandf.2015.09.030.

Su, Y., Zhang, Z., Wu, D., Zhan, L., Shi, H., & Xie, B. (2019). Occurrence of microplastics in landfill systems and their fate with landfill age. *Water Research, 164*, 114968, https://doi.org/10.1016/j.watres.2019.114968.

Sujathan, S., & El-Zein, A. (2025). Performance of Analytical Techniques for Microplastic and Nanoplastic Quantification in the Presence of Clay. *Water Research, 288*, 124716, https://doi.org/10.1016/j.watres.2025.124716.

Sun, H., Mašín, D., Najser, J., Neděla, V., & Navrátilová, E. (2019). Bentonite microstructure and saturation evolution in wetting–drying cycles evaluated using ESEM, MIP and WRC measurements. *Géotechnique, 69*(8), 713-726, https://doi.org/10.1680/jgeot.17.P.253.

Sun, H., Zhou, S., Jiang, Y., Qin, Z., Fei, J., Sun, Y., . . . Yin, X. (2022). Effect of cationic, anionic and non-ionic surfactants on transport of microplastics: role of adhesion of surfactants on the polyethylene surface. *Journal of Hydrology, 612*, 128051, https://doi.org/10.1016/j.jhydrol.2022.128051.

Sun, J., Zhu, Z., Li, W., Yan, X., Wang, L., Zhang, L., . . . Ni, B. (2021). Revisiting microplastics in landfill leachate: unnoticed tiny microplastics and their fate in treatment works. *Water research, 190*, 116784, https://doi.org/10.1016/j.watres.2020.116784.

Syngouna, V. I., & Chrysikopoulos, C. V. (2015). Experimental investigation of virus and clay particles cotransport in partially saturated columns packed with glass beads. *Journal of colloid and interface science, 440*, 140-150, https://doi.org/10.1016/j.jcis.2014.10.066.

Szulc, J., Okrasa, M., Nowak, A., Nizioł, J., Ruman, T., & Kuberski, S. (2022). Assessment of physicochemical, microbiological and toxicological hazards at an illegal landfill in Central Poland. *International Journal of Environmental Research and Public Health, 19*(8), 4826, https://doi.org/10.3390/ijerph19084826.

Taheri, S., & El-Zein, A. (2023). Desiccation cracking of polymer-bentonite mixtures: An experimental investigation. *Applied Clay Science, 238*, 106945, https://doi.org/10.1016/j.clay.2023.106945.

Tan, K. L., Ankathil, R., & Gan, S. H. (2011). Method development and validation for the simultaneous determination of imatinib mesylate and N-desmethyl imatinib using rapid resolution high performance liquid chromatography coupled with UV-detection. *Journal of Chromatography B, 879*(30), 3583-3591, https://doi.org/10.1016/j.jchromb.2011.09.048.

Tan, M., Liu, L., Zhang, M., Liu, Y., & Li, C. (2021). Effects of solution chemistry and humic acid on the transport of polystyrene microplastics in manganese oxides coated sand. *Journal of Hazardous Materials, 413*, 125410, https://doi.org/10.1016/j.jhazmat.2021.125410.

Tan, Y., Benson, C. H., Zhou, G., Bradshaw, S. L., & Edil, T. B. (2024). *Hydraulic conductivity of two geosynthetic clay liners with different bentonite granule sizes.* Paper presented at the E3S Web of Conferences.

Tehrani, R. S., Yang, X., & van Dam, J. (2025). Rainfall-induced microplastic fate and transport in unsaturated Dutch soils. *Journal of Contaminant Hydrology, 268*, 104456, https://doi.org/10.1016/j.jconhyd.2024.104456.

Thilagan, J., Kumar, A. V., Rajasekaran, K., & Raja, C. (2015). Continuous fixed bed column adsorption of copper (II) ions from aqueous solution by calcium carbonate. *International Journal of Engineering Research & Technology, 4*(12), 413-418, http://dx.doi.org/10.17577/IJERTV4IS120456.

Thompson, R. C., Olsen, Y., Mitchell, R. P., Davis, A., Rowland, S. J., John, A. W., . . . Russell, A. E. (2004). Lost at sea: where is all the plastic? *Science Advances, 304*(5672), 838-838, https://doi.org/10.1126/science.1094559.

Tian, K., Benson, C. H., & Likos, W. J. (2016). Hydraulic conductivity of geosynthetic clay liners to low-level radioactive waste leachate. *Journal of Geotechnical and Geoenvironmental Engineering, 142*(8), 04016037, https://doi.org/10.1061/(ASCE)GT.1943-5606.0001495.

Ting, H. Z. (2023). *Mechanical theory for particle detachment in porous media.* (Doctor of Philosophy, The University of Adelaide, Retrieved from https://digital.library.adelaide.edu.au/dspace/bitstream/2440/138957/1/Ting2023_PhD.pdf)

Topa, D., Cara, I. G., & Jităreanu, G. (2021). Long term impact of different tillage systems on carbon pools and stocks, soil bulk density, aggregation and nutrients: A field meta-analysis. *Catena, 199*, 105102, https://doi.org/10.1016/j.catena.2020.105102.

Torkzaban, S., & Bradford, S. A. (2016). Critical role of surface roughness on colloid retention and release in porous media. *Water Research, 88*, 274-284., https://doi.org/10.1016/j.watres.2015.10.022.

Trihadiningrum, Y., Wilujeng, S. A., Tafaqury, R., Radita, D. R., & Radityaningrum, A. (2023). Evidence of microplastics in leachate of Randegan landfill, Mojokerto City, Indonesia, and its potential to pollute surface water. *Science of the Total Environment, 874*, 162207, https://doi.org/10.1016/j.scitotenv.2023.162207.

Tufenkji, N., & Elimelech, M. (2005). Breakdown of colloid filtration theory: Role of the secondary energy minimum and surface charge heterogeneities. *Langmuir, 21*(3), 841-852, https://doi.org/10.1021/la048102g.

Utecht, S., Krause, S., & Schuetz, T. (2025). Particle size-dependent quantitative and qualitative differences of common microplastic detection procedures: Nile Red-assisted fluorescence microscopy and confocal micro-Raman spectroscopy. *Environmental Monitoring and Assessment, 197*(8), 934, https://doi.org/10.1007/s10661-025-14317-7.

van Praagh, M., Hartman, C., & Brandmyr, E. (2018). *Microplastics in Landfill Leachates in the Nordic Countries* (Retrieved from https://www.diva-portal.org/smash/get/diva2:1277395/FULLTEXT01.pdf)

Vasko, S., Jo, H. Y., Benson, C. H., Edil, T. B., & Katsumi, T. (2001). Hydraulic conductivity of partially prehydrated geosynthetic clay liners permeated with aqueous calcium chloride solutions. *Proc., Geosynthetics 2001*, 685-699.

Ventura, E., Marín, A., Gámez-Pérez, J., & Cabedo, L. (2024). Recent advances in the relationships between biofilms and microplastics in natural environments. *World Journal of Microbiology and Biotechnology, 40*(7), 220, https://doi.org/10.1007/s11274-024-04021-y.

Verma, M., Singh, P., & Dhanorkar, M. (2024). Exploring the abundance of microplastics in Indian landfill leachate: An analytical study. *Journal of Environmental Management, 360*, 121181, https://doi.org/10.1016/j.jenvman.2024.121181.

Verma, R., Vinoda, K. S., Papireddy, M., & Gowda, A. (2016). Toxic pollutants from plastic waste-a review. *Procedia Environmental Sciences, 35*, 701-708, https://doi.org/10.1016/j.proenv.2016.07.069.

Waldschläger, K., & Schüttrumpf, H. (2020). Infiltration behavior of microplastic particles with different densities, sizes, and shapes - from glass spheres to natural sediments. *Environmental Science & Technology, 54*(15), 9366-9373, https://doi.org/10.1021/acs.est.0c01722.

Walter, K., Don, A., Tiemeyer, B., & Freibauer, A. (2016). Determining soil bulk density for carbon stock calculations: a systematic method comparison. *Soil Science Society of America Journal, 80*(3), 579-591, https://doi.org/10.2136/sssaj2015.11.0407.

Walz, J. Y. (1998). The effect of surface heterogeneities on colloidal forces. *Advances in Colloid and Interface Science, 74*(1-3), 119-168, https://doi.org/10.1016/S0001-8686(97)00042-0.

Wan, Y., Chen, X., Liu, Q., Hu, H., Wu, C., & Xue, Q. (2022). Informal landfill contributes to the pollution of microplastics in the surrounding environment. *Environmental Pollution, 293*, 118586, https://doi.org/10.1016/j.envpol.2021.118586.

Wan, Y., Xue, Q., & Liu, L. (2014). Study on the permeability evolution law and the micro-mechanism of CCL in a landfill final cover under the dry-wet cycle. *Bulletin of Engineering Geology and the Environment, 73*(4), 1089-1103, https://doi.org/10.1007/s10064-014-0604-x.

Wang, C., O'Connor, D., Wang, L., Wu, W., Luo, J., & Hou, D. (2022a). Microplastics in urban runoff: Global occurrence and fate. *Water Research, 225*, 119129, https://doi.org/10.1016/j.watres.2022.119129.

Wang, C. Q., Wang, H., Gu, G. H., Fu, J. G., Lin, Q. Q., & Liu, Y. N. (2015). Interfacial interactions between plastic particles in plastics flotation. *Waste Management, 46*, 56-61, https://doi.org/10.1016/j.wasman.2015.08.041.

Wang, F., Wang, Q., Adams, C. A., Sun, Y., & Zhang, S. (2022b). Effects of microplastics on soil properties: current knowledge and future perspectives. *Journal of Hazardous Materials, 424*, 127531, https://doi.org/10.1016/j.jhazmat.2021.127531.

Wang, H., Ding, J., Xiong, C., Zhu, D., Li, G., Jia, X., . . . Xue, X. (2019a). Exposure to microplastics lowers arsenic accumulation and alters gut bacterial communities of earthworm Metaphire californica. *Environmental Pollution, 251*, 110-116, https://doi.org/10.1016/j.envpol.2019.04.054.

Wang, M., Gao, B., & Tang, D. (2016). Review of key factors controlling engineered nanoparticle transport in porous media. *Journal of Hazardous Materials, 318*, 233-246, https://doi.org/10.1016/j.jhazmat.2016.06.065.

Wang, S., Jian, Q., Zhang, P., Zhang, J., Zhao, L., Liu, D., & Kang, X. (2022c). Tracing land-based microplastic sources in coastal waters of Zhanjiang Bay, China: spatiotemporal pattern, composition, and flux. *Frontiers in Marine Science, 9*, 934707, https://doi.org/10.3389/fmars.2022.934707.

Wang, W., Gao, H., Jin, S., Li, R., & Na, G. (2019b). The ecotoxicological effects of microplastics on aquatic food web, from primary producer to human: A review. *Ecotoxicology Environmental Safety, 173*, 110-117, https://doi.org/10.1016/j.ecoenv.2019.01.113.

Wang, Z., Li, J., Qu, Z., Ayurzana, B., Zhao, G., & Li, W. (2024). Effects of microplastics on the pore structure and connectivity with different soil textures: Based on CT scanning. *Environmental Technology & Innovation, 36*, 103791, https://doi.org/10.1016/j.eti.2024.103791.

Wang, Z., Li, W., Li, W., Yang, W., & Jing, S. (2023). Effects of microplastics on the water characteristic curve of soils with different textures. *Chemosphere, 317*, 137762, https://doi.org/10.1016/j.chemosphere.2023.137762.

Wang, Z., & Sedighi, M. (2023). Dispersion properties of nanoplastic spheres in granular media at low Reynolds numbers. *Journal of Contaminant Hydrology, 259*(104244), https://doi.org/10.1016/j.jconhyd.2023.104244.

Weerasinghe, I. A., Gallage, C., & Dawes, L. (2021). Effect of overburden confining stress on hydraulic performance of geosynthetic clay liners (GCLs). *Heliyon, 7*(1), e05770, https://doi.org/10.1016/j.heliyon.2020.e05770.

Wireko, C., Zainab, B., Tian, K., & Abichou, T. (2020). Effect of specimen preparation on the swell index of bentonite-polymer GCLs. *Geotextiles and Geomembranes, 48*(6), 875-885, https://doi.org/10.1016/j.geotexmem.2020.06.006.

Wojnowska-Baryła, I., Bernat, K., & Zaborowska, M. (2022). Plastic waste degradation in landfill conditions: the problem with microplastics, and their direct and indirect environmental effects. *International Journal of Environmental Research and Public Health, 19*(20), 13223, https://doi.org/10.3390/ijerph192013223.

Wu, X., Lyu, X., Li, Z., Gao, B., Zeng, X., Wu, J., & Sun, Y. (2020). Transport of polystyrene nanoplastics in natural soils: Effect of soil properties, ionic strength and cation type. *Science of the Total Environment, 707*, 136065, https://doi.org/10.1016/j.scitotenv.2019.136065.

Xi, X., Ding, D., Zhou, H., Baihetiyaer, B., Sun, H., Cai, Y., . . . Yin, X. (2022). Interactions of pristine and aged nanoplastics with heavy metals: enhanced adsorption and transport in saturated porous media. *Journal of Hazardous Materials, 437*, 129311, https://doi.org/10.1016/j.jhazmat.2022.129311.

Xiao, D., Li, S., Chen, Z., Zou, S., Nugroho, W. A., Huo, M., . . . Fan, W. (2024). Microplastic and silica colloid transport in a saturated porous medium under various flow directions: the effect of gravity. *Water, Air, & Soil Pollution, 235*, 1-12, https://doi.org/10.1007/s11270-023-06824-5.

Xie, X., Zhou, H., Wu, L., & Man, J. (2024a). Numerical modeling of double-ring infiltrometers for determining saturated hydraulic conductivity of heterogeneous and anisotropic soils. *Pedosphere, 34*(6), https://doi.org/10.1016/j.pedsph.2023.07.016.

Xie, Y., Wang, H., Guo, Y., Wang, C., Cui, H., & Xue, J. (2024b). Effects of microplastic contamination on the hydraulic, water retention, and desiccation crack properties of a natural clay exposed to leachate. *Journal of Environmental Management, 351*, https://doi.org/10.1016/j.jenvman.2023.119858.

Xu, H., Shu, S., Wang, S., Zhou, A., Jiang, P., Zhu, W., . . . Chen, L. (2019). Studies on the chemical compatibility of soil-bentonite cut-off walls for landfills. *Journal of Environmental Management, 237*, 155-162, https://doi.org/10.1016/j.jenvman.2019.02.051.

Xu, L., Liang, Y., Zhang, R., Xu, B., Liao, C., Xie, T., & Wang, D. (2022). Facilitated transport of microplastics and nonylphenol in porous media with variations in physicochemical

heterogeneity. *Environmental Pollution, 315*, 120297, https://doi.org/10.1016/j.envpol.2022.120297.
Xu, S., Gao, B., & Saiers, J. E. (2006). Straining of colloidal particles in saturated porous media. *Water Resources Research, 42*(12), W12S16, https://doi.org/10.1029/2006WR004948.
Xu, Z., Sui, Q., Li, A., Sun, M., Zhang, L., Lyu, S., & Zhao, W. (2020). How to detect small microplastics (20-100 μm) in freshwater, municipal wastewaters and landfill leachates? A trial from sampling to identification. *Science of the Total Environment, 733*, 139218, https://doi.org/10.1016/j.scitotenv.2020.139218.
Xue, Q., Zhang, Q., & Liu, L. (2012). Impact of high concentration solutions on hydraulic properties of geosynthetic clay liner materials. *Materials, 5*(11), 2326-2341., https://doi.org/10.3390/ma5112326.
Yadav, H., Tadikonda, B. V., Gaurav, S., & Kumar, S. (2023). Fate and transport of coronavirus surrogate through compacted clays for pathogenic waste disposal. *Langmuir, 39*(23), 8042-8054, https://doi.org/10.1021/acs.langmuir.3c00110.
Yaghmaeiyan, N., Mirzaei, M., & Delghavi, R. (2022). Montmorillonite clay: Introduction and evaluation of its applications in different organic syntheses as catalyst: A review. *Results in Chemistry, 4*, 100549, https://doi.org/10.1016/j.rechem.2022.100549.
Yang, P., Jiang, T., Zhang, Y., & Li, Z. (2018a). Effect of osmotic pressure on migration behavior of nZnO in GCLs. *Advances in Civil Engineering, 2018*(1), 6703485, https://doi.org/10.1155/2018/6703485.
Yang, P., Liu, Y. H., Yang, K., & Ouyang, Z. B. (2020). Effects of pressure on graphene oxide nanoparticle deposition and transport in GCLs. *Geosynthetics International, 27*(6), 573-580, https://doi.org/10.1680/jgein.20.00015.
Yang, P., Wang, M., Zhang, Y., Song, L., Feng, S., & Xue, S. (2018b). Transport behavior of nZnO in geosynthetic clay liner used in municipal solid waste landfills under temperature effect. *Environmental Earth Sciences, 77*(1), 10, https://doi.org/10.1007/s12665-017-7188-2.
Yang, X., An, C., Feng, Q., Boufadel, M., & Ji, W. (2022). Aggregation of microplastics and clay particles in the nearshore environment: Characteristics, influencing factors, and implications. *Water Research, 224*, 119077, https://doi.org/10.1016/j.watres.2022.119077.
Yang, X., & Tang, D. W. (2025). Modeling microplastic transport through porous media: Challenges arising from dynamic transport behavior. *Journal of Hazardous Materials, 484*, 136728, https://doi.org/10.1016/j.jhazmat.2024.136728.
Ye, X., Cheng, Z., Wu, M., Hao, Y., Hu, B. X., Mo, C., . . . Lu, G. (2022a). Investigating transport kinetics of polystyrene nanoplastics in saturated porous media. *Ecotoxicology and Environmental Safety, 241*, 113820, https://doi.org/10.1016/j.ecoenv.2022.113820.
Ye, X., Cheng, Z., Wu, M., Hao, Y., Lu, G., Hu, B. X., . . . Wu, J. (2022b). Effects of clay minerals on the transport of polystyrene nanoplastic in groundwater. *Water Research, 223*, 118978, https://doi.org/10.1016/j.watres.2022.118978.
Yu, B., & El-Zein, A. (2019). Experimental investigation of the effect of airgaps in preventing desiccation of bentonite in geosynthetic clay liners exposed to high temperatures. *Geotextiles and Geomembranes, 47*(2), 142-153, https://doi.org/10.1016/j.geotexmem.2018.12.002.
Yu, B., El-Zein, A., & Rowe, R. K. (2020). Effect of added polymer on the desiccation and healing of a geosynthetic clay liner subject to thermal gradients. *Geotextiles and Geomembranes, 48*(6), 928-939, https://doi.org/10.1016/j.geotexmem.2020.08.001.
Yu, F., Wu, Z., Wang, J., Li, Y., Chu, R., Pei, Y., & Ma, J. (2022). Effect of landfill age on the physical and chemical characteristics of waste plastics/microplastics in a waste landfill

sites. *Environmental Pollution, 306*, 119366, https://doi.org/10.1016/j.envpol.2022.119366.
Yu, Y., Battu, A. K., Varga, T., Denny, A. C., Zahid, T. M., Chowdhury, I., & Flury, M. (2023). Minimal impacts of microplastics on soil physical properties under environmentally relevant concentrations. *Environmental Science & Technology, 57*(13), 5296-5304, https://doi.org/10.1021/acs.est.2c09822.
Zaman, F., Rahman, M. A., Haque, M. M., Akbor, M. A., & Tareq, S. M. (2024). Pervasiveness and classification of microplastics in Landfill Leachate: impacts, risks, and treatment efficiency. *Journal of Hazardous Materials Advances, 16*, 100502, https://doi.org/10.1016/j.hazadv.2024.100502.
Zeng, L., Yuan, C., Xiang, T., Guan, X., Dai, L., Xu, D., . . . Tian, C. (2024). Research on the Migration and Adsorption Mechanism Applied to Microplastics in Porous Media: A Review. *Nanomaterials, 14*(12), 1060, https://doi.org/10.3390/nano14121060.
Zhai, H., & Benson, C. H. (2006). The log-normal distribution for hydraulic conductivity of compacted clays: Two or three parameters? *Geotechnical & Geological Engineering, 24*(5), 1149-1162, https://doi.org/10.1007/s10706-005-1135-9.
Zhang, G., Ma, Q., Yu, M., Yin, J., Sun, H., Wang, N., . . . Yin, X. (2023a). Transport of functional group modified polystyrene nanoplastics in binary metal oxide saturated porous media. *Journal of Hazardous Materials, 441*, 129834., https://doi.org/10.1016/j.jhazmat.2022.129834.
Zhang, G. S., & Liu, Y. F. (2018). The distribution of microplastics in soil aggregate fractions in southwestern China. *Science of the Total Environment, 642*, 12-20, https://doi.org/10.1016/j.scitotenv.2018.06.004.
Zhang, G. S., Zhang, F. X., & Li, X. T. (2019). Effects of polyester microfibers on soil physical properties: Perception from a field and a pot experiment. *Science of the Total Environment, 670*, 1-7, https://doi.org/10.1016/j.scitotenv.2019.03.149.
Zhang, M., Hou, J., Xia, J., Wu, J., You, G., & Miao, L. (2024). Statuses, shortcomings, and outlooks in studying the fate of nanoplastics and engineered nanoparticles in porous media respectively and borrowable sections from engineered nanoparticles for nanoplastics. *Science of the Total Environment, 915*, 169638, https://doi.org/10.1016/j.scitotenv.2023.169638.
Zhang, Q., Li, X., Liu, J., Liu, J., Han, L., Wang, X., . . . Han, X. (2023b). The contribution of microbial necromass carbon to soil organic carbon in soil aggregates. *Applied Soil Ecology, 190*, 104985, https://doi.org/10.1016/j.apsoil.2023.104985.
Zhao, W., Su, Z., Geng, T., Zhao, Y., Tian, Y., & Zhao, P. (2022). Effects of ionic strength and particle size on transport of microplastic and humic acid in porous media. *Chemosphere, 309*, 136593, https://doi.org/10.1016/j.chemosphere.2022.136593.
Zheng, X. L., Shan, B. B., Chen, L., Sun, Y. W., & Zhang, S. H. (2014). Attachment–detachment dynamics of suspended particle in porous media: Experiment and modeling. *Journal of Hydrology, 511*, 199-204., https://doi.org/10.1016/j.jhydrol.2014.01.039.
Zhong, H., Liu, G., Jiang, Y., Yang, J., Liu, Y., Yang, X., . . . Zeng, G. (2017). Transport of bacteria in porous media and its enhancement by surfactants for bioaugmentation: a review. *Biotechnology advances, 35*(4), 490-504, https://doi.org/10.1016/j.biotechadv.2017.03.009.
Zhou, L., Zhang, H., Yan, M., Chen, H., & Zhang, M. (2013). Laboratory determination of migration of Eu(III) in compacted bentonite-sand mixtures as buffer/backfill material for high-level waste disposal. *Applied Radiation and Isotopes, 82*, 139-144, https://doi.org/10.1016/j.apradiso.2013.07.004.
Zhu, D., Chen, Q., An, X., Yang, X., Christie, P., Ke, X., . . . Zhu, Y. (2018). Exposure of soil collembolans to microplastics perturbs their gut microbiota and alters their isotopic

composition. *Soil Biology Biochemistry, 116*, 302-310, https://doi.org/10.1016/j.soilbio.2017.10.027.

Ziani, K., Ioniță-Mîndrican, C. B., Mititelu, M., Neacșu, S. M., Negrei, C., Moroșan, E., . . . Preda, O. T. (2023). Microplastics: a real global threat for environment and food safety: a state of the art review. *Nutrients, 15*(3), 617, https://doi.org/10.3390/nu15030617.